SAPIENZA
UNIVERSITÀ DI ROMA

Faculty of Civil and Industrial Engineering

Department of Civil, Constructional and Environmental Engineering

Ph.D. School of Civil Engineering and Architecture
Ph.D. Course in Environmental and Hydraulic Engineering - XXXIII Cycle

BIOCHAR AS REACTIVE MATERIAL FOR HEAVY METALS REMOVAL FROM CONTAMINATED WATER

Tutor

Prof. Maria Rosaria Boni

Ph.D. Student

Ing. Simone Marzeddu

Co-Tutor

Prof. Agostina Chiavola

Prof. Paolo Viotti

A.A. 2020/2021

"Try and leave this world a little better than you found it…"

Robert Baden-Powell

Summary

Figure index

Table index

Abstract

Several studies have recognized that biochar, obtained from pyrolysis of vegetable waste and by-product from agriculture and forestry, can be considered suitable for its adsorbent characteristics to remove different types of contaminants, both organic and inorganic, from soil and water. In fact, nowadays, due to its distinctive characteristics such as microporosity, high specific surface area, high adsorption capacity and ion exchange capacity, research is focusing on many other possible application of this promising material.

A further advantage is the fact that biochar can be considered a sustainable alternative to commercial adsorbents because, being a residual product, its use allows to avoid industrial production as well as to reduce the amount of waste to be disposed.

Furthermore, the scientific research, concerning the presence and the removal of pollutants from contaminated water, particularly persistent as heavy metals, is still evolving.

In this Ph.D. thesis, biochar will be investigated as a potential adsorbent media for heavy metals removal – in particular arsenic and lead – from contaminated water. Compared to commercial adsorbents biochar represents a new valid alternative from an economic and environmental point of view with good application prospects in many fields.

As a consequence, the interest in this material has grown enormously, due to its ability to improve the physical, chemical, biological and mechanical properties of the soil.

Biochar in Italy has been mainly used, until now, as a soil amendment in agriculture practices. Its capability in playing an adsorbent role can therefore be particularly interesting, focusing on its ability to remove heavy metals from contaminated water.

The research was mainly based on experimental activity, after an accurate bibliographic research and acquisition of the literature data, at a multidisciplinary level, in order to understand the emerging research fields of environmental engineering concerning biochar and its multiple use.

The first phase of experimental activity will be focused on the determination of the main physical-chemical characteristics of biochar, also carrying out a comparison with a commercial activated carbon.

In the successive phases batch and column tests will be used to investigate the performance of biochar, for arsenic and lead removal from aqueous solutions.

As regards the batch tests, the data, relating to experimental activities, will be interpreted through the most used models in the case of heavy metals adsorption from contaminated water, for the determination of kinetics and adsorption isotherms.

With regard to the experimentation in the column, breakthrough curves will be identified and the characteristic parameters of the system will be used to validate the obtained data.

Therefore, starting from the obtained experimental results, biochar may be considered as a useful alternative as adsorbent media for heavy metals removal from contaminated water.

Finally, some experimental hypotheses have been suggested in order to continue the research activity, with the aid of further targeted experimental tests.

Keywords: activated carbon; activated charcoal; adsorption kinetic; adsorption isotherm; arsenic; batch; biochar; breakthrough curve analysis; carbon-based sorbents; characterization; charcoal; circular economy; column; contaminated water; environmental processes; error analysis; lead; models; physical-chemical analysis; pyrolysis adsorption; remediation.

1 Introduction

In recent years, the traditional approach to the activities in the field of wastewater treatment and water purification, based primarily on the use of best remediation technologies at an affordable cost, is giving way to a new concept of sustainability, which involves, along with the economic environment, including environmental and social.

The new approach requires that the technologies used are evaluated and all the impacts to be given particular emphasis on those technologies that, from an environmental point of view, support the recovery and reuse of materials in the perspective of circular economy [1–4].

Agricultural and forestry activities produce a high amount of vegetable waste with a low economic value, the disposal of which has a significant cost. Often, moreover, the biomasses are intended for combustion even before they analyse the possibility of their possible reuse [5].

These wastes, after pyrolysis treatment, could be profitably used to produce biochar, not only for the consolidated and normed use as fertilizer of the soil, but also to remove the pollutants in the process of the contaminated water treatment [6–10].

Compared to commercial adsorbents [11–13] biochar represents a new valid alternative from an economic and environmental point of view with good application prospect in many fields [8,14].

The pyrolysis process is in fact be an excellent "*green*" alternative to the combustion being a technique not only carbon neutral but even carbon negative because it is able to sequester more carbon than it emits to produce energy [15–19].

Agriculture and forestry therefore offer a unique and valuable opportunity to reduce greenhouse gas emissions and to retract this waste in a sustainable supply chain of waste recycling, to be reutilized in a "*noble*" manner, before their final disposal [20–26].

As argued above, biochar is undoubtedly a reactive material that is the object of study in the most innovative research of the decade, as shown by the most recent scientific literature in the sector [27–34]. In fact, study results show that the use of biochar in the environmental field is exponentially increasing [35–40].

The multiple uses of biochar, identified in the different research fields under development, are listed below for explanatory purposes [4,16,33,41–45]:

1. Use of biochar in animal husbandry:
    - Feed additive and supplement;
    - Additive for litter;
    - Sewage treatment;
    - Manure fertilization;
    - Water treatment in fish farms.
2. Use as soil improver:
    - Fertilizer;
    - Compost;
    - Plant protection;
    - Vegetable supplement for trace elements.
3. Use in the construction sector:
    - Thermal insulation;
    - Air decontamination;
    - Humidity regulation;
    - Protection against electromagnetic radiation ("*electrosmog*").

4. Biogas production:
    - Biomass additive;
    - Biogas slurry treatment.
5. Wastewater treatment:
    - Activated carbon filter;
    - Pre-rinse additive;
    - Substrate of auxiliary soil support to be enhanced in artificially reproduced wetlands for phyto-purification assisted by macrophytes and phyto-extracting plants;
    - Composting services;
    - Treatment of sludge destined for reuse in agro-forestry.
6. Drinking water treatment:
    - Micro-filters;
    - Macro-filters in developing countries.
7. Other uses:
    - Exhaust filters (emission control, ambient air filters);
    - Industrial materials (carbon fibers, plastics);
    - Electronics (semiconductors, batteries);
    - Metallurgy (metal reduction);
    - Cosmetics (soaps, skin cream, additives for therapeutic baths);
    - Colours and dyes (food dyes, industrial paints);
    - Energy production (pellets, brown coal substitute);
    - Medicines (detoxification, active drug carrier ingredients);
    - Fabrics (additive fabric for functional underwear, thermal insulation for functional clothing).

Further to the above, biochar has been investigated as a renewable and low-cost precursor for activated carbon production, as it is cheaper than activated carbon.

The cost of biochar production is approximately also one-sixth of the commercially available activated carbon; in Italy the cost is indicated also per liter for its very low bulk density: on average is 10 € L^{-1}. Globally, the mean price for biochar was \$2.65 kg^{-1}, which was highly variable depending on the origin of biochar production sites and ranged from as low as \$0.09 kg^{-1} (Philippines) to \$8.85 kg^{-1} (UK) [8].

1.1 Heavy metals removal from contaminated water

Water is an invaluable asset and is often considered a renewable resource; but the amount of water available on the planet decreases every year [46,47]. It is essential for the devolvement of all types of life and sometimes part of them is disponible only as groundwater.

The water in the Earth's surface is irregularly distributed, 97% is in the oceans and 3% of is as freshwater [48]. The 69% of freshwater is in glaciers and ice caps in the Arctic and Antarctic circles, while the other 30% is groundwater [49,50] and less than 1% is surface water (lakes, rivers and swamps) and a small fraction (0.001%) is suspended in the air as vapours, clouds, etc [51].

Even though surface water is used extensively, groundwater is the major source of agricultural and drinking water in many countries where surface water is scarce [52,53]. For instance, in some arid climate countries as Denmark, Malta, Saudi Arabia, groundwater is the only water supply. Also, in many European countries (Austria, Belgium, Denmark, Hungary, Romania and Switzerland) groundwater use exceeds 70% of the total water consumption. Furthermore, cities like Budapest, Rome, among others, base their water supply almost completely on groundwater [54]. Groundwater is also the preferred source of drinking water in rural areas, particularly in developing countries, because no treatment is often required and the water source is often located near consumers [55].

Because of the wide and intensive use of water, it is necessary to monitor its quality in order to prevent water contamination. Among all contaminants in the water, heavy metals have been widely studied because they can be available for living organism [56,57]. Although organisms need some heavy metals in small concentrations, if concentrations are higher of their necessity, organisms life can be damaged [58].

Since many years, surface waters and aquifers have been contaminated by an increasing number of chemicals produced by human activities, as agricultural and industrial procedures: landfill leachate [59], sewage, leachate from mine tailings, seepage from industrial waste [56] and arbitrary waste disposal [60]. Many solutes introduced into the hydrological environment are reported as contaminants, whose concentrations reach levels that are considered harmful [61].

Nowadays, the scientific community defines the term "*heavy metals*" as a group of metals and metalloids with a higher density than water [62,63] and a toxic or poisonous effect at low concentrations for the human or the environment [64]. However, neither IUPAC or other institution have never defined the term "*heavy metals*" [65,66]. Thus, the term has suffered, along the time, of different changes by the scientific community. Examples of heavy metals include Arsenic (As), Cadmium (Cd), Chromium (Cr), Copper (Cu), Manganese (Mn) Lead (Pb), Nickel (Ni), Zinc (Zn).

The toxicity, mobility and reactivity of heavy metals depend on their oxidative states, which depends upon some conditions e.g. pH, ORP (mV), temperature, moisture, etc. [56,59]. Several previous studies reported that interaction of heavy metals to the microorganisms reduced the expression of several enzymes [67–69]. Furthermore, some heavy metals, at high concentrations, become toxic due to interaction with metal-sensitive enzymes, resulting in growth inhibition and death of organisms [63]. Another consequence is the bioaccumulation because heavy metals are not easily metabolized [67,70–73].

Currently, soils and groundwater contaminated by heavy metals have become a problem of international interest [74], because heavy metals represent an hazardous for the environment [48,75,76] and they can also reach the human food chain [77–79].

In order to avoid damage to the environment and to the public health, heavy metals need to be removed from contaminated water.

1.1.1 Arsenic (As) and Lead (Pb)

Arsenic (As) is the 12th most abundant element in the biosphere; it can be found into two different metalloids forms, respectively, crystalline metallic/grey or amorphous yellow [80]. Furthermore, it occurs as different species (inorganic and organic) in water [81,82].

Figure 1.1 – Arsenic.

Organic species, which are presented in minor concentration than inorganic ones, are Monomethylarsonous acid (MMA III), Dimethylarsinous acid (DMA III), Monomethylarsonic acid (MMA V), Dimethylarsinic acid acid (DMA V), Trimethylarsine (TMA III), Trimethylarsine oxide (TMAO V). These organic compounds are the result of various arsenic methyltransferases produced by several bacteria, fungi and mammals [67,82].

Among inorganic compounds, H_3AsO_3, $H_2AsO_3^-$ and $HAsO_3^{2-}$ for As(III) and H_3AsO_4, $H_2AsO_4^-$ and $HAsO_4^{2-}$ for As(V) are more common and toxic than organic species [81,83]. As inorganic in an aqueous environment can be in different oxidation states, that is (-3; 0; +3; +5); where 0 represents elemental arsenic, a very rare element; in water it is generally found in forms of arsenates, in conditions (As^{+5}); and arsenites, under reducing conditions (As^{+3}) [84,85]. Arsenite is more dangerous than arsenate, with serious effects that can be considered carcinogenic: long periods of exposure can lead to tumours of the skin or of internal organs such as liver, colon, brain [86].

Redox potential (Eh) and pH are the most important factors controlling arsenic speciation [87,88]. Under reducing conditions at pH less than 9.2, the uncharged arsenite species H_3AsO_3 will predominate. Under oxidizing conditions $H_2AsO_4^-$ is dominant at pH less than 6.9, whilst at higher pH, $HAsO_4^{2-}$ becomes dominant; $H_2AsO_3^-$ and H_3AsO_4 may be present, respectively, in extremely alkaline and acidic conditions.

Ingested elemental arsenic is poorly absorbed and eliminated unchanged in the human body [89], but ingestion of high levels of As compounds cause several human health effects. Numerous epidemiological studies informed a strong association between arsenic exposure and health effects [81,90,91]. Inorganic arsenic may accumulate in skin, bone, liver, kidney and muscle. Abdominal pain, diarrhoea, vomiting, muscular pain and weakness, with flushing of the skin are symptoms of an early intoxication [89].

However, the effects of a long-term ingestion of inorganic arsenic by humans are skin bladder, kidney lung, cancer skin lesions, developmental effects, cardiovascular disease, neurotoxicity and diabetes [67,92,93]. Furthermore, International Agency for Research on Cancer (IARC) classifies inorganic arsenic compounds in Group 1 (carcinogenic to humans) based on enough evidence for carcinogenicity in humans and limited evidence for carcinogenicity in animals [94].

Different technologies for arsenic removal from contaminated water are reported in literature as precipitation/dissolution, membrane processes, reverse osmosis, oxidation/reduction, ion exchange and

clotting processes [95–100]. Adsorption is the most widely used method; it does not require the addition of chemicals and does not produce dangerous by-products.

Lead is a shiny and bluish metal, it becomes dull grey in the air; it is quite soft, very malleable and ductile, the softest of the common heavy metals and is a poor conductor of electricity.

Figure 1.2 – Lead.

In nature it can be found in galena (PbS), one of the most common and abundant metallic minerals (mainly hydrothermal in nature), or in cerussite ($PbCO_3$), obtained by superficial alterations of galena. The crystal has a face-centered cubic structure.

Lead (Pb) is a heavy metal whose extensive use has caused environmental contamination (i.e. groundwater) and health problems.

Pb contaminated groundwater is due to volcanic activity, geochemical weathering and human activity. Anthropogenic contribution is done mainly because of mining, smelting, refining and informal recycling of lead; using of leaded petrol (gasoline); production of lead-acid batteries and paints, electronic waste, industrial wastewater contaminated with Pb [101].

Therefore lead is certainly one of the most persistent and toxic heavy metal which can be encountered in contaminated sites [102–105]; it is in 2nd place in the list of dangerous substances indicated by the ATSDR (Agency for Toxic Substances and Disease Registry) [106].

Pb absorption in the human body is 35 to 50% in adults and more than 50% in children [107]. Pb(II) enters the cells through the pathway of essential divalent metal transporters such as Fe^{++},Ca^{++},and Zn^{++} channels replacing Zn from proteins with Ca metabolism [67]. In the human body, Pb is taken into the kidney, liver , heart and brain [107]. Furthermore, acute and chronic Pb exposures are associated with hemolytic anemia, hypertension and cardiovascular and renal disease. In reproduction system, long-term Pb poisoning causes infertility in men [67,108]. Lead can be absorbed through respiration and nutrition, lead is not metabolized, but largely excreted, while the remaining 20% is distributed in the tissues.

Even if there are not enough studies respect of the carcinogenicity to humans of exposure to inorganic lead, but sufficient evidence in animals, the IARC classified inorganic lead as probably carcinogenic to humans (Group 2A) [109].

For all of this, there are several innovative technologies reported in literature studies finalized to remediation contaminated water [110–113] and contaminated soils [114–118]. Recently, numerous different materials have been investigated to adsorb heavy metals and specifically Pb from contaminated groundwater [119–121].

1.2 Biochar

A commonly used porous material is activated carbon, mainly containing carbon in the form of graphite micro-crystals, treated to obtain a porous structure with a large internal surface area [122–124].

Activated carbons are safe, processed, carbonaceous products, having a porous structure and a large internal surface area [125–128].

Activated carbon (AC) is one of the most used adsorbents for the removal of contaminants in the water due to its properties. AC is principally prepared from coal, coconut shells, lignite and wood, and activated by physical and chemical methods. Due to its high specific surface area, chemical stability, durability, high capacity of adsorption and not selective adsorption, AC has been widely used to remove heavy metals from contaminated water [129–131].

However, the regeneration cost of AC may limit its extensive use [83,132]. Therefore, it is important to develop low-cost adsorbents, like biochar, with high adsorption capacity for heavy metals removal from contaminated water.

The origin of the biochar is connected to the ancient Amerindian populations in the Amazon region, locally known as "*Terra Preta de Indio*", where the dark earth is formed through the use of techniques slash-and-char [133,134]. Research on the terrains of Terra Preta in the Amazon revealed the effects of biochar thanks to its beneficial effects on soil [135–137].

Biochar is a new scientific term: according to Lehmann and Joseph [134], it is defined as "*a carbon-rich product, which is formed when biomass such as wood, manure or leaves is heated in a closed container, in low air conditions or nothing*".

Shackley et al. [138] defined biochar as "*the porous carbonaceous solid produced by the thermochemical conversion of organic materials in an oxygen depleted atmosphere that has physicochemical properties suitable for safe and long-term storage of carbon in the environment*''.

Verheijen et al. [139] defined biochar as "*biomass which has been pyrolyzed in an environment in the absence of oxygen and which, when applied to the soil, is able to sequester carbon in a sustainable way and at the same time improve the characteristics of the soil, avoiding short-term and long-term adverse effects on the environment in general as well as for human and animal health*".

The International Biochar Initiative (IBI), in 2015, updated the definition of biochar as "*a solid material obtained from the thermochemical conversion of biomass in an oxygen-limited environment*" [140].

All these definitions are directly or indirectly related to the condition of biochar production and its application to the soil. In fact Lehmann and Joseph [134] have distinct from the operational point of view the biochar from coal. Mainly, the difference between these two terms resides in the end use of the material. Coal is a source of carbonized organic substance for the production of fuel and energy while the biochar can be applied for carbon sequestration and environmental management [42]. In general, the biochar is produced by carbonization or dry pyrolysis and/or gasification of feedstock, while coal is produced by a combustion; the two materials differ widely in chemical and physical properties [141].

Biochar obtained from by thermochemical decomposition, under controlled oxygen conditions, of biomasses or vegetable waste from agriculture and forestry can be used for a number of purposes, such as for soil improver [142–150] – also reducing contaminant leaching [151–156] –, as a low cost adsorbent [7,20,29,30,45,157–161], means for greenhouse emission reduction [8,19,162,163] etc..

Recently biochar is experiencing new attention because modern production methods, which also allow to diversify times and ways of the process and to use a wide variety of feedstocks. It is so allowed to obtain a huge variety of biochar that can be used in different fields.

1.2.1 Production techniques

Biochar is a co-product of thermochemical conversion of organic matter under conditions with low or near zero oxygen supply at temperatures usually between 300 and 1000 °C [164,165], generating by-products including syngas (e.g. carbon monoxide CO, hydrogen H_2, carbon dioxide CO_2 and methane CH_4) and liquids (tars and oils) [166–168].

Physical and chemical properties of biochar fundamentally depends on the technology used and on the production process parameters (temperature, residence time, heating rate and reactor type) [20,169–176].

Temperature plays a vital role in determining biochar quantity and quality [177]. The properties of biochar largely influenced by temperature are: ash, volatile matter, fixed carbon content, elemental composition, particle size, surface area, total pore volume and pore size distribution, heating value, pH, electrical conductivity and cation-exchange capacity.

Lignin, cellulose and hemicellulose, which constitute the feedstock, are thermally broken down during thermochemical process.

The systematic removal of the various elements (C, H, O) into gases and other volatile compounds consists in distinct molar ratios of O/C and H/C in biochar [178]. The molar ratio of O/C and H/C in the biochar is specifically associated with the aromaticity, biodegradability and polarity, which are highly favourable organic pollutant removal properties [179]. Biochar generated at higher temperatures has lower H/C and O/C ratios than biochar generated at lower temperatures, suggesting a rise in aromaticity and a decrease in polarity with increasing temperatures [168,180–183].

Another important factors is biochar pH, which rises with increasing process temperature due to the enrichment of ash content [178,184,185]. In biochar, the ash content typically indicates a growing tendency with increasing temperature. Ash comprises many inorganic elements from the initial biomass as well as impurities and usually contains silicate, carbonate, sulphate and phosphate species [186]. The inorganic composition of the ash is important during the thermochemical conversion process because it can lead to operational problems such as slag formation at higher temperatures, thus decreasing the productivity of the process.

In general, an increase in thermochemical conversion process temperature leads to a biochar with higher hydrophobicity, surface area, cation exchange capacity, aromatic carbon structure, alkalinity, nano-pore size, carbon content [169,187,188]. Nevertheless, if the temperature exceeded 700 °C, certain microporous structures on the biochar surface may be destroyed and, if the temperature exceeds 800 °C, the carbon skeleton structure of biochar may be unstable [189]. Biochar produced at higher temperatures (>500 °C) has a stronger presence of C–C bonds compared to C–O and C–H bonds [177]. All these properties, especially the surface area, are key parameters to evaluate the absorption by biochar, particularly for organic molecules. Indeed, the increase of the aromatic carbon structure could also enhance the resistivity to microbial decomposition [190].

On the other hand water-holding capacity, electrical conductivity, volatile matter content, functional groups containing O and N decrease with an increase in pyrolysis temperature [177,191–193].

The process temperature is the most important parameter which also affects the mass yield. However, the quantity of char produced may be increased also by enhance the residence time of thermochemical conversion process gases in the pore structure to stimulate secondary char formation [194,195]. Therefore, extending the contact time between the gas and the solid, for example with high pressure [195], slow heating rate [196] or long residence time [197], can be advantageous for biochar yield [198].

Biochar includes surfaces that are both positively and negatively charged [8,170]. Negative functional groups attract cations and lead to an increase in soil cation exchange capacity; in comparison, anion exchange capacity is also displayed by O-containing functional groups of biochar dependent on pH [178,199].

Table 1.4, in the next sub-chapter (related to feedstock), shows that lower temperature (< 500 °C) promotes partial carbonization and generates biochar with smaller pore size, lower surface area and higher O-containing functional groups [187,200,201], making biochar ideal for removal of inorganic contaminants thanks to increased ionic interactions by interaction with O-containing functional groups. In addition, biochar produced at relatively lower temperatures exhibits excellent activity in soil and have higher surface affinity for water because of the higher molar O=C ratio [190].

In general, technologies for biochar production comprise pyrolysis (slow, intermediate and fast), gasification, hydrothermal carbonization and torrefaction [202–204].

Among the mentioned biochar production systems, pyrolysis and gasification have the strongest economic viability and technological maturity [202,205], therefore are the prevailing technologies for the production of biochar. In addition, due to its moderate operating conditions and optimization of biochar yields, pyrolysis has gained further interest.

The final materials contain varying quantities of the relative quantity and content of liquid (bio-oil), solid (hydrochar, torrefied biomass or biochar) and gas (syngas, primarily consisting of CO and H_2), according to the reactor configuration and its operating parameters [206].

Table 1.1 summarizes the most important characteristics of the main biomass thermochemical conversion process for biochar production, the major products distribution and yield [16,20,213,165,170,207–212].

Table 1.1 – Characteristics of the main biomass thermochemical conversion processes.

Process	Temperature	Residence time	Heating rate	Yields		
				Biochar	Bio-oil	Syngas
	(°C)		(°C min^{-1})	(%)	(%)	(%)
Slow pyrolysis	300-700	hour-days	5-7	35	30	35
Intermediate pyrolysis	~500	10-20 s	Up to 100	20	50	30
Fast pyrolysis	500-1000	<2 s	300-800	12	75	13
Gasification	~750-900	10-20 s	-	10	5	85
Hydrothermal carbonization (HTC)	180-300	1-16 h	5-10	50-80	5-20	2-5
Torrefaction	~290	10-60 min	-	61-84	0	39-16

The characteristics of the biomass thermochemical conversion processes mentioned above will be discussed in detail in the following sub-paragraphs.

1.2.1.1 Pyrolysis

Pyrolysis is the most important current thermochemical biomass-conversion technologies. It consists in the thermal decomposition of biomass in the absence of oxygen or with limited oxygen supply and under the influence of heat, which transforms the solid organic matter into three different products: biochar, bio-oil and syngas [214–221]. In pyrolysis, biomass is decomposed at a temperature range of 300–1000 °C (generally < 700 °C) [222]. Bio-oil is typically used as a fuel or enhanced and refined for specialty chemicals [223]. Syngas, which mainly consists of CO, CO_2, CH_4 and H_2 [224], is usually combusted to provide heat for the pyrolysis reaction and to generate power. The yields and the quality of the final products depend on the operating conditions such as temperature, residence time, heating rate, pressures, reactor configuration and feedstock type [225,226]. In general, the proportion of the final products is relatively balanced. Although biomass chemical energy is stored in the biochar, the amount of energy emitted during pyrolysis may be higher than that of combustion. In comparison to combustion, in terms of carbon emissions, pyrolysis is more efficient and has a greater mitigation potential for carbon storage [177].

From a thermal point of view, the pyrolysis process can be divided into four phases [194]:

- **Drying** (~100 °C). The process starts with the drying of biomass, where the particle is further heated and release moisture, some loosely bound water and volatile matter.
- **Initial stage** (100-300 °C). The exothermic dehydration of the biomass occurs with the release of water and low molecular weight gases (e.g. CO and CO_2).
- **Intermediate stage** (> 200 °C). In this stage primary pyrolysis takes place and much of the vapor or precursor to bio-oil is produced. Large biomass particulate molecules are decomposed into char (primary char), condensable gases (vapours and liquid yield precursors) and non-condensable gases.
- **Final stage** (> 300 °C). In this final stage, the secondary cracking of volatiles and molecules polymerization into biochar and non-condensable gases takes place. Relatively large-molecular-weight condensable gases may crack if they remain in the biomass long enough, yielding extra biochar (called secondary biochar) and gases. The condensable gases, if extracted easily from the reaction site, condense outside as bio-oil in the downstream reactor.

Moderate temperatures, slower heating rates and longer residence times greatly favour the production of biochar, because cause the formation of heavy molecular weight compound. On the other hand, high temperatures and longer residence times increase biomass conversion to gas, while moderate temperatures, faster heating rates and short residence times are optimum for producing bio-oils [227]. For optimizing bio-oil yield that promotes biomass pyrolysis by restraining secondary cracking reactions, a temperature about 500 °C is preferable [228]. After all, the carbonaceous solid product is the main interest in biochar production. The evaporation of water and the release of volatile elements lead to an increase in comparative fixed carbon content of the solid. Polymerization of organic compounds in vapours and gases is assumed to contribute to secondary char formation and to an increase in solid yield [39].

There are different types of pyrolysis, based on temperature, heating rate, pressures and residence times: slow pyrolysis, intermediate pyrolysis and fast pyrolysis [27,229–231].

Slow pyrolysis is characterized by low heating rate (5-7 °C min^{-1}), long residence time (from hours to days) and temperatures around 300-700 °C [223,232–234]. The slow pyrolysis is designed to give a high yield of biochar, about 35% of the total. In this types of pyrolysis, relatively high biochar yields are favoured by biomasses with a high lignin and ash content, along with large particle size [235]. Technologies applied are generally agitated drum kilns, rotary kilns ,wagon reactor and paddle pyrolysis kiln [236].

Fast pyrolysis has a high heating rate (up to 100 °C min^{-1}), very short residence time (<2s) and a process temperature up to 500-100 °C [214,227,237,238]. The main goal is the production of bio-oil, about 75% of the dry matter of the feedstock [166,239], therefore this processing system also requires a small size of the feedstock particles and a moisture content below 10%, allowing the vapor to be quickly cooled from the hot solid to avoid cracking into light gases or polymerization into biochar [137]. The most used types of reactors are bubbling fluidized bed, circulating bed, rotating-cone and ablative reactors [236].

The other option is intermediate pyrolysis, which operates in between conditions of fast and slow. It is generally characterized by a heating rate up to 100 °C min-1, a short residence time (ranging from 10 to 20 s) and a temperature of about 500 °C. Biochar yield is around 20%.

1.2.1.2 Gasification

Gasification is a biomass thermochemical conversion process in which a gasification reaction occurs at high temperature (~750-900 °C) and under a controlled amount of oxidizing agent to produce, as already indicated by its name, a gaseous mixture (syngas) with small amounts of char and liquids [237,240,241].

In gasification processes, the biomass is partially oxidized in the gasification chamber [239] with a residence time of about 10-20 s, a moderate heating rate, at atmospheric or elevated pressure [211,242,243].

As the key product of gasification (about 85 wt%), syngas is a mixture of gases mainly consisting of CO, CO_2, CH_4 ,H_2 and N_2 which can be catalytically converted into liquid fuel, value-added chemicals (e.g. methanol), or directly used as a fuel for power generation and to provide heat for the process itself [244–246].

The typical biochar yield of gasification is about 10 wt% of biomass, with a higher degree of aromatization compared with pyrolytic carbonization and a high level of alkali and alkaline earth metals (Ca, K, Si, Mg, etc.) [202–204,247]. Emerging information and data on the commercialization and use of biochar shows that biochar will potentially increase the overall economic and environmental efficiency of a gasification device.

While pyrolysis is a thermochemical conversion process that doesn't involve the additional input of an oxidant and thus exposes the produced biochar to its own product gas, gasification requires a gasifying agent such as oxygen, air, steam or a mixture of these gases, which reacts with solid carbon and heavier hydrocarbons to turn them into low-molecular-weight gases like CO and H_2 [182,194].

The product compositions are affected by the gasification agent type, reaction temperature, particle size, residence time, pressure and gasification agent/biomass ratio [27]. Usually, the production of H_2, CO and carbon was enhanced and the contents of CO_2, CH_4, hydrocarbons and tar were reduced with the rise of temperatures [248].

A gasification process generally involves a sequence of four reaction stages: drying, pyrolysis, combustion and reduction [194,249–251]:

- **Drying**. In this stage, the moisture content of the biomass is decreased before being fed into the gasifier. Typically, the moisture content of biomass varies from 10 to 35%. The temperature is usually between 100 and 200 °C, which is not enough to thermally decompose the feedstock, with a reduction in the moisture content of the biomass of <10% [252,253].
- **Pyrolysis**. During this stage, biomass is decomposed, in the absence of oxygen, under increased temperatures (300-1000 C°). Pyrolysis consist in the thermal breakdown of larger hydrocarbon molecules into volatile matter and carbonaceous solid residue (biochar). The hydrocarbon gases can condense at a sufficiently low temperature to produce liquid tars.
- **Combustion**. This stage involves the complete or partial oxidation of carbonaceous materials and some pyrolysis gas species (CO, H2, CH4 and CnHm), generating H2O, CO2 and CO. This exothermic oxidation stage typically occurs in a temperature range from 700 to 1500 °C and provides heat to the endothermic drying process as well as pyrolysis and reduction reactions [254,255]. Under a high temperature from 900 to 1100 °C, some heavy molecules are broken down to lighter molecules and some of the tar is thermally cracked. During the subsequent reduction stage, the steam produced by combustion serves as the reactant of the water gas reaction and water gas shift reaction. The main reactions in this phase are the following:
  - ✓ *Carbon complete oxidation:*

$$C + O_2 \leftrightarrow CO_2 + 393{,}8\ \frac{kJ}{mol}$$

  - ✓ *Gas oxidation:*

$$H_2 + \frac{1}{2}O_2 \rightarrow H_2O + 242\ \frac{kJ}{mol}$$

$$CO + \frac{1}{2}O_2 \rightarrow CO_2 + 283\ \frac{kJ}{mol}$$

$$CH_4 + \frac{1}{2}O_2 \rightarrow CO + 2H_2 + 35{,}7\ \frac{kJ}{mol}$$

- Reduction. In this stage the biochar reacts with the gasifying agent to produce a mixture of combustible gases such as CO, CO2, H2, CH4. These reactions are mostly endothermic. Reduction takes place in the 800–1000 °C temperature range. Typical reduction reactions are:
  - ✓ *Water gas reaction:*

$$C + H_2O \rightarrow H_2 + CO - 131{,}4\ \frac{kJ}{mol}$$

✓ *Boudouard reaction:*

$$C + CO_2 \rightarrow 2CO - 172{,}6\ \frac{kJ}{mol}$$

✓ *Water gas shift reaction:*

$$CO + H_2O \leftrightarrow CO_2 + H_2 + 41{,}2\ \frac{kJ}{mol}$$

✓ *Methane reaction:*

$$C + 2H_2 \leftrightarrow CH_4 + 75\ \frac{kJ}{mol}$$

Although these steps are classified into separate stages, there is no clear boundary between them and there are often overlaps between the reactions of the stages.

Based on the sequencing of the above process, the major types of gasification systems are: fixed bed and fluidized bed [253].

The oldest and most modern reactors used to synthesize syngas are fixed-bed gasifiers [253], generally consisting of a cylindrical space for fuel and gasifying agent with a fuel supply unit, an ash-removal unit and a gas exit [251]. In this type of system, the four gasification steps correspond to four stratified temperature zones [249]. Depending upon the direction and entry of airflow, the fixed-bed gasifiers are classified as updraft, downdraft, or cross-draft [256]. In an updraft gasifier, the biomass is supplied from top of the gasifier, while air is fed from the bottom of the gasifier. The reduction zone is located above the combustion region [257]. In a downdraft fixed bed gasifier, the gas is fed above the reduction zone and flows in the same direction as the descending feedstocks towards the bottom of reactor. The reduction region is placed below the combustion region [249]. In the cross-draft gasifiers the gasifying agent and gas are fed from one side of the reactor and emitted from the other side on the same horizontal level [251]. In fluidized bed gasifiers the gasifying agent is blown through a solid particles bed at a sufficient velocity to keep the particles in a suspended state. Fuel particles are introduced at the bottom of the reactor, mixed very quickly with the bed material and almost instantaneously heated to the bed temperature [251].

Fluidized beds are emerging as the best gasifiers due to their versatility in terms of type of fuel and high efficiency. One of the main characteristics is the uniform temperature distribution in the reduction zone. This temperature uniformity is obtained using a bed of fine granular material (e.g. sand) into which air is circulated. There are two major types of fluidized-bed gasifiers in current use: circulating fluidized bed and bubbling bed [257]. Circulating fluidized-bed gasifier relies on the continuous circulation mechanism of the bed material between the reaction vessel and a cyclone separator, where the ash is separated and the bed material and char return to the reaction vessel [253]. In a bubbling-bed gasifier, the air is pumped from the bottom of the reactor into the grid. The fine bed material is located above the grid into which the feedstock is introduced [253].

Compared to fluidized bed, fixed bed gasifiers have weaker heat transfer and mixing of gases and solids, resulting in an irregular radial temperature distribution and multiple problems such as slagging, bridging and clinkering in the gasifiers [249].

1.2.1.3 Hydrothermal carbonization

Hydrothermal carbonization (HTC) is a cost-effective system to produce biochar, also called hydrochar, carried out at low temperatures of 180-300 °C, under high pressure in water for several hours (1-16 h) [208]. Libra et al. (2011) define hydrothermal carbonization as "*wet pyrolysis*", since no oxygen is supplied to the reactor with the biomass-water suspension [208]. Different from pyrolysis and gasification processes, that are commonly used for the biomass with low moisture content, HTC is more suitable for processing biomass with high moisture content [258,259]. Hydrochar yield is very high assuming values between 50-80% of the dry matter of the feedstock [212,260–262].

Hydrochar results very different compared to the chars created in a gaseous environment [171,263]. Reaction temperature, pressure, residence time and water-to-biomass ratio are the principal parameters that determine the characteristics of the products [208,264]. It is mostly composed of alkane structures that have low stability [39,203,204]. The surface of biochar shows a greater degree of aromatization with larger number of groups containing oxygen [265]. The presence of these groups on the surface of biochar is useful for affinity with water and therefore it can be used to improve water retention capacity of soil [266].

Krysanova et al. (2019) found that hydrochar obtained from peat has a larger specific surface in contrast with the initial peat and a higher exothermic effect during decomposition and has a more dispersed structure [267].

Liu et al. (2013) studied the production of hydrochar from coconut fiber and dead eucalyptus leaves and their analysis revealed that carbon content, fixed carbon content and energy density of hydrochar increased with rising temperature [268].

1.2.1.4 Torrefaction

Torrefaction is a thermochemical process in an inert or limited oxygen environment where biomass is slowly heated in the temperature range between 200 and 300 °C, with a residence time of about 10-60 min [213]. The major objectives are to improve the specific energy density with higher calorific value and heating values in the solid by increasing carbon content, decreasing oxygen and hydrogen content, decomposing hemicellulose and considerably enhance physical properties of the biomass (such as grindability and pelletability) [39,194,247]. These characteristics raise the commercial value of biomass (i.e. wood) for energy production and transportation [194,269].

Torrefaction in general generates biochar with a yield of about 70%, which retains 90% of the starting energy content, while the remaining mass is converted into condensable (water, organics and lipids) and non-condensable gases (CO_2, CO and CH_4) [213]. Common biomass reactions during torrefaction include devolatilization and carbonization of hemicelluloses, depolymerization and devolatilization of lignin and cellulose [213].

In conclusion, torrefaction can be considered as a more promising solution for clean energy production compared with fossil energy.

1.2.2 Feedstocks

Apart from the process conditions, the physicochemical properties and the yield of biochar can vary widely depending on the characteristics of the feedstock [20,156]. It was previously mentioned that biochar is the carbon-rich product of biomass produced by thermal decomposition of organic materials, under limited supply of oxygen, therefore before proceeding it is appropriate to clarify what is meant by biomass.

The term biomass refers to non-fossilized and biodegradable organic matter originating from plants, animals and microorganisms derived from biological sources [270]. A more detailed definition was given by Demirbas (2008), according to which the term biomass refers to wood, short-rotation woody crops, agricultural wastes, short-rotation herbaceous species, wood wastes, bagasse, industrial residues, waste paper, municipal solid waste, sawdust, biosolids, grass, waste from food processing, aquatic plants and algae animal wastes and a range of other materials [271]. Researchers characterize the various types of biomass in different ways, but a simple method is to define four main types [272]:

- woody plants;
- herbaceous plants/grasses;
- aquatic plants;
- manures.

Hemicellulose, cellulose and lignin are the main components, in different percentage, of the feedstock organic matter [273]. The composition and proportion of the various constituents differ depending on the type of biomass [274–277]. Some examples of their typical relative composition are shown in Table 1.2 [225,270].

Table 1.2 – Structural composition of some plant materials (wt% of dry and ash free sample).

Plant material	Cellulose (%)	Hemicelluloses (%)	Lignin (%)	Others (%)
Hardwood	43 – 48	27 – 35	16 – 24	2 – 8
Softwood	40–44	24 – 29	26–33	1–5
Orchard grass (medium maturity)	32	40	4.7	23.3
Rice straw	34	27.2	14.2	24.6
Birchwood	40	25.7	15.7	18.6

Cellulose is a glucose polymer with an unbranched structure and a high molecular-weight (106 or more) [272]. It is thermally more stable, decomposing at temperatures between 315 and 400 °C to produce anhydrocellulose and levoglucosan [278].

Hemicellulose is a mixture of various polymerized monosaccharides (i.e. glucose, mannose, galactose, xylose etc.) with a branched chain-structure and a lower molecular weights than cellulose. It is the most reactive of the three main components and it decomposes at temperatures of about 220–315 °C [278], giving rise to more volatiles, less tars and less chars than cellulose [225].

Lignin is an amorphous cross-linked resin with a complex three-dimensional structure and chemically related compounds of high molecular-weight, [272]. Due to the large number of functional groups with different thermal stabilities, the decomposition does not occur in a limited temperature range such as for hemicellulose and cellulose.

Thermal degradation begins at 200 °C and may require temperatures as high as 900 °C to be completed (depending on the residence time) [278].

As mentioned above, the quantity of the product that can be obtained from the biomass pyrolysis depends on the conditions of the process, including temperature and residence time. In addition, because of their different thermal stability, the cellulose, hemicellulose and lignin composition, as well as the alkaline and alkali earth-metal content, affects the required treatment temperature and obviously the mass yield. Cellulose

and hemicellulose contribute more to the yield of the volatile products, while lignin contributes mainly for the biochar yield [279,280].

Biomass with higher lignin content was reported to produce a higher biochar yield because lignin preferably forms char during pyrolysis [235,281]. In general, higher biochar yield can be obtained from feedstock with higher ash contents, although with an ash content >5% the effect is less noticeable [281].

Based on current knowledge on the biochar properties of different feedstocks, it is clear that the C content and compositions of wood biochar were comparatively higher than those of agricultural residues and other feedstocks biochars derived, which is attributable to the higher abundance of recalcitrant carbon and lignin in wood biomass that already has an aromatic alcohol polymer component [282].

Moreover, due to the high volume of aromatic C compound, cellulose and hemicellulose become abundantly hydrophobic, displaying recalcitrance and resistance to microbial decomposition and carbon-sequestration ability, demonstrating increased adsorption capabilities due to alkaline pH and high surface area [283].

Owing to their distinct sources, waste biomasses such as animal manure and sewage sludge contain no notable concentrations of these three components and thus need to be defined differently. Since they contain more nutrients itself, such as N, P, Ca, Mg and K, the biochar produced will also have a high nutrient content [284–290], having better effects on soil quality improvement [190].

The higher amounts of N and P and other micronutrients and macronutrients in sewage sludge biochar are also the key reasons for the usage of wastewater sludge in biochar production and agricultural utilization [291]. Biochar derived from woody biomass and crop residues usually has a higher surface area compared to biochar derived from solid urban waste or animal manure biochar, both of which generated at the same pyrolysis temperature [20].

Previous researches have carried on in-depth studies about the impact of the type of feedstock and conversion technologies used on biochar properties including various types of wood [215,274,292–294], corn cob and corn stalk [295–297], wheat residues [298], rice husk [299,300], sugar beet tailing [301], sawdust [302], sewage sludge [284,303,304], chicken manure [305] and ipomoea fistulosa [306], observing that the composition of the feedstock is a decisive factor in determining the differences in the elemental composition and functionalities of the biochars, which in consequence has an impact on the performance of the various biochars and therefore on its application.

Ronsse et al. (2013) studied yield and physicochemical characteristics of biochar produced by fixed-bed slow pyrolysis under a range of process conditions from pine wood, wheat straw, green waste and dried algae [175]. Of the various feedstocks tested, the highest biochar yield was obtained using straws at the highest treatment temperature of 300 °C with a residence time of 10 minutes, reaching 98.4 wt% (biochar on dry and ash-free basis).

Table 1.3 shown average biochar pH, calcium carbonate equivalent (CCE), surface area and cation exchange capacity (CEC) based on various feedstock sources [222].

Table 1.3 – pH, CCE, CEC and surface area with various types of feedstock.

Source	pH (-)	CCE (%)	Surface Area ($m^2\ g^{-1}$)	CEC ($mmol\ kg^{-1}$)
Corn	9.27	---	107.2	607.0
Wheat/barley	8.80	---	26.65	103.0
Rice straw/husk	9.17	---	42.15	212.0
Soybean stover	9.30	---	4.375	---
Peanut shell	8.52	---	115.1	---

Source	pH (-)	CCE (%)	Surface Area (m^2 g^{-1})	CEC (mmol kg^{-1})
Pecan shell	6.97	---	111.5	---
Hazelnut shell	7.86	---	467.5	83.8
Switchgrass	9.28	---	52.96	---
Bagasse	7.59	---	113.6	115.0
Coconut coir	---	---	114.8	---
Food waste	9.09	---	0.803	81.0
Other (grass, leaves, orange peel, other green wastes)	8.72	---	119.8	290.0
Hardwoods	7.94	---	171.3	138.0
Softwoods	7.48	---	194.2	145.0
Papermill waste	9.13	---	10.08	52.0
Poultry manure/litter	9.80	18.4	50.35	538.0
Turkey manure/litter	8.95	---	24.70	---
Swine manure	9.37	---	26.89	---
Dairy manure	9.45	---	33.38	342.0
Cattle manure	8.99	13.4	73.27	---
Biosolids/sewage sludge	6.90	12.9	102.1	23.6

In contrast with terrestrial biomass, this could be due to a different composition in terms of extractives and cell wall materials. Furthermore, algae had the high ash content (38.4 wt%). When comparing the different biomass feedstocks also pH variations may be observed: the biochar derived from wood had an average pH in solution that is typically 2 pH units lower than the values for the three other feedstocks produced under comparable conditions of pyrolysis.

Woody biochar gave the highest BET surface area, exceeding the value of 100 m^2 g^{-1} under three process conditions, while the other raw materials have never exceeded the value of 46 m^2 g^{-1}. Also, wood had the lowest ash content of all feedstocks used (0.2, 7.9, 3.5 and 38.4 wt% for wood, straw, green waste and algae, respectively). From these findings, the greater quantity of inorganic substances in the biomass feedstock, such as ash content, is negatively associated with the specific surface area of the biochar produced.

Generally, compared to the widely-used biochar feedstock, algae tend to be relatively low in carbon but often high in N, P and other nutrients [307,308]. Necessarily, these biochar feedstocks could be an appealing choice for carbon sequestration and soil amelioration.

Srinivasan et al. (2015) analysed the biochar properties derived from pyrolysis of six biomass wastes including pine sawdust, paunch grass, broiler litter, dewatered pond sludge, dissolved air-floatation sludge and sewage sludge [309]. Among all, due to biochar's high specific surface area (795 m^2 g^{-1}), aromaticity and carbon content (90.9 %), biochar derived from pine sawdust has the highest potential for carbon sequestration and contaminant remediation, for example as a cheap landfill filter medium to mitigate the movement of contaminants or for the creation of storm-water filter media.

In addition, considering its low ash content (1.01 %), pine sawdust biochar may also theoretically be used as a filler in wood plastic bio composites.

Wang et al. (2014) assessed the characterization and utilization of biochars derived from rice husk and elm sawdust using fast pyrolysis and the results showed that rice husk biochar exhibited higher ash content,

lower volatile and fixed carbon content, larger surface areas (78.15 $m^2 g^{-1}$) than elm sawdust biochar [310]. Rice husk biochar contained more function groups and a new functional group (C-H deformation vibration, aromatic hydrocarbons) was generated in rice husk biochar, which made it more stable.

Compared to elm sawdust biochar, incorporation of the rice husk biochar significantly improved the quality of acid soil properties, increasing total C, nitrogen, pH, extractable Ca, Mg, K, Na contents and decreasing the Al and Pb contents.

An overview of the main characteristics of biochars produced by pyrolysis from several feedstocks is provided in Table 1.4.

Table 1.4 – Overview of the characteristics of biochars produced from several feedstocks.

Biomass feedstocks	Apple branch	Dairy manure	Dairy manure	Dairy manure
Reactor type	Furnace	Furnace with gas tight retort	Furnace with gas tight retort	Muffle furnace
Reactor temperature (°C)	400-800	350	700	100-500
Residence time (h)	10.0	2.0	2.0	4.0
Heating rate (°C min^{-1})	10.0	2.5	8.3	25.0
Biochar size (mm)	0.5	-	-	<1
Yield (%)	11.9-545.4	1.6	186.5	< 2-13
BET Surface area ($m^2 g^{-1}$)	-			-
Micropore volume ($cm^3 g^{-1}$)	7.0-10	9.2	9.9	-
pH	28.3-15.5	54.9	35.0	>90-15-25
Mobile matter (%)	32.4-6.8	53.5	27.7	-
Fixed matter (%)	-	23.2	34.7	-
N (%)	0.8-0.3	2.6	1.5	3.1-0.0
O (%)	20.6-5.8	18.7	4.1	-
H (%)	4.1-0.6	4.3	0.9	-
C (%)	70.2-84.8	55.8	56.7	36.8-1.7
Specific weight (mg kg^{-1})	-			0.91-2.66 a
Ash content (wt%)	-	24.2	39.5	35-40-80-90
References	[283]	[290]	[290]	[287]

Biomass feedstocks	Goat manure	Human manure	Miscanthus sacchari-florus	Orange peel	Orange peel	Orange peel
Reactor type	Vertically fixed-bed reactor	Tube furnace	Lab scale SS reactor in furnace	Furnace	Furnace	Furnace
Reactor temperature (°C)	400-800	300-700	300-600	400-700	150-600	700
Residence time (h)	0.5	0.7	1.0	2.0	6.0	6.0
Heating rate (°C min^{-1})	−263.2	15.0	10.0	-	-	-
Biochar size (mm)	-	-	-	2.0	0.2	0.2
Yield (%)	3.3-93.5	-	0.6-381.5	428.0-110.2	7.8-51	201.0
BET Surface area (m^2 g^{-1})	0.0	-	-	-	-	-
Micropore volume (cm^3 g^{-1})	-	7.3-11.1	8.3-10.1	11.6-12.3	-	-
pH	44.5-33.8	51.9-30.6	53.8-88.6	-	82.4-61.6	22.2
Mobile matter (%)	-	60.5-6.3	75.8-1.5	-	-	-
Fixed matter (%)	-	13.2-31.2	53.8-88.6	-	-	-
N (%)	2.1-1.1	4.8-2.4	0.3-0.4	2.0-1.7	1.8-2.4	1.7
O (%)	30.1-21.7	44.4-58.3	25.7-6.7	19.8-13.4	41.0-14.4	22.2
H (%)	1.7-0.8	6.7-1.8	5.5-2.3	4.8-1.6	6.2-2.0	1.8
C (%)	42.7-43.6	42.9-36.4	68.5-90.7	68.4-74.8	50.6-77.8	71.6
Specific weight (mg kg^{-1})	3.8-5.0. a	5.4-8.1. a	-	-	-	-
Ash content (wt%)	-	26.6-62.5	2.2-2.7	5.0-8.5	0.5-4.3	2.8
References	[311]	[220]	[312]	[313]	[314]	[314]

Biomass feedstocks	Peanut shells	Peanut shells	Pine needle	Pine needle	Pine needle litters	Pine needle litters
Reactor type	Muffle furnace	Muffle furnace	Muffle furnace	Muffle furnace	Furnace	Furnace
Reactor temperature (°C)	300	700	300-500	700	100-300	400-700
Residence time (h)	3.0	3.0	3.0	3.0	6.0	6.0
Heating rate (°C min^{-1})	7.0	7.0	7.0	7.0	-	-
Biochar size (mm)	1.0	1.0	1.0	1.0	0.2	0.2
Yield (%)	3.1	448.2	4.1-13.1	390.5	0.7-19.9	112.4-490.8
BET Surface area (m^2 g^{-1})	-	0.2	-	0.1	-	0.0-0.2
Micropore volume (cm^3 g^{-1})	7.8	10.6	-	-	-	-
pH	36.9	21.9	57.6-31.8	25.0	91.2-48.6	30.0-14
Mobile matter (%)	-	-	38.6-15.8	6.2	-	-
Fixed matter (%)	-	-	54.2-72.4	75.0	-	-
N (%)	1.9	1.1	3.9-4.1	3.6	0.7-1.1	1.2-1.1
O (%)	25.9	13.3	7.6-3.7	2.1	42.3-25.7	18.0-11.1
H (%)	3.9	1.8	4.4-2.1	0.6	6.2-4.3	3.0-1.3
C (%)	68.3	83.8	84.2-90.1	93.7	50.9-68.9	77.9-86.5
Specific weight (mg kg^{-1})	-	-	-	-	-	-
Ash content (wt%)	1.2	8.9	7.2-11.8	18.7	0.9-1.9	2.8-2.2
References	[167]	[167]	[315]	[315]	[316]	[316]

Biomass feedstocks	Pine pitch	Pine wood shavings	Pine wood shavings	Poultry litter	Poultry litter	Poultry litter (Pelletized)
Reactor type	Fluidized bed reactor	Muffle furnace	Muffle furnace	Furnace with gas tight retort	Furnace with gas tight retort	Lindberg box programmable furnace equipped
Reactor temperature (°C)	300-400	150-250	350-700	350	700	350
Residence time (h)	2s	6.0	6.0	2.0	2.0	-
Heating rate (°C min^{-1})	-	5.0	5.0	2.5	8.3	-
Biochar size (mm)	0.4	0.2	0.2	-	-	0.3
Yield (%)	2.9-4.8	1.8-5.9	166.0- 637	3.9	50.9	1.1
BET Surface area (m^2 g^{-1})	-	0.0	0.0	-	-	-
Micropore volume (cm^3 g^{-1})	-	-	-	8.7	10.3	8.7
pH	60.7-33.5	88.9-64.7	32.6-15.3	54.3	36.7	72.0
Mobile matter (%)	-	-	-	19.0	14.8	36.7
Fixed matter (%)	-	-	-	42.3	18.3	-
N (%)	0.3-0.4	0.3	0.4-0.0	4.5	2.1	4.9
O (%)	30.4-25.5	43.6-36.3	29.8-9.4	15.6	10.5	8.6
H (%)	5.4-3.4	6.2-4.3	2.6-1.0	3.8	2.0	3.7
C (%)	63.9-70.7	49.2-57.7	65.4-84.9	51.1	45.9	46.1
Specific weight (mg kg^{-1})	-	-	-	-	-	2.94. a
Ash content (wt%)	4.5-7.9	1.0-1.7	2.3-4.7	30.7	46.2	35.9
References	[317]	[318]	[318]	[290]	[290]	[319]

Biomass feedstocks	Poultry litter (Pelletized)	Rubber wood sawdust	Sludge	Sow manure	Sow manure	Soybean stover	Soybean stover
Reactor type	Lindberg box programmable furnace equipped	Fixed bed reactor (stainless steel)	Fixed bed horizontal tubular reactor	Muffle furnace	Muffle furnace	Muffle furnace	Muffle furnace
Reactor temperature (°C)	700	450-850	300-700	300	500	300	700
Residence time (h)	-	1.0	-	2.0	2.0	3.0	3.0
Heating rate (°C min^{-1})	-	-	10.0	26.0	26.0	7.0	7.0
Biochar size (mm)	0.3	2-3		< 0.154	< 0.154	1.0	1.0
Yield (%)	9.0	-	-	3.8	12.7	5.6	420.3
BET Surface area (m^2 g^{-1})	-	-	-			-	0.2
Micropore volume (cm^3 g^{-1})	10.3	-	5.3-12.0	8.9	10.3	7.3	11.3
pH	44.0	41.9-28.9	72.3-52.4	60.0	46.0	37.0	21.6
Mobile matter (%)	14.1	-	33.8-15.8			46.3	14.7
Fixed matter (%)	-	-	9.1-6.8			38.8	67.7
N (%)	2.8	0.4-0.0	3.3-1.2	2.9	1.8	1.9	1.3
O (%)	< 0.01	14.0-0.5	8.3-0.0	11.7	3.1	25.0	15.5
H (%)	0.3	3.2-1.1	2.6-0.5	3.2	1.3	4.3	1.3
C (%)	44.0	82.3-93.4	25.6-20.2	38.4	34.2	68.8	82.0
Specific weight (mg kg^{-1})	4.28. a	-	-	7931.0	8501.0	-	-
Ash content (wt%)	52.4	14.5-20	52.8-72.5	43.9	59.6	10.4	17.2
References	[319]	[320]	[291]	[321]	[321]	[167]	[167]

Biomass feedstocks	Swine solid	Swine solid	Turkey litter	Turkey litter	Weaner manure	Weaner manure
Reactor type	Furnace with gas tight retort	Furnace with gas tight retort	Furnace with gas tight retort	Furnace with gas tight retort	Muffle furnace	Muffle furnace
Reactor temperature (°C)	350	700	350	700	300	500
Residence time (h)	2.0	2.0	2.0	2.0	2.0	2.0
Heating rate (°C min^{-1})	2.5	8.3	2.5	8.3	26.0	26.0
Biochar size (mm)	-	-	-	-	< 0.154	< 0.154
Yield (%)	0.9	4.1	2.6	66.7	3.8	13.0
BET Surface area (m^2 g^{-1})	-	-	-	-	-	-
Micropore volume (cm^3 g^{-1})	-	-	-	-	-	-
pH	62.3	36.4	58.1	39.9	59.5	43.0
Mobile matter (%)	49.8	13.4	42.1	20.8		
Fixed matter (%)	17.7	33.8	23.1	29.2		
N (%)	3.5	2.6	4.1	1.9	2.7	1.9
O (%)	11.1	4.0	15.4	5.8	10.4	4.3
H (%)	4.9	0.7	3.6	0.9	2.9	1.2
C (%)	51.5	44.1	49.3	44.8	38.7	34.1
Specific weight (mg kg^{-1})	-	-	-	-	8108.0	8801.0
Ash content (wt%)	32.5	52.9	34.8	49.9	45.4	58.5
References	[290]	[290]	[290]	[290]	[321]	[321]

1.2.3 Biochar certifications

When considering environmental and health safety, two main initiatives, the International Biochar Initiative (IBI) and the European Biochar Certificate (EBC), have defined biochar production criteria and properties and limits on hazardous pollutants. Those guidelines provide safety and quality criteria, aiming to prevent the cutting down of native forests to produce biochar, to except production processes with high pollutant emissions and to prevent biochar with high quantities of toxic elements from entering the food chain. In Italy, the use of biochar is regulated by a Ministerial Decree of 2015, which indicates the characteristics that biochar must possess in order to be marketed and used as a soil improver.

1.2.3.1 International biochar certificate

The International Bio-char Initiative (IBI) (www.biochar-international.org) released on November 2015 the "*Standardized product definition and product testing guidelines for biochar that is used in soil*" [140]. The purpose was to provide a uniform definition of biochar and standardized testing and measurement methods to identify certain biochar qualities and characteristics related to the use of biochar as a soil improver.

Figure 1.3 – IBI figurative mark [www.biochar-international.org].

The IBI Standards refer only to the physicochemical properties of biochar and not to production methods or feedstocks.

There are three categories of tests for biochar materials, that are necessary for biochar to be sold on market:

- Test Category A "*Basic Utility Properties*", refers to the most basic properties of biochar (Table 1.5);
- Test Category B "*Toxicant Assessment*", measures maximum allowable threshold of many toxic compound (Table 1.6);
- Test Category C "*Advanced Analysis and Soil Enhancement Properties*", consists of additional tests and evidence of soil enhancement properties (Table 1.7).

The first two categories are required for all biochars, while the third is optional.

Table 1.5 – Test Category A: Basic Utility Properties.

Parameter	Criteria	Unit	Test Method
Moisture	Declaration	% of total mass, dry basis	ASTM D1762-84 Standard Test Method for Chemical Analysis of Wood Charcoal (specify measurement date with respect to time from production)
Organic Carbon (Corg)	10% Minimum Class 1: ≥60% Class 2: ≥30% and <60% Class 3: ≥10% and <30%	% of total mass, dry basis	Total C and H analysis by dry combustion-elemental analyzer. Inorganic C analysis by determination of CO2-C content with 1N HCl, as outlined in ASTM D4373 Standard Test Method for Rapid Determination of Carbonate Content of Soils. Organic C calculated as Total C – Inorganic C.
H:Corg	0.7 Maximum	Molar ratio	
Total Ash	Declaration	% of total mass, dry basis	ASTM D1762-84 Standard Test Method for Chemical Analysis of Wood Charcoal
Total Nitrogen	Declaration	% of total mass, dry basis	Dry combustion-elemental analyzer following the same procedure for total C and H above.

Parameter	Criteria	Unit	Test Method
pH	Declaration	pH	pH analysis procedures as outlined in section 04.11 of TMECC (2001) using modified dilution of 1:20 biochar:deionized H2O (w:v) and equilibration at 90 minutes on the shaker, according to Rajkovich et al. (2011) [322].
Electrical Conductivity	Declaration	dS/m	EC analysis procedures as outlined in section 04.10 of TMECC (2001) using modified dilution of 1:20 biochar:deionized H2O (w:v) and equilibration at 90 minutes on the shaker, according to Rajkovich et al. (2011) [322].
Liming (if pH is above 7)	Declaration	% CaCO3	AOAC 955.01 potentiometric titration on "as received" (i.e., wet) samples. Use dry weight to calculate % CaCO3 and report "per dry sample weight".
Particle size distribution	Declaration	% <0.5 mm; % 0.5-1 mm; % 1-2 mm; % 2-4 mm; % 4-8 mm; % 8-16 mm; % 16-25 mm; % 25-50 mm; % >50 mm	Progressive dry sieving with 50 mm, 25 mm, 16 mm, 8mm, 4mm, 2 mm, 1 mm and 0.5 mm sieves.

Table 1.6 – Test Category B: Toxicant Assessment.

Parameter	Range of Maximum Allowed Thresholds		Test Method
Germination Inhibition Assay	Pass/Fail		OECD methodology (1984) using three test species, as described by Van Zwieten et al. (2010) [323].
Polycyclic Aromatic Hydrocarbons (PAHs), total (sum of 16 US EPA PAHs)	6 – 300	mg/kg dry wt	US EPA 8270 (2007) using Soxhlet extraction (US EPA 3540) and 100% toluene as the extracting solvent
Dioxins/Furans (PCDD/Fs)	17	ng/kg WHO-TEQ dry wt	US EPA 8290 (2007)
Polychlorinated Biphenyls (PCBs)	0.2 – 1	mg/kg dry wt	US EPA 8082 (2007) or US EPA 8275 (1996)
Arsenic	13 – 100	mg/kg dry wt	TMECC (2001)
Cadmium	1.4 – 39	mg/kg dry wt	TMECC (2001)
Chromium	93 – 1200	mg/kg dry wt	TMECC (2001)
Cobalt	34 – 100	mg/kg dry wt	TMECC (2001)
Copper	143 – 6000	mg/kg dry wt	TMECC (2001)
Lead	121 – 300	mg/kg dry wt	TMECC (2001)
Mercury	1 – 17	mg/kg dry wt	US EPA 7471 (2007)
Molybdenum	5 – 75	mg/kg dry wt	TMECC (2001)

Parameter	Range of Maximum Allowed Thresholds		Test Method
Nickel	47 – 420	mg/kg dry wt	TMECC (2001)
Selenium	2 – 200	mg/kg dry wt	TMECC (2001)
Zinc	416 – 7400	mg/kg dry wt	TMECC (2001)
Boron	Declaration	mg/kg dry wt	TMECC (2001)
Chlorine	Declaration	mg/kg dry wt	TMECC (2001)
Sodium	Declaration	mg/kg dry wt	TMECC (2001)

Table 1.7 – Test Category C: Advanced analysis and soil enhancement properties.

Parameter	Criteria	Unit	Test Method
Mineral (available) Nitrogen (ammonium and nitrate)	Declaration	mg kg^{-1}	2M KCl extraction followed by spectrophotometry (Rayment and Higginson 1992)
Total Phosphorus & Potassium*	Declaration	mg kg^{-1}	Modified dry ashing (Enders and Lehmann 2012). Elements in the digest determined by common analytical techniques.
Available Phosphorous	Declaration	mg kg^{-1}	2% formic acid followed by spectrophotometry [324].
Total Calcium, Magnesium and Sulfur	Declaration	mg kg^{-1}	Modified dry ashing (Enders and Lehmann 2012). Elements in the digest determined by common analytical techniques.
Available Calcium, Magnesium and Sulfate-S	Declaration	mg kg^{-1}	1M HCl extraction [222]. Elements in the digest determined by common analytical techniques.
Volatile Matter	Declaration	% of total mass, dry basis	ASTM D1762-84 Standard Test Method for Chemical Analysis of Wood Charcoal
Total Surface Area	Declaration	$m^2 g^{-1}$	ASTM D6556 Standard Test Method for Carbon Black – Total and External Surface Area by Nitrogen Adsorption.
External Surface Area	Declaration	$m^2 g^{-1}$	

* Total K is sufficiently equivalent to available K for the purpose of this characterization

1.2.3.2 European biochar certificate

The European Biochar Certificate (EBC) (www.european-biochar.org) is a project that dates back to 2012 of the non-profit European Biochar Foundation. Similarly to the IBI, the EBC provide assurances around biochar safety and efficacy for its applications.

Figure 1.4 –EBC figurative mark [www.european-biochar.org].

Further than the IBI Standards, EBC addresses sustainability and environmental impacts of feedstock procurement and biochar production technology. According to the EBC guidelines, biochars are divided into four different application classes, each with different threshold values and ecological requirements: EBC-Feed, EBC-AgroOrganic, EBC-Agro, EBC-Material [325]. Depending on the application classes there are restrictions to be followed for allowed feedstocks. Currently, the European Biochar Certificate is a voluntary industry standard in Europe. Biochar with EBC-feed certification meets all requirements of the EU feed regulation and may be used as feed or feed additive in animal husbandry. Biochars certified with EBC-Agro and EBC-AgroOrganic meet all requirements of the new EU fertilizer regulations [326]. Several EU countries such as Austria, Sweden and Hungary have approved the use of biochar according to the requirements of EBC-Agro. The EBC-Material Certificate guarantees sustainably produced biochar, which can be used in industrial materials such as building materials, plastics, electronics, or textiles without risk to the environment and users. The EBC requires that biochar materials respect the parameters presented in the following Table 1.8 and Table 1.9 [325].

Table 1.8 – EBC biochar limit values.

EBC - Label **EBC - Class**		**EBC-Feed** **Class I**	**EBC-AgroBio** **Class II**	**EBC-Agro** **Class III**	**EBC-Material** **Class IV**
Elemental analysis	C-total, Corg, H, N, O, S, ash				
	H/Corg	< 0,7	< 0,7	< 0,7	< 0,7
	O/Corg	< 0,4	< 0,4	< 0,4	< 0,4
Physical parameters	Water content, dry matter (DM), bulk density (TS), specific surface area (BET), pH, salt content				
TGA	Only once for the first production batch of a pyrolysis unit				
Nutrients	at least N, P, K, Mg, Ca				
Heavy metals	Pb	10 g t-1 (88%DM)	45 g t-1 DM	150 g t-1 DM	250 g t-1 DM
	Cd	0.8 g t-1 (88% DM)	0.7 g t-1 DM	1,5 g t-1 DM	5 g t-1 DM
	Cu	70 g t-1DM	70 g t-1DM	100 g t-1 DM	250 g t-1 DM
	Ni	25 g t-1 DM	25 g t-1 DM	50 g t-1 DM	250 g t-1 DM
	Hg	0.1 g t-1 (88% DM)	0.4 g t-1 DM	1 g t-1 DM	1 g t-1 DM
	Zn	200 g t-1 DM	200 g t-1 DM	400 g t-1 DM	750 g t-1 DM
	Cr	70 g t-1 DM	70 g t-1 DM	90 g t-1 DM	250 g t-1 DM
	As	2 g t-1 (88% DM)	13 g t-1 DM	13 g t-1 DM	15 g t-1 DM
Organic contaminants	16 EPA PAH	4±2 g t-1 DM	4±2 g t-1 DM	6.0+2.2 g t-1 DM	30g t-1 DM
	Benzo[a] pyrene	25 mg t-1 (88% DM)			
	PCB, PCDD/F	[325]	Once per pyrolysis unit for the first production batch. For PCB: 0.2 mg kg-1 DM, for PCDD/F: 20 ng kg-1 (I-TEQ OMS), respectively		

Table 1.9 – Thresholds for heavy metals according to the EBC application classes.

	EBC-Feed	**EBC-AgroOrganic**	**EBC-Agro**	**EBC-Material**
Pb	10 g t-1 (88% DM*)	45 g t-1 DM	150 g t-1 DM	250 g t-1 DM
Cd	0.8 g t-1 (88% DM)	0.7 g t-1 DM	1,5 g t-1 DM	5 g t-1 DM
Cu	70 g t-1 DM	70 g t-1 DM	100 g t-1 DM	250 g t-1 DM
Ni	25g t-1 DM	25 g t-1 DM	50 g t-1 DM	250 g t-1 DM
Hg	0.1 g t-1 (88% DM)	0.4 g t-1 DM	1 g t-1 DM	1 g t-1 DM
Zn	200 g t-1 DM	200 g t-1 DM	400 g t-1 DM	750 g t-1 DM
Cr	70 g t-1 DM	70 g t-1 DM	90 g t-1 DM	250 g t-1 DM
As	2 g t-1 (88% DM)	13 g t-1 DM	13 g t-1 DM	15 g t-1 DM

*DM: dry matter

1.2.3.3 Italian biochar legislation

In Italy, the progress related to biochar is mainly the result of the work carried out by ICHAR, a non-profit association supporting Italian researchers, commercial entities, development agents, farmers and all those who are committed to supporting the sustainable use of biochar systems as a means to remove carbon from the atmosphere and improve the planet's soils. The Association was founded in 2009 by representatives of the National Research Council CNR-IBIMET Institute of Biometeorology of Florence and of the University of Udine (Department of Agriculture and Environmental Sciences), by commercial enterprises with a general interest in the promotion of research , development, demonstration, use and commercialization of the potential biochar production technology in Italy.

Figure 1.5 – ICHAR figurative mark [www.ichar.org].

ICHAR is the Italian reference of the IBI and currently has 55 members belonging to the most diverse categories: researchers, companies, public administrators, gardeners, associations, students, environmental and university certifiers. In 2012, ICHAR, considering the regulatory vacuum related to biochar and aware that the affirmation of this product could not be separated from its legislative recognition, presented to the Ministry of Agricultural, Food and Forestry Policies an application for the inclusion of this material as soil improver in Italian law. Following the Ministerial Decree of 22 June 2015, published in the Official Gazette n. 186 of 12 August 2015 [327], biochar was officially included among the amendments allowed in agriculture (Legislative Decree n. 75 of 29 April 2010, annex 2, order number 16 [328]).

In the decree, biochar is defined as a material produced through a process of carbonization of products and residues of vegetable origin from agriculture and forestry, as well as from olive pomace, pomace, bran, fruit pits and shells, untreated waste of wood processing, as by-products of related activities.

Therefore, waste and any organic matter of animal origin are excluded. The carbonization process is defined by the Decree as the loss of hydrogen, oxygen and nitrogen by organic matter as a result of the application of heat in the absence, or reduced presence, of the oxidizing agent, typically oxygen. This thermochemical decomposition is given the name of pyrolysis or cracking. Gasification involves a further redox process involving the coal produced by pyrolysis. Stringent limits have been placed on heavy metals, polycyclic aromatic hydrocarbons (IPA), polychlorinated biphenyls (PCB) and dioxins, as well as on the need to test the possible phytotoxicity of biochar through a specific biological test. The regulatory limits that the biochar must satisfy are shown in Table 1.10.

In addition to national regulations, biochar will have to deal with the new European regulation on fertilizers, regulation (EU) 2019/1009 of the European Parliament and of the Council of 5 June 2019 [326], which establishes rules relating to the making available on the market of fertilizer products. The new text entered into force on July 15, 2019, but will only be applied starting from July 16, 2022, the day on which the current 2003/2003 EC regulation, which exclusively regulates mineral fertilizers, will cease to apply [329].

Table 1.10 – Amendments to Annex 2 of Legislative Decree 75/2010.

Minimum titer in useful elements and/or substances. Criteria concerning evaluation. Other requirements required	**Useful elements or substances whose title must be declared. Different characteristics to declare. Other requirements required**	**Limits to chemical-biological parameters**	**Notes**
Total C of biological origin (#) % DM (Dry Matter)	Grain size (passing 0.5-2-5 mm)		
≥ 20 and ≤ 30 (CI (*) 3)	Total nitrogen		(#) Subtracted C from carbonates
> 30 and ≤ 60 (CI (*) 2)	Total potassium		
> 60 (CI (*) 1)	Total phosphorus	IPA (Σ 16 molecules) <6 mg/kg DM	(*) Quality class
Salinity mS / m ≤ 1000 (§)	Total calcium		(§) For use as soil improver for horticultural substrates ≤ 100
pH (H_2O) 4-12	Total magnesium	PCB <0.5 mg/kg DM	
Humidity % ≥20 for powdery products (°)	Total sodium		(^) Carbon stability index
Ashes % DM	% C from carbonate	Dioxins <9 ng/kg	
> 40 and ≤ 60 (CI (*) 3)	Phytotoxicity and growth test		(°) Data to be declared in any case
≥ 10 and ≤ 40 (CI (*) 2)	(earthworm test and or germination / growth test)		
<10 (CI (*) 1)			
H / C (molar) (^) ≤ 0.7	Max water retention % m/m		

1.2.4 Uses and Benefits

Biochars produced via different feedstock and conversion technologies generally have different properties due to the variety of operating conditions (reactor technology, temperature, heating rate, residence time, oxidation medium) and potential post-processing treatments [202,330–332]. The performance of biochar in its applications considerably depends on its carbon content, surface area, pH, pore volume, pore size distribution, alkalinity, cation-exchange capacity, surface functional groups, chemical structure and the form of carbon (aromatic or non-aromatic C) and elemental composition [169–171,177]. Because of this variability, the determination of the optimal feedstocks and conversion technologies method of biochar for a particular application has to be done primarily on a case-by-case basis.

In order to provide a broad and comprehensive picture, the uses and benefits of biochar have been classified as follows: application related to soil (as an agent for soil improvement and for remediation of contaminated soil), application related to water, mitigation of GHG emissions and other uses (i.e. biomaterials production, chemical reactions and pharmacy).

1.2.4.1 Soil

Lehmann and Joseph (2009) sustain that there are complementary and synergistic objectives that could provide an incentive for applying biochar to soil: soil amelioration (amendment and fertilizer), waste management and to mitigate the effects of climate change [165].

Properties of biochar are believed to assess the quality of a given biochar as soil improver [331]. Biochar used as a soil amendment can:

- improve soil health and fertility, soil structure, nutrient availability, water holding capacity, cation exchange capacity;
- mitigate nutrient leaching and increase biological activity;
- reduce cationic nutrient leaching and aluminium toxicity. [139,288,333–336]

In addition, biochar is known to be relatively stable in soil against decay with slower rates of mineralization than those observed in the initial biomass and superior ability to retain essential plant nutrients than any other form of soil organic matter [337,338]. The improvements listed above can increase seed germination, plant growth and crop yield [164,339,340].

Jeffery et al. (2011) conducted a meta-analysis which shows that the largest increases in crop productivity occurred in soils with acidic and neutral pH, along with soils with coarse or medium texture [164]. Biochar application has been shown to have a positive impact on the stabilization of soil C, particularly in soils with a lower concentration of native organic matter [170,341,342]. Furthermore, soil properties and climatic conditions are also considered to be critical factors controlling the consequences of the biochar effects [330,338,343,344].

The key relevant potential functions of biochar in soil are listed and defined below.

Modification of physical characteristics

Depending on the rate and nature of biochar, its application to soil affects the soil pore size distribution, texture, structure, enhances formation of macroaggregates and increase the water holding capacity [345,346]. Char porosity affects the proportion of water that can be retained and therefore the accessibility to plants to held water and solutes which can induce enough tension to extract macropore contents that cannot be drained naturally [338,347,348]. High porosity of biochar is commonly associated with augmented water retention in soils [169,323,349–351].

Water scarcity is one of the main issues related to climate change and global warming [352]. Approximately 75% of the freshwater resources are used for irrigation in the agriculture field, while just a limited fraction of this water is currently made available to plants [353]. Biochar, in addition to being a promising soil improver that can be used to increase productivity, it also allows to reduce crop water requirements, to ensure crop yield stability under drought or water scarcity conditions [354,355]. A good rise

in water holding capacity of the soil, particularly in the rhizosphere (the soil portion surrounding plants roots), can enrich nutrient movement and leaching [338].

Obviously, the biochar soil water retention capacity varies depending on the type of soil.

Karhu et al. (2011) found that adding 9 t ha^{-1} biochar (a by-product of birch charcoal production, from pyrolysis at 400 °C for 2–2.5 h, C%: 77.83, N%: 0.77, BET surface area: 3.6 m^2 g^{-1}) on an agricultural soil in Southern Finland, increased the water-holding capacity by 11% [356]. Yu et al. (2013) observed that water-holding capacity of a loamy sand soil can still double in mass using biochar from yellow pine scrap lumber (pyrolysis at 400°C for 3 h, C%: 71.2, N%: 0.2, surface area: 0.19 m^2 g^{-1}) [353].

Nutrient delivery vehicle

Soils generally contain a relatively large total pool of most nutrients, but only a small fraction of these is generally bioavailable. The application of biochar to soils can have effects on soil nutrient dynamics increasing the bioavailability and the uptake of many nutrients to plants due to the adsorption of nutrients by the biochar particles or biochar high carbon-to-nitrogen ratio, leading to microbial nitrogen immobilization during decomposition of the labile fraction [336,357,358]. In particular, biochar produced from nutrient-rich feedstocks (i.e. animal manure, poultry litter, sewage sludge), can be a direct source of highly accessible nutrient salts that offer a direct short-term source of nutrition to plants [338]. Indeed, the greatest effects about soil analyses have usually been observed in coarse soils with biochar from feedstocks containing sufficient nutrients itself [222]. Cow manure biochar applied at a rate of between 10 and 20 t ha-1 [288] and poultry litter biochar [289] showed a significant positive effect. Due to the high number and volume of biochar pores, it imparts such as good adsorption/sequestration and subsequent slow release of adsorbed nutrients. Biochar may stores the nutrients dissolved in the water making them accessible to plants [165]. Some evidence suggests that biochar can also sorb nutrients such as N, P and K (K particularly from the top soil layer) from soil solution and act to improve the availability of nutrients to the shallow root system vegetable crops by reducing loss by run-off and leaching [322,359,360]. Generally, nitrogen is the most essential plant nutrient and the most expensive input. Studies indicate that, even with the significant loss of labile N in the thermochemical conversion process (70-90%), biochar residues may contain considerable amounts of N [361].

Biochar can minimize nitrogen losses in soil, such as N2O emissions, NH3 volatilization and leaching [362] and increase nitrogen inputs with higher nitrogen fixation rates [277], resulting in higher nitrogen availability for the crop and greater nitrogen efficiency.

In general, the addition of nutrients, such as from chemical or organic fertilizers, in soils where biochar has been applied, results in an enhanced efficiency and may be a management strategy [363,364].

Modification of pH

One of the most significant limits to agricultural production worldwide is represented by acid soils (pH < 5.5). Such soils may limit options for crop growth and yields, especially for staple food crops (in particular grain crops). Therefore, increasing the pH of such soils is likely to have beneficial effects on crop productivity [222]. Most biochars have a neutral to basic pH and this have been recognized as providing a positive effect on acidic soils [365]. A liming effect may be one of the key mechanisms behind the observed positive effects of the application of biochar to soils on plant productivity and thus the amount of carbon substrate added to the soil through roots and residues [164]. Benefits of a liming effect include optimizing nutrient availability and utilization (mainly P, but also N, Ca, Mg and Mo), reducing available levels of some toxic elements plant growth (i.e. Al3+ and Mn2+), enhancing the N2 fixation in legumes and improving the decomposition process of organic matter [222]. The liming effect of biochar reduces the concentration of Fe and Al in the soil, therefore the previously bound P then becomes well accessible to plants [366].

Wang et al. (2014) showed that the addition of 4% of rice husk biochar in the tea garden soil appreciably improved the quality of acid soil properties, rising the levels of soil pH, K, Ca, Mg, Na and total C and N, while the available Al and Pb contents decreased [310].

From an economic point of view, it may not be economically feasible for farmers to use biochar in agricultural production solely for pH adjustment as it would represent a relatively higher cost than agricultural lime [367]. Though, it is possible that the economic returns from using biochar may be higher than those from using lime after accounting for any of the other non-pH associated plant growth advantages or carbon sequestration credits.

CEC and sorption

Advanced abiotic and biotic surface oxidation of biochar results in surface proliferation of carboxyl groups and a growing capacity to sorb cations [368,369], clarifying high cation exchange capacity (CEC) in archaeological soils [370]. Negative charge presents the possibility for reversible storage of accessible nitrogen (ammonium, $NH4^+$) relevant to soil-based $N2O$ emissions and nitrate leaching [371].

Biochar is capable of sorbing polar compounds, including several environmental contaminants [372], certain polycyclic aromatic hydrocarbons (PAH) for which it may be the major sink in soils [373]. Furthermore, biochar can increase the potential soil CEC to allow for the retention of nutrients such as K, while reducing P losses by leaching due to its ability to absorb this nutrient on its surface [374,375].

Microbial activity

The probability that biochar catalyzes organic matter breakdown by supplying microbial habitat alone is doubtful, but rises in microbial activity and biomass have been reported with the addition of biochar, along with improvements in composition and abundance of the microbial community [340]. Many of these improvements may be due to biochar, which provide a habitat for microbial colonization [376] and protection against the predators or harsh environment [340,377]. Additionally, in the short term, biochar can induce the microbial community by supplying organic C substrates and can retains essential nutrients and moisture, which are also beneficial factors for peripheral microbial colonization [378].

Biochar can affect microbial activity to the detriment of some metabolizable plants, including mycorrhizal fungi, whose filamentous hyphae provide extension to plant roots in the majority of crop species which can enhance both nutrient and water acquisition [379], by providing a favourable microhabitat such as pore space, due to its weak alkalinity and by being an unfavourable substrate for saprophytes [380]. Besides microbial activity, longer term and more relevant effect derive mainly from structural effects of biochar and indirect effects such as on the soil moisture regime, better aggregate formation and retention of mobile nutrients like N and P as discussed above.

Effects on crop yield

There are lot of studies (field trials and pot experiments) demonstrating that biochar application to soil enhances plant growth by supplying nutrients efficiently and increases crop production and yields [139,164,388,389,339,381–387]. The potential benefit of biochar application in the agronomic field must be considered because of its overall effect on the increase in soil productivity, which is determined both by the set of biochar properties examined previously and by the soil properties, such as:

- physical attributes (soil structure): size and continuity of pores, aggregates stability and texture;
- chemical properties: organic matter content and composition, pH, mineralogy, nutrient stocks and availability, salinity and quantity of elements that are averse to plant growth;
- biological attributes: activity and diversity of microbial biomass and soil fauna [390].

Results of the meta-analysis (a technique which statistically combines data from different studies to provide an estimate of the overall effect size) conducted by Jeffery et al. (2011) showed an increase in crop productivity by 10% after biochar application [164]. The response differs according to the characteristics of the biochar, the mode of application and the soil conditions [137,391]. What turned out was that biochar improved crop yields for nutrient-poor or degraded soils, while the effects were minor on healthy soils [323,392].

Lehmann and Joseph (2015) updated and increased the meta-analysis by Jeffery et al. (2011) to include more studies and to provide further conclusions [222]. From the application rate point of no significant yield

increases were found only for biochar application rates lower than 1-5 t ha-1 and higher than 150 t ha-1. This suggests that if the biochar application rate is relatively low the induced effects are negligible, while at high application loads the biochar can introduce a lot of salt rich ash leading to salinity problems [382]. Generally, if the mentioned limits were not exceeded, an increase in the application rate of biochar corresponds to an increase in yield. At the crop type level, the responses to cultivation with a biochar soil amendment are highly variable. For example, rice, wheat, maize and soybeans (certainly the most important commercial crops globally) revealed statistically considerable increases in crop productivity of about 16, 17, 19 and 22 percent. For other crops such as sugar cane, sugar beet, oats, there were no significant effects of being grown with biochar compared to soil alone.

Table 1.11 – Effects of the biochar amendment on the growth and yield characteristics of different types of crops.

Soil type	Crop	Biochar type	Application rate	Effects on crops	Reasons	Ref.
Ferrosol	Soybean Radish Wheat	Papermill sludge	Biochar was mixed with 25 kg soil to give an equivalent rate of 10 t ha−1	Increase height especially in presence of fertilizer (+20-40%).	Increased pH, soil carbon, CEC. Reduced exchangeable Al. Elevated exchangeable Ca	[323]
Reclaimed tidal land soil	Maize	Rice hull-derived biochar	1, 2 and 5% (w/w)	Increased in yield of maize	Increased in soil organic carbon content and the percentage of water stable aggregate. Decrease in exchangeable sodium percentage. Mitigation of Na uptake due to increased potassium. Decline in antioxidant activities of APX and GR	[393]
Alfisol (chromosol)	Radish (Raphanus sativus var. Long Scarlet)	Green waste (cotton trash/ stalks, grass cutting, plant prunings)	10-100 t/ha	280% increase over biochar unamended soil	The changes in soil properties, such as increases in organic carbona and pH and reduction in soil strength were consistent with the properties of the greenwaste biochar used in this investigation, which was alkaline and high in carbon content.	[336]
Sandy loam	Potato (Solanum tuberosum L. cv. Folva)	Mixture of hardwood (80 %) and softwood (20 %)	Biochar (0 and 5% w/w)	Increase in tuber yield and improvement in plant growth and yield by mitigating the negative effect of salinity through its high sorption ability.	Decrease in Na+, Na+/K+ ratio and increase in K+ content in xylem. Decrease in ABA concentration in the leaf and xylem sap. Increase in shoot biomass, root length and volume, An, gs, midday leaf water potential	[394]

Soil type	Crop	Biochar type	Application rate	Effects on crops	Reasons	Ref.
Clayey	Wheat and maize	Rice straw	Control, biochar (2.0 Mg fed-1), compost tea (400 L fed-1), magnetic iron ore (Fe_3O_4; M: 150 kg fed-1), B + M, C+ M, B + C and B + C+ M.	Significant increase in the yield of wheat and maize	Significant increase in CEC and soil porosity. Increase in soil nutrients availability, yield, water use efficiency and NPK uptake	[395]
Sandy loam	Wheat	Mixture of hardwood (80 %) and softwood (20 %)	0 and 5% (w/w)	Increase in growth and yield of crop	Reduction in plant sodium uptake by transient Na^+ binding; Decrease in osmotic stress and release of mineral nutrients (particularly K^+, Ca^{2+}, Mg^{2+})	[396]
Sandy Loam	Wheat and corn	Biochar	5, 10 and 20 ton/fed	Significant increase in the grain yields of wheat and corn plants	Decrease in soil bulk density, hydraulic conductivity, pH, EC, soluble Na, SAR and ESP values; Increase in CEC capacity, organic matter content, total N and available amounts of P, K, Fe, Mn, Zn and Cu in soil	[397]
Aqui-Entisol	Maize	Wheat straw	Compost (12 t ha-1) of wheat straw biochar and poultry manure compost and a diluted pyroligneous solution (0.15 t ha-1)	Increased maize grain yield	Decrease in sodium and chloride, improvement in leaf bioactivity related to osmotic, increase in leaf sap nitrogen, phosphorus and potassium	[398]
Calcareous inceptisol	Maize	Wheat straw	0, 20 and 40 t ha-1	Increased significantly maize yield in both years	Addition of nutrients and soil structure and moisture improvement	[399]
Clay loam	Maize (Zea mays L.)	Maize straw	0, 10, 20 and 30 t ha-1	Increased by 9 and 13% in BC20 and BC30 in year 1 and by 11 and 14% in year 2, respectively, compared with BC0	Increase in soil organic carbon, total soil nitrogen, C:N ratio, available phosphorus and potassium	[400]
Sandy soil	Tomato (Solanum	Conocarpus biochar	0.0, 4.0 and 8.0% (w/w)	Increased 14.0–43.3% total yield	Biochar addition decreased the suppressing effects of salt on	[401]

Soil type	Crop	Biochar type	Application rate	Effects on crops	Reasons	Ref.
	lycopersicum L.)			over the control	the vegetative growth and yield components of tomato plants	

Biochar is emerging as an attractive option to improve fertilizer use efficiency [165,402]. Incorporating biochar along with chemical fertilizer could be an appropriate option for yield improvement when crops are grown in cultivated land [403].

This combined application can increase the availability and uptake of plant nutrients supplied through fertilizers and can reduce the loss of nutrients by leaching, reducing the requirement for chemical fertilizers. Therefore, the co-application of biochar and chemical fertilizers to the soil or their prior mixing is necessary [403].

For example, Blackwell et al. (2010) [404] demonstrated that banded application of woody biochar increased wheat yield and fertilizer efficiency in dryland south-western Australia. A few recent field-based studies have found increased fertilizer use efficiencies of chemical [351] and chemical-organic [399,405] fertilizers in biochar amended low fertility soils.

Ye et al. (2020) [406] carried out a meta-analysis to explain field responses in crop yield across different climates, soils, biochars and management practices worldwide. Based on a large dataset, in which the short-term effect (1 year) of biochar applications ≤ 20 t ha-1 on crop yield were considered, they have found that if the soil received both biochar and inorganic fertilizer the contribution of biochar to the yield increase beyond that of the addition of fertilizer was, on average, ≥ 15%.

Part of this increase could be attributed to the short-term liming value of biochar, especially considering that there was a trend in the results due to the predominance of low-pH soil in the dataset considered.

Hence, increase in nitrogenous fertilizer use efficiencies mean their reduced losses to environment via leaching and greenhouse gas emissions [336,402,407].

Generally, it is important to consider that each crop may not have been grown on the same type of soil, with the same type of biochar (feedstocks, thermochemical reduction process, temperatures, residence times, post activation treatments or post production procedures such as enrichment of nutrients or mixing with compost), with the same application rates, plus a wide range of other factors that may differ, such as practical operation conditions and environmental and management factors. [408]

Although positive effects on plant productivity and soil chemical, biological and physical properties have mostly been observed [135], a closer look at the published literature shows that negative responses in some instances have been reported by many researchers [164], with no positive yield [409,410] or even negative impact on the yield [411,412].

Additionally, the long-term stability of biochar in soil has not been completely demonstrated, the preservation for human health not totally assessed, while the effect on the radiative balance due to alterations in soil albedo has only been partially discussed [413].

In conclusion, more long-term and comprehensive assessment of direct biochar effects on crops and on the environment as well as an evaluation of socioeconomic implications should be conducted, in order to gain a mechanistic understanding behind many of the observed effects to permit widespread understanding and global assessment.

Greenhouse gases emission storage

Climate change is one of the biggest challenges of our times. Human influence on the climate system is clear and recent anthropogenic emissions of greenhouse gases (GHG) are the highest in history. Climate changes have had widespread impacts on human and natural systems. Anthropogenic GHG emissions, which are mainly released through the combustion of fossil fuels and also through the decomposition of organic matter in the soil, since the pre-industrial era have driven large increases in the atmospheric concentrations of carbon dioxide (CO_2), methane (CH_4) and nitrous oxide (N_2O). It is estimated that soil emissions of carbon dioxide (CO_2), methane (CH_4) and nitrous oxide (N_2O) represent 35%, 47% and 53% of the total annual global emissions of these greenhouse gases (GHG), respectively [414,415]. Between 1750 and 2011, cumulative anthropogenic CO2 emissions to the atmosphere were 2040 ± 310 Gt CO_2. About 40% of these emissions have remained in the atmosphere (880 ± 35 Gt CO_2); the rest was removed from the atmosphere and stored on land (in plants and soils) and in the ocean. About half of the anthropogenic CO_2 emissions between 1750 and 2011 have occurred in the last 40 years and are continuing to increase exponentially, despite a growing number of climate change mitigation policies.

Carbon dioxide (CO_2)

Mitigation, in the context of climate change, can be accomplished in two principally ways: reducing the emissions or enhancing the sinks of greenhouse gases in the environment [416]. However, since some emissions are obviously unavoidable, it is right to focus also on the second way. An existing approach to removing carbon from the atmosphere is to grow plants that sequester carbon dioxide in their biomass or in soil organic matter. By the way, methods for subtracting amounts of CO_2 from the atmosphere through afforestation have already been accepted as tradable carbon offsets under the Kyoto Protocol on Climate Change of 1997, which was adopted in the United Nations Framework Convention on Climate Change [334]. Howeewr, this sequestration can be taken a step further by the application of biochar to soil, a novel approach to establish a significant, long-term, sink for atmospheric carbon dioxide in terrestrial ecosystems [417,418].

The global carbon cycle is made up of flows and pools of carbon (terrestrial, atmospheric, ocean, and geological) in the Earth's system. In order to decrease carbon in the atmosphere, it is necessary to move carbon in the active pool into a passive pool containing stable or inert carbon. Biochar provides a facile flow of carbon from the active pool to the passive pool [419]. Plants subtract carbon dioxide (CO_2) from the atmosphere through the photosynthetic process and once their life cycle is over, they return part of it to the soil and to the atmosphere through the degradation and mineralization of the organic substance. This natural cycle is considered as carbon neutral [420]. If the plant residues or, more generally, biomass organic matter are converted by pyrolysis into biochar, ~50% of the C contained in the biomass is immediately released as bio-oils and gases, leaving the remaining part as a stable biochar residue with a high resistance to microbial degradation [335]. So, given a certain amount of carbon that cycles annually through plants, half of it can be taken out of its natural cycle and sequestered in a much slower biochar cycle [334]. Non-charred carbonaceous materials such as non-living plant or animal matter decompose in the soil to release carbon slowly over time. The release of carbon from natural decomposition of dead matter continues until most of it is lost within a relatively short period of time from the soil, whereas biochar carbon will be stored in the soil for much longer periods of time. The estimated residence time of biochar-carbon, with its stable aromatic carbon, is in the range of hundreds to thousands of years while the residence time of carbon in plant material is in the range of decades [177]. As said, this would reduce the CO_2 release back to the atmosphere if the carbon is indeed persistently stored in the soil [139], and the net process might be carbon negative [139,421].

About four times more organic carbon is stored in the Earth's soil than in atmospheric CO_2 and every 14 years, the entire atmospheric CO_2 has cycled once through the biosphere [16]. The annual uptake of CO_2 by plants from the atmosphere through photosynthesis is 8 times greater than anthropogenic GHG emissions [419]. Switching even a small amount of the carbon cycling between the atmosphere and plants into a much slower biochar cycle would impact greatly to atmospheric CO_2 concentrations. It is estimated that the deviation of only 1% of net annual plant uptake into biochar would mitigate almost 10% of current anthropogenic carbon emissions [165]. Lehmann (2007) calculated emissions reductions for three separate

biochar approaches (pyrolysis of existing forest residues, or crop wastes, or fast growing biomass established on idle cropland) that can each sequester about 10% of the annual US fossil-fuel emissions (1.6 billion tonnes of carbon in 2005) [334]. In each case, the biochar generated by pyrolysis is returned to the soil and not burned to offset fossil-fuel use.

To understand in principle how much carbon can be stored in soils through biochar, it is necessary to estimate the maximum amount of biochar which can be stored in soils without compromising other soil functions, the effects on plant productivity and the surrounding ecosystem. Obviously the biochar loading capacity and the amendment capacity will vary according to the soil properties and other factors, such as the climatic conditions [330,343,344]. Most of the results of biochar additions to soil shows that crops respond positively to biochar additions from 50 Mg C ha^{-1} increasing crop yields with increasing additions up to 140 Mg C ha^{-1} [422]. However, it should be noted that some experiments report that some crops experience a loss of the positive effects of biochar addition to soil at a much lower application rate [277].

Moreover, there are other factors that make the use of biochar an even more virtuous practice with multiplier effects that lock up additional carbon. Firstly, as discussed previously, biochar application to soils concurrently improve soil quality and fertility. Secondly, bio-oil and gases produced during pyrolysis can be used for energy production, reducing fossil fuel usage and consequently other greenhouse gas emissions [423]. Therefore, when combined with bioenergy production, it is a clean energy technology that reduces emissions as well as sequesters carbon [423]. For example, under a current practice of complete combustion (burning) more than 90% of the C in an organic material is oxidized to form CO_2, whereas under the various systems of biochar production discussed above only 45–48% of the organic C is oxidized to CO_2. Consequently, by switching from burning of residues to a biochar system 420–450 kg C of emissions per ton of C used as feedstock are avoided. Further, the energy produced, if used to displace energy produced by fossil fuel burning, leads to a further reduction in emissions [335].

The ability of biochar to sequester carbon and therefore its stability in soil will depend on its physical and chemical properties, which can be varied significantly on the basis of the feedstock choice and in the production process [319].

Because degraded soils in different regions around the world have specific quality issues, it follows that one biochar type will not solve all soil quality problems. Biochars with a highly aromatic composition, which are obtained by pyrolyzing organic feedstocks at high temperatures (400-700 °C) [187], may best be suited for long-term carbon sequestration because the aromatic structures have low O/C ratios that are highly resistant to microbial degradation and mineralization [135,424,425]. On the other hand, biochars produced at lower temperatures (250-400 °C) have higher yield recoveries and contain more C=O and C-H functional groups that can serve as nutrient exchange sites after oxidation [135]. So, from a carbon sequestration perspective biochar produced at high pyrolysis temperatures is better because it contains a higher proportion of the stable fraction [263].

Case et al. studied a 2-year biochar amendment in a miscanthus bioenergy crop field and found that soil CO_2 emissions decreased by approx. 33% and the annual net soil CO_2 equivalent emissions by 37%, lower than the data obtained in the laboratory [426].

The dominant mechanisms may be decreased enzymatic activity, improved carbon use efficiency and CO_2 adsorption on the biochar surface.

Carbon dioxide is not the only gas emitted from soil with the possibility to affect the climate. Methane (CH_4) and nitrous oxide (N_2O) are the second and third largest contributors to radiative climate forcing after CO_2, and soil is a key source of both gases, which are emitted through natural microbial processes. The contributions of GHG to the greenhouse effect are affected by the properties and abundance of these gas. CH_4 and N_2O have, respectively, a global warming potential (GWP) of 25 and 298, over a 100-year time horizon [427]. Hence, these gases are more impactful than CO_2, however, the contribution rate of CO_2 is approx. 55% for its large amount [428,429]. 50% of CH_4 and 80% of N_2O emitted are produced by soil processes in managed

ecosystems [427]. Global emissions of all major greenhouse gases increased between 1990 and 2010, N2O emissions increased the least, 9%, while CH_4 emissions increased by 15% [427].

Methane (CH4)

The earth's atmospheric CH_4 concentration has increased by about 150% since 1750, and it accounts for 20% of the anthropogenic warming effect [430]. CH_4 is one of the six GHG to be mitigated under the Kyoto Protocol and is the major component of natural gas and associated with all hydrocarbon fuels. Significant emissions occur as a result of animal husbandry and agriculture, and their management represents a major mitigation option [431].

Methane in soil is primarily produced under anaerobic conditions by methanogenic Archaea through a process known as methanogenesis and can be taken up in oxic soils via consumption by methanotrophic bacteria [432]. It has been shown that biochar decreases [296,433,434], on CH_4 emissions from soils. The mechanisms by which biochar can influence soil CH_4 fluxes mainly consist of CH_4 sorption to biochar surfaces [435], and soil aeration by adding biochar, which can increase CH_4 diffusive uptake [323,356], since microbial oxidation of CH_4 in upland soils is mainly a-limited substrate [436]. Though, in anoxic environments, the C labile pool of biochar can serve as a methanogenic substrate, stimulating CH_4 production [437]. Biochar has also been shown to stimulate methanotrophic CH_4 consumption at oxic/anoxic interfaces in anoxic environments, reducing CH_4 emissions via the biofilter function of CH_4 consumption [296,434].

To assess the actual benefits of biochar for the mitigation of CH4 emissions, it is necessary to quantify the effect of biochar on CH_4 production from modified soils. However, other studies showed that biochar has no considerable effect [438] or increased soil CH_4 emissions [402,439–441], possibly because biochar provided a substrate for methanogens [442] or inhibited the activity of methane oxidizing bacteria [443].

Dong et al. compared the CH_4 emission responses of biochar and straw applications in a two-year experiment on a paddy field [433]. The results showed that rice straw derived biochar was able to reduce CH4 emissions by 47.30%-86.43% during the rice growing cycle. Another experiment using straw biochar was conducted in China by Wang et al. (2018) [444]. The results experiment indicated that biochar amendment at 24 t ha−1 could decrease annual total CH_4 emissions by 20–51% in four years. Similar findings were achieved by Proyuth et al. [445]. Based on the average values of continuous field measurements in situ for 3 years, Chen et al. founded that biochar treatments slightly increased biomass by 0.5-8.0% (while significantly reduced total CH_4 emissions to the soil of the 33.8-43.1% compared to the treatment without adding straw and without biochar, suggesting the high potential of biochar to increase crop biomass and reduce emissions [446]. In a rice cropping system, biochar reduced soil CH_4 emissions notably [296] and increased soil net absorption of CH_4 [447].

Nitrous oxide (N_2O)

N_2O is one of the six GHG to be mitigated under the Kyoto Protocol and it is now also the major ozone-depleting substance in the stratosphere. [448]. The atmospheric concentration of N_2O before industrialization was 270 parts per billion by volume, while its current atmospheric abundance is ~324 parts per billion by volume [449].

The main anthropogenic source of N_2O is agriculture (soil and animal manure management) due to the extensive use of nitrogen fertilizers, but critical contributions also come from wastewater treatment, fossil fuel combustion and chemical industrial processes. N_2O is also naturally produced from a broad range of biological sources in soil and water, particularly from microbial action, but the underlying processes are very complex and depend on the interaction between soil characteristics, climate, land use and management practices [431,450–452].

Biochar has a significant effect on the nitrogen cycles of transition in the soil. The application of biochar reduces soil N_2O emission through both abiotic mechanisms and biotic mechanisms [450,453,454] which includes:

- change in the proportion of the transformation of N_2O into N_2 during denitrification due to the change in pH (liming effect) [183,455];
- interaction with dissolved organic C [452,456];
- modification of the abundance of soil microbes, in particular increasing the growth and activity of microorganisms involved in denitrification [340,457];
- improvement of soil adsorption capacity to NH_4^+ or NO_3^- [323,458,459];
- increase in soil aeration and decrease of denitrification rate [460,461];
- release of toxic/inhibitory compounds [462,463].

Overall, biochar demonstrates a significant effect on the soil N cycle, although the effects are not exactly the same due to differences in soil characteristics, climate conditions, management practices and application methods [437,464].

Rondon was the first to report the decrease in N_2O emissions after the biochar amendment [465]. N_2O emission decreased by approx. 50% for soy and approx. 80% for grass, which grew in an arid oxisol in the Colombian savannah. Yanai et al. (2007) evaluated N_2O emissions from the soil after rewetting in the laboratory and found variable results, namely an 89% suppression of N_2O emissions in a porous space filled with water for 73-78%, in contrast with a 51% increase in the porous space filled with water [466]. They also reported that these effects change over time, but their experiment only lasted 5 days and therefore it is not possible to extrapolate the results to time scales where biochar is likely to persist in soil. Cayuela et al. (2014) conducted a meta-analysis using 261 experiments [450]. They found a 54% reduction in N_2O emissions to soil in both laboratory studies and field tests and that the results were closely related to pyrolysis parameters, feedstock types and C/N ratios. In comparison, the meta-analysis conducted by Borchard et al. (2019), which involved 88 publications, showed overall reduction in N_2O was approximately 38%, but the reductions in N_2O emissions tended to be negligible after one year [467]. Moreover, the biochar amendment had the largest N_2O emission reduction effect in rice fields and sandy soils. Cayuela et al. (2013) investigated the amount of reduced N_2O emissions and reduction mechanisms, founding that biochar significantly affects denitrification, reducing N_2O emissions by 10–90% in 14 different soils [468]. With the N gas flow method, they found a substantial reduction in the $N_2O/(N_2 + N_2O)$ ratio, indicating that the biochar facilitated the last stage of denitrification. Ameloot et al. (2016) performed a field experiment with biochar for 7 months, concluding that adding biochar reduced N_2O and N_2 emissions in all cases, but did not reduce the $N_2O/(N_2 + N_2O)$ ratio [469].

Further research and long-term field trials are still needed, but the results achieved to date are so positive that biochar has been incorporated on the agenda of the upcoming international negotiations on climate change as one of the most promising strategy for mitigating climate change [431]. Logically, biochar must be considered together with other mitigation strategies and cannot be seen as an alternative to reducing GHG emissions [139].

Table 1.12 – Application of several types of biochar for soil improvement, carbon sequestration, and GHG reduction.

Biochars	Soil	Experiment type	Biochar application rate (t ha^{-1})	N fertilization (kg ha^{-1})	Time (day)	Soil carbon	CO_2 emission	CH_4 emission	N_2O emission	Ref.
Bamboo	Paddy soil	Bottle (anaerobic)	2,50%	–	49	–	No difference	51.1% decreased	–	[470]
Corn stalk	Paddy inceptisol	Pot	24	250	116	Soil DOC* increased	–	63% decreased	–	[296]
Corn stalk	Paddy inceptisol	Pot	24	250	116	Soil DOC increased	–	61% decreased	–	
Maize straw	Vegetable field	Pot	20	400	67	–	–	No difference	77% decreased	[453]
Maize straw	Vegetable field	Pot	40	400	67	–	–	No difference	82% decreased	

Mixed sawdust	Corn field	Serum vials	20–60%	–	100	–	Decreased	Decreased when biochar ≥ 20%	57–74% decreased	[471]
Municipal biowaste char	Grassland soil	Petri dish	10%	–	3	–	–	–	89% decreased	[466]
Pinus radiata	Dairy farm soil	Soil core	20	760	55	No difference initially and then increased	–	–	No difference	[472]
Pinus radiata	Pasture soil		30	133	70	–	–	–	70% decrease	[473]
Poultry manure & Wood	Alfisol	Column	10	45	183	–	Fluctuated	–	14–73% decreased	[474]
Poultry manure & Wood	Vertisol	Column	10	45	183	–	Fluctuated	–	23–52% decreased	
Straw	Paddy soil	Bottle (anaerobic)	2,50%	–	49	–	No difference	91.2% decreased		[470]
Wheat straw	Agricultural soil	Pot (40% moisture)	1%	150	55	Soil DOC decreased	Increased	–	Decreased	[457]
Wheat straw	Agricultural soil	Pot (40% moisture)	3%	150	55	Soil DOC decreased	3.3 times increased than 1%	–	Decreased	
Wheat straw	Rice paddy	Field	40	300	150	–	–	34% increased	40–51% decreased	[402]
Wheat straw	Rice paddy	Field	40	0	150	–	–	41% increased	21–28% decreased	
Wood	Wheat soil	Field	30	222	420	–	No difference	No difference	26–76% decreased	[475]
Wood	Wheat soil	Field	60	222	420	–	No difference	No difference	59–88% decreased	

*DOC: Dissolved organic carbon

Remediation of contaminated soils

Biochar-based contamination management has been extensively studied [476]. In recent years, large research efforts have been conducted to investigate the use of biochar for the removal of various inorganic and organic pollutants from the soil [477,478].

The potential use of biochar for soils contaminated with heavy metals, volatile organic compounds (VOC), industrial chemicals including polycyclic aromatic hydrocarbons (PAH) or agrochemicals (e.g. pesticides, herbicides, fungicides, insecticides) depends on its ability to reduce mobility and absorption of plant pollutants [275,309,487,488,479–486]. Biochar can be used in both in-situ and ex-situ remediation techniques such as landfarming, bioventing, composting, bioaugmentation and as an adsorbent in permeable reactive barrier (PRB) [489–493].

The removal processes are basically regulated by the interactions between these contaminants and different biochar attributes. Heavy metal removal mechanisms with the biochar amendment could be attributed to electrostatic interactions, precipitation and formation of metal complexes [494–497], whereas the removal of organic contaminants by biochar could be primarily attributed to surface adsorption [498–500].

Thus, the following sections summarize the main aspects and characteristics related to the removal of inorganic and organic contaminants by biochar.

Inorganic Contaminants

Heavy metals are a group of elements which are important both from an industrial and a biological point of view [501]. Excessive concentrations of heavy metals can cause a toxic response to biota or humans. Those considered most dangerous and harmful to the environment are cadmium (Cd), chromium (Cr), copper (Cu), mercury (Hg), nickel (Ni), lead (Pb) and zinc (Zn), and some of these (Cu, Ni, Zn) are essential for plant metabolism [502]. Their presence in urban and rural environments is mainly related to activities such as mining, smelting, industrial processing and waste disposal, while the prevalence of high concentrations of heavy metals in agricultural systems is due to the use of fertilizers, herbicides and pesticides [502]. The factor that makes heavy metals highly dangerous is that they are not biodegradable and persist for a long time in contaminated soils. Therefore, it is very costly and time consuming to remove heavy metals from contaminated soils with traditional technologies or hard engineering solutions. An alternative strategy, that appears to be effective and justified by the relatively low cost to reduce the bioavailability of metals and minimize plant uptake, is stabilization of heavy metals in situ by adding soil amendments such as lime and compost [503,504]. Therefore as demonstrated by many field applications, the application of biochar as soil amendment can potentially provide a new solution for in-situ remediation of metal-contaminated sites for a significant reduction in crop uptake of heavy metals [150,495,505].

Biochar has several favourable properties that facilitate chemical modifications of heavy metals [479,494,506–508], such as its high porous structure, high aromatization, active surface functional groups, high pH and CEC [203,204,509]. When biochar is to be used as an amendment for the remediation of soils contaminated with heavy metals, the types of heavy metals present in the contaminated soil and the characteristics of the biochar related to the type of feedstock used and the production parameters should be taken into account [510].

According to current research, the mechanisms for heavy metal remediation by biochar could involve different possible mechanisms, including adsorption (both chemisorption and physisorption), reduction, oxidation and most importantly, immobilization of heavy metals [205]. The adsorption mechanisms between biochar and heavy metals consist of ion exchange, surface mineral adsorption, electrostatic attraction, cation–π interactions and precipitation of surface functional groups [511].

Lu et al. (2012) indicated different mechanisms for sludge-derived biochar sorption of Pb2 +:

- heavy metal exchange with Ca^{2+}, Mg^{2+} and other biochar-associated cations, attributing to co-precipitation and inner-sphere complexation with complexed organic matter and mineral oxides of biochar;
- surface complexation of heavy metals with other functional groups, and inner-sphere complexation with the free hydroxyl of mineral oxides and other surface precipitation;
- physical adsorption and precipitation of the soil contributing to Pb2+ stabilization [495].

There are strong interactions among heavy metals and abundant surface groups (primarily oxygen-containing groups, such as -COOH and OH), which can be shown by shifts in functional groups of biochar before and after metal adsorption [28]. Ion exchange depends mainly on the CEC. Electrostatic attraction is mainly attributed to negatively charged surfaces [512]. When biochar is applied to soil, the electrostatic attraction between positively charged heavy metals and soil increases, increasing the adsorption capacity of heavy metals [505]. The electron cloud of the benzene ring can be polarized and create a weak electrostatic effect when heavy metal ions are close to the benzene ring, resulting in physisorption [513]. Cation–π is a complex combination of electrostatic adsorption and π–π conjugation. Commonly, the effect of cation–π depends primarily on the aromaticity of the biochar surface, which is a measure of the number of π–π conjugations [489].

To influence heavy metals there are also a series of indirect effects resulting the application of biochar as soil amendment. Adding biochar to soil can increase water holding capacity, soil pH, organic C content, microbial biomass, and nutrient use efficiency [330,338,340,479], which in turn can affect the retention and release of heavy metals.

The pH of the soil solution impacts metal removal efficiency and the amount of which depends on the metal [505]. Biochar is more alkaline and can significantly increase soil pH, which indirectly reduces the bioavailability of heavy metals [514,515]. Sorption studies have found that the optimum pH for Cr sorption is at pH of 2 resulting in up to 98% Cr removal [494]. On the other hand, Pb sorption processes were faster at a higher pH between 2 and 5 [494,495]. For Cu, biochar sorbed increasing quantities as the pH reduced from 9 to 6 [150].

Another important role in the stabilization of heavy metals in the soil is also played by mineral components present in biochar, such as phosphates and carbonates, because these salts can precipitate with heavy metals reducing their bioavailability [489]. Cao and Harris (2010) indicated that the major process for the biochar of dairy manure to retaining Pb was the precipitation of insoluble Pb phosphates [287].

Also, biochar can alter soil moisture condition and aeration, and influence soil redox potential, thus modifying the toxicity of a variety of charge-sensitive toxic heavy metals (i.e. Cd) [516].

Organic Contaminants

Organic pollutants are known to be serious soil and water pollutants and can be divided into persistent (polychlorinated biphenyls, polyaromatic hydrocarbons) and emerging (phthalate acid esters, naturally released estrogenic steroid hormone and its metabolites, pharmaceutical and personal care products) [510]. Soil contamination with organic pollutants is usually caused by a broad range of industrial processes, farming practices (many organic pollutants are currently or were in the past used as pesticides), and inappropriate application of wastes. Some of the organic pollutants are recalcitrant to degradation and some are carcinogenic or mutagenic [517], and the pollution caused can be harmful for agricultural production and ecological health, culminating in a serious threat to human survival. Thus, there is a strong need for adsorption or remediation/catabolization using different bioremediation techniques [510], and biochar application to soil appear to be a useful in situ remediation strategies for different types of organic pollutants [510,518]. Biochar, when incorporated into the soil, is an effective adsorbent of organic compounds (i.e. polycyclic aromatic hydrocarbons, polychlorinated biphenyls, naphthalenes, and phenols) having the ability to immobilize them, reducing bioaccessibility for plant absorption and accumulation in the soil, reducing the risk of the pollutants entering human food chain or leaching to groundwater [519]. Biochar characteristics which plays important roles in the ability to adsorb organic pollutants are: highly aromatic nature, high surface area, elemental composition, pH, micropore volume, and the presence of abundance of polar functional groups [332,518,520].

For organic pollutants, the biochar removal mechanism mainly includes chemisorption (electrophilic interaction) and physisorption (e.g., pore diffusion, hydrophobic, electrostatic attraction/repulsion via π-π electron donor-acceptor, and H-bonding) through COOH, OH, and R-OH functional groups [6,205,521], but the adsorption process is normally governed by the combination of several mechanisms [514,515]. In addition, other processes including partitioning (due to substratum polarity reduction in the non-carbonized phase), chemical transformation (through reductive reactions or electrical conductivity) and most of the bonded contaminants are mineralized by biodegradation (by different microorganisms present on the surface and in biochar micropores) [20,161,173,522].

The main factor affecting the biochar interactions with organic pollutants are pH, pyrolysis temperature, feedstock type and ratios of pollutant-to-biochar [32]. As previously discussed, higher pyrolysis temperature leads to higher surface area and microporosity in the biochar. Although these are advantageous attributes for the removal of non-polar organic contaminants, these properties are lacking in the biochar produced at lower temperatures [20,173]. High pyrolysis temperature (>500 °C) results in high aromaticity, low polarity and acidity on biochar due to the loss of functional groups containing O and H [187]. Hydrophobic interactions are primarily encouraged by reduced O-bearing functional groups, while biochar produced at <500 °C contains more O and H-containing functional groups so they are likely to have a high affinity for polar organic compounds [167].

Generally, with increasing biochar adds, adsorption and degradation of organic pollutants in soil has been improved. For instance, with growing quantities of biochar in soil, the loss of both pesticides (chlorpyrifos and carbofuran) degradation and/or sequestration in soils decreased dramatically [523].

Normally, soil conditions affect contaminant degradation and adsorption. The persistence and effectiveness of isoproturon (IPU) [524] and benzonitrile [525] pesticides and herbicides such as (4-chloro2-methylphenoxy) acetic acid (MCPA), atrazine and trifluralin in soil have also been shown to be affected by the application of biochar [526]. Biochar absorption for pesticides was typically preferred at a low pH level [527].

As imagined, surface activation increases the uptake of organic contaminants due to the higher surface area of the activated biochar compared to an untreated biochar of analogous composition and production process [528,529].

Currently, most of the studies based on the adsorption mechanism of organic pollutants are at a qualitative stage although quantitative structure-activity relationship study is being performed gradually [530]. This is because the biochar reduction mechanism of the bioavailability of organic pollutants is not easy to quantify in the soil ecosystem as it contains complex microbial metabolic processes.

1.2.4.2 Water

Aquatic ecosystems are often subject to contamination by organic, inorganic and microbial contaminants originate from either anthropogenic or natural sources and the exposure to these toxic substances can cause various health problems [531,532]. Water-soluble heavy metals can make a potent biological effective, even in very low concentrations. Without proper treatment, industrial wastewater, urban wastewater and agricultural production wastewater carry heavy metal pollution into natural water bodies and caused one of the most serious global environmental problems [533].

In general, for the treatment of water the conventional technologies currently used include coagulation-flocculation, sedimentation, filtration, and disinfection, while the advanced ones are represented by membrane technology, advanced oxidation process, biofiltration, granular activated carbon [534]. Though, the disadvantages of current technologies, including high costs, and uneven distribution around the world underline the need to implement a new purification method based on an ecological and economical technology to overcome current limitations [428].

In addition to the benefits described so far, biochar would appear to provide a sustainable and economical solution for water treatment (water purification and wastewater treatment) thanks to its low production cost and feasibility in many contexts [20]. It can be used in water treatment as an adsorbent alternative to activated carbon (AC) for the removal of various contaminants from water such as nutrients, trace metals, pharmaceuticals, pesticides, dyes, metals (loids), organic compounds volatiles and polycyclic aromatic hydrocarbons [535,536]. Recently developed hybrid techniques in water purification systems include for example biochar-based membrane filtration (e.g., micro-sized biochar + polysulfone mixed matrix hollow fiber membrane), permeable reactive barriers and biochar-augmented biofilters [537].

The factors that regulate the adsorption rate are the specific surface, the nature and initial concentrations of the adsorbate, the pH of the solution, the temperature, the interfering substances, the properties and the amount of adsorbent.

There are several mechanisms responsible for removing contaminants from aqueous solutions using biochar, including electrostatic interactions, ion-exchange, hydrogen bonding, surface complexation, pore-filling mechanisms and π–π electron donor–acceptor (EDA) interactions [538]. Adsorption is basically proportional to the surface area available for adsorption [539]. Consequently, higher porosity and specific surface area typically increase adsorption due to the enhanced mass transfer mechanisms, but there are other factors that need to be taken into consideration such as the chemical composition of the adsorbate, its size and its speciation. Furthermore, pH has an important impact on the adsorption process as it directly affects both the chemical form of the contaminant and the surface charge, as well as the ionization or speciation of the adsorbate [540].

Inorganic Contaminants

Presence of elevated trace metals concentrations in natural ecosystem potentially leads to severe environmental concerns [484]. Most commonly inorganic contaminants found in aquatic ecosystem are Pb, Hg, Cr, As, Cd, Zn and Cu, as well as troublesome ions, including F-, NH_4^+, PO_4^{3-}, and NO_3^-.

Heavy metal removal studies have recently been conducted using biochar together with advanced spectroscopic techniques to elucidate the adsorption capabilities in aqueous media and, depending on the state of the contaminant, the results have shown that biochar can act as a dominant adsorbent, showing a very high degree of removal [150].

The process of adsorption of heavy metals by biochar in aqueous solution is very varied as it is a complex material, its surface oxygen-containing functional groups and binding sites can easily allow the complexation of the biochar or ion exchange with metal ions heavy. In addition, certain insoluble inorganic salt (formed in the biochar preparation process) may co-precipitate on the surface with heavy metal ions.

The abundance of negatively and positively charged biochar sites makes it possible to absorb water cations and anions [476,541]. Usually, on the surface of the biochar, carboxyl and hydroxyl groups are involved

in metal immobilization by three major mechanisms: complex formation, electrostatic attraction, and exchange of H+/light metal ion exchange [537,542].

Several studies examined the efficiency of sewage sludge, animal wastes and agriculture by-products derived biochars for removal of Cu2+, Pb2+, Ni2+, Zn2+, Sb2+ and Cd2+ in aqueous system and the results were encouraging [173,484,495].

Boni et al. (2020) investigated biochar produced by a wood biomass pyrolysis process as adsorbent for remediating a Pb-contaminated solution [543]. The complete removal in batch process was achieved within 4-h contact time using a biochar dosage of 5 g L^{-1}. Continuous flow column tests showed that adding biochar to the soil of the adsorbent bed significantly extended the breakthrough and exhaustion times, with respect to the column filled with soil only.

As reported by Mohan et al. (2011), cellulose and hemicelluloses provide unsaturated anhydro sugars, diols and other compounds that can reduce Cr(VI) [544]. Therefore, these pyrolytic chars can easily reduce and bind to Cr(VI). Consequently, biochar is an effective reductant agent for Cr(VI) due to its reactive surface functional groups and large surface area [545,546]. It has been suggested that the dominant mechanism for the adsorption of Cr (VI) on biochar consists in the absorption of Cr(VI) and the subsequent reduction of sorbed Cr(VI) to Cr(III) [546].

Beiyuan et al. (2017) demonstrated that permeable reactive barriers produced with wood waste biochar showed the highest adsorption capacity for Pb (10.2 mg g^{-1}), while Cu and Zn (7.51 and 2.44 mgg^{-1}, respectively) showed a slightly lower affinity to Pb [2]. Cao and Harris (2010) also reported the precipitation of Pb2+ with phosphate in water on biochar derived from dairy manure (enriched with P) [287]. Similar to Cu and Pb, water-soluble Hg can be precipitated as Hg(OH)2 or HgCl2 on alkaline biochar surfaces containing a high chloride content [173]. Sorption of Cr(VI) on biochar has been attributed to binding to active negatively charged biochar sites after its reduction to Cr (III) due to O-containing functional groups [494].

Organic contaminants

In general, the main organic contaminants in aqueous bodies are agrochemicals, such as pesticides, herbicides, fertilizers, liming and acidifying agents, pharmaceuticals and polycyclic aromatic hydrocarbons.

Sorption of organic contaminants from water onto biochar occurs due to its high surface area, surface polarity, aromaticity and microporosity [316,547,548]. In fact, biochars produced at >400 °C are more effective for the sorption of organic contaminants due to their high surface area and the development of micropores [167,549]. As mentioned, being the surface of the biochar negatively charged due to the presence of different functional groups, the adsorption of organic contaminants can be controlled by electrostatic attractions and by π–π (EDA) interactions between biochar and aromatic groups of organic [550]. The positively charged organic contaminants can be retained on the surface of the biochar. This interaction occurs as a result of the donation or the acceptance of electrons to/from an organic compound or biochar [551]. The electrostatic attraction was reported by Qiu et al. (2009) and Xu et al. (2011) referred to studies on the adsorption of cationic dyes including methyl violet and rhodanine from water [486,552].

For example, the exchange of electrons between the hydrophobic graphite regions of carbon nanotubes (CNTs) or biochar and the amino group in the sulfapyridine created π–π bonds, which allowed the retention of the sulfapyridine by the CNT and the CNT-modified biochar [553]. Thus, phenanthrene removal performance is dominated by π–π EDA interactions as well as by surface adsorption, partitioning and electrostatic attractions [554].

Other studies described the adsorption of hydrophobic compounds, such as humic acids and phenanthrene, onto different biochars through π–π interactions [555–557]. The presence of functional groups containing oxygen, such as carboxyl and hydroxyl groups (-OH, -COOH), facilitates the adsorption of organic pollutants through hydrogen bonding and complexation between the biochar and the contaminant [16,558]. The formation of H-bonds between biochar polar functional groups and organic contaminants facilitates stronger retention of adsorbate on biochar [559]. Essandoh et al. (2017) studied different hydrogen bonds

between switch grass biochar and the herbicide 2,4-dichlorophenoxyacetic acid (2,4-D) in an aqueous solution and concluded that carboxylic acid (-COOH), carboxylate (-COO) and phenolic functional groups contained in the biochar surface can act as hydrogen donors or hydrogen acceptors with the -COOH and -COO groups of 2,4-D [560], and the maximum adsorption capacities was ~134 mg g-1 at pH 2. The adsorption mechanisms of herbicides (e.g., metribuzin) and of antibiotics (e.g., sulfathiazole) with biochar were also demonstrated by with H-bonding between biochar and the adsorbate [561].

In biochar-organic contaminant retention, the formation of complexes and pore filling also play a significant role. Jin et al. (2017) and Ahmed et al. (2017) stated that phenanthrene and sulfonamide antibiotic retention is predominantly due to pore filling via the diffusion process [16,556]. Some organic farming by-products that can potentially be found in water sources, such as furfural and carbofuran, have been successfully removed from bamboo rice husk biochars [562,563]. Hydrophobic organic compounds, such as naphthalene and p-nitrotoluene, have been found to adsorb on modified magnetic orange peel biochar [564]. Removal of pesticides, such as carbofuran, from aqueous solutions with steam activated rice husk biochar has also been shown to have high adsorption [563].

Factors such as pH and ionic strength can certainly influence the sorption of organic contaminants on the biochar. The sorption capacity of a crop residues derived biochar at 350 °C for methyl violet increased significantly from pH 7.7 to 8.7 [486]. The electrostatic attraction between biochar and methyl violet improved with increasing pH due to the dissociation of the biochars phenolic -OH group, thus increasing the net negative charge on their surfaces [486].

Microbial contaminants

Given the porous nature and high surface area of biochar, it can provide more surface-active sites for the removal of microbial contaminants from water through various mechanisms.

It was reported that biofilters could be used to remove both E. coli and Enterococci from natural storm water [565]. Forestry wood waste biochar produced at 700°C was able to remove E. coli by 96.6% in a bioretention columns [566]. In addition, biochar filters showed an excellent E. coli removal percentage than sand filters within a short period of time [566].

The presence of lipid-containing compounds, such as phospholipids and lipopolysaccharides, on the membrane of some species of bacteria makes these organisms hydrophobic [567,568] and the attachment to the surface via hydrophobic attraction is a common mechanism for the deposition of E. coli on biochar [565,566].

Table 1.13 summarizes the recent studies on the capability of various biochar for removing contaminants from water.

Table 1.13 – Summary of contaminants removal from water.

Biochar	Pyrolysis temperature (°C)	Contaminant	Temperature (°C)	pH	R (%)	q_{max} (mg g^{-1})	Isotherm	Mechanism/Effect	Ref.
Heavy metals									
Broiler litter	500	Cu	–	4.8	75.2	–	–	Chemisorption onto a negatively charged inorganic fractions	[229]
Broiler litter	500	Cd	–	4.8	21.7	–	–		
Broiler litter	500	Ni	–	4.8	10.1	–	–		
Broiler litter	500	Zn	–	4.8	16.4	–	–		
Broiler litter	700	Cu	–	4.8	95	–	–		[569]

Biochar	Pyrolysis temperature (°C)	Contaminant	Temperature (°C)	pH	R (%)	q_{max} (mg g^{-1})	Isotherm	Mechanism/Effect	Ref.
Broiler litter	700	Cd	–	4.8	82.3	–	–	Adsorption by inorganic constituents (e.g. phosphorus)	
Broiler litter	700	Ni	–	4.8	5.1	–	–		
Broiler litter	700	Zn	–	4.8	90.9	–	–		
Broiler litter	800	Cu	–	4.8	86.9	–	–	Adsorption by inorganic constituents (e.g. phosphorus)	[569]
Broiler litter	800	Cd	–	4.8	59.9	–	–		
Broiler litter	800	Ni	–	4.8	6	–	–		
Broiler litter	800	Zn	–	4.8	75.7	–	–		
Canola straw	400	Cu(II)	25	5	–	0.59a	Langmuir	Surface complexation with carboxylic and hydroxyl functional groups/Adsorption through electrostatic attraction operating between biochar surface and Cu	[570]
Cattle manure	100	Al	25	4,3	–	0.2424 a	Langmuir	Surface complexation of Al to oxygen containing functional groups and surface adsorption/coprecipitation	[571]
Cattle manure	400	Al	25	4,3	–	0.2963 a	Langmuir		
Cattle manure	700	Al	25	4,3	–	0.2432 a	Langmuir		
Corn straw	600	Cu(II)	22	5	–	12,52	Langmuir	Adsorption by inorganic constituents	[572]
Corn straw	600	Zn(II)	22	5	–	11	Langmuir		
Dairy manure	100	Pb	–	–	92.8	–	–	Precipitation with phosphate	[287]
Dairy manure	200	Pb	–	–	99.8	–	–		
Dairy manure	350	Pb	–	–	99.7	–	–		
Hardwood	450	Cu(II)	22	5	–	6.79	Langmuir	Adsorption by inorganic constituents	[572]
Hardwood	450	Zn(II)	22	5	–	4.54	Langmuir		
Miscanthus saccharifloru s	300	Cd(II)	25	7	–	11.4	Langmuir	Chemisorption/surface precipitation	[312]
Miscanthus saccharifloru s	400	Cd(II)	25	7	–	11.99	Langmuir		
Miscanthus saccharifloru s	500	Cd(II)	25	7	–	13.24	Langmuir		
Miscanthus saccharifloru s	600	Cd(II)	25	7	–	12.96	Langmuir		
Peanut straw	400	Cu(II)	25	5	–	1.40a	Langmuir	Surface complexation with carboxylic and hydroxyl functional groups/Adsorption through electrostatic attraction operating between biochar surface and Cu	[570]

Biochar	Pyrolysis temperature (°C)	Contaminant	Temperature (°C)	pH	R (%)	q_{max} (mg g^{-1})	Isotherm	Mechanism/Effect	Ref.
Pine needles	200	U(VI)	25	–	–	62.7	Langmuir	pH dependent adsorption	[573]
Pinewood	300	Pb(II)	25	–	–	3.89	Langmuir	Adsoption/diffusion into pores	[574]
Rice husk	300	Pb(II)	25	–	–	1.84	Langmuir		
Rice straw	100	Al	25	4.3	–	0.1309 a	Langmuir	Surface complexation of Al to oxygen containing functional groups and deposition of albite	[571]
Rice straw	400	Al	25	4.3	–	0.3976 a	Langmuir		
Rice straw	700	Al	25	4.3	–	0.3537 a	Langmuir		
Sludge	550	Pb(II)	25	–	–	–	Freundlich	Surface complexation with carboxyl and hydroxyl functional groups	[495]
Sludge	400	Pb(II)	25	5	–	–	Langmuir	Surface complexation with carboxyl and hydroxyl functional groups	[575]
Sludge	400	Cr(VI)	25	5	–	–	Freundlich	Cr (VI) reduction to Cr (III)	[575]
Soybean straw	400	Cu(II)	25	5	–	0.83a	Langmuir	Surface complexation with carboxylic and hydroxyl functional groups/Adsorption through electrostatic attraction operating between biochar surface and Cu	[570]
Spartina alterniflora	400	Cu(II)	25	6	–	48,49	Langmuir	Ion exchange	[576]
Sugar beet tailing	300	Cr(VI)	22	2	–	123	Langmuir	Cr (VI) reduction to Cr (III)	[494]
Switchgrass	300	U(VI)	25	3,9	–	2,12	Langmuir	pH dependent adsorption	[226]
Organic contaminants									
Broiler litter	350	Deisopropylatrazine	–	5,5	–	3.27b	Freundlich	Sorption due to aromaticity and high surface area	[549]
Broiler litter	700	Deisopropylatrazine	–	5,5	–	5.89b	Freundlich		
Dairy manure	100	Atrazine	–	–	27,7	–	–	Partitioning to organic C	[287]
Dairy manure	200	Atrazine	–	–	77,3	–	–		
Dairy manure	350	Atrazine	–	–	33,9	–	–		
Eucalyptus	400	Methylene blue dye	40	–	–	2,0	Langmuir	Monolayer chemical and physical adsorption	[577]
Maize straw	300	Oxytetracycline	25	5,5	–	759.4b	Freundlich	Sorption to biochar surfaces	[578]
Palm bark	400	Methylene blue dye	40	–	–	2,95	Langmuir	Monolayer chemical and physical adsorption	[577]
Peanut shells	300	Trichloroethylene	25	–	–	12,12	Langmuir	Sorption	[167]

Biochar	Pyrolysis temperature (°C)	Contaminant	Temperature (°C)	pH	R (%)	q_{max} (mg g^{-1})	Isotherm	Mechanism/Effect	Ref.
Peanut shells	700	Trichloroethylene	25	–	–	32,02	Langmuir		
Peanut straw	350	Methyl violet	25	–	–	256.4a	Langmuir	Interaction with phenolic and carboxylic functional groups	[486]
Rice hull	350	Methyl violet	25	–	–	123.5a	Langmuir		
Soybean stover	300	Trichloroethylene	25	–	–	12,48	Langmuir	Sorption	[167]
Soybean stover	700	Trichloroethylene	25	–	–	31,74	Langmuir		
Soybean straw	350	Methyl violet	25	–	–	178.6a	Langmuir	Interaction with phenolic and carboxylic functional groups	[486]
Swine manure	400	Paraquat	25	–	–	14.79	–	Sorption due to increased negatively charged surface	[579]
Wastewater sludges	550	Fluoroquinolone antibiotics	25	–	80–96	19.8	Freundlich	Sorption	[580]

1.2.4.3 Other uses

In addition to the goals of carbon storage, soil improver and contamination control, there is growing interest in the use of biochar for other value-added applications, as fillers for composites, catalysts or materials for electronic, bioenergy applications etc. [16,165,177,237,581]. The versatile properties of biochar make it possible to use it also in metallurgical processes and in the chemical and pharmaceutical industries [177]. The main applications that the researchers are studying for biochar are summarized in Table 1.14.

Table 1.14 – Other uses of biochar.

Use	Description	Reference
Additives for anaerobic digestion and composting	Biochar can be used as an additive for anaerobic digestion reducing the CO2 content in the biogas, contributing to the buffering capacity of the system and forming a surface area for the colonization of microbial cells. Additionally, biochar improves the digestate quality through the retention of nutrients, enriches the micro and macronutrients in the digestate, making it appropriate for the use of fertilizer. Biochar has the capacity to catalyze anaerobic digestion by mitigation of mild ammonia inhibition, support of archaeal growth and methanization of the biochar labile carbon.	[21,582–584]
Animal feeding	The use of biochar as a feed additive has the potential to improve animal health, feed efficiency and livestock productivity, to reduce nutrient losses and GHG emissions and to increase manure quality. The analysis of scientific articles on biochar feed supplements has revealed that for farm animal species, positive effects on different parameters (i.e. growth, digestion, feed efficiency, toxin adsorption, blood levels, meat quality and emissions) could be found. In a program, biochar was provided as a dietary supplement to 60 cows, and the findings were the potential to reduce costs for the farmer, to improve soil properties, and to improve pasture health. Animals cause GHG emissions due to the anaerobic decomposition of their liquid and solid excretions, while ruminants cause direct methane emissions through flatulence and burps. Feeding of biochar might reduce cattle methane emissions by 10 to 12.7%. Biochar and its b wood vinegar by-product have disease resistance and antibacterial effects.	[585–589]

Use	Description	Reference
Biomedical applications	Activated charcoal has shown its functionality in preventing the gastrointestinal absorption of many toxic agents and drugs. Studies have demonstrated that activated biochar can prevent systemic absorption of drugs when administered within 1-2 h of ingestion or longer after ingestion of sustained-release preparations.	[590–593]
Electrochemical energy storage	Several researchers used different biochars for the production of supercapacitors. Results are encouraging and show that biochar can be used as an electrode due to its abundant and low-cost raw materials, flexible preparation methods, non-toxicity, biodegradability, high chemical stability. Thanks to its large specific surface area and large pore structure, it facilitates the rapid penetration of electrolytes to enable rapid electron transfer for charge storage and delivery. It can be used directly or as a template in the field of rechargeable battery systems by blocking the dissolution of the reaction intermediates in lithium-sulfur batteries.	[594–597]
Fuel cell systems	Biochar can be used to generate electricity in a Direct Carbon Fuel Cell system, an efficient device that converts the carbon fuel directly into electricity with 100% theoretical efficiency. An experiment has shown that using as fuel a biochar issued from almond shell carbonization has been achieved a peak power density of 127 mW cm2 for a cell performance at 700 °C. In another study biochar from the pyrolysis of corn cob was used and the maximum power output reached 185 mW cm2 at 750 °C.	[598,599]
Gas biofiltration (adsorbents)	Biochar can be converted into activated carbon, for example through the chemical activation of biochar by KOH, which is an effective method of developing highly microporous activated carbon, comparable to commercial one. Activated carbons are used in air purification systems for removing trace or dilute organic impurities, solvent vapours, hydrocarbons, odour forming compounds from air or other industrial gases by selectively adsorbing the impurity. Adsorption by activated biochars provides an efficient technology for the removal of volatile organic compounds (VOC) from air pollution sources due to their large specific surface areas, high micropore volumes and rapid adsorption capabilities.	[600–602]
Precursor of catalysts	Due to its high specific surface area, biochar can be used as a supporting material or catalysts in various spheres such as power generation, waste management, biorefinery (syngas production, tar removal, biodiesel production). By providing more active sites for reactions, biochar-based materials act as catalysts and mineralize or reduce pollutants to derived products with less toxicity and better degradability.	[603–606]
Specialty materials manufacturing	Biochar is a promising candidate for the synthesis of new carbon-based materials with a wide variety of potential applications such as carbon nanotubes, graphitic carbon materials, nanocells, olivary carbon particles, ellipsoidal carbon microparticles and mono-dispersed carbon microspheres from biomass and organic wastes. Another application being tested is the use of biochar as a filling material to develop biocomposites with improved thermal and mechanical properties.	[177,264,607]
Carbonized bio-coal	Biochar has desirable combustible properties, exhibiting H/C and O/C ratios and calorific value comparable to coal. Growing evidence from studies on the mixed combustion of coal and biochar showed that biochar could efficiently reduce the ignition and burnout temperatures of fuel blends and improve their conversion efficiency and combustion characteristics. This revealed that biochar could be used in the future for the co-firing of charcoal for large boilers. Biochar molding has been proposed as a practical energy strategy to improve the volumetric energy density of powdered biochar and reduce particulate formation during combustion. Chen et al. (2011) developed "carbonized biofuel" to replace fossil fuels in China's rural energy regeneration process.	[274,564,608,609]

1.2.5 Biochar activation and modification

In many cases, it is required to modify the biochar surface to enhance its affinity with target pollutants and increase its adsorption capacity, and further to improve the removal rate of contaminants from contaminated water.

The big number of studies available on biochar must be appropriately used to select the most suitable one for the environmental project; furthermore, the possibility of using engineering methods to be able to select increasingly specialized biochar for the various areas [610,611], should not be underestimated [137,612].

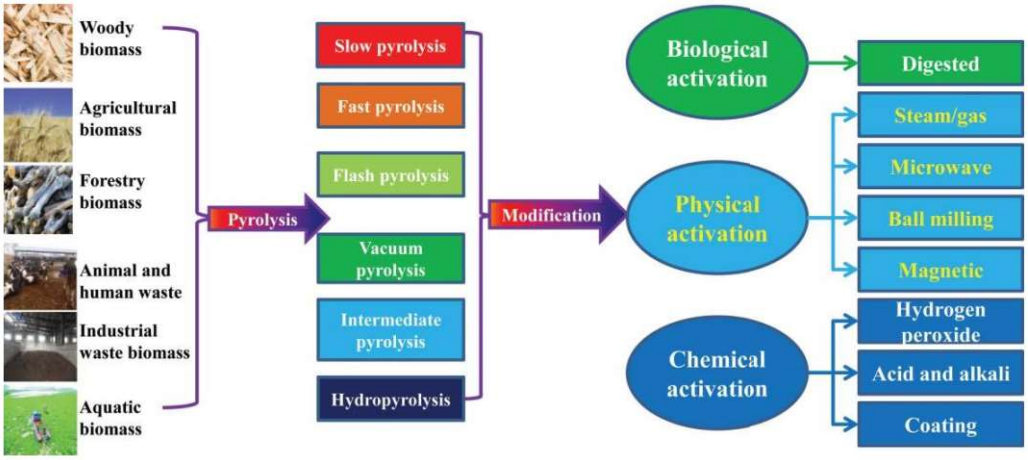

Figure 1.6 – Some engineering methods for biochar production.

For this purpose, it is important to know what conditions the functionality of biochar, starting from the material with which it is produced [613–616], the technology with which it is made [206,617] and the operating condition [172,615,618], the possible modifications to which it can be subjected [31,612,619] for the specific use consequential (Figure 1.7).

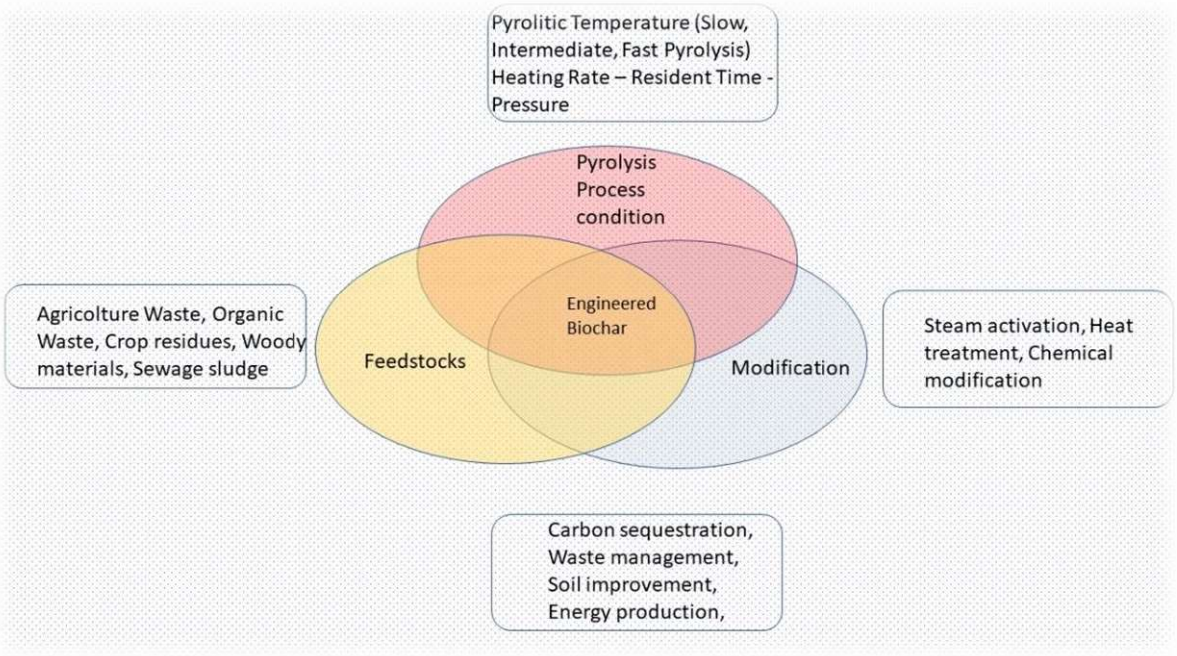

Figure 1.7 – Biochar: origin, preparation, modification and use.

Therefore, the effectiveness of biochar in the various environmental fields can be increased by suitably modifying its characteristics through the activation or chemical-physical modification of the product [5,620]. Some modification methodologies [8,612] are shown in Table 1.15.

Table 1.15 – Some biochar methodologies modification/activation.

Modification Method	Mechanism	Reference
Chemical Oxidation	Introduction of an acidic functional group on the biochar surface	[562]
H_2O_2 Modification	Increased Carboxyl Groups	[1]
KOH modification	Increase of surface area and changes of porous texture	[300]
Physical activation	Improved the pore structures, higher surface area, larger surface area and pore volume, increase in sorption capacity	[621]
Steam Activation	Suppress CH_4 and NO_2 emission. Increase sorption capacity	[621]
Mineral addition	Enhanced carbon retention and stability of biochar with mineral treatment due to enhanced formation of aromatic C	[622]
Magnetic Modification	Significantly improved sorption capacity	[623]

These methods increase its specific surface area and pore fraction and create new functional groups prior to use. The administration of steam flows has shown positive effects on nutrient retention and adsorption properties related to the increase of the specific surface. Also, the use of magnetization has shown an improvement in the adsorption capacity of organic contaminants and inorganic anions.

The most widely used method is the chemical one. It mainly includes acid modification, alkalinity modification, oxidizing agent modification, metal salts or oxidizing agent modification and carbonaceous materials modification.

The activation methodology must be chosen based on the wanted effects. In remediation, it must be considered the type of contaminant, the environmental situation and the final goal that can be reached.

By narrowing the field down to soil heavy metal pollution, it is well known that the main mechanism that allows the decontamination of these pollutants is adsorption, which includes several mechanisms such as ion exchange, physical and chemical adsorption, complexation, precipitation and so on. In this specific case, the biochar will have to be modified, for example, using a technology that allows increasing the functional groups on its surface and the pore volume to increase the adsorption capacity such as magnetic or steam modification [28].

In aqueous solution, instead, it must be taken into account the inner and outer share complexation, the electrostatic interaction, the ionic exchange and precipitation and so physical or chemical activation are the most suitable methods that can be used to develop these removal mechanisms [624].

1.2.6 Regeneration of biochar

Furthermore, biochar offers the possibility of being regenerated after use, in generally biochar regeneration is an inverse process of adsorption. Dai et al. (2019) reviewed regeneration methods of sorting the biochar [500].

The regeneration of biochar and the reduction of cost can be achieved by adopting different technologies to treat different biochar. The main regeneration methods and their advantages and disadvantages are shown in Table 1.16 [500].

Table 1.16 – Main regeneration methods features.

Regeneration method	Scope of application Advantages	Advantages and disadvantages	Ref.
Thermal regeneration	Widely used in industrial and sewage treatment plants Suitable for the desorption of pyrolyzable organics.	Advantages: regeneration process is more mature; low cost; strong economic applicability. Disadvantages: higher carbon loss rate.	[625]
Solvent regeneration	Simple device flow and used a lot in industry Desorption of adsorbate suitable for the treatment of refractory organics.	Advantages: simple process and equipment. low operating cost when using inorganic solvent. Disadvantages: the corrosion of equipment is serious; regeneration liquid could cause secondary pollution.	[626,627]
Microwave irradiation	Currently in the research and experimental stage Not yet applied on a large scale in industry.	Advantages: regeneration time is short; the heating temperature is easy to control. Disadvantages: complex equipment; high cost.	[31,628,629]
Supercritical fluid regeneration	Suitable for adsorption of highly volatile substances.	Currently in the experimental stage, the process is complicated.	[630]

However, studies on biochar regeneration are few and still at an early stage. Currently the cost seems to be high, but the future perspectives are positive and make biochar an even more interesting material also from the circular economy point of view.

1.2.7 Biochar in the circular economy

The circular economy is one of the most central issues of the 21st century. According to Preston (2012), "*circular economy is an approach that would transform the function of resources in the economy. Waste from factories would become a valuable input to another process – and products could be repaired, reused or upgraded instead of thrown away*" [631]. Thanks to its systemic and holistic nature, the circular economy is a new business model and a new way of seeing products and services, in clear contrast to the concept of traditional linear economy. The primary focus of the circular economy is the reduction of resource consumption, pollution and waste in each step of the life cycle of the product [632].

Biochar, is a carbon negative climate change mitigation technique because it is able to sequester more carbon than it emits to produce energy. Its peculiarities have led it to be included in the agenda of the next international negotiations on climate change as a climate change mitigation strategy. In addition, also in terms of circular economy, biochar can play a very important role from various points of view.

What was previously considered a waste, today is instead a valuable secondary raw material, usable in various fields, from agriculture as a soil improver to the other applications examined in paragraph Uses and Benefits.

Use of biochar represents a more economically and environmentally sustainable alternative because it offers a new opportunity for the reuse of green wastes from agriculture and forestry, or in general from organic waste such as sewage sludge. Therefore, its use completely fits the goals of the circular economy which require to limit waste materials and associated environmental issues, transforming them into valuable resources.

Agricultural waste is often directly associated with the cultivation and collection of products with nutritional value or with their processing.

The conversion of different types of biomass into value-added products via thermochemical conversion has many advantages [633]:

It allows the production of renewable energy, replacing that produced using fossil fuels. This permits to reduce carbon dioxide (CO_2) from the atmosphere and help to mitigate climate change by reducing GHG emissions.

It prevents these types of materials from being landfilled with potential environmental hazards such as surface and groundwater pollution, odors and other noxious gases, and degrading under conditions that can lead to the emission of greenhouse gases such as methane and nitrous oxide [634];

It prevents direct combustion in open-air of the materials by users with no pollution or particulate controls. In fact, in many countries, agricultural waste such as stalks, leaves and husks are burned to reduce agricultural residues [635];

When used as a soil improver, biochar allows to reduce the quantity of conventional fertilizers, and, when used as an alternative of commercial adsorbents, it allows to avoid the environmental impact of the industrial activities related to their production.

To conclude with respect to the above, biochar is easier to prepare and less expensive than active AC [205] [22,636].

Figure 1.8 shows a general picture of the entire biochar supply chain, in which real-scale applications and those currently being researched are represented, together with the potential of this material in environmental and circular economy terms.

The entire biochar concept can be a solution that will allow countries, companies and consumers to reduce damage to the environment and close the product life cycle through three main approaches of reuse, reduction and recycling of materials, energy and waste.

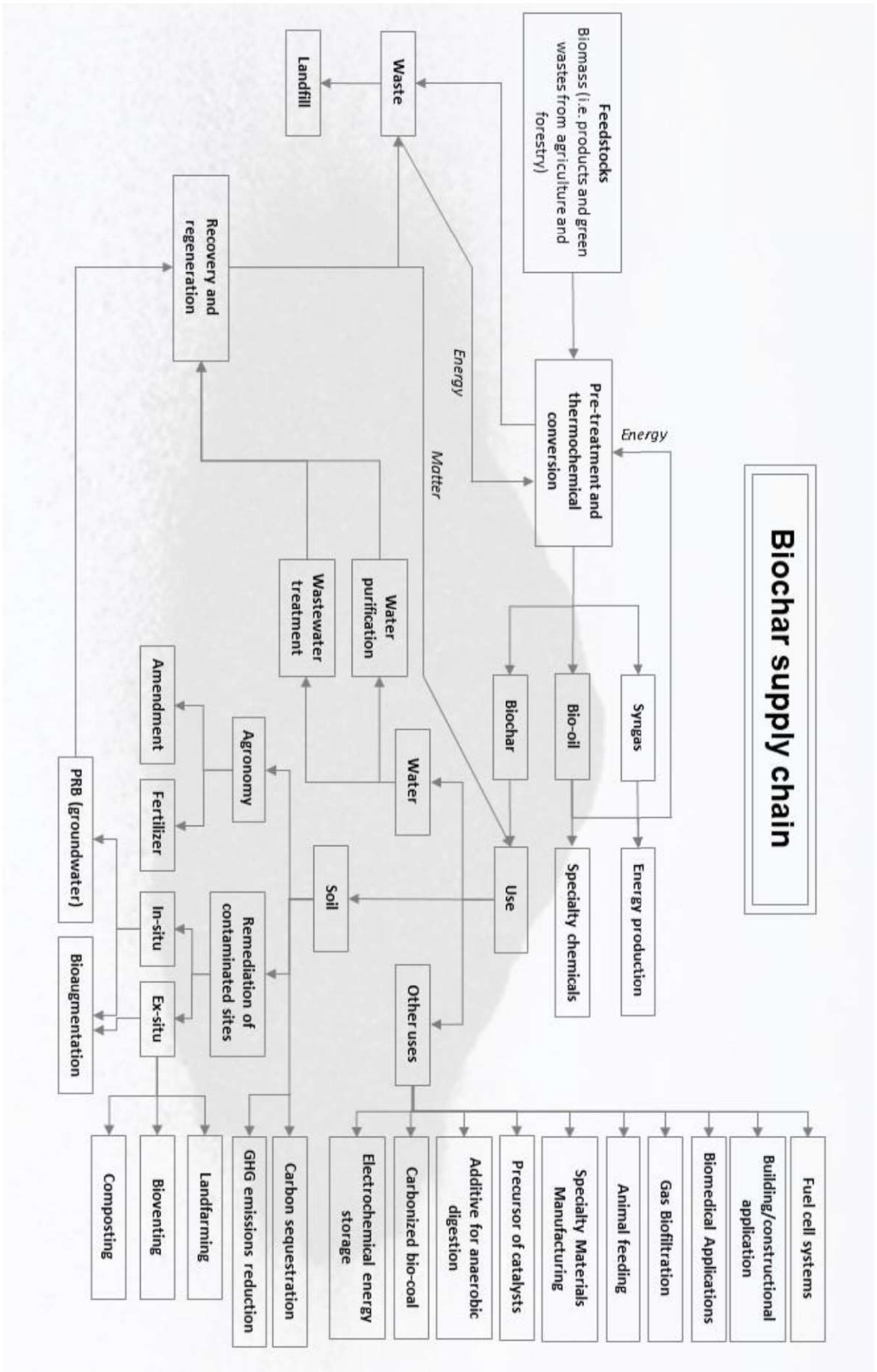

Figure 1.8 – General framework of the biochar supply chain.

1.3 Objective of the Ph.D. thesis

The present Ph.D. thesis has set itself the goal of studying the behaviour of biochar as a possible adsorbent media for heavy metals removal from contaminated water.

In particular, it was verified that this material represents a valid alternative - from the point of view of sustainability, economy, efficacy, efficiency and eco-compatibility - to activated carbon and adsorbent media currently on the market, used in the field of treatment technologies of contaminated water.

To this end, a laboratory-scale analysis, characterization and validation methodology was developed, aimed at studying these materials.

The research was mainly based on experimental activity, after an accurate bibliographic research and acquisition of the literature data, at a multidisciplinary level, in order to understand the emerging research fields of environmental engineering concerning biochar and its multiple use.

The first phase of experimental activity will be focused on the determination of the main physical-chemical characteristics of biochar, also carrying out a comparison with a commercial activated carbon.

In the successive phases, experimental tests were carried out aimed at the removal of heavy metals (lead and arsenic were selected as targets), using batch and column systems.

As regards the batch tests, the data, relating to experimental activities, will be interpreted through the most used models in the case of heavy metals adsorption from contaminated water, for the determination of kinetics and adsorption isotherms.

With regard to the experimentation in the column, breakthrough curves will be identified and the characteristic parameters of the system will be used to validate the obtained data.

Therefore, starting from the obtained experimental results, biochar may be considered as a useful alternative as adsorbent media for heavy metals removal from contaminated water.

Finally, some experimental hypotheses have been suggested in order to continue the research activity, with the aid of further targeted experimental tests.

2 Materials and methods

2.1 Biochar

RE-CHAR®, supplied by RECORD IMMOBILIARE S.r.l. (Lunano, Italy), is a biochar produced from a pyrolyzation process of virgin coniferous wood (mainly pine), conducted under the following operating conditions: 600 °C average gasification temperature, 750 °C effluent gas temperature and 300 °C inlet air temperature. The pyrolysis plant aimes at energy production, and generates biochar as a solid residue product; it is classified as Biochar class A1 according to ISO 17225- 4: 2014 from forestry.

AMBIOTON® (or BIOTON®), supplied by the LATERIZI REATO S.r.l., is produced by a wood biomass pyrolysis process, at a temperature below 750 °C, in a controlled atmosphere with low oxygen content. Due to processing issues, semi-decorticated and large-sized wood was used, in particular poplar, oak, robinia, platanus, willow, apple, and pear wood; resinous wood like fir, larch, pine or conifers was not used. The biochar had a capacity of imbibition above 250% by volume, a specific weight ranging from 0.125 to 0.150, which was evaluated on the anhydrous product after the production process at humidity less than 7%.

Figure 2.1 – AMAMBIOTON® and RE-CHAR® logo.

Both two biochar (AMBIOTON® and RE-CHAR®), provided by the two Italian companies (RECORD IMMOBILIARE Srl and LATERIZI REATO Srl), who have duly completed the registration in the "Register of fertilizer manufacturers" and "Register of fertilizers ", established by the Ministry of Agricultural, Food and Forestry Policies, for the purposes of product traceability, following the amendments to annexes 1, 2, 3, 6 and 7 of Legislative Decree n. 75, containing: «Reorganization and revision of the regulations on fertilizers, pursuant to article 13 of the law of 7 July 2009, n. 88."

Figure 2.2 – RECORD IMMOBILIARE Srl and LATERIZI REATO Srl logo.

Table 2.1 compares Italian limit value established for biochar and the values declared by the companies using official documents made available, by the two companies compares some chemical-physical parameters of the material.

The comparison takes place between them and the Italian limit value established for biochar. Being two Italian companies, the limit present in Italian legislation was considered as a limit, through official documents of the ICHAR (Italian Biochar Association) so as to more easily notice the difference between the two products as the limits are much more restrictive than the American limits or of some European nations.

Table 2.1 – Comparison between main physical and chemical properties of biochar.

Chemical-physical parameters	Italian limits	AMBIOTON®	RE-CHAR®
Salinity (electrical conductivity) ms m^{-1}	≤ 1000	430	<1000
pH (H_2O)	4 - 12	10.4	<12
Humidity %	≥ 20	6.9	>20
Ashes %	Quality class 3 (40 – 60) Quality class 2 (30 – 60) Quality class 1 (<10)	25	<30
H/C (*mole fraction*)	≤ 0.7	0.35	0.1
Maximum water retention %	n.r.	265	>80

** Data from: ICHAR, Italian Biochar Association; Laterizi Reato s.r.l Documents; Record Immobiliare s.r.l. Documents*

It is noted that the two products are different in all the parameters considered but the values that have the greatest impact are salinity, as well as electrical conductivity, and maximum water retention.

Table 2.2 compares the chemical parameters of both biochars (Figure 2.3), the unit of measurement and the related method for the determination of the specific parameter.

Table 2.2 – Chemical properties of AMBIOTON® and RECHAR®.

			AMBIOTON®		RE-CHAR®	
Parameters	**Symbol**	**Unit**	**Value**	**Methods**	**Value**	**Methods**
Nitrogen	N	%	0.2	UNI EN ISO 16948:2015	0.39	UNI EN ISO 13654-2:2001
Cadmium	Cd	mg g^{-1} s.s.	<0.5	DM 17/06/2002 GU n°220	<1	UNI EN 13650:2002 ISO 11885:2007
Copper	Cu	mg g^{-1} s.s.	25	DM 17/06/2002 GU n°220	62	UNI EN 13650:2002 ISO 11885:2007
Mercury	Hg	mg g^{-1} s.s.	<0.5	EPA 3050B 1996 EPA 7471B 2007	<1	UNI EN 16174:2012 UNI CEN/TS 16175-1:2013
Nickel	Ni	mg g^{-1} s.s.	7	DM 17/06/2002 GU n°220	22	UNI EN 13650:2002 ISO 11885:2007
Lead	Pb	mg g^{-1} s.s.	82	DM 17/06/2002 GU n°220	18	UNI EN 13650:2002 ISO 11885:2007
Zinc	Zn	mg g^{-1} s.s.	257	DM 17/06/2002 GU n°220	174	UNI EN 13650:2002 ISO 11885:2007

			AMBIOTON®		RE-CHAR®	
Parameters	**Symbol**	**Unit**	**Value**	**Methods**	**Value**	**Methods**
Hexavalent Chromium	Cr VI	mg g^{-1} s.s.	<0.5	DM 08/05/2003 GU n°116	<1	EPA 3550C 2007 EPA 7196 A 1992
Potassium	K	% s.s	2.2	UNI EN 16174:2012 UNI CEN/TS 16170:2013	3.52	UNI EN 13650:2002 ISO 11047:1998
Phosphorus	P	% s.s.	0.21	UNI EN 16174:2012 UNI CEN/TS 16170:2013	0.64	UNI EN ISO 13650:2002 ISO 11885:2007
Calcium	Ca	% s.s.	7.3	UNI EN 16174:2012 UNI CEN/TS 16170:2013	7.59	UNI EN 13650:2002 ISO 11047:1998
Magnesium	Mg	% s.s.	0.55	UNI EN 16174:2012 UNI CEN/TS 16170:2013	0.55	UNI EN 13650:2002 ISO 11047:1998
Sodium	Na	% s.s. mg kg^{-1} s.s	0.17	UNI EN 16174:2012 UNI CEN/TS 16170:2013	2.734	UNI EN 13650:2002 ISO 11047:1998
Carbon	C	%	67.7	UNI EN 16948:2015	58.9	D.L. 7276/2016
Hydrogen	H	%	2.0	UNI EN 16948:2015	n.r.	
IPA (polycyclic aromatic hydrocarbons)		mg kg^{-1} s.s.	n.r.		<1	EPA 3545 A 2007 EPA 8270 D 2014
PCB (polychlorinated biphenyls)		mg kg^{-1} s.s.	n.r.		<0.25	EPA 3550 C 2007 EPA 8270 D 2014

**Data from Laterizi Reato s.r.l. and Record Immobiliare s.r.l.*

It can be shown in Table 2.2, which also being similar, show substantial differences. RECHAR® has a Copper value three times higher, as well as for Nickel and Phosphorus while it is evident that AMBIOTON® is much richer in Lead (+ 355%) and Zinc (+ 47%).

2.2 Activated carbon

CARBOSORB NC 1240 from COMELT is a granular activated carbon, produced from coconut shells by physical activation (gasification, T > 900 °C). This coal is suitable for the removal of organic micropollutants (chlorinated solvents, chlorine, etc.), as well as compounds that cause odours and flavours, in the water purification processes.

The CARBOSORB NC 1240 is complies with the UNI EN 12915-1: 2004 standard "Granular Activated Carbon for use for the treatment of water for human consumption". By virtue of the porous structure and high mechanical strength, the CARBOSORB NC 1240 can be thermally reactivated.

Table 2.3 describes the parameters and chemical-physical characteristics of the material through official documents granted by the company, specifying the scientific method used to perform the measurement of the parameter and the value declared by the factory.

Table 2.3 – Physical and chemical properties of CARBOSORB NC 1240.

Parameters	Methods	Unit	Declared data**
Iodine index	AWWA B0804	mg g^{-1}	>1.000
Methylene blue index	CEFIC (DAB IV)	mg g^{-1}	18
CCl4 Specific surface (*Carbon tetrachloride*)	Astm D3467	%	70
Specific surface (B.E.T)	Astm D3663	$m^2 g^{-1} g$	1.150
Granulometry	Astm D2862	Mesh	12 x 40
	-	mm	0.425 – 1.700
	> 12 Mesh	%	5 max
	< 40 Mesh		5 max
	> 50 Mesh		1 max
Apparent density	Astm D	kg m^{-3}	500 ± 20
Moinsture content	Astm D	%	5 max.
Hardness	Astm D	%	> 98
Ashes (water soluble)	Astm D	%	< 2
pH	Astm D	-	10 ± 2

** *Data from COMELT technical folder - Document n°: ST-CFG-NC1240*

Figure 2.3 – Carbon-based sorbent investigated for physical-chemical characterization.

2.3 Characterization of carbon-based sorbents

Characterization in the field of materials science is necessary and fundamental to have a scientific understanding of the materials to be used.

The characterization of a material is essential for its subsequent use because let to define a correct use in environmental processes and also to improve the production process [637–640]. The physical chemicals analyses carried out onto the material depending on its application field and use [636].

The analyses highlight the composition of the material, the structure properties of its transformation processes and the adsorption capacity with special reagents and elements [641–644]. Furthermore knowing the chemical composition of a material guarantee the quality and safety of a final product [645], with attention to the environment and the health of consumers, [646–648].

Physical-chemical analyzes carried out on carbon-based materials were particle size distribution, pH, Scanning Electron Microscope, Cation-Exchange Capacity, Anion-Exchange Capacity, Atomic Force Microscope and others. The results were compared with other studies on similar materials permeating to define the potential of the analyzed materials according to their use.

The analysis carried out made possible to know the characteristics of the materials in an effective and efficient way [649,650].

2.3.1 Composition and particle size distribution

The particle size distribution (PSD) is a fundamental parameter as it characterizes the grain size of the coal and provides an indication of the uniformity of its dimensions. In general, larger dimensions lead to lower pressure drops but slower adsorption kinetics.

Particle size distribution of the material was determinate by sieving. About 30 g of activated carbon was sieved by different diameter size sieves, and the fraction of solid retain in each sieving interval was weighed considering the percentage of the material withheld from the total. The sieving was carried out in the most appropriate the range of sizes taking account the technical data sheets of the carbonaceous materials.

2.3.2 Density, bulk density and specific weight

Bins containing 25 mL of H_2O and known quantities of carbonaceous material were weighed and subjected to a stirring process. Blank samples were weighed before and after the addition of the material. Subsequently a quantity of water was added until reaching the initial volume and weighed again.

2.3.3 Water content, volatile matter, ash content and fixed carbon

All experiments were performed on a TA Instruments SDTQ600 TG-DSC electronic thermobalance, which can reach a maximum temperature of 1600 °C and heating rates from 0.001 to 50 °C min^{-1}. To avoid limitations on mass and heat transfer, about 10 ± 10^{-6} kg of sample and uncovered platinum crucibles were used [651]. All experiments were initially conducted under an inert nitrogen flow at a rate of 45 mL min^{-1} to prevent the samples from oxidizing and to determine the moisture and volatile material concentration. Next, dry air (45 mL min^{-1}) was used to determine the ash content.

The water (or moisture) content was determined by heating the sample to ≈105 °C in an N_2 atmosphere until a constant weight was reached. The moisture content (θ) was obtained from the following equation:

$$\theta\ (\%) = 100 * \left(\frac{m_1 - m_2}{m_1}\right) \quad (1)$$

where θ (10^{-6} kg) is the difference between the initial mass (m_1) of the sample and the constant mass (m_2) at ≈105 °C. Volatile matter was determined as weight loss due to heating from ≈105 °C to ≈600 °C in an atmosphere of N_2. The volatile content (VM, %) was calculated according to the following equation:

$$\text{VM (\%)} = 100 * \left(\frac{m_2 - m_3}{m_1}\right) \quad (2)$$

where m_3 (10^{-6} kg) is the mass of the sample at ≈600 °C. Ash is the residual inorganic matter remaining after combustion and the ash content (ASH, %) was obtained from the equation:

$$\text{ASH (\%)} = 100 * \left(\frac{m_4}{m_1}\right) \quad (3)$$

where m_4 (10^{-6} kg) is the mass remaining after the passage to dry air. Subsequently, the amount of fixed carbon (FC, %) was determined by the formula:

$$\text{FC (\%)} = 100 - \theta - \text{VM} - \text{ASH} \quad (4)$$

where ASH, VM and FC were calculated on the dry weight basis and θ was calculated on the wet basis.

2.3.4 Conductance

The conductance, S (Ω^{-1}), was misused using a conductivity meter FiveEasy FE30.

2.3.5 Ion exchange capacity

To measure Cation exchange capacity (CEC, cmol(+)/kg_{DW}): 1 g each of material carbonaceous and 42 mL of $BaCl_2$ were put in contact and stirred for 90 minutes and subsequently subjected to an evapotranspiration process in the oven for 24 hours. After filtration with $MgSO_4$, and consequently stirring and filtration, 10 mL of each sample were recovered and the solution was prepared with 100 mL of H_2O, 10 mL of NH_4Cl (ammonium chloride) and eriochrome black used as indicator. This solution was titrated by adding EDTA (Ethylenediaminetetraacetic acid) until the color change was found depending on the addition of EDTA. The measurement is based on how many mL of EDTA have been added to the solution. A neutral sample was also analyzed, without the addition of carbon inside and was composed of: 100 mL of H_2O, 10 mL of $MgSO_4$, 10 mL of NH_4Cl and eriochrome black.

Anion exchange capacity (AEC, cmol(+)/kg_{DW}) was measured putting in contact 0.1of each carbonaceous material and 50 mL of different solutions. Six different samples were prepared, each one containing a substance in quantities calculated in 50 mL, containing 0.1 g of the different carbon-based sorbent. The quantities of substance it adds are:

- 600 mg L^{-1} of K_2SO_4;
- 600 mg L^{-1} of NaCl;
- 600 mg L^{-1} of Na_2CO_3;
- 450 mg L^{-1} of $NaNO_3$;
- 450 mg L^{-1} of $NaHCO_3$;
- 450 mg L^{-1} of $NaHPO_4$.

Through a stirring process with a magnetic stirrer, the samples were subjected to titration by adding an EDTA reagent, in order to determine the amount in mL of reagent added.

2.3.6 pH analysis

The pH (potential of Hydrogen) of the solution affects the surface charge of the carbon by altering the electron density of the graphite layer, consequently modifying its polarity and therefore its adsorbing properties towards hydrophobic molecules [192].

The pH of the solution, in turn, is influenced by the acid-base characteristics of the surface functional groups of the coal. Other studies [652] argue that generally a neutral pH of the solution favours the adsorption of halogenated aliphatic organic compounds. Furthermore, they state that the point of zero charge (pH_{PZC}) of a carbon-based sorbent depends on the pH of the solution and the type of activation treatment received.

pH_{PZC} is defined as the pH value of a water/solid suspension, in correspondence with which an equal adsorption of the H^+ and OH^- ions (called "*potential determining ions*"). Under these conditions the electric charge present on the surface of the solid may not be zero. The condition in which the positive and negative charges on the surface of the solid are equivalent is instead identified by a pH value which is indicated by pH_{IEP} (iso-electric point) [653,654].

Consequently, for pH values of the solution lower than the pH_{PZC} value, the external surface of the carbonaceous materials will be positively charged, vice versa for pH values higher than the pH_{PZC}. In conclusion, carbons with a pH_{PZC} above 7 are basic; but given that the surface charge may depend on the pH of the solution, it follows that the carbons are amphoteric solids [655].

The analysis method involves entering known quantities of samples of carbonaceous materials (the suggested values are 0.01, 0.1, 1, 5, 10 % by mass) in 45 ml of 0.1 M H_2O solution with a known initial pH: as the quantity of carbon-based sorbent increases, the pH of equilibrium of the solution tends progressively to an asymptotic value which is, in fact, the pH_{PZC}.

2.3.7 Elemental analysis

CHNOS elemental analyzer, determine the percentage content of total hydrogen (H), nitrogen (N), carbon (C), sulphur (S) and oxygen (O). CHNOS elemental analysis technique is based on the combustion of the sample. During combustion, the sample produces uniform gaseous compounds consisting of the elements C, H, N and S. These combustion products (e.g., CO_2, H_2O, NO_2, etc.) are determined using gas chromatography and the ratio of the elements present in the original sample is determined accordingly. The quantities of C, H, N and S can be determined simultaneously, while the presence of O can be examined later by pyrolysis. In order to have a significant sample of material to be analysed, the samples have been homogenized and finely ground; the analyses are repeated three times and the average values have been reported.

XRF (X-Ray Fluorescence) is a technique that allows you to identify the chemical elements that make up a sample, using x-rays and the radiation emitted by it following atomic excitation with appropriate energy. The X radiation that hits the sample has a maximum energy of about 10 KeV and the information obtained comes from the most superficial layers of the sample, exactly the layers that the re-emitted characteristic radiation is able to cross. The main advantage is its ability to directly analyse solid and liquid samples, avoiding having to handle the sample or at least minimizing contact with it. However, XRF has a number of limitations especially when using aqueous samples, such as a short linear range, the requirement for closely matched standards to overcome matrix effects, and poor sensitivity [656]. This technique has also been used for the analysis of natural waters containing Hg Cr particles [657].

2.3.8 Boehm analysis

Functional groups present onto carbonaceous material were identified by Boehm analysis [654,658]. Practically 1 g of carbonaceous material was put in contact with 50 mL of different solution (0.05 M HCl, 0.05 M NaOH, 0.05M Na_2CO_3 0.05M, or 0.05M $NaHCO_3$) to determinate the presence of stirred until constant pH (approximately for 3 hours) filtered and titrated to evaluate the final concentration of the compounds measured the pH value.

2.3.9 Methylene Blue Index (MBI)

The methylene blue index (MBI) is a quantitative measurement of the adsorption of methylene blue dye (MB) on the surface of the carbon-based sorbents [659]. Results are normally expressed in milliequivalents of dye adsorbed per 100 grams of clay.

The absorbance of the sample prepared with 0.1 g of the carbonaceous materials in 50 mL of solution of H_2O, 10 mg L^{-1} of methylene blue was measured, after having centrifuged and left the carbon sample in contact with the solution for 24 hours and diluted 1: 100.

Methylene Blue Index was measured by spectrophotometry UV. Briefly 0.1 g of carbonaceous material and in 50 mL of a 10 mg L^{-1} solution of methylene blue was put in contact for 24 h centrifuged at 150 rpm. After thar the supernatant was diluted 1/100 and measured the absorbance of amount of dye adsorbed.

2.3.10 Iodine adsorption value (IV)

The iodine value (or iodine adsorption value or iodine number or iodine index, commonly abbreviated as IV) in chemistry is the mass of iodine in grams that is consumed by 100 grams of a chemical substance.

Above 0.1 g of carbonaceous material was added to 10 mL of 5% (V/V) HCl. Boiled for 30 s and then cooled at room temperature. Subsequently 100 mL of 0.1 N iodine solution is immediately added to carbonaceous material and stirred for 30 s. The suspension was filtered and 50 mL of the filtrate is titrated with 0.1 N ($NaSO_2O_3$) sodium thiosulphate solution using thyodene (or starch) as indicator. The amount of iodine adsorbed per gram of adsorbent is plotted against the residual iodine concentration, using logarithmic axes. If the residual iodine concentration is not within the range (0.008–0.04 N), the procedure is repeated using different carbon masses for each isotherm point. A regression analysis is applied to the three points and the iodine number is calculated as the amount adsorbed at a residual iodine concentration of 0.02 N.

2.3.11 Brunauer-Emmett-Teller (BET) analysis

Surface area and porosity are physical properties that affect the quality and behaviour of porous materials, produced by pyrolysis or gasification [660]. These characteristics can be derived from an 2.3.9 Brunauer-Emmett-Teller (BET) analysis.

The measurement is carried out at low temperatures and pressures and consists in evaluating the volume of gas adsorbed by the carbonaceous materials at various pressures.

The instrument with which the laboratory is equipped is the Micromeritics 3Flex 4.05 (USA), which performs the measurement of the specific surface using a continuous flow method of adsorbent gas (N_2) mixed with an inert gas (He) on a sample maintained at atmospheric pressure.

Figure 2.4 – Micromeritics 3Flex 4.05 (USA).

The measurement is based on the determination of the quantity of mixture adsorbed gas as a monomolecular layer on the sample under examination. The parameters and operating conditions adopted are shown in the Table 2.4 below.

Table 2.4 – Operating conditions adopted for Brunauer-Emmett-Teller (BET) analysis.

Operating conditions	CARBOSORB NC 1240	AMBIOTON®	RE-CHAR®
Sample mass (g)	1.7872	0.5830	0.3855
Analysis free space (cm^3)	63.9745	57.75486	57.4380
Low pressure dose	None	None	None
Automatic degas	No	No	No
Analysis adsorptive	N_2	N_2	N_2
Analysis bath temperature (°K)	77.297	77.296	77.296
Thermal correction	No	No	No
Ambient free space measured (cm^3)	16.0510	16.3163	16.5698
Equilibration interval (s)	10	10	10
Sample density ($g\ cm^{-3}$)	1.000	1.000	1.000

Degassing of samples was primarily applied and then N_2 adsorption-desorption was studied. Based on the N_2 isotherms collected at 77°K and employing the Brunauer Emmett-Teller (BET) equation, the surface area was calculated.

The BET model is based on several assumptions regarding solid-gas interaction. It is an extension of the Langmuir model valid in the hypothesis of multilayer adsorption on the surface of the solid. It hypothesizes the formation of gaseous multilayers on the surface of the coal following the contact of adsorbable gases and the surface of the three carbonaceous materials. [661]. The BET equation is presented below, in its linear form [662]:

$$\frac{1}{W\left(\left(\frac{P_0}{P}\right)-1\right)} = \frac{1}{W_m C} + \frac{C-1}{W_m C}\left(\frac{P}{P_0}\right) \tag{5}$$

Where W and W_m are, respectively, the weight of gas adsorbed and the weight of adsorbate as monolayer, P/P_0 is the relative pressure and C is the BET constant. The following are the formulas – equations (6) and (7) – obtained for the slope (m) and the intercepts (Q), starting from the plot of the variables of the linearized equation:

$$m = \frac{C-1}{W_m\ C} \tag{6}$$

$$Q = \frac{1}{W_m\ C} \tag{7}$$

From these it is possible to determine the weight of adsorbate as monolayer (W_m):

$$W_m = \frac{1}{s+i} = W\left(1 - \frac{p}{p_0}\right) \quad (8)$$

Total surface area (S_t) can then be derived [662]:

$$S_t\ (m^2) = \frac{W_m\ N\ A_{cs}}{M} \quad (9)$$

Where M is the molecular weight of adsorbate (mol), N is the Avogadro's number (6.023×10^{23} mol^{-1}) and A_{cs} is adsorbate cross sectional area (16.2Å^2 for N_2); therefore Specific Surface Area (S) is determined by the ratio between the total surface area and the sample weight (g):

$$S\ (m^2 g^{-1}) = {}^{S_t}/_{W} \quad (10)$$

Furthermore, BET equation can be linearized in the range 0.05 – 0.35 [663]:

$$\frac{\mathrm{P}}{W(\mathrm{P_0} - \mathrm{P})} = \frac{1}{W_m \mathrm{C}} + \frac{\mathrm{C}-1}{W_m \mathrm{C}} \frac{\mathrm{P}}{\mathrm{P_0}} \quad (11)$$

By plotting the first member as a function of $\frac{P}{W(P_0-P)}$ the constants C e W_m are obtained by the slope and the intercept. From the constant C, it is possible to deduce the average heat of adsorption of the first layer (E_1):

$$\mathrm{c} = \frac{\mathrm{e}^{(\mathrm{E1}-\mathrm{E_L})}}{\mathrm{RT}} \quad (12)$$

where E_L is the enthalpy of evaporation of the adsorbent. By introducing another parameter n, the maximum number of layers that can be adsorbed, the linearized equation becomes (with $x = \frac{\mathrm{P}}{\mathrm{P_0}}$) [663]:

$$W = \frac{W_m \mathrm{C\,x}}{1-\mathrm{x}} \frac{1 - (\mathrm{n}+1)\mathrm{x}^{\mathrm{n}} + \mathrm{n}\mathrm{x}^{\mathrm{n}+1}}{1 + (\mathrm{C}-1)\mathrm{x} - \mathrm{c}\mathrm{x}^{\mathrm{n}+1}} \quad (13)$$

The parameters W_m, c and n are obtained from experimental data by non-linear regression.

As for the pore volume, it was obtained using the t-plots and the Barrett–Joyner–Halenda (BJH) equations [664]. In fact, Barrett, Joyner and Halenda (1951) proposed a method for evaluating pore size distribution through the desorption isotherm [664]. The pore curve is expressed as a percentage change in pore volume ($\Delta V_p/\Delta r_p$) respect to the radius of the micropore (r_p).

In the area where capillary condensation is present, the radius of the cylindrical shaped pore (r_p) is the sum of the thickness of adsorption layer at the arbitrary pressure (t) and the radius of the nucleus of the meniscus part (r_k):

$$\mathrm{r_p} = \mathrm{t} + \mathrm{r_k} \quad (14)$$

The generalized equation for calculating the pore volume is [663]:

$$V_{p_n} = R_n \Delta V_n - R_n \Delta t_n \sum_{j=1}^{n-1} c_j * A_j \quad (15)$$

Where A_j is the average area from which the physically adsorbed gas is desorbed, c is a coefficient to be entered in accordance with the thickness of the physically adsorbed layer and Δt_n is the change in thickness of the physically adsorbed layer of a pore, obtained from the instrument. Furthermore:

$$c = \frac{r_p - t_r}{r_p} \text{ and } R_n = \frac{r_{pn}^2}{(r_{k_{n-1}} + \Delta t_n)^2} \quad (16)$$

Measurement of the surface area, pore size, and average volume of pores was achieved using a Micromeritics ASAP2020 accelerated surface area and porosimetry system.

2.3.12 Raman analysis

Raman spectroscopy is a materials analysis technique through a phenomenon of diffusion of an electromagnetic radiation by the analysed sample; in fact the Raman spectral response is sensitive to the microscopic structure of the carbonaceous material. For the acquisition of the Raman spectra, a micro-Raman spectrometer (SENTERRA, Bruker Optics) equipped with laser Nd-YAG ($\lambda 0$ = 532 nm) and a 20x objective (Olympus B41) was used.

2.3.13 Scanning electron microscope (SEM)

The morphological studies were carried out by scanning electronic microscopy (SEM) technique. The studies were carried out by a HR-FE-SEM (High Resolution Field Emission Scanning Electron Microscopy) Zeiss Auriga and FE-SEM (Field Emission Scanning Electron Microscopy) TESCAN Mira-3 scanning microscope [665].

Figure 2.5 – HR FESEM Zeiss Auriga at the CNIS (Research Center for Nanotechnologies applied to Engineering).

2.3.14 Energy-dispersive X-ray spectroscopy (EDS)

Energy-dispersive X-ray spectroscopy (EDS, EDX, EDXS or XEDS), sometimes called energy dispersive X-ray analysis (EDXA), indicates an analytical method that uses the emission of X-rays by an accelerated electron beam that affects the sample under examination. The analysis was performed using EDX (Energy Dispersive X-ray spectroscopy) EDAX and analyzed by software Team.

2.3.15 X-Ray Diffraction Analysis (XRD)

The XRD (X-Ray Diffraction) technique is one of the most widely used analytical techniques for the study of the crystalline structure of substances by exploiting the X-ray diffraction produced by the lattice of the material, information is obtained on the atoms that constitute it, on their distribution and on the distances between the reticular planes of the same.

The analysis was performed using a Philips X'Pert diffractometer (PANalytical B.V.). The diffractometer works at 40 KV and 40 mA with radiation CuKα1 with scanning range of 20–60° (2θ), step of 0.02° and counting time of 2 seconds.

2.3.16 Atomic force microscopy (AFM)

The atomic force microscope (AFM) is nowadays used for the study, at the scale of atomic dimensions, of the surfaces of compounds of various kinds: thin or thick films of ceramic materials, glasses, synthetic or biological membranes, metals, polymers etc. It has a resolution of 0.01-1 nm along the x, y axes and 0.01 nm along the z axis. With AFM it is possible to have the micro-topography of a sample on a scale that varies between 100 nm and 150 μm.

To obtain images by Atomic Force Microscope, a few mg of carbonaceous material was dispersed in deionized H_2O (between 20 and 40 mL). Once a stable suspension was obtained, an aliquot of sample was taken from the bin with a pipette and a drop was placed on the specific support for observations with the AFM.

2.4 Chemicals and reagents

All chemicals used are conform with the standard conditions of use and are stored correctly as required on the label of each product. All chemicals and reagents that have been used during laboratory tests are analytical grade and were used without any further purification; moreover they have been listed in the description of the analytical methods.

Pb^{2+} stock solution was prepared by dissolving lead(II) nitrate salt [$Pb(NO_3)_2$] – supplied by Carlo Erba, Milan, Italy; solubility in water = 52 g 100 mL^{-1}, at 20 ± 0.1 °C – into Milli-Q water (18.5 MΩ cm^{-1}).

As stock solution was prepared by dissolving accurately weighed quantity of a specific arsenic salt, respectively, meta-sodium arsenite ($NaAsO_2$) and disodium hydrogen arsenate heptahydrate ($Na_2HAsO_4{\cdot}7H_2O$), in order to obtain an As(III) and As(V) concentrated solution.

Lead (or arsenic) contaminated waters will be implemented through a subsequent dilution from the stock solution, in order to obtain the required concentrations for the experimental tests. The volumes used for the dilutions are obtained using the Eq. (17):

$$V_s * C_s = V_c * C_c \tag{17}$$

Where Vs and Vc are, respectively, the volume of the stock solution (L) and the volume of aqueous solution that we intend to prepare; Cs and Cc are, respectively, the concentration of the stock solution (mg L-1 or µg L-1); and the concentration of the contaminated water prepared (mg L-1 or µg L-1).

Stock solutions and contaminated waters were stored at 4 °C until their use.

2.5 Analytical Methods

In order to analyze lead contaminated waters, the samples were adequately filtered with a suitable vacuum filtration system and subsequently acidified (0.1 M HNO_3) to determine the concentration values (mg L^{-1}) by emission spectrometry with atomic absorption (F-AAS; Perkin-Elmer®, model 3030B), whose detection limit was 0.1 mg L^{-1}. The calibration curve was determined using Standard Methods-3230 [666] and standard solutions at 2 and 4 mg L^{-1} Pb. Samples were properly diluted using the relative method to fall within the instrument's calibration curve.

The arsenic samples were filtered by 1 µm and 0.45 µm syringe filters (25 mm FLL/MLL Acrylic Yellow and white membranes, GVS Filter Technology) and analyzed for the residual As total concentration in solution. Total arsenic concentration in the aqueous phases was determined using mass spectrometry with inductive plasma source (ICP-MS; Perkin-Elmer®, model NexION 300x), whose detection limit was 1 µg L^{-1}. The calibration curve was determined using Standard Methods-3125 [666] and arsenic solutions at four concentration (0, 10, 50 and 100 µg L^{-1} As).

pH and redox potential (ORP, mV) of the aqueous solution were measured using a pH-meter HACH HQ40D or a pH-meter Hanna Instruments HI2002-02 edge pH/ORP. pH meter was calibrated under non-agitated conditions with buffer at pH 4, 7 and 10, with Hanna certification. Any heavy metals percentage removal (R, %), adsorption capacity (mg g^{-1} or µg g^{-1}) at time t (q_t) and at the equilibrium time (q_e) were calculated through the following Eqs. (18) and (19) respectively, obtained through the mass balance of heavy metal between the liquid and the solid phases:

$$R(\%) = \frac{(C_0 - C)}{C_0} * 100 \quad (18)$$

$$q = \frac{(C_0 - C) * V}{m} \; or \; \frac{(C_0 - C)}{d} \quad (19)$$

where V is the volume of the aqueous solution (L); m is the mass of biochar (g); d is the dosage of biochar (g L-1); C0 and C (mg L-1 or µg L-1) indicate respectively heavy metal initial concentration in the liquid phase, and time = t (Ct) and equilibrium (Ce).

2.6 Pb and As Batch tests

The experiments are conducted in batch mode to analyse the kinetic and thermodynamic characteristics of the reaction between the contaminated waters and the investigated biochars and possible to study the adsorption process through the determination of the kinetic characteristics and the isotherms specifications.

All tests are conducted using a jar-tester apparatus (Figure 2.6) in a room with a controlled temperature (20 ± 0.1 °C), under a fume hood. All batch experiments were conducted in duplicate and the results obtained averaged.

Figure 2.6 – Flocculator VEPL mod. FC6S.

Batch tests for lead removal were conducted at 50 and 100 Pb mg L^{-1} as initial concentrations; these values were selected, being very high and far above the limits imposed by the Italian legislation (5 μg L^{-1} for groundwater), in order to test the adsorption capacity of the biochar at high concentrations (similar to what has been reported by other studies [667]), such as in wastewater.

Batch tests for arsenic adsorption were conducted at 90 μg L^{-1} as initial concentrations; this value was selected, as it is nine times higher than the limits of drinking water (10 μg L^{-1}), in order to test the material in the field of dearsinification, possibly to make water potable.

In the batch tests, a known dosage of biochar (5 g L^{-1} and 0.5 g L^{-1}, respectively, for Pb and As tests) was added to the contaminated water and maintained (for 6 h and 24 h, respectively, for Pb and As tests) under mixing conditions at 120 rpm constant stirring speed. Liquid samples were collected at different times: 5, 15, 30, 45 and 60 min within the first hour, and afterwards at 1 h intervals until the end of the tests.

Through the above batch tests, it was possible to determine the equilibrium time of the adsorption process.

Another series of batch tests was conducted with the aim of obtaining the equilibrium data, collecting samples: the following adsorbent dosages of biochar were added to the solutions at the same concentrations mentioned above: 0.5, 1, 2, 4, 5, 6, 8 and 10 g L^{-1} for Pb tests; 0.5, 1, 2 , 3, 5, 7.5, 10, 15, 20 g L^{-1} for As tests. The content was maintained under mixing conditions at 120 rpm for a duration equal to the equilibrium time previously determined.

2.7 Models for heavy metals adsorption

The parameters for each arsenic adsorption kinetics and isotherm model were obtained using a non-linear (NL) and linear (L) regression of Microsoft Excel [668–670].

In NL regression method, a trial-and-error procedure was used by the solver add-in with Microsoft's spreadsheet. Four different objective functions were used, in detail: the maximization of the coefficient of determination (R^2) and the minimization of the following errors SSE, HYBRID and χ^2; R^2 and the errors mentioned will be explained in the following paragraphs.

In L regression method , the procedure was differentiated according to the number of parameters of the model (p):

- For two-parameter models, through slope and intercept, derived from the least squares methodology of the interpolating line, using the variables of linearized equations, starting from experimental data;
- For three-parameter models, the first – starting from the linearized variables – was obtained using the excel solver, through four different conditions (explained previously); the second and third through the slope and intercept, derived from the least squares methodology of the interpolating line (explained previously).

2.7.1 Adsorption isotherm models

The study of equilibrium is essential in supplying the fundamental information required for the design and operation of sorption process.

Adsorption isotherms are used to study the relationship between the concentration of the solute (mg L^{-1} or µg L^{-1}) and the corresponding amount of adsorbate per mass unit of adsorbent material (mg g^{-1} or µg g^{-1}) under equilibrium conditions (time, temperature and pH remain unchanged).

Therefore, the adsorption isotherms were studied to provide a basis for revealing adsorption behavior, indicating possible adsorption mechanism, and estimating adsorption capacity.

In literature, Langmuir and Freundlich isotherm models have been most commonly used to analysis the equilibrium data.

In the next sections, six isotherm models are descripted to study arsenic adsorption from contaminated water; some of these, in their linear forms, have also been used for the study of lead adsorption.

2.7.1.1 Langmuir

Langmuir adsorption was designed to describe gas-solid phase adsorption [671]. It is also used to quantify and contrast the adsorptive capacity of various adsorbents like activated carbon [672]. Langmuir isotherm assumes for the surface a monolayer by balancing the relative rates of adsorption and desorption [673]. The equation (20) that describes Langmuir model is presented below:

$$q_e = \frac{q_{max}\, K_L\, C_e}{1 + K_L\, C_e} \tag{20}$$

Langmuir isotherm model can be linearized into at least four different types as shown in Table 2.5; m and Q are, respectively, the slope and the intercept of the linearized equations.

Table 2.5 – Linear forms of Langmuir isotherm model.

Linear form		Plot	K_L	q_{max}	Ref.
$\frac{C_e}{q_e} = \frac{1}{q_{max}} Ce + \frac{1}{q_{max} K_L}$	(21)	$\frac{C_e}{q_e}$ vs C_e	$\frac{m}{Q}$	$\frac{1}{m}$	[100,674]
$\frac{1}{q_e} = \frac{1}{q_{max} K_L} \frac{1}{C_e} + \frac{1}{q_{max}}$	(22)	$\frac{1}{q_e}$ vs $\frac{1}{C_e}$	$\frac{Q}{m}$	$\frac{1}{Q}$	[675]
$q_e = -\frac{1}{K_L} \frac{q_e}{C_e} + q_{max}$	(23)	q_e vs $\frac{q_e}{C_e}$	$-\frac{1}{m}$	Q	[676,677]
$\frac{q_e}{C_e} = -K_L q_e + q_{max} K_L$	(24)	$\frac{q_e}{C_e}$ vs q_e	$-m$	$-\frac{Q}{m}$	[678]

In the above equations, q_{max} indicates the maximum saturation capacity by monolayer adsorption at the given parameters (mg g^{-1} or μg g^{-1}), K_L is a constant that indicates the measure of the affinity between the adsorbent and the adsorbate (L mg^{-1} or L μg^{-1}); it is related to the free energy of adsorption [679]. Both Langmuir isotherm parameters can be evaluated from the intercept and slope of linear plot of each linear formula.

The essential characteristics of Langmuir isotherm can be expressed in terms of the dimensionless constant separation factor (R_L) for the equilibrium conditions, defined by Weber and Chakravorti [680]. This parameter is defined as:

$$R_L = \frac{1}{(1 + K_L C_0)} \tag{25}$$

where C_0 is the initial concentration of adsorbate (mg L^{-1}) and K_L is the Langmuir constant previously mentioned. According to Hall et al. [681], using mathematical calculations, it has been shown that the parameter R_L indicates the isotherm to be irreversible ($R_L = 0$), favourable ($0 < R_L < 1$), linear ($R_L = 1$) or unfavourable ($R_L > 1$) [672].

2.7.1.2 Freundlich

Freundlich adsorption isotherm model describes the reversible and non-ideal adsorption process; it is applicable to adsorption processes that occur on heterogonous surfaces [682], with a non-uniform distribution of adsorption heat. Therefore, this empirical mode gives an expression which defines the surface heterogeneity and the exponential distribution of active sites and their energies [683,684]. It is expressed by the following equation:

$$q_e = K_F C_e^{1/n} \tag{26}$$

Where:

- K_F is the constant of Freundlich, (mg g^{-1})(mg L^{-1})$^{-n}$ or (μg g^{-1})(μg L^{-1})$^{-n}$, an indicator of adsorption capacity. Adsorption is considered favourable if value of K_F is found in range of 1–20 [669].
- n (-) is an indicator of adsorption intensity or surface heterogeneity, indicating the energy relative distribution and the adsorbate sites' heterogeneity; therefore the type of the isotherm is indicated by

the value of n: when $1/n$ is greater than zero ($0 < 1/n < 1$) the adsorption is favorable, when $1/n$ is greater than 1, the adsorption process is unfavorable, and it is irreversible when $1/n = 1$.

The linear form of the Freundlich isotherm is as follows:

$$\ln q_e = \ln K_F + \frac{1}{n} \ln C_e \tag{27}$$

Both Freundlich (K_F, $\frac{1}{n}$) parameters are dependent on temperature and there are obtained from the intercept and slope of linear plot of $\ln q_e$ versus $\ln C_e$. To determine the maximum adsorption capacity it is necessary to operate with the initial constant concentration and variable weights of reactive material; thus according to Halsey [685]:

$$q_{max} = K_F C_0^{1/n} \tag{28}$$

where C_0 is the initial concentration of the solute in the contaminated water (mg L^{-1} or μg L^{-1}) and q_{max} is the Freundlich maximum adsorption capacity (mg g^{-1} or μg g^{-1}).

2.7.1.3 Dubinin-Radushkevich

Dubinin-Radushkevich (D–R) isotherm was designed as an empirical model for adsorption of subcritical vapours onto micropore solids [686]. Dubinin and Radushkevich and have reported that the characteristic sorption curve is related to the porous structure of the sorbent; it can be successfully applied for adsorption of heterogeneous system including solid and liquid [687]. The D–R model is expressed as follows [688]:

$$q_e = (q_{max})\, exp(K_{DR}\varepsilon^2) \tag{29}$$

Where: q_{max} is the theoretical saturation capacity (mg g^{-1} or μg g^{-1}), K_{DR} is a constant related to the mean free energy of adsorption per mole of the adsorbate ($mol^2\ kJ^{-2}$) and ε is the Polanyi potential (), which is equal to:

$$\varepsilon = RT\ ln(1 + \frac{1}{C_e}) \tag{30}$$

where R represent the universal gas constant (8.314 J mol^{-1} K^{-1}) and T the absolute temperature (K). The linear form of the Dubinin–Radushkevich isotherm is as follows:

$$ln\, q_e = ln\, q_{max} - K_{DR}\varepsilon^2 \tag{31}$$

q_{max} and K_{DR}, of Langmuir equation can be determined from the linear plot. The constant K_{DR} gives an idea about the mean free energy E of adsorption per mole of the adsorbate (kJ mol^{-1}) as it is transferred to the surface of the solid; it can be calculated using the relationship [688]:

$$E = \frac{1}{(2K_{DR})^{1/2}} \tag{32}$$

2.7.1.4 Temkin

The Temkin isotherm equation assumes that the fall in the heat of adsorption decreases linearly [689], therefore the adsorption is characterized by a uniform distribution of the binding energies and a coverage due to adsorbent–adsorbate interactions [690]. The Temkin isotherm has generally been applied in the following form [691]:

$$q_e = \frac{RT}{b_t} ln\, A_t\, C_e \tag{33}$$

Where R is the universal gas constant (8.314 J mol^{-1} K^{-1}), T the absolute temperature (K), A_t is the Temkin equilibrium constant, corresponding to the maximum binding energy (L mg^{-1} or L μg^{-1}) and b_t is the variation of adsorption energy (J mol^{-1}); the linearized equation is the following:

$$q_e = \frac{RT}{b_t} ln\, A_t + \left(\frac{RT}{b_t}\right) ln(C_e) \tag{34}$$

the Temkin equilibrium constant (A_t) and the variation of adsorption energy (b_t) can be calculated from the slope and the intercept of the plot q_e versus $ln(C_e)$.

2.7.1.5 Redlich-Peterson

The Redlich-Peterson (R–P) isotherm [692] is a three-parameter empirical adsorption model [693] that incorporates elements from both the Langmuir and Freundlich isotherms and amends the inaccuracies [694]. It is extremely versatile as it is applicable in either homogenous or heterogeneous systems. The model can be described as follows:

$$q_e = \frac{K_{RP} C_e}{1 + b_{RP} C_e^{n_{RP}}} \tag{35}$$

Where: K_{RP} is the Redlich-Peterson adsorption capacity constant (L g^{-1}), b_{RP} is an isotherm constant (L mg^{-1} or L $\mu g^{-1})^n$, and n_{RP} is the exponent of the R–P isotherm ($0 < n < 1$) [695]. The linear expression of the R-P isotherm model is defined as:

$$\ln\left(K_{RP}\frac{C_e}{q_e} - 1\right) = n_{RP} \ln C_e + \ln b_{RP} \tag{36}$$

Using the linear formula, K_{RP} is determined via trials and errors to obtain the maximum linear regression value of the isotherm graph [696]. The other parameters (b_{RP}, n_{RP}) can be obtained from the intercept and slope of the linearized equation [695].

2.7.1.6 Koble-Corrigan

Koble-Corrigan (K–C) isotherm model is another three-parameter empirical model based on the combination of Langmuir and Freundlich isotherm equations [697]. It is represented in one non-linear equation of the equilibrium adsorption data for heterogeneous sorbent surfaces [698,699], which has an exponential

dependence on concentration in the numerator and denominator [670], unlike that of R–P. The model is commonly expressed by:

$$q_e = \frac{A_{KB} {C_e}^{n_{KB}}}{1 + B_{KB} C_e^{n_{KB}}} \tag{37}$$

where A_{KB} is related to the thermodynamic equilibrium constant (L g^{-1}), B_{KB} is a constant related to the total number of active centers (L μg^{-1}) and n_{KB} is the exponent of K–C isotherm model. The linear expression of the K–C isotherm model is defined as:

$$\frac{1}{q_e} = \frac{1}{A_{KB} {C_e}^{n_{KB}}} + \frac{B_{KB}}{A_{KB}} \tag{38}$$

Using the linear formula, n_{KB} is determined using a trial and error optimization [698], in order to obtain the maximum linear regression value [696]. The other parameters (b_{RP}, n_{RP}) can be obtained from the intercept and slope of the linearized equation [695].

2.7.2 Adsorption Kinetic models

In batch adsorption process, kinetic studies provide information about optimum conditions, mechanism of sorption, and possible rate controlling step.

Adsorption kinetics can be represented by the relation between the contact time (independent variable) and the adsorption capacity, (time dependent variable). This plot forms the basis of all kinetics studies because its shape represents the underlying kinetics of the process.

In the next sections, six kinetic models are descripted to study arsenic adsorption from contaminated water; some of these, in their linear forms, have also been used for the study of lead adsorption.

2.7.2.1 Pseudo-first order

Pseudo First Order (PFO) was introduced initially by Lagergren [700]; its model is a good simulation when mass transfer to the active sites is a controlling factor during the adsorption process [701]. PFO model is described by the following equation [702,703]:

$$\frac{dq_t}{dt} = K_{PFO}(q_e - q_t) \tag{39}$$

Integrating the equation in the boundary conditions t = 0 to t = t and q_t = 0 to q_t = q_t, the following expression is obtained:

$$q = q_{e,cal}(1 - \exp((-K_{PFO} t)) \tag{40}$$

With the following linear form; it is generally used one proposed by Ho and McKay [704]:

$$\ln(q_e - q_t) = \ln q_{e,cal} - K_{PFO}\, t \text{ or } \log(q_e - q_t) = \log q_{e,cal} - \frac{k_{PFO}}{2.303} t \tag{41}$$

Where $q_{e,cal}$ is the calculated concentration of the adsorbate at equilibrium time (mg g^{-1} or μg g^{-1}) by the model and K_{PFO} is the rate constant of the pseudo first order equation (min^{-1}).

2.7.2.2 Pseudo-second order

The Pseudo second order (PSO) assumes that the sorption process is a pseudo-chemical reaction process. The PSO kinetic model is expressed as below (42):

$$\frac{dq_t}{dt} = K_{PSO}(q_e - q_t)^2 \tag{42}$$

Integrating between the boundary conditions t = 0 to t = t and $q_t = 0$ to $q_t = q_t$ [705,706], the last equation becomes as below (43):

$$q = \frac{q_{e,cal}^2 K_{PSO} t}{1 + q_{e,cal} K_{PSO} t} \tag{43}$$

Where K_{PSO} represents the adsorption reaction rate constant of the PSO (g mg^{-1} s-1 or g μg^{-1} min^{-1}) and $q_{e,cal}$ is the calculated concentration of the adsorbate at equilibrium time (mg g^{-1} or μg g^{-1}) by the model.

Eq. (43) can be linearized as four different types as shown in Table 2.6 [706].

Table 2.6 – Linear forms of pseudo-second-order kinetic model.

Linear form	Plot	K_{PSO}	$q_{e,cal}$
$\frac{1}{q_t} = (\frac{1}{K_{PSO} q_{e,cal}^2})\frac{1}{t} + \frac{1}{q_{e,cal}}$	$\frac{1}{q_t}\ VS\ \frac{1}{t}$	$\frac{Q^2}{m}$	$\frac{1}{Q}$
$q_t = q_{e,cal} - (\frac{1}{q_{e,cal}})\frac{q_t}{t}$	$q_t\ VS\ \frac{q_s}{t}$	$-\frac{1}{mQ}$	Q
$\frac{q_t}{t} = K_{PSO} q_{e,cal}^2 - k q_{e,cal} q_t$	$\frac{q_t}{t}\ VS\ q_t$	$\frac{m^2}{Q}$	$-\frac{Q}{m}$
$\frac{t}{q} = \frac{1}{K_{PSO}\ q_{e,cal}^2} + \frac{1}{q_{e,cal}} t$	$\frac{t}{q_t}\ VS\ t$	$\frac{m^2}{Q}$	$\frac{1}{m}$

Both constants K_{PSO} and $q_{e,cal}^2$ can be calculated from the intercept (Q) and slope (m); obtained by plotting the variables of the four linearized equations. Of all the equations mentioned above, the one proposed by Ho and McKay [704] is generally used:

$$\frac{t}{q} = \frac{1}{K_{PSO}\ q_{e,cal}^2} + \frac{1}{q_{e,cal}} t \tag{44}$$

The initial adsorption rate of the PSO, h_{PSO} (mg g^{-1} min^{-1} or μg g^{-1} min^{-1}) is expressed as [679,705]:

$$h_{PSO} = K_{PSO}\ q_{e,cal}^2 \tag{45}$$

2.7.2.3 Elovich

Elovich equation is used to describe an adsorption kinetic model assuming that the actual solid surfaces are energetically heterogeneous. This model also considers the adsorption as a process limited by the linking of the adsorbate in the active sites, therefore the equation does not propose any definite mechanism for adsorbate–adsorbent [679,691,703]. The equation is as follows:

$$\frac{dq_t}{dt} = \alpha \, exp\,(-\beta q_t) \tag{46}$$

This expression, integrated between the boundary conditions: $q_t = 0$ at $t = 0$ and $q_t = q_t$ at $t = t$, gives rise to the equation (47):

$$q_t = \left(\frac{1}{\beta}\right) \ln\,(1 + \alpha\beta t) \tag{47}$$

or, in linear form, assuming that $\alpha\beta t \gg 1$:

$$q_t = \frac{1}{\beta}\ln(\alpha\beta) + \frac{1}{\beta}\ln t \tag{48}$$

where constants α (mg g^{-1} s^{-1} or μg g^{-1} min^{-1}) and β (g mg^{-1} or g μg^{-1}) are related, respectively, to the initial adsorption rate and to the number of sites available for adsorption [701]. The Elovich coefficients could be computed from the intercept and slope of the straight-line plots of q_t versus $\ln t$.

2.7.2.4 Weber and Morris

In Weber and Morris model (or intra particle diffusion model, IPD) the internal diffusion determines the adsorption rate in most of the liquid systems. Eq. (49) is a general representation of the kinetics, where the intercept is related to the mass transfer across the boundary layer and the expected value of the exponent is 0.5. The Weber-Morris model is expressed using the following equation:

$$q = k_{WM}\sqrt{t} + c \tag{49}$$

Both processes are generally observed for adsorption kinetics on activated carbons – the external mass transfer from the solution to the liquid-solid interface and the diffusion of the adsorbed species inside the porous particle.

$$q = K_{WM}\sqrt{t} + c \tag{50}$$

where K_{WM} is the intra-particle diffusion rate constant (mg g^{-1} $min^{-1/2}$ or μg g^{-1} $min^{-1/2}$), and c is a constant that increases with the thickness of the boundary layer (mg g^{-1} or or μg g^{-1}) [701]. Both constant are obtained from the plot of q versus $t^{0.5}$.

2.7.2.5 Avrami

This model was recently developed based on Avrami's kinetic model to simulate phase transition and crystallization kinetics. It has been also applied to describe the adsorption of CO_2 on amine-functionalized adsorbents [707]. The general form of the model is as follows [703]:

$$\frac{d_q}{d_t} = K_{Av} t^{\,n_{Av}-1}(q_e - q) \tag{51}$$

The integrated form for the above-mentioned boundary conditions is expressed as:

$$q_t = q_e\{1 - exp\,[-(K_{Av}t)]^{\,n}_{Av}\} \tag{52}$$

Where K_{Av} is the Avrami kinetic constant (μg g^{-1} min^{-1}) and n_{Av} is the Avrami exponent, a factionary number that expresses the dimensionality of growth of adsorption sites.

2.7.2.6 Bangham

Bangham model, or also called the power model [694], assumes that the kinetics of the adsorption process is determined by the pore diffusion. The equation is as follows [691]:

$$q_t = K_B t^{\theta_B} \tag{53}$$

Where K_B and θ_B are respectively the model constant (μg g^{-1}) and a exponent (μg g^{-1} min^{-1})(< 1)

$$lnq_t = \theta_B \ln(t) + \ln(K_B) \tag{54}$$

Both parameters of Bangham model can be obtained from the intercept (e^Q) and slope (θ_B) of the straight line plots of lnq_t against $\ln(t)$.

The model can be also represented by an another linear equation [703,708]:

$$\log\left(\log\frac{C_0}{C_0 - q_t\,\frac{m}{V}}\right) = \log\left(\frac{k_B\,\frac{m}{V}}{2.303\,V}\right) + \alpha \log t \tag{55}$$

Where: α (<1, -) and k_B (mg g^{-1} $s^{-\alpha}$ or μg g^{-1} $s^{-\alpha}$) are constants which can be obtained from slope and intercept from the data plot, using the linearized variables; m/V (or M) is the weight of adsorbent used per liter of aqueous solution (g L^{-1}); C_0 and V, are respectively, the initial concentration (mg L^{-1} or μg L^{-1}) and the volume of solution (mL or L); m is the mass of adsorbent media (g).

2.8 Column test

2.8.1 Remediation of lead-contaminated water

The capability of AMBIOTON® and RE-CHAR® as adsorbent media were investigated at lab-scale by means of an experimental apparatus consisting of three Pyrex glass columns, three peristaltic pumps and suitable tanks to stoke Pb contaminated water.

The column tests were performed following the procedures reported [709]. In these studies, laboratory-scale equipment has been optimized to remove lead from aqueous solutions using the characterized commercial biochar as reactive material. Water containing 100 mg L^{-1} (C_0) of dissolved lead was flushed inside the columns through a peristaltic pump using a flow rate of 60 mL h^{-1}. To avoid any preferential routes within the columns, a suitable hydraulic head together with a perforated plate has been fixed at the top of the column. The value of the lead concentration in the feeding flow has been chosen in accordance with other studies previously conducted [710].

Three columns were carried out to compare Pb adsorption capacity of AMBIOTON® and RE-CHAR® and that of an agricultural soil as a possible target of contamination; in fact, the columns simulate a leaching of lead, where biochar is investigated as a possible protective layer of the environmental matrix (soil) to be preserved.

Biochar and sand particle having a size smaller than 2 mm were previously discarded, in order to limit by-pass phenomena along the column walls [711]. Agricultural soil was made by 29% clay, 28% silt, 43% sand and 2% organic matter, by weight. Columns were utilized for the tests were characterized by 1 cm of diameter and 18 cm of high.

In order to simulate a Pb leaching into the soil, several layers were arranged in two of the three columns; in order from bottom to top: a layer of draining sand, a layer of soil, a layer of sand, a filter layer mixing sand and biochar (AMBIOTON® or RE-CHAR®) and a last layer of draining sand. In the mixed layer biochar (AMBIOTON® or RE-CHAR®) was used with a percentage by weight of around 50% respect to the soil.

The filling of the columns and the synthesis of the different layers are shown in the following Table 2.7.

Table 2.7 – Configuration of the layers of the experimental columns.

Soil with AMBIOTON®			Soil with RE-CHAR®			Soil		
Layer	High (cm)	Weight (g)	Layer	High (cm)	Weight (g)	Layer	High (cm)	Weight (g)
sand	3.00	3.93	sand	3.00	3.93	sand	3.00	3.93
sand and AMBIOTON®	2.65	0.50	sand and RE-CHAR®	3.75	0.50	sand	6.00	7.87
	3.35	4.39		2.25	2.95			
sand	0.50	0.66	sand	0.50	0.66	sand	0.50	0.66
soil	1.09	1.00	soil	1.09	1.00	soil	1.09	1.00
sand	6.41	8.40	sand	6.41	8.40	sand	6.41	8.40

The third column was filled with the soil to evaluate the specific adsorption capacity of the investigated soil. The remaining part of the column was filled with quartz sand, a non-reactive medium. This column was also operated under the same conditions as a control.

Eluate samples were collected at the columns outlet every hour in order to analyze the residual lead concentration and to determine the breakthrough curves. Then, the saturation and breakthrough times were calculated, assuming to correspond to the time when Pb concentrations in the eluate, C, corresponds to $C/C_0 = 95\%$ and $C/C_0 = 5\%$ and respectively [712,713].The experimental data of the column tests were fitted using the Yoon–Nelson [714], Thomas [715] and Bohart–Adams [716] models to determine the adsorption capacity of the model.

2.8.2 Adsorption of arsenic from aqueous solutions

The column tests were carried out using the experimental apparatus described in [717,718]. It was composed of a Pyrex column with an internal diameter of 8 cm and a length of 60 cm (with a volume about 3.3 L). The column has been connected from the top to a peristaltic pump, in order to maintain the flow rate approximately constant and a tank to stock the inflowing solution.

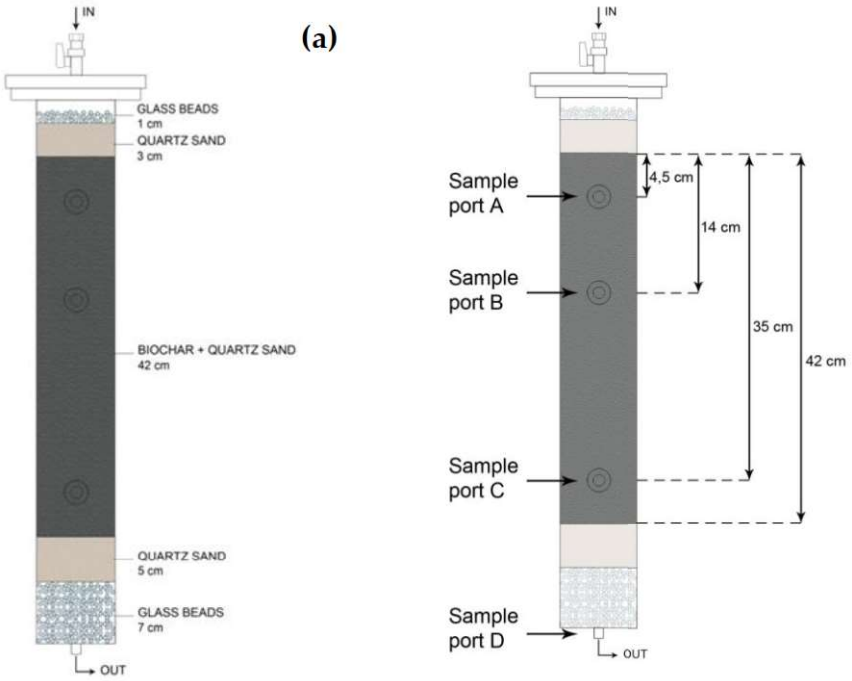

Figure 2.7 – (a) Identification of the layer thicknesses of the elements within the column; (b) Arrangement of the four column sample ports.

The column was filled with different elements as shown in Figure 2.7 (a): the reactive zone composed of biochar and sand mixture in the middle part of the column and two filter zones placed at the bottom and the top of the column.

The Table 2.8 reports the values of the measured physical parameters of the inert quartz sand, determined by the UNI EN 13242 standard.

Table 2.8 – Main physical properties of the inert quartz sand.

Parameters	Unit	Values	Methods
Dry density	Kg L^{-1}	2.65	UNI EN 13242
Medium grain size d_{50}	µm	700	UNI EN 13242
Medium grain size d_{10}	µm	450	UNI EN 13242
Medium grain size d_{60}	µm	800	UNI EN 13242
Hydraulic conductivity	m s^{-1}	$3.0*10^{-3}$	-

The grain size of the quartz sand was estimated by laboratory measurements [113] and the hydraulic conductivities was evaluated using the formula proposed by Hazen.

The filter zones were composed of two layers: glass beads and quartz sand. The bottom filter is used to avoid the materials escape from the column outlet [719] and the upper filter to assure the best distribution of the inlet solution.

The layers of quartz sand and glass beads have the function of distributing the inlet flow evenly also to limit by-pass phenomena [712,720].

Two tests were carried out using different volume ratio between biochar and sand in the reactive zone, respectively, in the test 1 was utilized a biochar-sand volume ratio of 7:100, in the test 2 of 3:100.

The column was equipped with sample ports positioned along the reactive zone and at the outlet in order to monitoring the process inside the column Figure 2.7 (b).

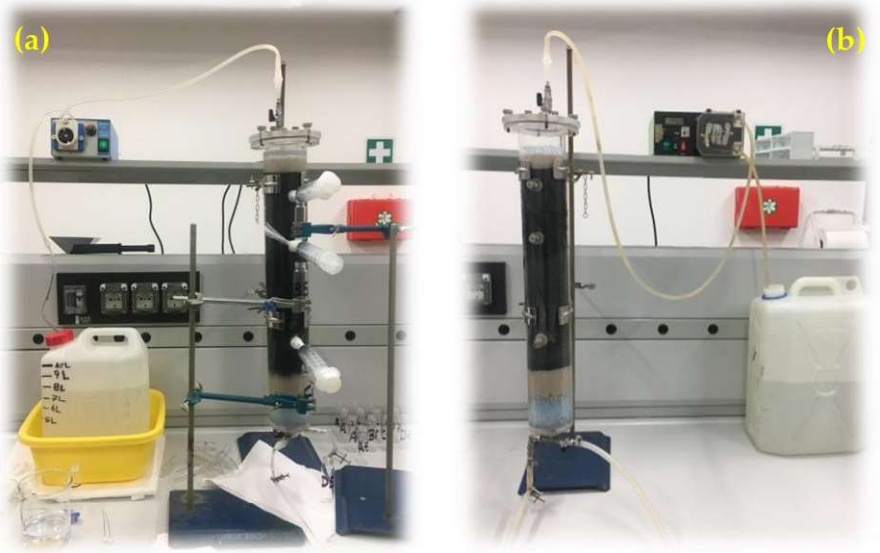

Figure 2.8 – Photographic documentation of the filled column, connected to the peristaltic pump; respectively, (a) for the Test 1 and (b) for the Test 2.

At the first step, the column was saturated with deionized water; successively a solution containing 1 mg L^{-1} of As(V) (at pH 7.5) was continuously fed to the top of the column through the peristaltic pump with constant flow rate equal to 5 mL min^{-1}.

To quantify the adsorption capacity of the sand a blank test was also conducted: a column was filled with pure sand (still including the glass marbles on top and at the bottom), and arsenic solution was flowed through the column.

During the tests, water samples were collected from the ports in order to monitoring in time the arsenic concentration along the column.

A numerical model was implemented on MATLAB environment to reproduce the laboratory tests. To simulate the solute transport through the saturated porous media the model utilizes the classical advection-dispersion equation (56):

$$\frac{\partial C}{\partial t} + u_i \frac{\partial C}{\partial x_i} = \frac{\partial C}{\partial x_i}\left(D_{ij} \frac{\partial C}{\partial x_j}\right) \tag{56}$$

where C is the solute concentration, t is the time, x_i are the axes, u_i are the components of velocity vector and D_{ij} is the hydrodynamic dispersion tensor.

Equation (56) can be considered as one-dimensional because the length of the column used for laboratory tests is much larger than its diameter, so the motion can be considered occurring mainly along the x-axe. Furthermore, for the characteristics of the material, the sample can be considered homogeneous, so, porosity as well as hydrodynamic dispersion are constant along the whole column.

In order to consider the affinity of the solute for adsorption onto solid particles of the biochar, the adsorption term is incorporated to the advection-dispersion equation (57) [721] as follow:

$$\frac{\rho_b}{p}\frac{\partial S}{\partial t}+\frac{1}{p}\frac{\partial C}{\partial t}=\frac{D}{p}\frac{\partial^2 C}{\partial x^2}-\frac{u}{p}\frac{\partial C}{\partial x} \quad (57)$$

where S is the amount of solute absorbed on the biochar particles, p the porosity and ρ_b the bulk density.

In order to investigate the most suitable isotherm [722] to describe the contaminant partition (adsorbed/dissolved), Linear [672,673], Langmuir [671] and Freundlich isotherms were implemented in the numerical model. The equations are numerically solved using the explicit finite difference technique proposed by Karahan [723]. The technique is based on the Saulvey scheme [724] and it gives highly accurate results even for high values of the Courant number.

One-dimensional simulation domain was divided into a regular grid with spacing Dz=1.4*10^{-2} m. As boundaries conditions the Dirichlet (up) and the Neumann (bottom) conditions were used respectively.

In summary, using the code three different phases are distinguished:

1. Initial phase: Setting of variables and operating parameters, spatial and temporal discretization were carried out; the input operating parameters and the analytical variables are:
    a. Flow;
    b. Diameter and section area of the column;
    c. Speed;
    d. Porosity;
    e. Number of nodes.
2. Unfolding: Setting of initial/boundary conditions and the delay factors (associated with the various adsorption isotherms); the input operating parameters for the second phase are:
    I. Dirichlet condition in which the value is assigned to the variable u in the contour points to the variation of the time;
    II. Neumann condition the value of the gradient of u in the contour points is assigned to the variation of the time;
    III. Transport equation.
3. Final phase: Implementation to transpose returning values from the equation in Excel to build a graphical representation upon which final implications are considered.

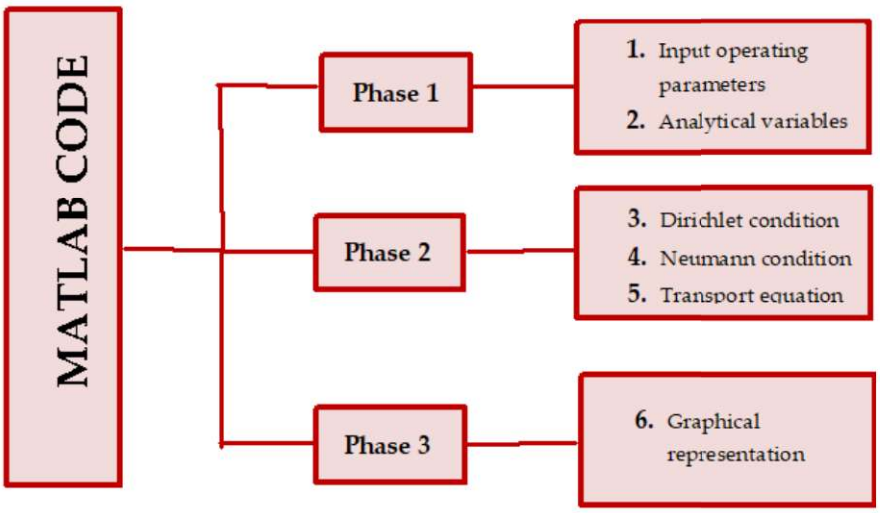

Figure 2.9 –Flowchart of the Matlab code.

2.9 Error analysis/statistics

In order to determine best fitting of linear or non-linear models, it is necessary to calculate the error function The following are the formulas used to validate the results obtained during some stages of experimental research; where y_{exp}: experimental value, y_{cal}: calculated value, $\overline{y_{exp}}$: means of experimentals data points, $\overline{y_{cal}}$: means of calculated data points, n: number of experimental data points, p: number of parameters in each model.

2.9.1.1 Sum square error

Sum square error (ERRSQ or SSE) is the most widely used error function [725]; it is a measure of the discrepancy between the data and an estimation model. A small ERRSQ indicates a tight fit of the model to the data.

$$ERRSQ\ or\ SSE = \sum_{i=1}^{n} [y_{cal} - y_{exp}]_i^2 \tag{58}$$

2.9.1.2 Sum of absolute error

Sum of absolute error (SAE or EABS) is similar to the ERRSQ function but here there is no square elevation [703,726–729]:

$$SAE\ or\ EABS = \sum_{i=1}^{n} (y_{cal} - y_{exp})_i \tag{59}$$

2.9.1.3 Mean squared error (MSE)

Mean squared error (MSE) represent the average squared difference between the estimated value and the experimental data; its value almost always strictly positive [703]:

$$MSE = \frac{1}{n} \sum_{i=1}^{n} [y_{cal} - y_{exp}]_i^2 \tag{60}$$

2.9.1.4 Root mean sum-of-squares error

Root mean sum-of-squares error (RMSE) is the square root of MSE [730–733]:

$$RMSE = \sqrt{\frac{1}{n} \sum_{i=1}^{n} [y_{cal} - y_{exp}]_i^2} \tag{61}$$

2.9.1.5 Hybrid fractional error function

Hybrid fractional error function (HYBRID) was aimed to improve the applicability of ERRSQ at a lower concentration. Hereby, each ERRSQ value is divided by the experimental concentration obtained in the laboratory and the sum of it is divided by a specific term that represent the degrees of freedom of the system; the number of data points minus the number of parameters within the model equation [727–729,734–736].

$$HYBRID = \frac{100}{n-p}\sum_{i=1}^{n}\left[\frac{y_{exp}-y_{cal}}{y_{exp}}\right]_i \quad (62)$$

2.9.1.6 Average relative error

The average relative error (ARE), or mean relative percent error (MRPE), indicates a tendency to under or overestimate the experimental data, attempts to minimize the fractional error distribution across the entire studied concentration range [696,698,703,722,727,729,735,737].

$$ARE\ or\ MRPE = \frac{1}{n}\sum_{i=1}^{n}\left[\frac{y_{exp}-y_{cal}}{y_{exp}}\right]_i \quad (63)$$

2.9.1.7 Average percentage error

The average percentage error (APE or E%), is calculated according to equation indicated the fit between the experimental and predicted values of adsorption capacity used for plotting models curves [696,703,727,729,735].

$$APE\ or\ E(\%) = \frac{100}{n}\sum_{i=1}^{n}\left[\frac{y_{exp}-y_{cal}}{y_{exp}}\right]_i \quad (64)$$

2.9.1.8 Normalized standard deviation

Normalized standard deviation (Δq) is also known as average relative standard errors (ARS) [693,703,737].

$$\Delta q(\%)\ or\ ARS = 100\sqrt{\frac{1}{n-1}\sum_{i=1}^{n}\left(\frac{y_{exp}-y_{cal}}{y_{exp}}\right)_i^2} \quad (65)$$

2.9.1.9 Marquardt's percent standard deviation

Marquardt's percent standard deviation (MPSD) is a modification of geometric mean distribution and it is usually practiced by a great number of researchers in the isotherm studies. It is based on the number of degrees of freedom of a system as the Hybrid fractional error function [703,727–729,734,735,738].

$$MPSD = 100\sqrt{\frac{1}{n-p}\sum_{i=1}^{n}\left(\frac{y_{exp}-y_{cal}}{y_{exp}}\right)_i^2} \quad (66)$$

2.9.1.10 Coefficient of determination

Coefficient of determination (R^2), which represents the percentage of variability in the dependent variable (the variance about the mean) is employed to analyse the fitting degree of isotherm and kinetic models with the experimental data [696,705,733,739].

$$R^2 = 1 - \frac{\sum_{i=1}^{n}\left[y_{cal}-y_{exp}\right]_i^2}{\sum_{i=1}^{n}\left[y_{exp}-\overline{y_{exp}}\right]_i^2} \quad (67)$$

2.9.1.11 Coefficient of non-determination

Nother statistical term, coefficient of non-determination (K_2), is much useful in describing the extent relationship between the transformed experimental data and the predicted data, and minimization of the error distribution [740].

$$K_2 = 1.000 - R^2 \tag{68}$$

2.9.1.12 Spearman's correlation coefficient

Spearman's correlation coefficient (r^2) (or coefficient of correlation) and standard deviation of relative errors are individually determined to evaluate the global correlation and the dispersion of its relative errors [78].

$$r^2 = \frac{\left[\sum_{i=1}^{n}(y_{exp} - \overline{y_{exp}})(y_{cal} - \overline{y_{cal}})\right]^2}{\left[\sum_{i=1}^{n}(y_{exp} - \overline{y_{exp}})^2{}_i \sum_{i=1}^{n}(y_{cal} - \overline{y_{cal}})^2{}_i\right]} \tag{69}$$

2.9.1.13 Adjusted R^2

The Adjusted R^2 is a variant of the R^2; while R^2 is used for the analysis of simple linear regression as the main index of the goodness of the regression curve, Adjusted R^2 is used for the analysis of multiple linear regression, by taking into account the high number of experimental data and the model parameters [703].

$$R^2_{adj} \; or \; \overline{R}^2 = 1 - \left[\frac{(1 - R^2)}{(n - p - 1)}(n - 1)\right] \tag{70}$$

2.9.1.14 Standard deviation of relative errors

The standard deviation of a relative errors (S_{RE}) is equal to the standard error of a survey estimate divided by the survey estimate and then multiplied by 100 [737].

$$S_{RE} = \sqrt{\frac{\sum_{i=1}^{n}\left[\left(y_{exp} - y_{cal}\right)_i - ARE\right]^2_i}{n - 1}} \tag{71}$$

2.9.1.15 Nonlinear chi-square test (χ^2)

Nonlinear chi-square test (χ^2) is a statistical tool necessary for the best fit of an adsorption system; this test is obtained through the sum squares differences between the experimental and the calculated data, where each squared difference is divided by its corresponding value calculated from the models [696,703,739,741,742].

$$\chi^2 = \sum_{i=1}^{n} \frac{\left(y_{exp} - y_{cal}\right)^2}{y_{cal}}_i \tag{72}$$

3 Results and discussion

The results obtained during the experimental activity are analyzed and discussed in the following chapter. The following paragraphs show the results obtained in the characterization, in the batch and column tests, the results of which, for reasons of clarity, have been reported in three different sections.

3.1 Characterization of carbon-based sorbent

3.1.1 Composition and particle size distribution

The particle size distribution is a fundamental parameter as it characterizes the grain size of the material and provides an indication of the uniformity of its dimensions. In general, larger dimensions lead to lower pressure drops but slower adsorption kinetics.

The Table 3.1 shows the particle size distribution of the three different carbon-based materials.

Table 3.1 – Particle Size Distribution (PSD, %) of CARBOSORB NC 1240, AMBIOTON® and RE-CHAR®.

Diameter	CARBOSORB NC 1240	AMBIOTON®	RE-CHAR®
>850 x10^{-6} m	86.77	85.448	17.230
>600 x10^{-6} m	12.143	11.922	33.017
>500 x10^{-6} m	0.949	1.547	7.134
>355 x10^{-6} m	0.084	0.947	4.307
>300 x10^{-6} m	0.054	0.091	2.492
>212 x10^{-6} m	<	0.019	9.014
>180 x10^{-6} m	<	0.070	3.173
>90 x10^{-6} m	<	0.018	8.984
>75 x10^{-6} m	<	0.002	13.704
>53 x10^{-6} m	<	<	0.750
>45 x10^{-6} m	<	<	0.180
>38 x10^{-6} m	<	<	0.007
<38 x10^{-6} m	<	<	0.002

From the Table 3.1 it can be shown that the mode (d_{50}) of the CARBOSORB NC 1240 and AMBIOTON® is equal to (850) x10^{-6} m, while for what the RE-CHAR® is about to (850-600) x10^{-6} m.

In the Figure 3.1 below are presented the granulometric curves, inputting the percentage of passing along the ordinate axis.

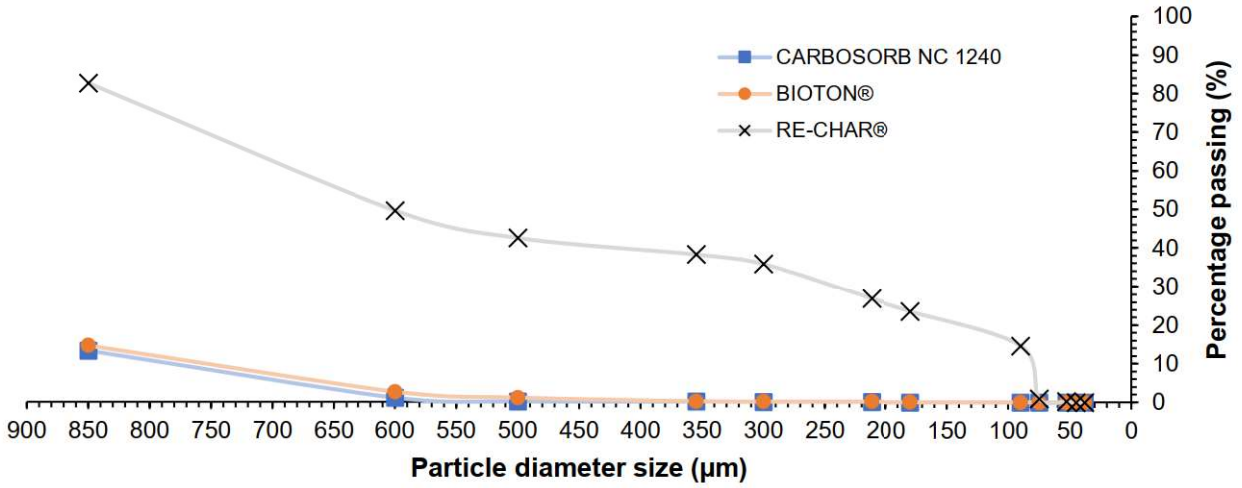

Figure 3.1 – Composition and grain size distribution (Granulometric curve) of CARBOSORB NC 1240, AMBIOTON® and RE-CHAR®.

It can be shown from the results that CARBOSORB NC 1240, present a homogeneous size, where almost all the material is distributed between 850 µm and 500 µm. AMBIOTON® has similar characteristics to CARBOSORB NC 1240 but with small percentages even on smaller sieves up to 90 µm. On the other hand, RE-CHAR® presents a very varied and fine size reaching over 13% at 75 µm sieve and small percentages at 38 µm.

Major et al. [743] has shown how, with the same starting particle sizes, the size of the particles decrease as the temperature at which pyrolysis occurs (from 450 to 700 °C) increases. Furthermore, during pyrolysis, by increasing the pressure to 10 and 20 bars, particles with larger dimensions are obtained due to melting and joining phenomena between particles.

3.1.2 Density, bulk density and specific weight

The Table 3.2 shows the estimate of the real one and the determination of the apparent one. In addition it is also estimated specific weight.

Table 3.2 –Bulk density, apparent density and specific weight of carbon-based sorbents.

Parameter	Symbol	Unit	CARBOSORB NC 1240	AMBIOTON®	RE-CHAR®
Density (estimate)	ϱ	kg m^{-3}	2,048.0	1,136.0	528.0
Bulk density	ϱ_b	kg m^{-3}	512 ± 4.1	284 ± 3.4	132 ± 2.0
Specific weight (estimate)	γ	N m^{-3}	20,082.69	11,139.62	5,177.57

Density is strongly influenced by the porosity of the material; precisely for this reason density and apparent (or bulk) density are different, since the first refers to the density calculated by subtracting the open porosity from the volume, otherwise the second is calculated by including both open and closed pores from the volume. The bulk density refers to the density calculated considering the volume including both open and closed pores that may be present inside the material. Generally bulk density of biochar is in the range from 470 to 600 kg m^{-3}, as it is reported by Singh et al. [744].

3.1.3 Water content, volatile matter, ash content and fixed carbon

Table 3.3 reported the percentage values, of water content (θ), volatile matter (VM), ash content (ASH) and fixed carbon (FC) of the carbonaceous material studied (on a dry weight basis).

Table 3.3 – Water content, volatiles, fixed carbon and ash of CARBOSORB NC 1240, AMBIOTON® and RE-CHAR®.

Parameter	Symbol	Unit	CARBOSORB NC 1240	AMBIOTON®	RE-CHAR®
Water content	θ	%	3.48 ± 0.2	3.18 ± 0.11	0.98 ± 0.1
Volatile matter	VM	%	3.22 ± 0.04	5.91 ± 0.04	6.63 ± 0.04
Fixed carbon	FC	%	91.35 ± 0.1	84.40 ± 0.1	80.84 ± 0.1
Ash content	ASH	%	2.45 ± 0.44	6.57 ± 0.34	11.55 ± 0.44

As can be shown from the results, CARBOSORB NC 1240 and AMBIOTON® have a similar moisture value while RE-CHAR® is about one third. Different situation for volatile matter and ash content where RE-CHAR® has the highest values, while CARBOSORB NC 1240 the lowest. AMBIOTON® appears to have values in the middle between those of the two substances.

In fact, the four main constituents of biochar as the fraction of the biochar that consists of water and volatile matter, the ash content, that refers to the inorganic portion of biochar, and the organic portion of biochar that will remain stable in the soil for a very long time (FC); also there is a small percentage that can eventually leach into the soil or be ingested by soil microbes. Fixed carbon is therefore generally more valuable in biochar than mobile matter [745]. In Yargicoglu et al. [746] moisture content of the analysed biochar was in range between 0.33 and 66.2%, ash content ranging from 1.5 to 65.7% and the percentage of volatile matter was in range between 28.0 and 74.1%.

In the Figure 3.2 it is shown the variation in weight (%) and the derivative of variation in weight (% min^{-1}) of the volatile substances in CARBOSORB NC 1240 (Sample A.001), AMBIOTON® (Sample B.001) and RE-CHAR® (Sample C.001).

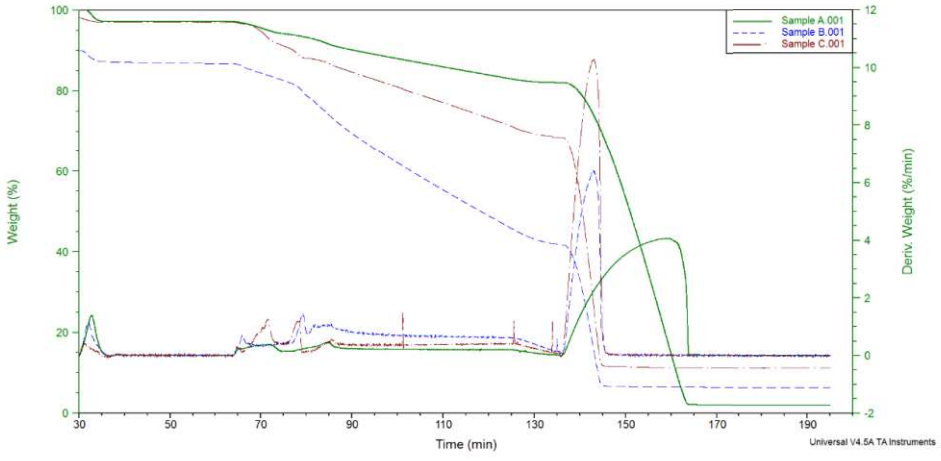

Figure 3.2 – Weight (%) of volatile matter in CARBOSORB NC 1240, AMBIOTON® and RE-CHAR®.

Leeq et al. [747] on biochar reports volatile matter between 7.6 and 12.7% and ash values equal to 58.0%. The quantities of ash in the biochar are consistent with the raw materials used in the gasification process: pine and wood derivatives are materials with a low ash content, consisting mainly of alkali metals (Ca, K, Mg) as also reported by Brewer et al. [748]. Erto et al. [749] reported for activated carbon the ash values are reported, ranging between 1.80 and 10.49%.

3.1.4 Conductance and Ion exchange capacity

The Table 3.4 shows the values of conductivity, cationic and exchange capacity, determined for each carbonaceous material. The values found for the ion exchange capacity analysis are shown below. The cationic values of the CEC and the anionic values of the CSA are reported.

Table 3.4 – Conductance, CEC and AEC of carbon-based sorbents.

Parameter	Symbol	Unit	CARBOSORB NC 1240	AMBIOTON®	RE-CHAR®
Conductance (1 g L^{-1})	G	S (Ω^{-1})	$31.3 \pm 0.4 \times 10^{-6}$	$47.1 \pm 0.6 \times 10^{-6}$	$132.3 \pm 1.7 \times 10^{-6}$
Cationic exchange capacity	CSC	cmol(+) /kg_{DW}	75 ± 1.2	58.75 ± 1.4	12.5 ± 0.8
Anionic exchange capacity	AEC	cmol(+) /kg_{DW}	18.40 ± 0.87	13.02 ± 0.11	5.3 ± 0.45

From the results of Table 3.4 it is easy to see how for CARBOSORB NC 1240 and AMBIOTON® the conductivity value is quite similar even if higher towards AMBIOTON®. While for RE-CHAR®, it is noted how the value has almost tripled compared to AMBIOTON®. So, the RE-CHAR® is among the three, the material with the most electrical conductivity. Several values have been reported in the literature: 54.2 (dS m^{-1}) by Smider et al. [750] and 0.04 (dS m^{-1}) by Rajkovich et al. [322].

Furthermore, the results show that CARBOSORB NC 1240 has a higher CEC and CSA value than the two biochars. CEC of AMBIOTON® is four times larger than that of RE-CHAR®, as far as the AEC of the letter is less than half of the AMBIOTON®. Leeq et al. [747] reported CEC values of the investigated biochar was about 20.0 (cmol(+) kg^{-1}). Lawrinenko et al. [751] reports AEC values between 2.6 and 18.1 (cmol(+) kg^{-1}).

3.1.5 pH analysis

The pH of the solution affects the surface charge of the carbon by altering the electron density of the graphite layer, consequently modifying its polarity and therefore its adsorbing properties towards hydrophobic molecules [192].

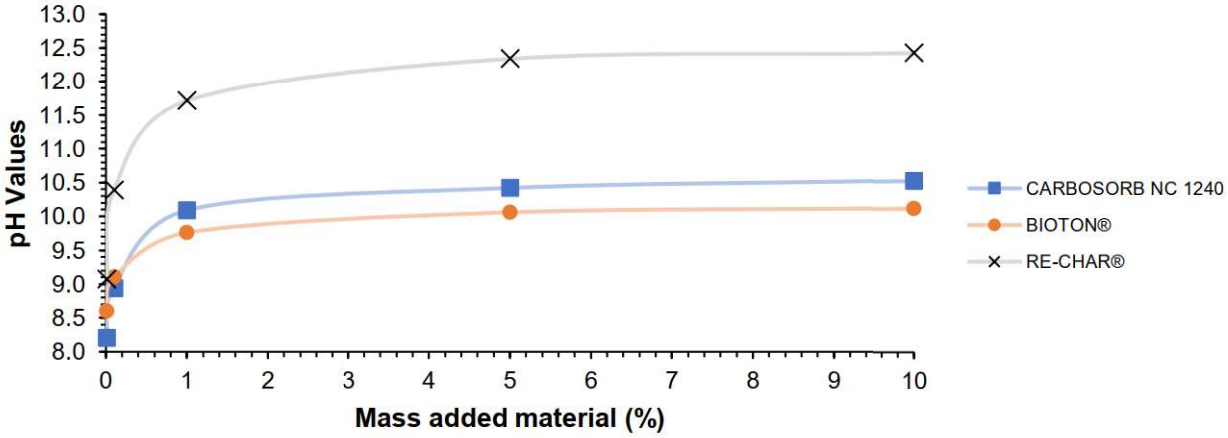

Figure 3.3 – pH as a function of the added material (%).

Table 3.5 shows the values of pH, PI and pH_{PZC} of the carbonaceous materials investigated.

Table 3.5 – Values of pH, pI and pHPZC.

Measurement	CARBOSORB NC 1240	AMBIOTON®	RE-CHAR®
pH (1%)	10.09±0.1	9.76±0.1	11.71±0.1
pI	10.5±0.05	10.1±0.04	12.4±0.1
pHPZC	10.5±0.05	10.1±0.04	12.4±0.1

Observing Table 3.5 it is noted that all three materials are strongly alkaline. Regardless of the starting raw material, the high temperatures reached during the pyro-gasifier process strongly influence the pH of the final products, inducing alkalinity, as also reported by Yuan et al. [752].

Yargicoglu et al. [746] detected variable pH values based on the type of biochar analyzed, with values ranging from 6.24 to 8.86. Awtar Singh et al. [744] showed pH values from 8.5 to 10.4.

3.1.6 Elemental analysis

The results of the elementary analysis, carried out via CHNOS elemental analyzer and XRF are shown in Table 3.6 and Figure 3.4.

Table 3.6 – Elemental analysis and molar ratios of CARBOSORB NC 1240, AMBIOTON® and RE-CHAR®.

Measure	Symbol	Unit	CARBOSORB NC 1240	AMBIOTON®	RE-CHAR®
Carbon	C	%	92.6 ± 0.1	77.65 ± 14.1	84.5 ± 0.1
Hydrogen	H	%	0.35 ± 0.02	0.9 ± 0.1	0.85 ± 0.04
Nitrogen	N	%	0.05 ± 0.004	0.07 ± 0.01	0.15 ± 0.02
Oxygen	O	%	2.67 ± 0.21	1.1 ± 0.12	9.99 ± 1.05
Phosphorus	P	%	0.32 ± 0.19	0.65 ± 0.19	1.79 ± 0.59
Potassium	K	%	1.45 ± 0.13	4.57 ± 1.03	1.4 ± 0.11
Sulfur	S	%	1.88 ± 0.39	0.2 ± 0.02	0.32 ± 0.02
Calcium	Ca	%	<L.D. (0.5)	<L.D. (0.5)	<L.D. (0.5)
Magnesium	Mg	%	<L.D. (0.5)	1.03 ± 0.03	<L.D. (0.5)
	O/C	-	0.029	0.014	0.118
	H/C	-	0.004	0.012	0.010
	C/N	-	1,852.000	1,109.285	563.333

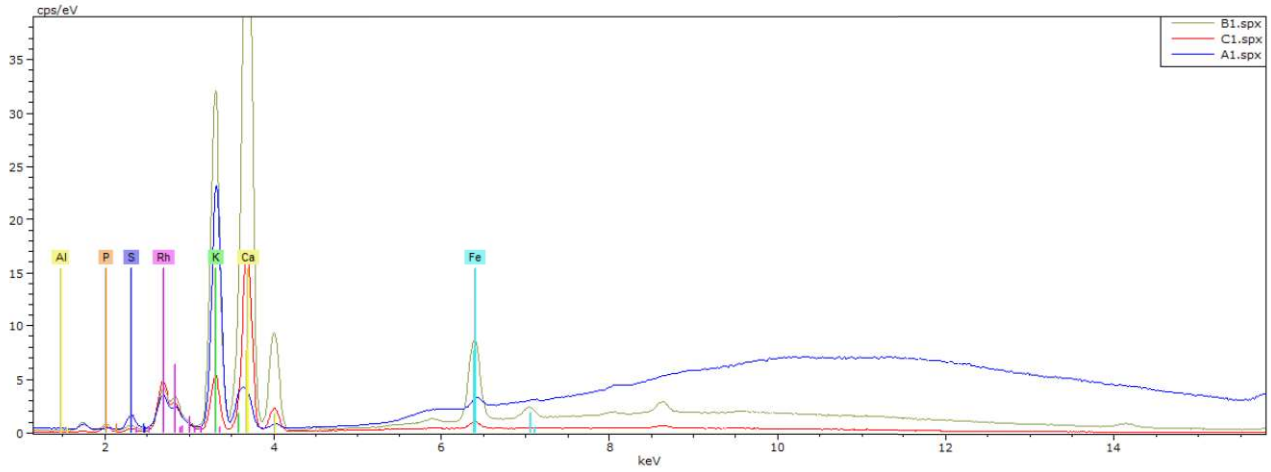

Figure 3.4 – XRF Analysis spectrum of CARBOSORB NC 1240, AMBIOTON® and RE-CHAR®.

Through elemental analysis, XRF analysis and EDS analysis (carried out later) the composition of the three materials can be clearly seen. CARBOSORB NC 1240 is an activated carbon with a high% of C inside it inside it; to the completion of the unit value is added in small part of O, K and S.

AMBIOTON® and RE-CHAR® are slightly relatively different from each other, in fact there is a higher% of carbon for RE-CHAR®, such as the% of O and P is also high compared to AMBIOTON®, which has a good% of Mg and K.

The nitrogen in the RE-CHAR® is three times that of CARBOSORB NC 1240; this could be due to the different production process [753]. Potassium is mostly present in AMBIOTON®, unlike sulfur in coal. Only in AMBIOTON® magnesium is present, as in the other does not reach the limit of detection. The XRF spectrum also detects the presence of iron, calcium and potassium only in the AMBIOTON®.

CARBOSORB NC 1240 is an activated carbon with a high% of carbon inside it and a good presence of O, K, S. The biochar are relatively different from each other, in fact there is a higher% of carbon for RE-CHAR®, such as the% of O and P is also high compared to AMBIOTON®, which has a good% of Mg and K.

Compared to the results obtained it is possible to make a comparison with the values reported by Singh et al. [744] and Yargicoglu et al. [746].

3.1.7 Boehm analysis

The results of the Boehm's titration method are shown in the Table 3.7.

Table 3.7 – Analysis of functional groups through Boehm's method.

Group	CARBOSORB NC 1240	AMBIOTON®	RE-CHAR®	Unit
OH-	0.41 ± 0.03	0.40 ± 0.02	0.44 ± 0.05	mmol g^{-1}
Acid	1.19 ± 0.0.9	0.98 ± 0.06	1.31 ± 0.09	mmol g^{-1}
Lactone	0.45 ± 0.03	4.34 ± 0.12	<0.001	mmol g^{-1}
Carboxyl	0.80 ± 0.05	0.29 ± 0.03	0.29 ± 0.02	mmol g^{-1}

From the results of Table 3.7 it can be show that the OH- values are similar for all the materials analysed, unlike the Acid and Lactone group which is high, respectively, in RE-CHAR® and AMBIOTON®. Furthermore,

Lactone group is very low in CARBOSORB NC 1240 and almost absent in RE-CHAR®. As for the carboxyl group it is greater in CARBOSORB NC 1240 and the same in the two biochar.

The following Table 3.8 shows some values from the literature data.

Table 3.8 – Boehm's analysis performed in other studies.

Materials	OH-	Acid	Lactone	Carboxyle	Units	Reference
DFW Biochar	0.10	0.20	0.07	0.06	mmol g^{-1}	[168]
DF Biochar	0.09	0.06	0.06	0.01	mmol g^{-1}	
HP Biochar	0.08	0.08	0.06	0.03	mmol g^{-1}	
EUC-450	0.23 ± 0.011	0.63 ± 0.004	0.17 ± 0.012	0.23 ± 0.003	mmol g^{-1}	[754]
EUC-600	0.09 ± 0.017	0.32 ± 0.006	0.10 ± 0.0016	0.14 ± 0.003	mmol g^{-1}	
Pica 150	0.64	2.51	0.75	0.87	mmol g^{-1}	[755]
Picaflo	0.27	1.34	0.51	0.51	mmol g^{-1}	
KN	0.27	0.78	0.09	0.42	mmol g^{-1}	[756]

Pica 150 and Picaflo can be comparable with the investigated CARBOSORB NC 1240.

3.1.8 MBI and IV analysis

The Table 3.9 shows the values of the methylene blue index and iodine adsorption value.

Quantifies the mg of methylene blue adsorbed by 1g of material in equilibrium with a 1 mg L^{-1} solution of methylene blue. Methylene blue has a 320 molecular weight and an effective molecular diameter of about 15 Å, therefore this index gives information on the adsorption capacity of the material on molecules of this order of magnitude. Thanks to the size of the adsorbed molecules, the iodine index indicates the surface area in pores of 10 Å or greater.

Table 3.9 – Methylene blue index and iodine adsorption value of of CARBOSORB NC 1240, AMBIOTON® and RE-CHAR®.

Index	Unit	CARBOSORB NC 1240	AMBIOTON®	RE-CHAR®
Methylene blue (MBI)	g kg^{-1} DW	30.18 ± 1.4	35.04 ± 2.7	25.56 ± 3.4
Iodine (IV)	g kg^{-1} DW	>1,000 (1,044 ± 22.1)	211 ± 8.9	202 ± 12.4

The results show that the value of the methylene blue index is greater for AMBIOTON®, but the iodine index value is similar to that of RE-CHAR®. CARBOSORB NC 1240 is different which has a very high iodine index value compared to the two biochar.

Erto et al. reported the following values for activated carbon: iodine index between 1000 and 1278 g kg-1 and methylene blue index between 180 and 332 g kg^{-1}. Saka et al. [757], the iodine index value varies depending on the material from 37 to 1200 g kg^{-1}. Zhang et al. [758], the value for methylene blue equal to 862 g kg^{-1} is reported.

3.1.9 Specific surface area, microporous volume and pore size distribution

The specific surface area (S_{BET}) was determined by nitrogen adsorption at 77 °K on which carries out the measurement of the specific surface using a continuous flow method of adsorbent gas mixed with an inert gas on a sample maintained at atmospheric pressure. The measurement is based on the determination of the quantity of adsorbed gas (nitrogen) as a monomolecular layer on the sample under examination.

The adsorption and desorption of CARBOSORB NC 1240, AMBIOTON® and RE-CHAR® prepared to nitrogen under different pressures have the similar laws, with the details shown in Figure 3.5 and Figure 3.6.

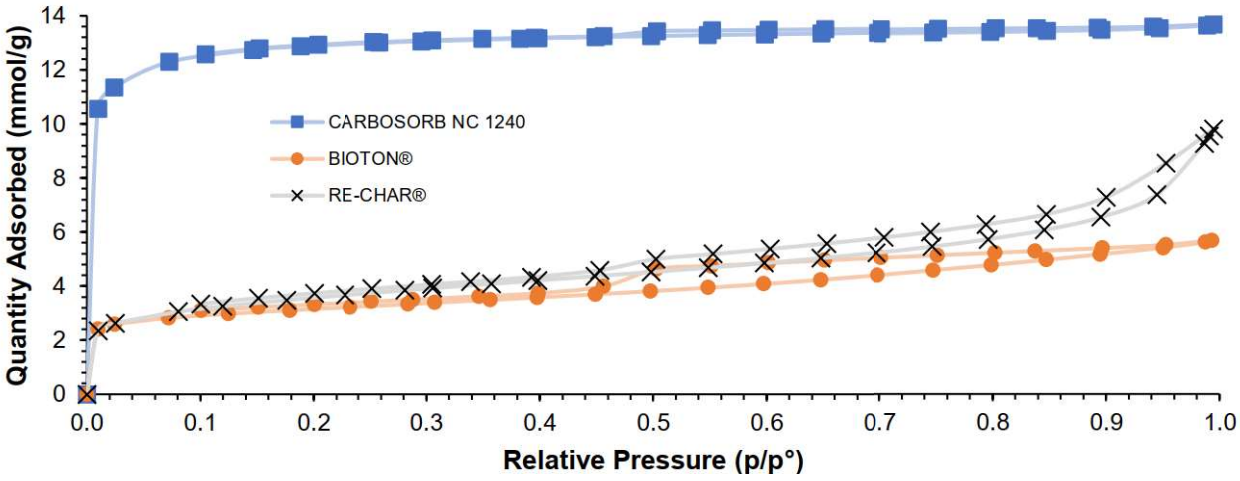

Figure 3.5 – Relative pressure vs Adsorption and desorption of CARBOSORB NC 1240, AMBIOTON® and RE-CHAR® to N_2.

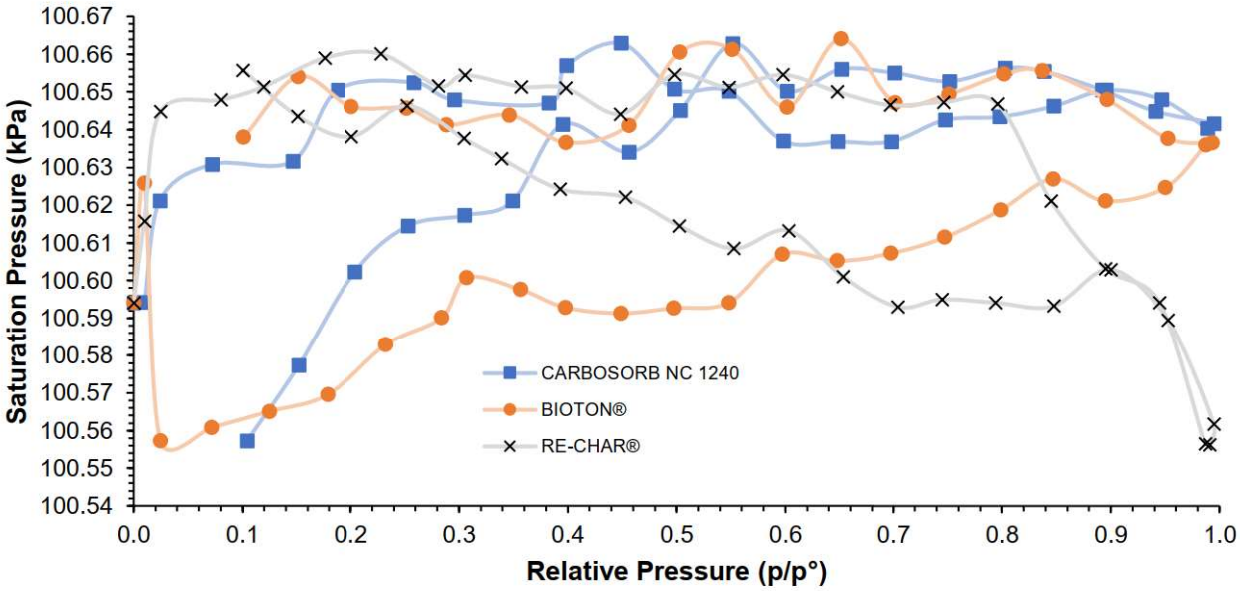

Figure 3.6 – Saturation pressure in adsorption/desorption of CARBOSORB NC 1240, AMBIOTON® and RE-CHAR® to N_2.

From the Figure 3.6, it is appreciable that the passage from adsorption to desorption both in CARBOSORB NC 1240 than in AMBIOTON® takes place in the same conditions of pressure to saturation (above 100.64); in RE-CHAR® this occurs at a slightly lower pressure, but different (approx 100.56).

In Table 3.10 the summary report of the BET analysis is shown. The single point surface area of CARBOSORB NC 1240, AMBIOTON® and RE-CHAR® have been determined, respectively, at p/p° 0.072457619, 0.124814317 and 0.227864757. BJH adsorption and desorption cumulative surfaces area were determined between 17.000 Å and 3,000.000 Å width for all carbon-based sorbent.

Table 3.10 – Summary report of surface area for CARBOSORB NC 1240, AMBIOTON® and RE-CHAR®.

	Single point surface area ($m^2 g^{-1}$)	BET Surface Area ($m^2 g^{-1}$)	BJH Adsorption cumulative surface area of pores ($m^2 g^{-1}$)	BJH Desorption cumulative surface area of pores ($m^2 g^{-1}$)
CARBOSORB NC 1240	1,112.1743	1,126.6411	71.8756	71.7123
AMBIOTON®	254.1408	256.2287	104.2323	115.8626
RE-CHAR®	276.1552	280.2516	164.0660	158.5556

Through the data shown in the report (Table 3.10), the deviations related to the instrumental response, caused by the matrix effect of the three carbon-based sorbents, were also investigated.

The Table 3.11 shows the parameters used for the linearization of the BET equation, in the range allowed to validate these results with the linear equation.

Table 3.11 – Linearization parameters of the BET equation.

	CARBOSORB NC 1240	AMBIOTON®	RE-CHAR®
BET surface area ($m^2 g^{-1}$)	1,126.6411 ± 0.9436	256.2287 ± 1.3481	280.2516 ± 2.0686
Slope ($g\ mmol^{-1}$)	0.086504 ± 0.000072	0.380430 ± 0.001998	0.347361 ± 0.002548
Y-intercept ($g\ mmol^{-1}$)	0.000089 ± 0.000003	0.000320 ± 0.000146	0.000752 ± 0.000336
C	976.880829	1,190.154960	463.079552
Qm ($mmol\ g^{-1}$)	11.54829	2.62639	2.87263
Correlation coefficient	0.9999996	0.9999724	0.9998924
Molecular cross-sectional area (nm^2)	0.1620	0.1620	0.1620

Starting from linearization, further statistical analysis have therefore made it possible to determine the specifics surface areas, also considering the deviation, equal to 1126.64 ± 12.44 $m^2 g^{-1}$, 256.23 ± 9.44 $m^2 g^{-1}$ and 280.25 ± 7.12 $m^2 g^{-1}$ respectively for CARBOSORB NC 1240, AMBIOTON® and RE-CHAR®.

From the adsorption of biochar to nitrogen, it may be seen that, CARBOSORB NC 1240>RE-CHAR®>AMBIOTON®, which shows that the activated carbon has good adsorption performance.

The value of specific surface of CARBOSORB NC 1240 is higher than in Luperto et al. [759], where the specific surface value of its active carbons analyzed varies from 550 to 899 $m^2 g^{-1}$.

Furthermore, the values found by Yargicoglu et al. [746] for the biochar samples analyzed vary from 5.41 to 611.87 $m^2 g^{-1}$, while Leeq et al. [747] reported BET values from 26.0 to 154 $m^2 g^{-1}$.

In the following figures (Figure 3.7, Figure 3.8 and Figure 3.9) are shown the compositions of absolute pressure as a function of different adsorption/desorption of the three carbonaceous materials.

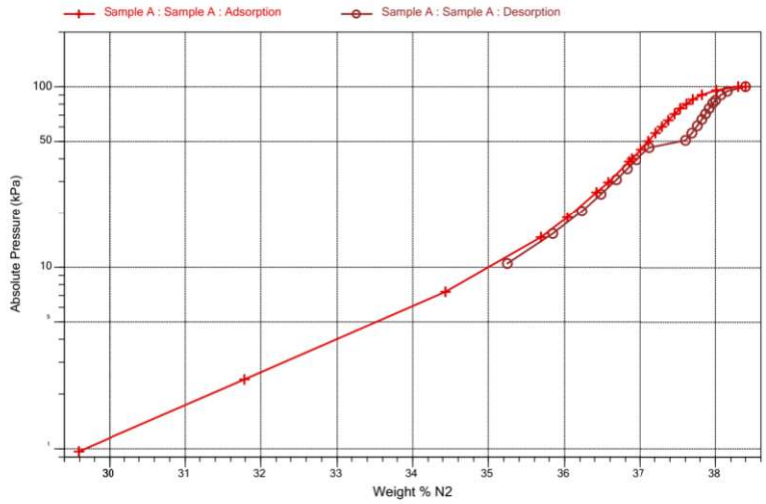

Figure 3.7 – Pressure composition in adsorption/desorption of CARBOSORB NC 1240 to N_2.

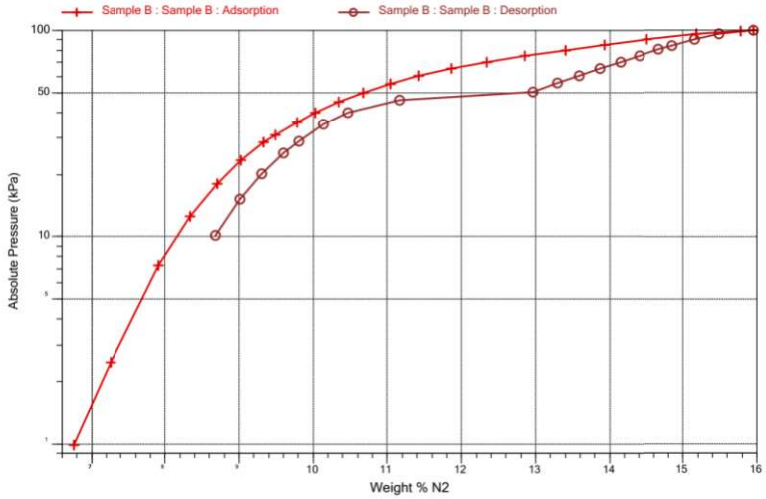

Figure 3.8 – Pressure composition in adsorption/desorption of AMBIOTON® to N_2.

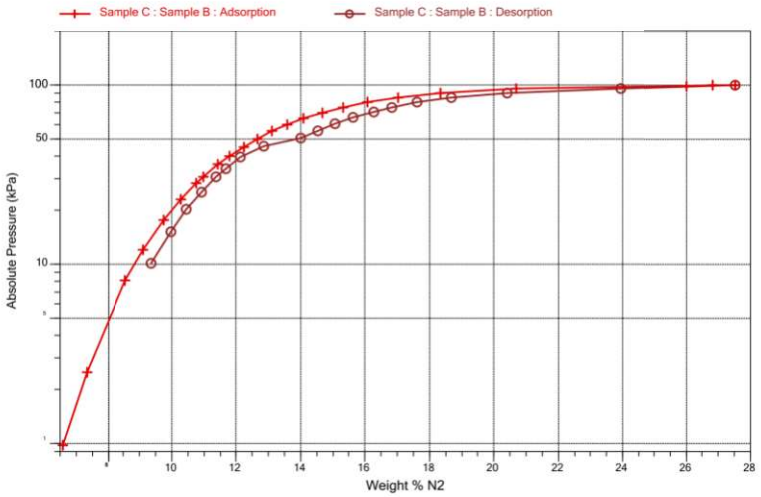

Figure 3.9 – Pressure composition in adsorption/desorption of RE-CHAR® to N_2.

Both Biochar have a type IV isotherm of the International Union of Pure and Applied Chemistry (IUPAC) classification. One of the characteristics of type IV is the hysteresis cycle. Initially, the isotherm follows the same profile as the type II isotherm in which the formation of the monolayer occurs and to follow the formation of the multilayer.

In Table 3.12 is shown the summary report of pore volume and pore size. BJH adsorption and desorption cumulative volumes of pores were determined between 17.000 Å and 3,000.000 Å width for all carbon-based sorbent.

Table 3.12 – Summary report of pore volume and pore size for CARBOSORB NC 1240, AMBIOTON® and RE-CHAR®.

	Pore volume		Pore size	
	BJH Adsorption cumulative volume of pores ($cm^3\ g^{-1}$)	**BJH Desorption cumulative volume of pores ($cm^3\ g^{-1}$)**	**BJH Adsorption average pore width [4V/A] (Å)**	**BJH Desorption average pore width [4V/A] (Å)**
CARBOSORB NC 1240	0.057615	0.056178	32.064	31.335
AMBIOTON®	0.129858	0.127704	49.834	44.088
RE-CHAR®	0.283416	0.274866	69.098	69.342

Through the data shown in the report (Table 3.12), the deviations related to the instrumental response, caused by the matrix effect, were also investigated.

For the t-plot, the equation (73) adopted for the thickness curve (Figure 3.10) and the Table 3.13 relating to the report with the parameters adopted are presented below.

$$t = \sqrt{\frac{13.99}{[0.034 - \log(^{p}/_{p_0})]}} \tag{73}$$

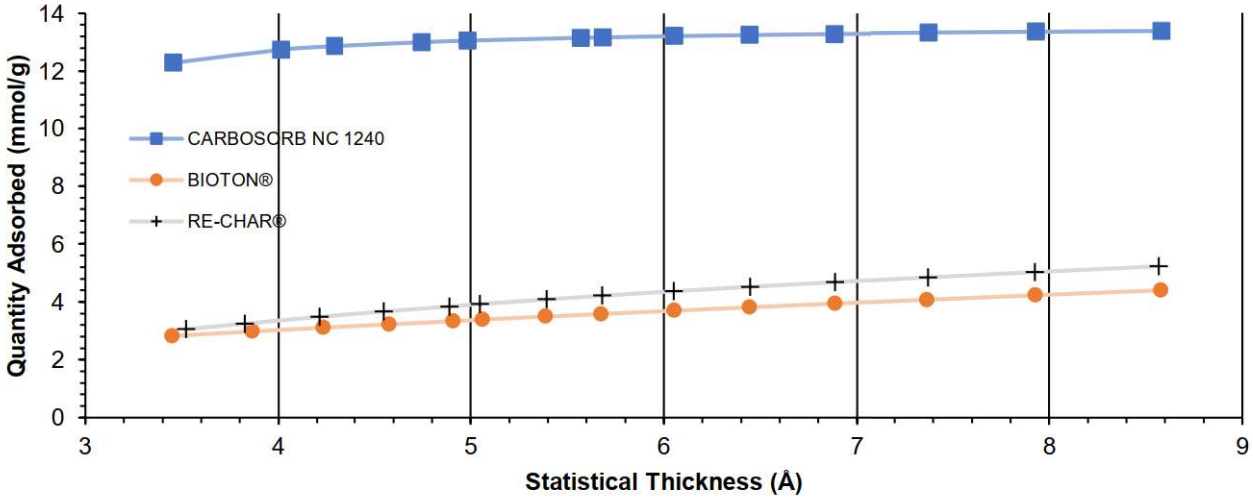

Figure 3.10 – t-Plot in adsorption/desorption of CARBOSORB NC 1240, AMBIOTON® and RE-CHAR® to N_2.

Table 3.13 – Summary t-plot report for CARBOSORB NC 1240, AMBIOTON® and RE-CHAR®.

	CARBOSORB NC 1240	AMBIOTON®	RE-CHAR®
Micropore volume ($cm^3\ g^{-1}$)	0.398410	0.057996	0.035743
Micropore area ($m^2\ g^{-1}$)	1,014.9686	138.4452	79.3663
External surface area ($m^2\ g^{-1}$)	111.6726	117.7835	200.8853
Slope (mmol $(g \cdot Å)^{-1}$)	0.321440 ± 0.027400	0.339032 ± 0.004225	0.578234 ± 0.014587
Y-intercept (mmol g^{-1})	11.467873 ± 0.123943	1.669383 ± 0.018636	1.028823 ± 0.061652
Correlation coefficient	0.992812	0.999845	0.999047
Surface area correction factor	1.000	1.000	1.000
Density conversion factor	0.0015500	0.0015500	0.0015500
Total BET surface area ($m^2\ g^{-1}$)	1,126.6411	256.2287	280.2516
Thickness range	3.5000 Å to 5.0000 Å	3.5000 Å to 5.0000 Å	3.5000 Å to 5.0000 Å
Thickness equation	Harkins and Jura	Harkins and Jura	Harkins and Jura

Further statistical analysis have therefore made it possible to determine the average porosity and pore size of the three carbon-based sorbents, also considering the deviation, equal to: 0.057 ± 0.004 $cm^3\ g^{-1}$ and 32 ± 0.6 Å for CARBOSORB NC 1240; 0.128 ± 0.009 $cm^3\ g^{-1}$ and 47 ± 1.5 Å for AMBIOTON®; 0.28 ± 0.012 $cm^3\ g^{-1}$ and 69±1.1 Å for RE-CHAR®.

The quality of a material as a function of porosity depends on the size, density and distribution of the particles, their shape and how they bond together [760]. The pores communicating with the external surface are named open pores and are accessible to ions or molecules [761]; the non-communicating ones are named closed pores and do not contribute to the adsorption properties of a porous material but influence its mechanical properties [762].

The graphs relating to the volume and area of the pores are shown, during the adsorption (Figure 3.11 and Figure 3.12) and desorption of N_2 (Figure 3.13 and Figure 3.14). This curves are typical of many mesoporous industrial adsorbents.

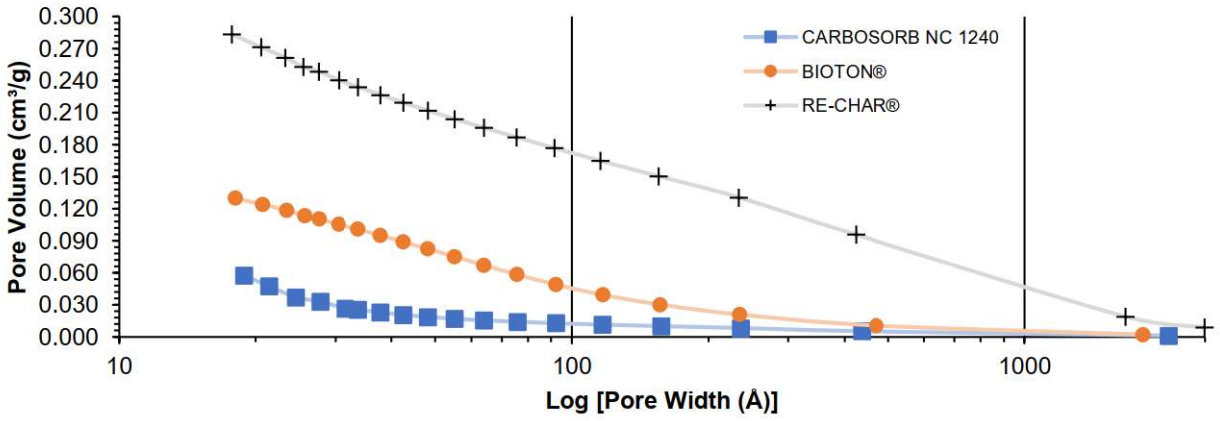

Figure 3.11 – Pore volume in adsorption of CARBOSORB NC 1240, AMBIOTON® and RE-CHAR® to N_2.

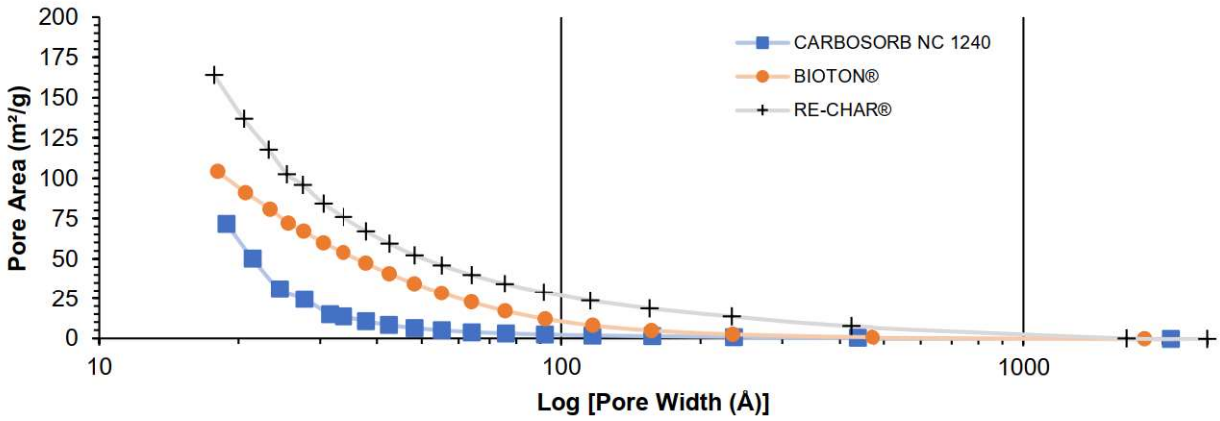

Figure 3.12 – Pore area in adsorption of CARBOSORB NC 1240, AMBIOTON® and RE-CHAR® to N_2.

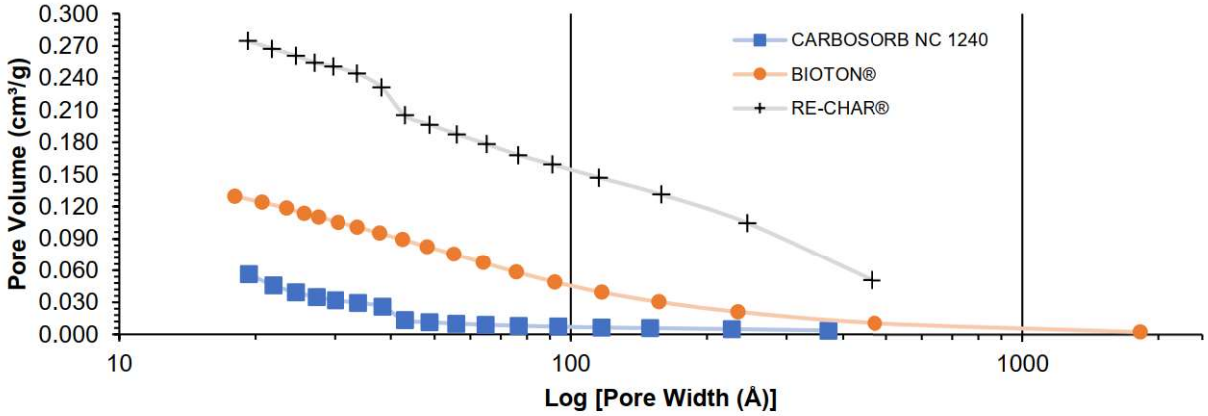

Figure 3.13 – Pore volume in desorption of CARBOSORB NC 1240, AMBIOTON® and RE-CHAR® to N_2.

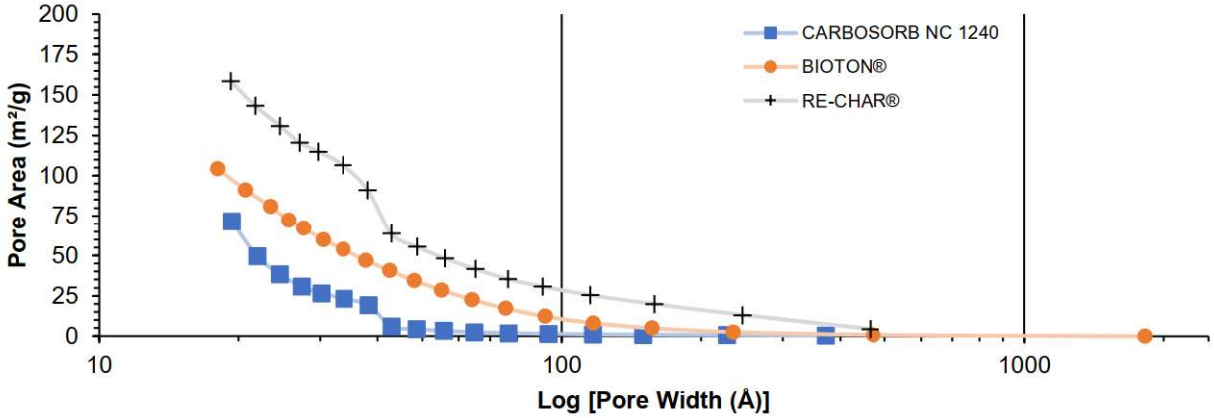

Figure 3.14 – Pore area in desorption of CARBOSORB NC 1240, AMBIOTON® and RE-CHAR® to N_2.

Both Biochar belong to the category of mesopores having a pore size between 2 and 50 nm (20 - 500 Å). These results are like the values of Yang et al. equal [763] to 5.93 nm and 6.23 nm. IUPAC has classified pores based on its size [764]: micropores with a width of < 2 nm; mesopores with a width between 2 and 50 nm; macropores with a width of > 50 nm [21,765]. In summary, the found values of specific surface area and porosity property make both biochar more suitable for the candidates of porous mediums [766–768].

3.1.10 Raman analysis

Figure 3.15 shows the Raman Spectroscopy of carbonaceous substances. CARBOSORB NC 1240, AMBIOTON® and RE-CHAR® are indicated, respectively, with A, B and C.

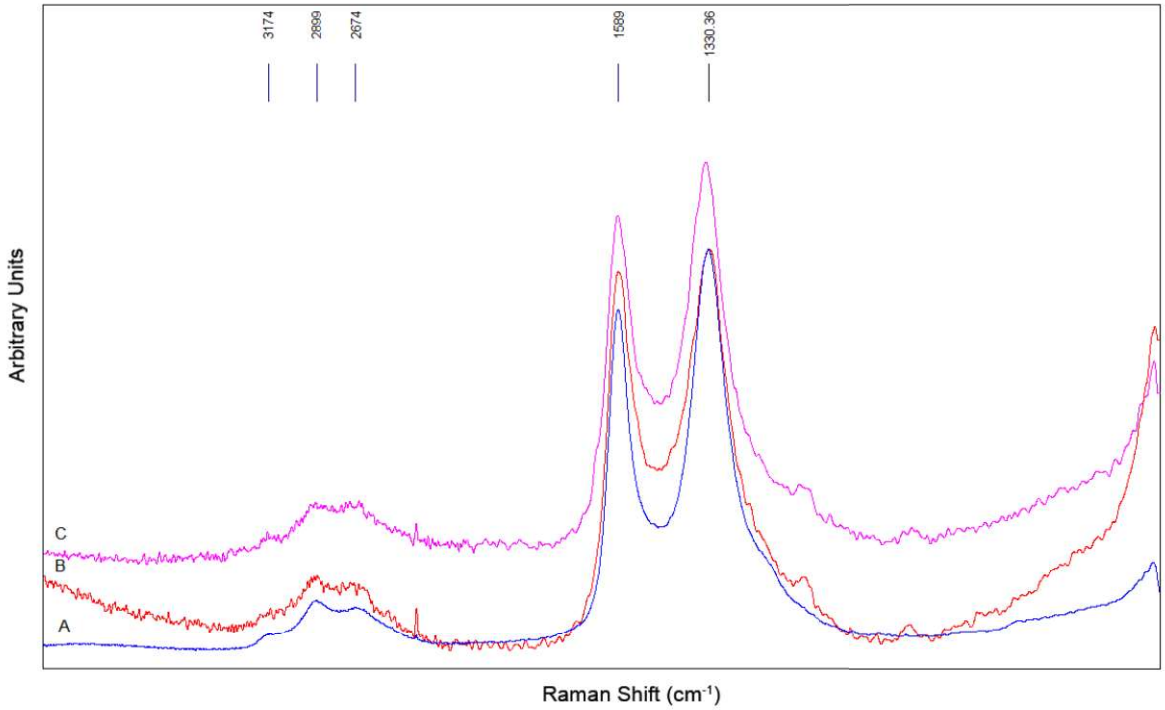

Figure 3.15 – Raman spectroscopy of CARBOSORB NC 1240, AMBIOTON® and RE-CHAR®.

The Raman spectrum is composed of several bands, linked to the vibrations of different intensity that characterize the molecule [769]. Raman spectroscopy allows to study the vibrations that modulate the polarizability of the molecule under examination [770] and high-level structural features of disordered carbon-based sorbents, such as biochar [237].

Two main peaks, D and G, can be notices at approximately at 1330 and 1580 cm^{-1}. Respectably the G band is an intrinsic Raman-active band for the ideal graphite structure and corresponds to the E2g vibration due to the C-C stretching in the longitudinal symmetry axis of the graphite plane. This band represents a high degree of graphitization on the other hand, Band D, usually identified as A1g vibration, is assigned to defects present at the edges of the carbon layers.

Table 3.14 – Positions of characteristic Raman bands and their integrated intensity ratios.

Carbon-based sorbent	D Band (cm^{-1})	G Band (cm^{-1})	I_D/I_G
CARBOSORB NC 1240	1334.0	1590.0	3252.056/2,829.469 = 1.149
AMBIOTON®	1334.0	1590.0	286.933/299.411 = 0.958
RE-CHAR®	1341.0	1595.0	327.702/302.060 = 1.084

Table 3.14 shows the positions of the characteristic Raman bands and the integrated intensity ratios (I_D/I_G) of the analysed samples. The ratio of integrated intensities is a measure of the orientation of the graphite planes and the degree of graphitization.

3.1.11 Scanning electron microscope (SEM)

Scanning electron microscopy (SEM) is a microscopic technique in determining the image macro porosity and physical morphology of solid substances [744]. SEM allows a three-dimensional view of the external surfaces of biological structures. It uses an electron beam that hits the sample. The sample is kept under vacuum to prevent air from disturbing the creation of the electron beam. The sample must be conductive, otherwise it would produce electrostatic charges that would disturb the detection of the signal; in the case of non-conductive samples, they can be metallized through surface metallization through a thin layer of Gold or Carbon, or by ultra-high vacuum bombardment with Ar radicals.

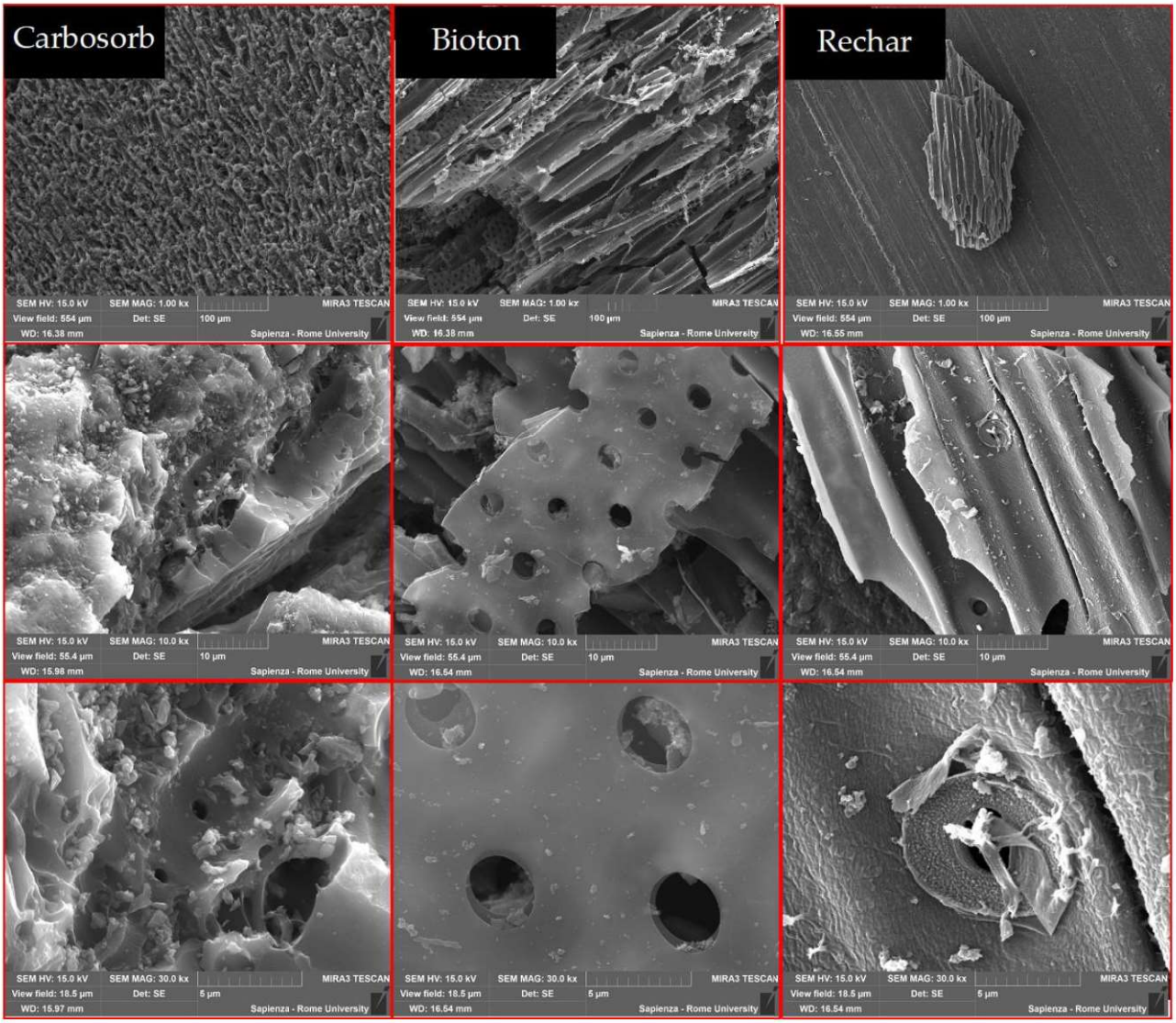

Figure 3.16 – SEM images for CARBOSORB NC 1240, AMBIOTON® and RE-CHAR®. Comparison with the three samples at the same magnifications (from the top: 1kX, 10 kX and 30 kX).

The Figure 3.16 shows the homogeneous and compact surface of CARBOSORB NC 1240 and the heterogeneous repetitive structure of AMBIOTON® (such as cellulose structures); it is also clear that RE-CHAR® is completely different from the other two carbonaceous materials in terms of at least dimensions, longitudinal and transverse section. In both biochar particles related to the different production process of traditional activated carbon are evident.

In Figure 3.17, a Scanning Electron Microscope (SEM) images of AMBIOTON® (A1, B1, C1 and D1) and RE-CHAR® (A2, B2, C2 and D2) surface are shown, at various magnifications: (A1) 79 x; (A2) 100 x; (B1) 2.50 kx; (B2) 500 x; (C1) 2.00 kx; (C2) 1.00 kx; and (D1 and D2) 100.00 kx.

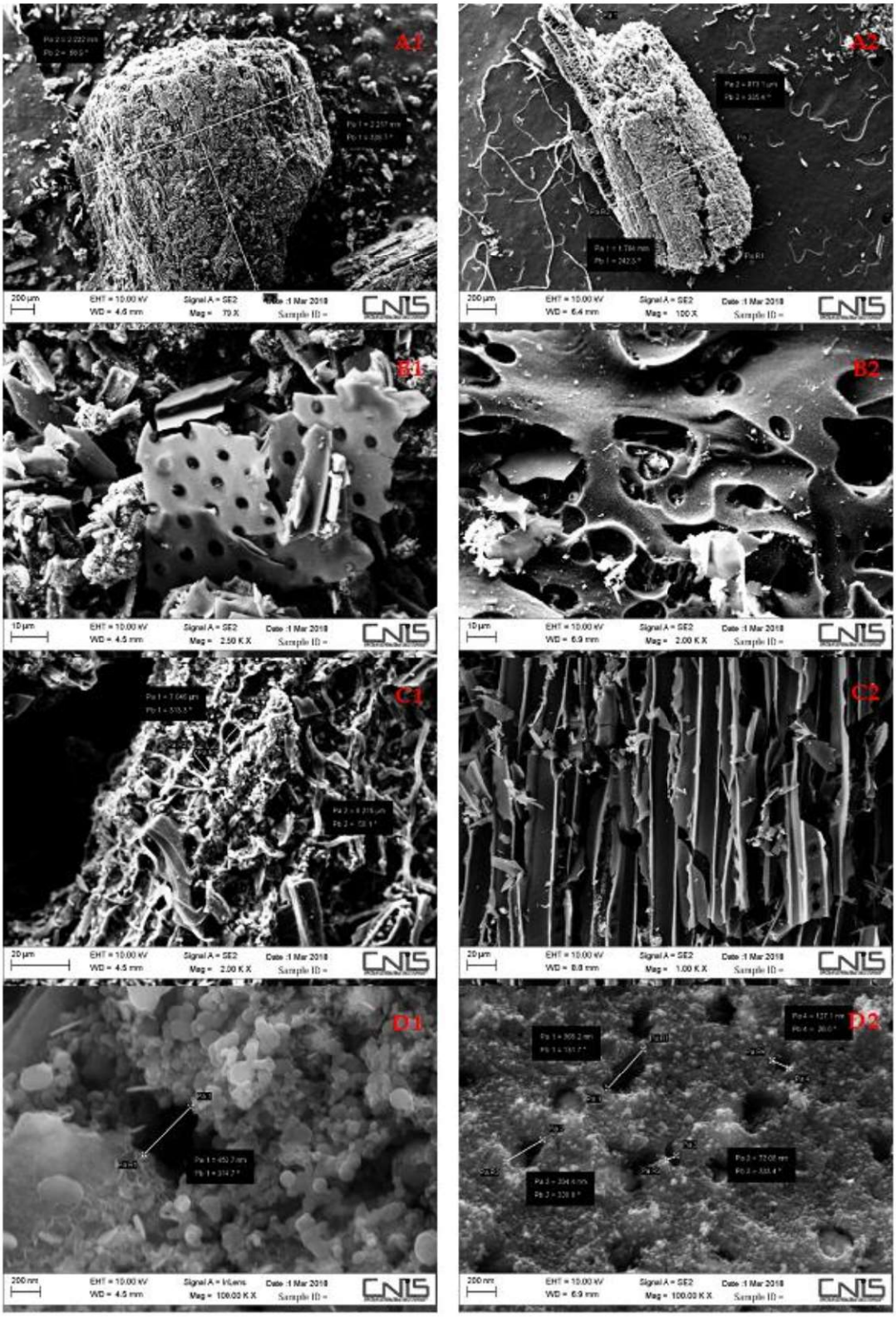

Figure 3.17 – SEM images of the surface of AMBIOTON® and RE-CHAR®.

Particularly in Figure 3.17 are highlighted; (A1) the particle size of AMBIOTON®, (A2) one chip of RE-CHAR®, (B1) the different feedstocks used for AMBIOTON® production, (B2) the transversal cut cross section of RE-CHAR®, (C1) the cross-section of AMBIOTON®, (C2) the longitudinal vertically cut cross section of RE-CHAR®, (D1) the internal pores of AMBIOTON® and (D2) variously sized pores of RE-CHAR®.

Below in the figures, from Figure 3.18 to Figure 3.22, the various particles are represented in different zoom functions (45x, 500x, 1kx, 3kx, 10kx, 30kx).

Two different particles of the same sample for CARBOSORB NC 1240 and AMBIOTON® were visualized at SEM, while only one particle for RE-CHAR®.

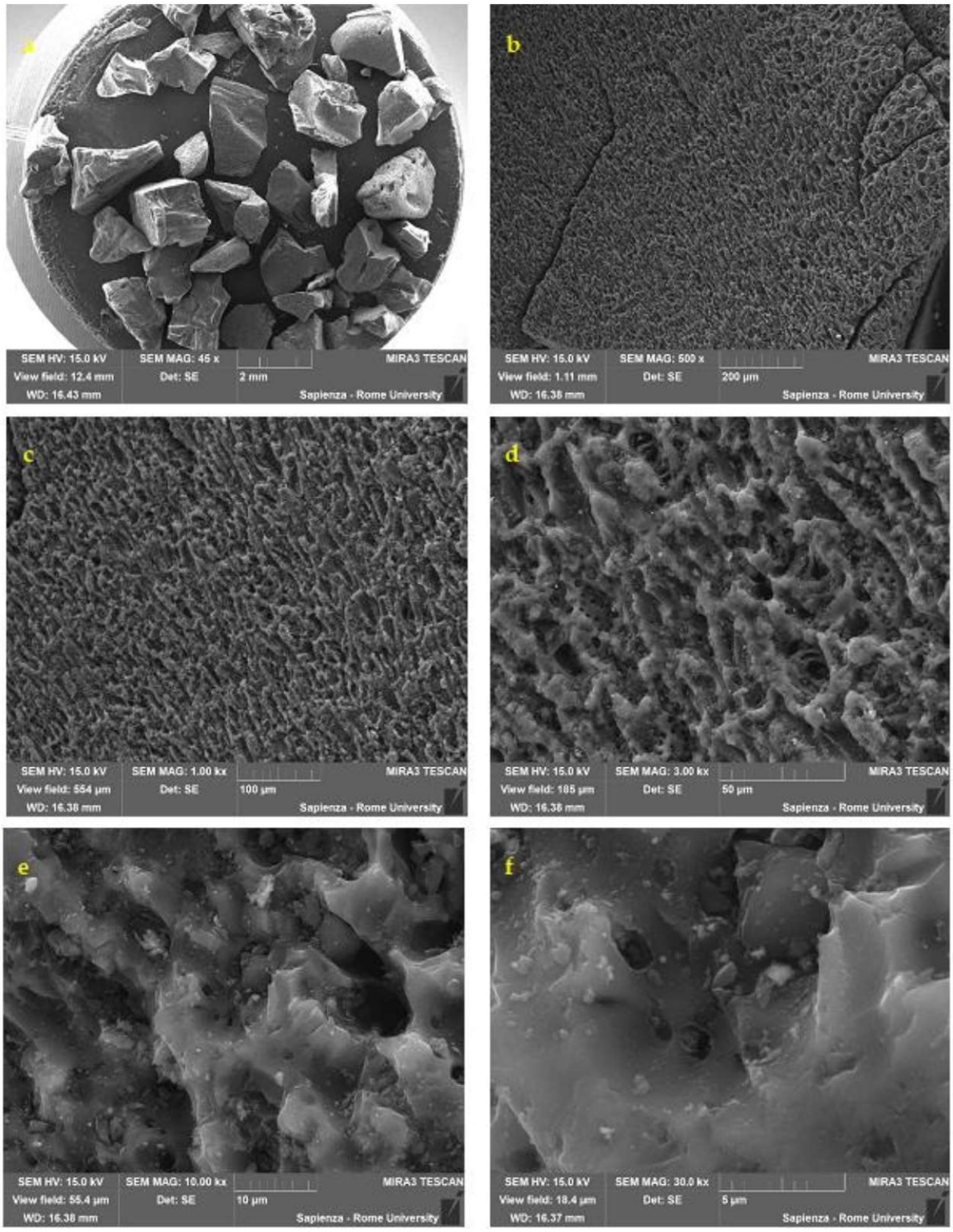

Figure 3.18 – Scanning Electron Microscope (SEM) images of CARBOSORB NC 1240 (particle 1) in magnification order: (a) 45 x; (b) 500 x; (c) 1.00 kx; (d) 3.00 kx; (e) 10.00 kx; (f) 30.0 kx.

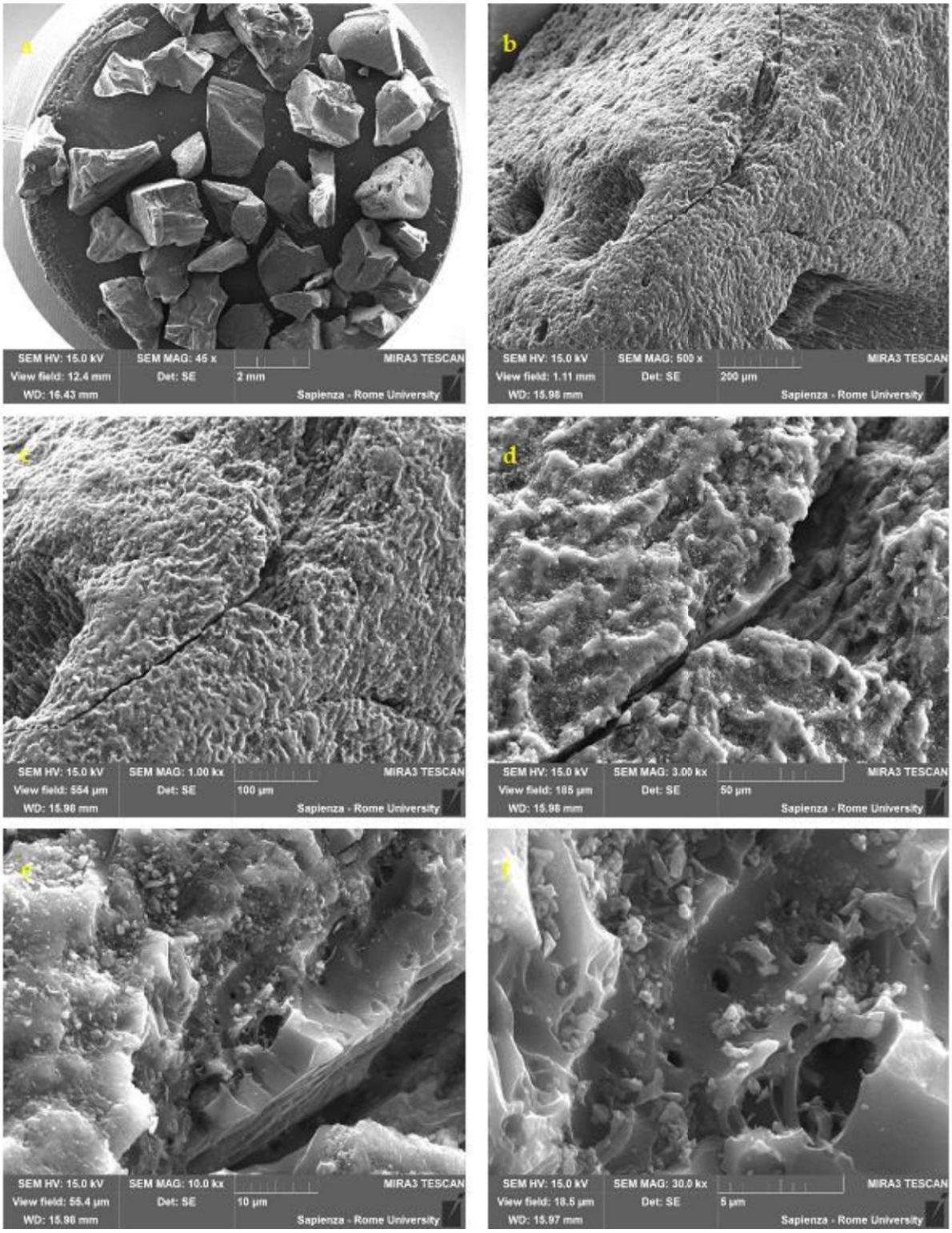

Figure 3.19 – Scanning Electron Microscope (SEM) images of CARBOSORB NC 1240 (particle 2) in magnification order: (a) 45 x; (b) 500 x; (c) 1.00 kx; (d) 3.00 kx; (e) 10.00 kx; (f) 30.0 kx.

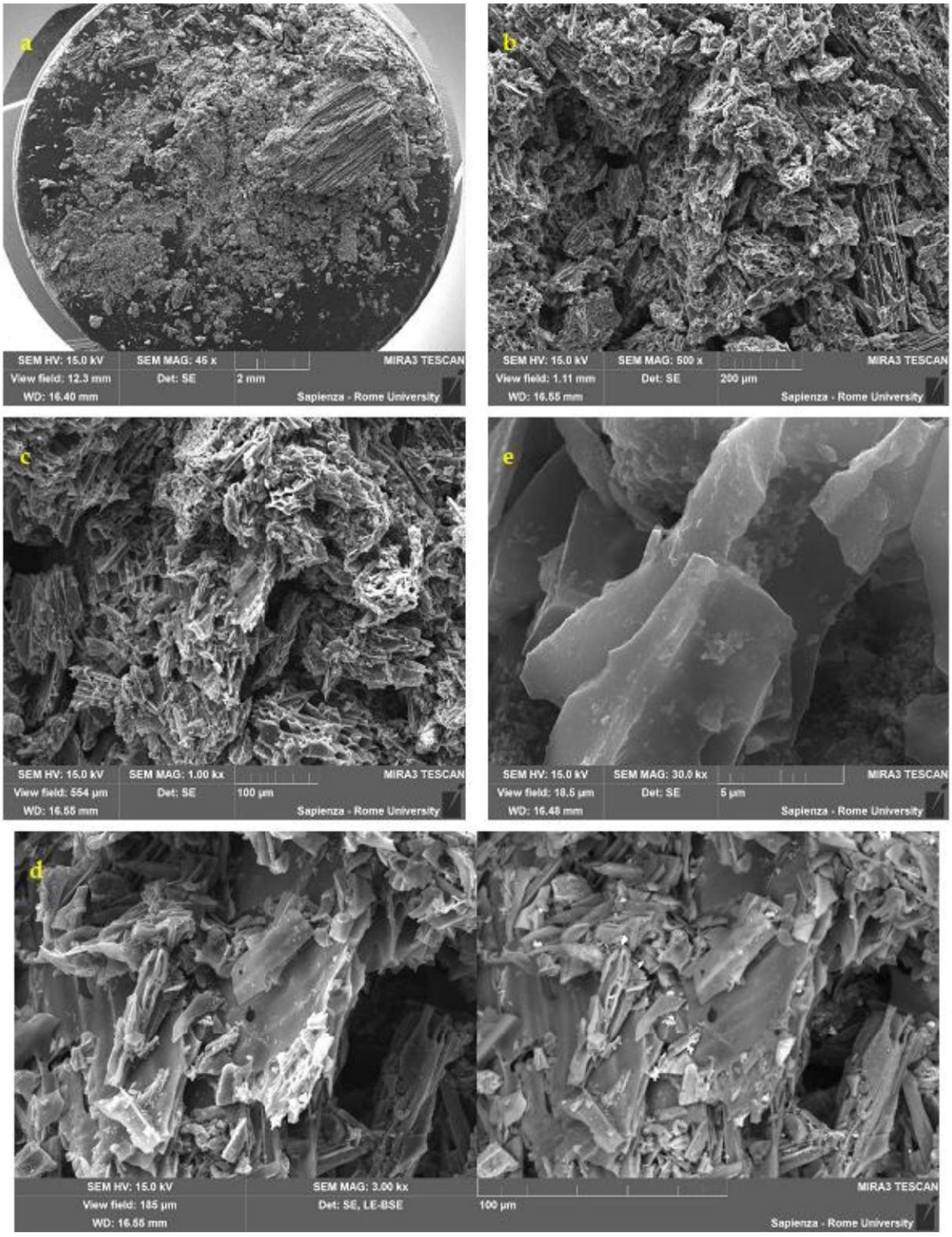

Figure 3.20 – Scanning Electron Microscope (SEM) images of AMBIOTON® (particle 1) in magnification order: (a) 45 x; (b) 500 x; (c) 1.00 kx; (d) 3.00 kx; (e) 30.0 kx.

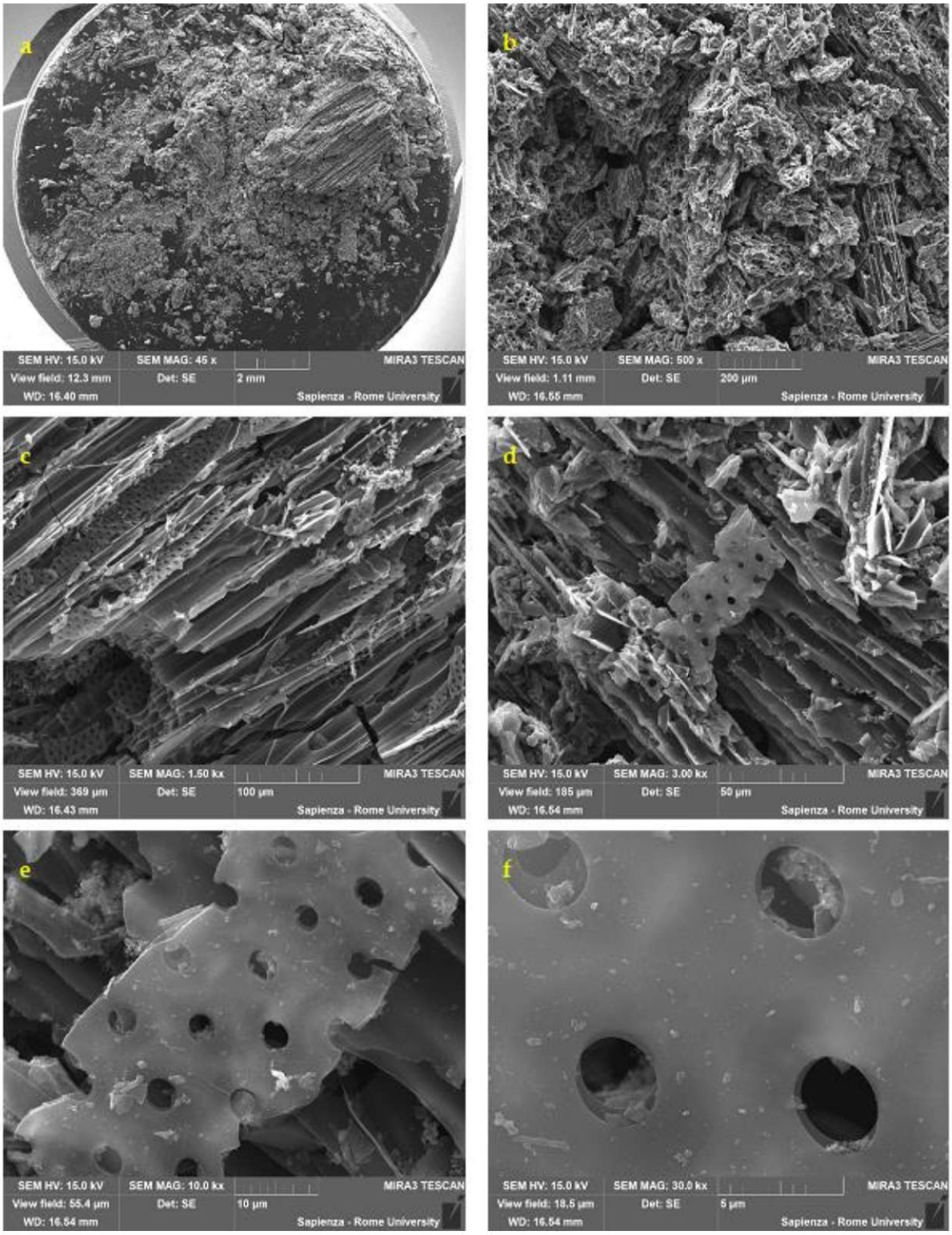

Figure 3.21 – Scanning Electron Microscope (SEM) images of AMBIOTON® (particle 2) in magnification order: (a) 45 x; (b) 500 x; (c) 1.50 kx; (d) 3.00 kx; (e) 10.00 kx; (f) 30.0 kx.

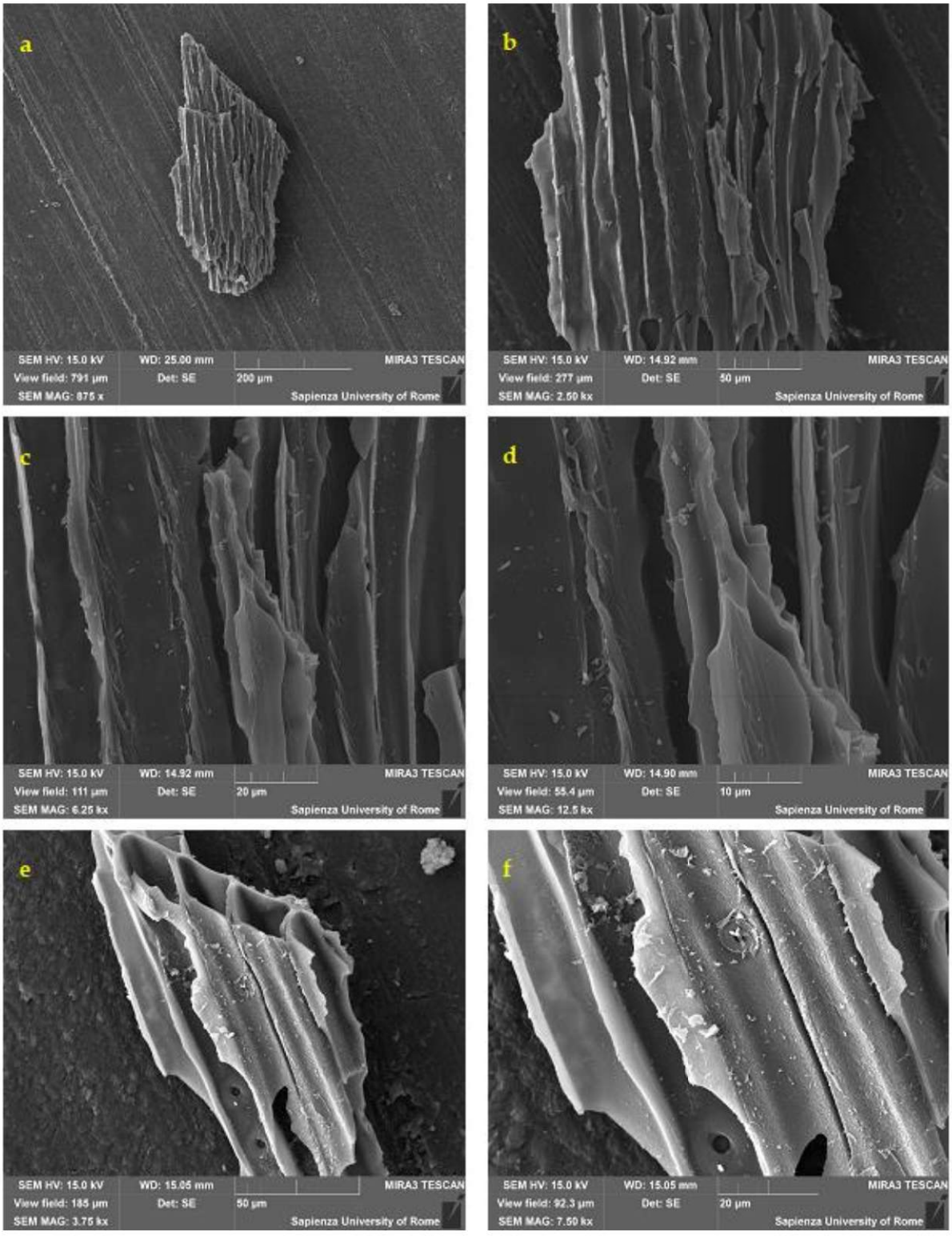

Figure 3.22 – Scanning Electron Microscope (SEM) images of RE-CHAR® in magnification order: (a) 875 x; (b) 2.5 kx; (c) 6.25 kx; (d) 12.5 kx; (e) 3.75 kx; (f) 7.50 kx.

3.1.12 Energy-dispersive X-ray spectroscopy (EDS)

Energy Dispersive X-ray Spectrometry indicates an analytical method that uses the emission of X-rays by an accelerated electron beam that affects the sample under examination. It is a non-destructive and relatively rapid methodology that allows to study samples of solid material that must be stable under an electronic bombardment and an electrical conductor. The EDS allows an instant qualitative analysis of the elements present in the sample and their proportions in a very short time [771].

Below are the images (Figure 3.23) for each analysed area of each sample and the respective data analysis with all the parameters studied through the Energy-dispersive X-ray spectroscopy (EDS). Two different areas of the same sample were analysed, for each sample considered, in order to evaluate the variability of the material.

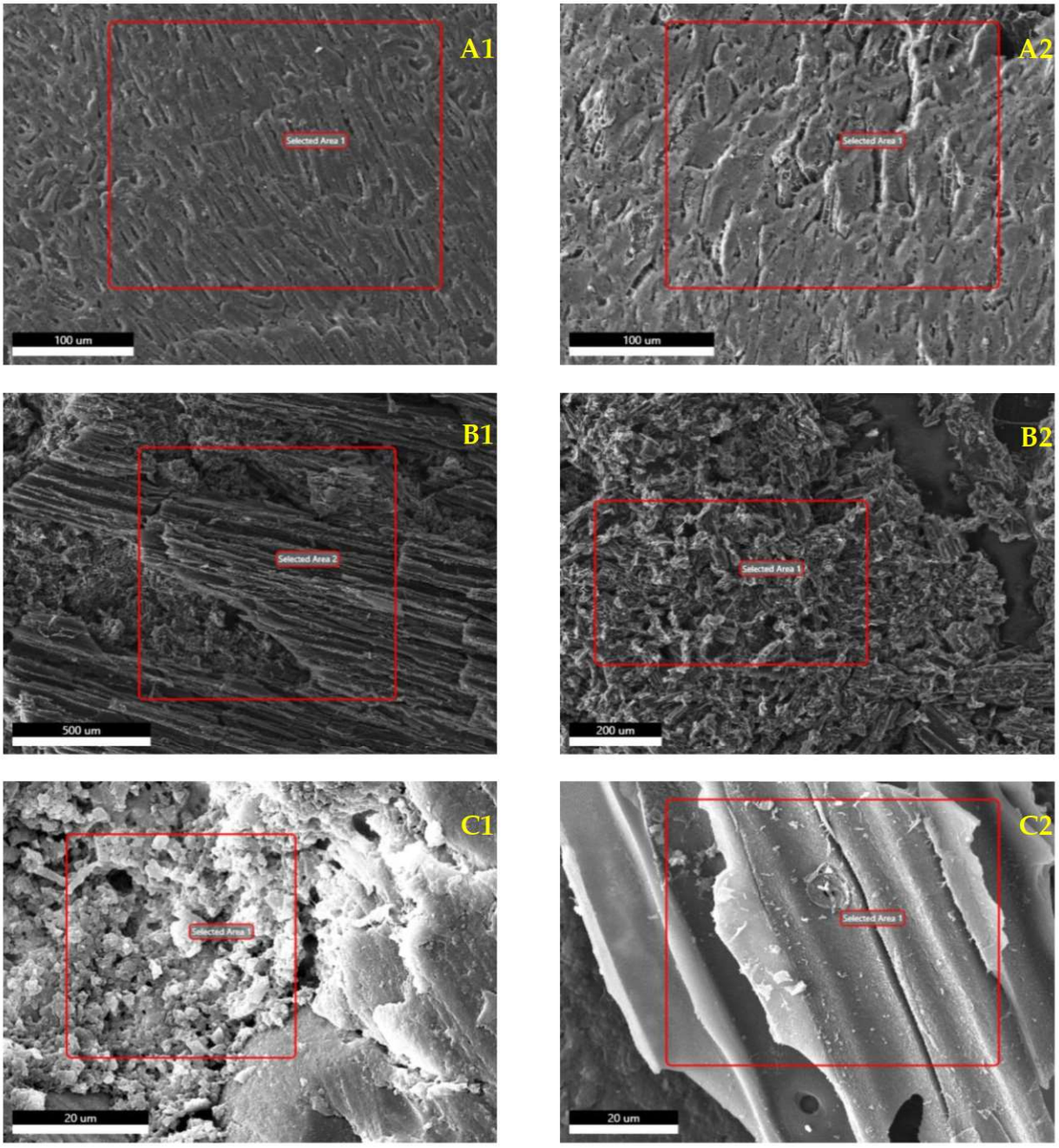

Figure 3.23 – SEM images of selected areas of CARBOSORB NC 1240 (A1, A2), AMBIOTON® (B1, B2) and RE-CHAR® (C1, C2).

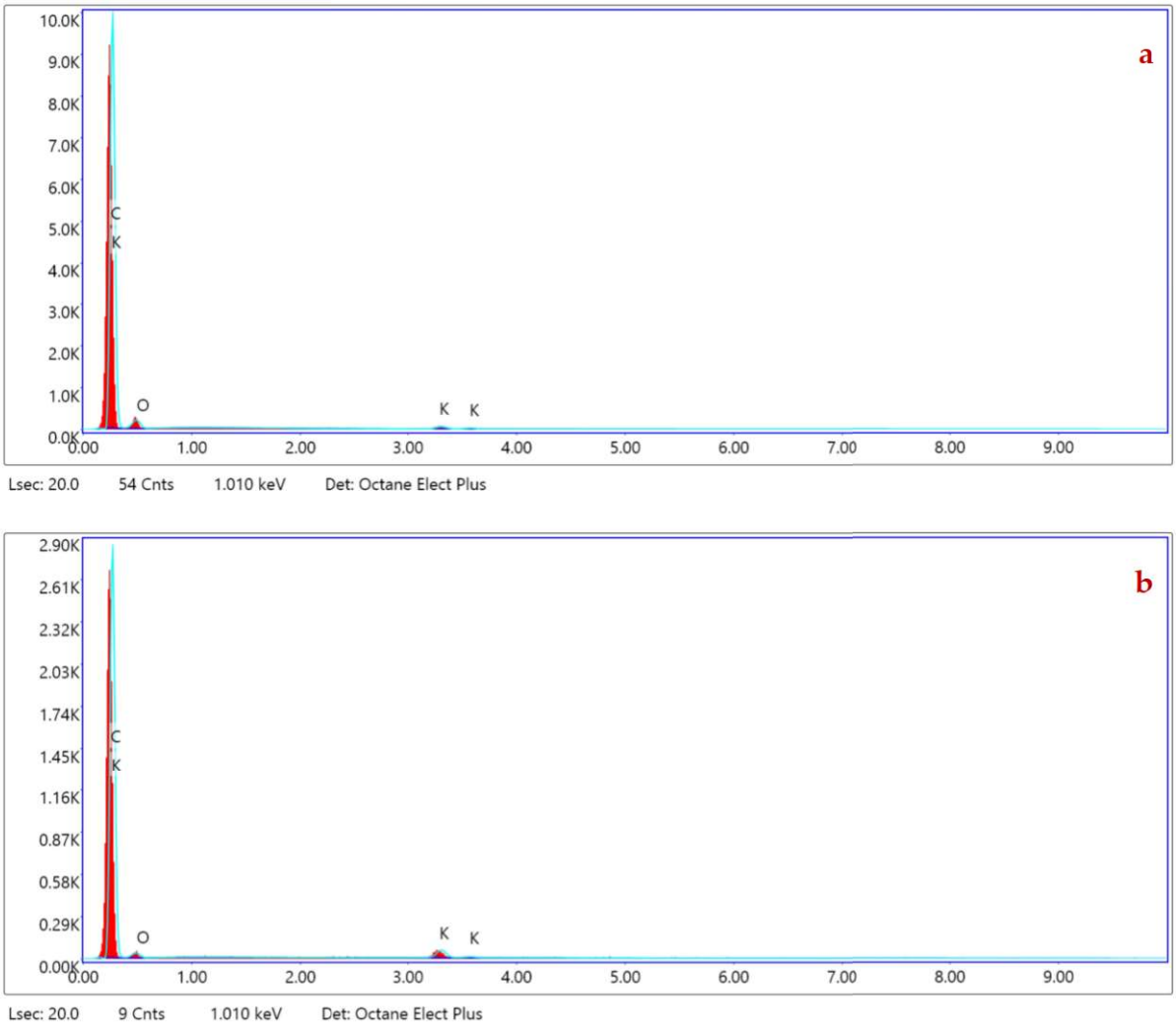

Figure 3.24 – EDS analysis graph of two areas of CARBOSORB NC 1240 (kV: 15, Mag.: 780, Takeoff: 34.9, Live Time: 20 s, Amp. Time: 0.96 μs, Resolution: 130 eV).

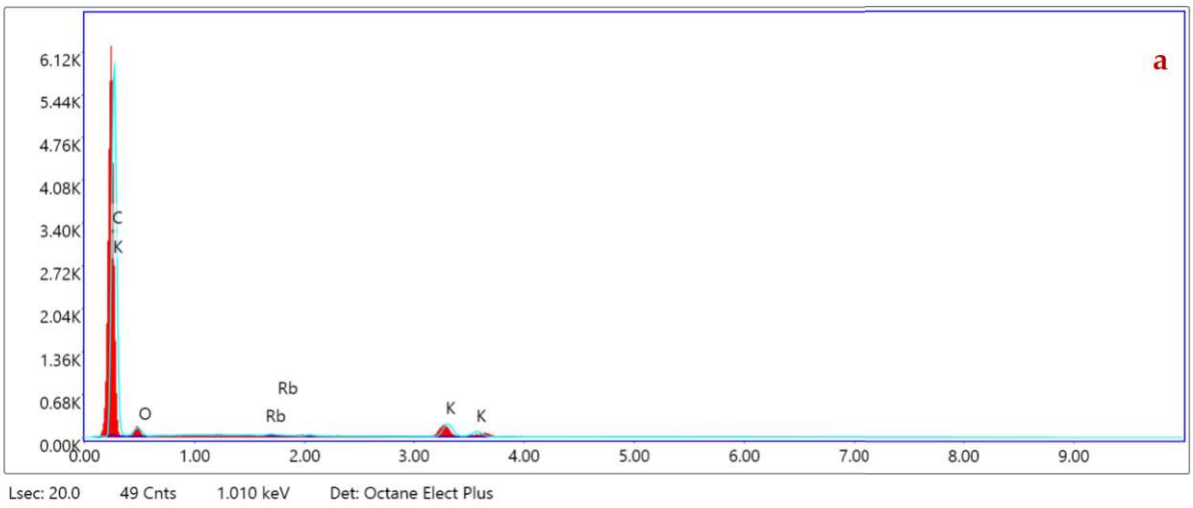

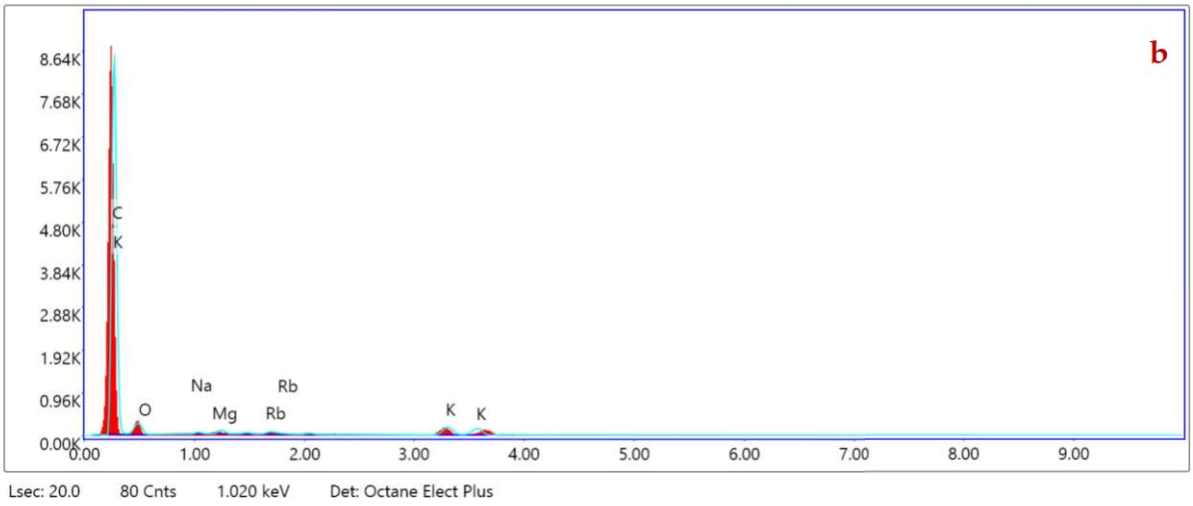

Figure 3.25 – EDS analysis graph of two areas of AMBIOTON® (kV: 15, Mag.: 780, Takeoff: 34.9, Live Time: 20 s, Amp. Time: 0.96 µs, Resolution: 130 eV).

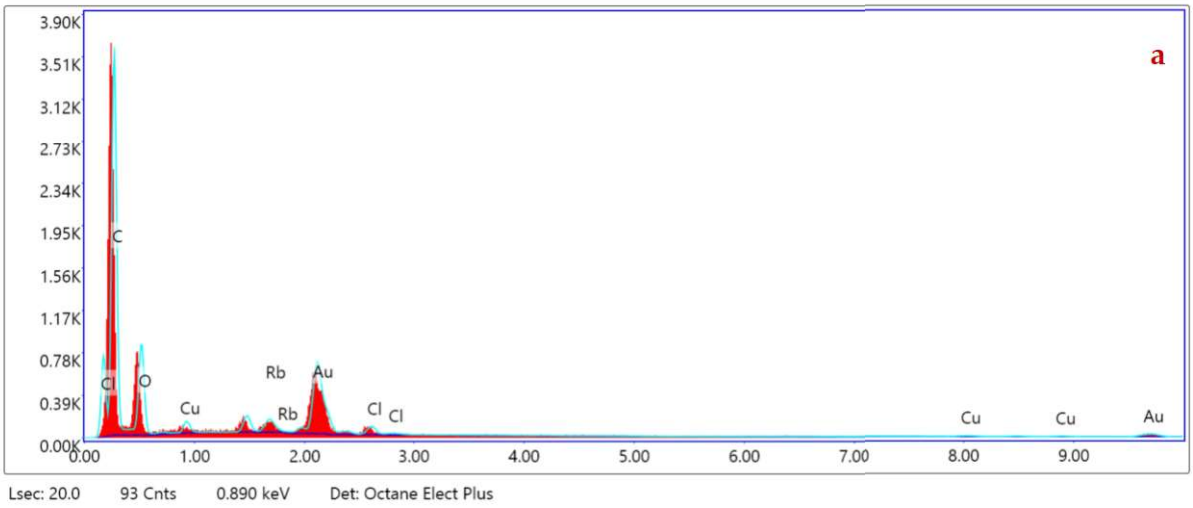

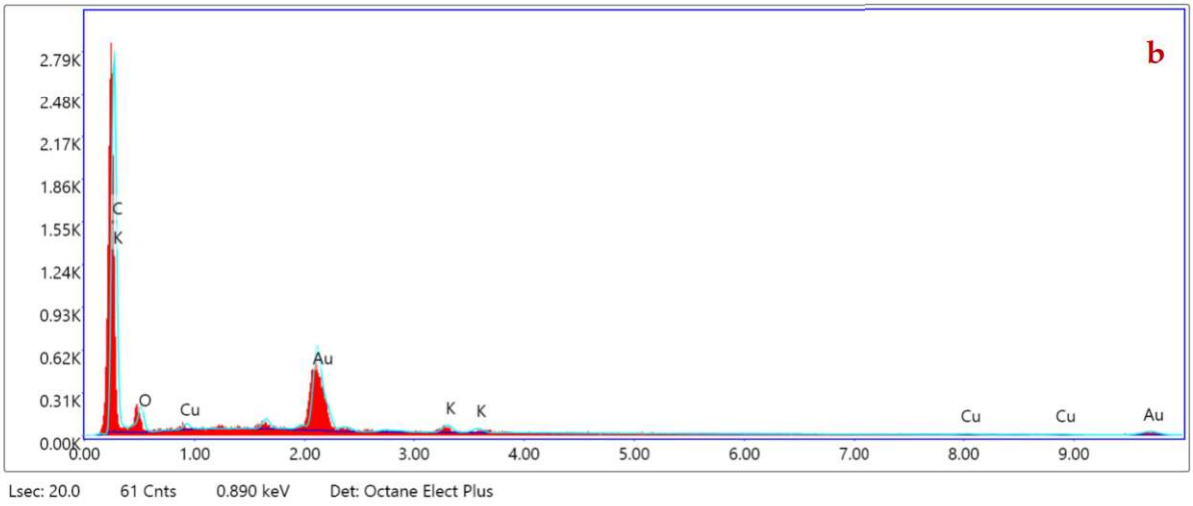

Figure 3.26 – EDS analysis graph of two areas of RE-CHAR® (kV: 15, Mag.: 249, Takeoff: 35.3, Live Time: 20 s, Amp. Time: 0.96 µs, Resolution: 130 eV).

In the above figures (Figure 3.24, Figure 3.25 and Figure 3.26), the EDS analysis of graphs of selected areas SEM are shown.

ZAF corrections has been applied to EDX measurements in the SEM to convert apparent concentrations (raw peak intensity) into (semi-quantitative) concentrations corrected for inter-element matrix effects. Very simplistically, Z is the atomic number correction related to stopping power of the element, A is the absorption correction - less energetic X-rays from lighter elements are absorbed upon leaving the sample by heavier elements, F is the fluorescence correction - A more energetic X-ray leaving the sample can fluoresce a lower energy X-ray from a lighter element. The ZAF routine is iterative, it needs information on concentrations in order to proceed but these are absent at the start. So the results from the first iteration are fed back to the second and so on until a limit is reached that is statistically satisfactory.

Table 3.15 – EDS analysis of CARBOSORB NC 1240, AMBIOTON®, RE-CHAR®.

CARBOSORB NC 1240		AMBIOTON®		RE-CHAR®	
Element	**Weight %**	**Element**	**Weight %**	**Element**	**Weight %**
C K	95.13	C K	88.19	C K	59.00
O K	3.43	O K	2.88	O K	6.69
K K	1.45	RbL	0.65	AuM	30.67
		K K	8.28	K K	1.94
				CuK	1.71

From the results it's visible that CARBOSORB NC 1240 has a much higher percentage of carbon (95.13%) than RE-CHAR® (59.00%). Different situation for the quantity of oxygen equal to 3.43% for CARBOSORB NC 1240 compared to 6.69% for RE-CHAR®. AMBIOTON® has a high amount of K (8.28%) compared to RE-CHAR® (1.94%) and CARBOSORB NC 1240 (1.45%).

Furthermore, through electron microscope scanning it was possible to have an elementary analysis of the surface, even if only by comparing the images of the samples.

Figure 3.27 shows the elemental maps of carbon, oxygen, calcium, potassium, magnesium, silicon and sodium within the biochar samples (AMBIOTON® and RE-CHAR®), whose percentage contents are reported in Table 3.6.

Particularly, amber colour is used to indicate carbon, aquamarine for oxygen, dark violet for calcium, magenta for potassium, red for magnesium, light green for silicon and green for sodium.

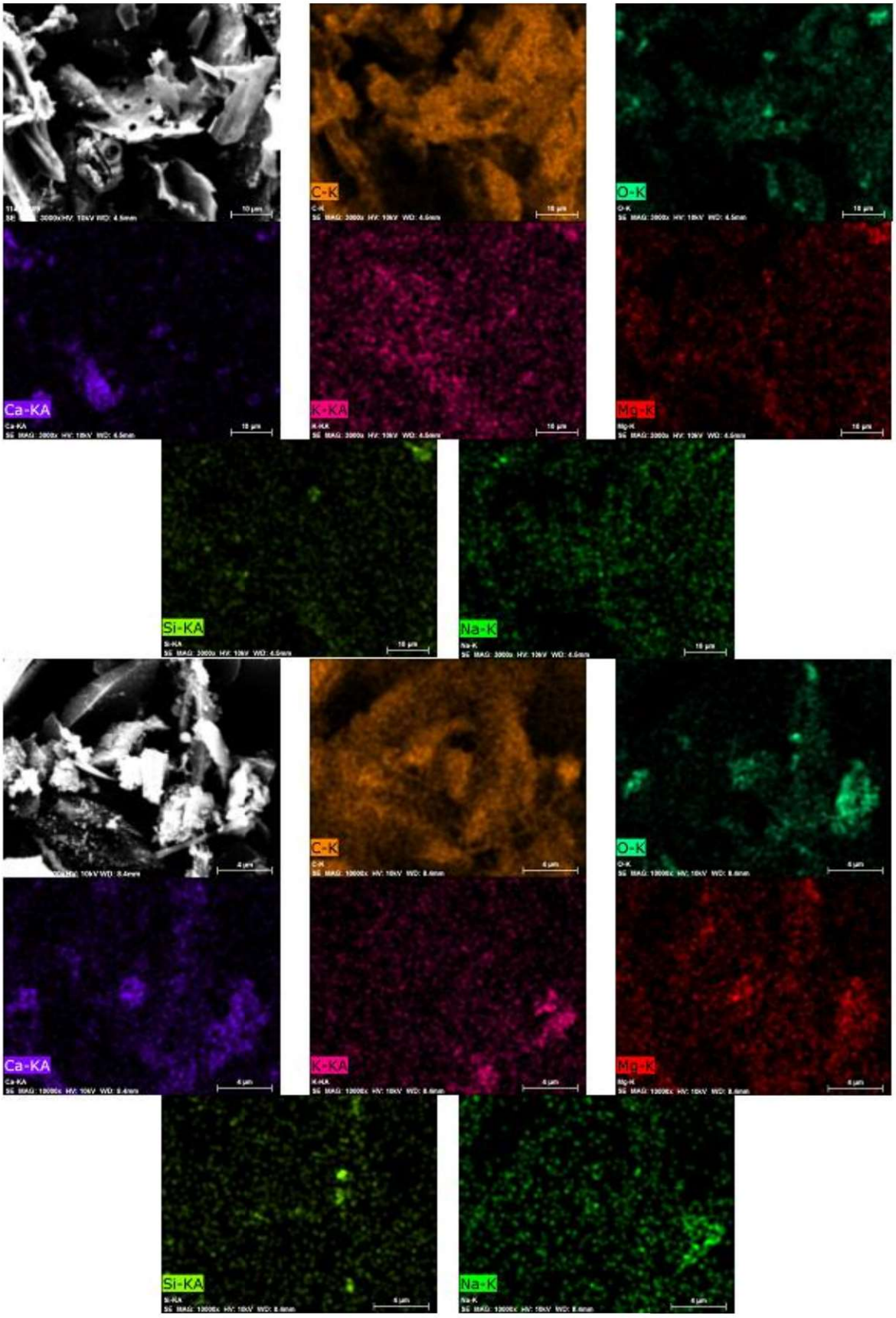

Figure 3.27 – Image and color coded EDS analysis dot maps AMBIOTON® and RE-CHAR®.

3.1.13 X-Ray Diffraction (XRD)

The X-rays produced by the tube affect the sample and are diffracted. They are then collected by the detector, which transforms the signal into an electrical impulse that is sent to a computer and allows data processing. The analysis is based on the study of the spectrum, which reports the X-ray counts as a function of the angular position ϑ e 2 ϑ and consists of a series of peaks of different intensity and angular position, characteristic of the various mineralogical phases present in the investigated sample. In XRD analysis, the value on the abscissa is the diffraction angle.

The diffraction peaks are identified both manually and with automated systems, in the first case the peaks obtained are compared with the data contained in the databases that contain information according to different organization criteria, for example, based on the counts (a.u.) of the most intense peak.

Figure 3.28, Figure 3.29 and Figure 3.30 are shown the spectra of the three samples (CARBOSORB NC 1240, AMBIOTON® and RE-CHAR® respectively). In Figure 3.31 are shown the comparison between all the spectra, to compare and give a first quick visual analysis of the three materials.

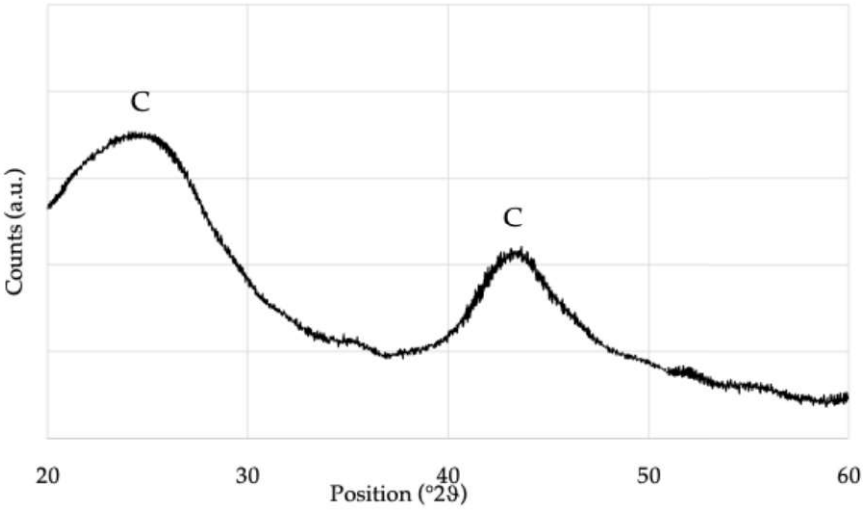

Figure 3.28 – XRD spectrum of CARBOSORB NC 1240.

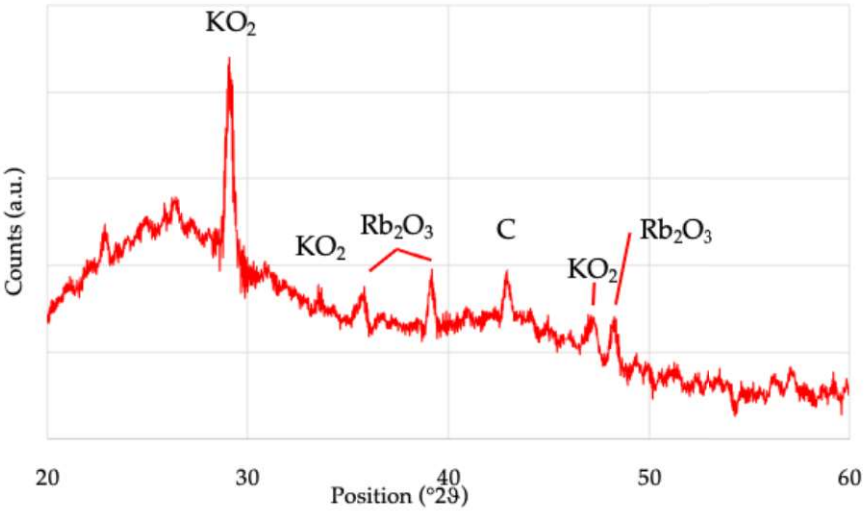

Figure 3.29 – XRD spectrum of AMBIOTON®.

EDS and XRD for the AMBIOTON® sample has shown the presence of C in high concentration (more than 80 wt%) and small traces of Rb and K (as confirmed in the form of Rb_2O_3 and KO_2 from XRD analysis). As

reported previously, the AMBIOTON® is obtained by fast pyrolysis of softwood and hardwood essences (birch, willow, black locust or turkey oak, plane tree, fruit tree wood, vine, walnut) in which it is possible to detect some traces of heavy elements (including Rb).

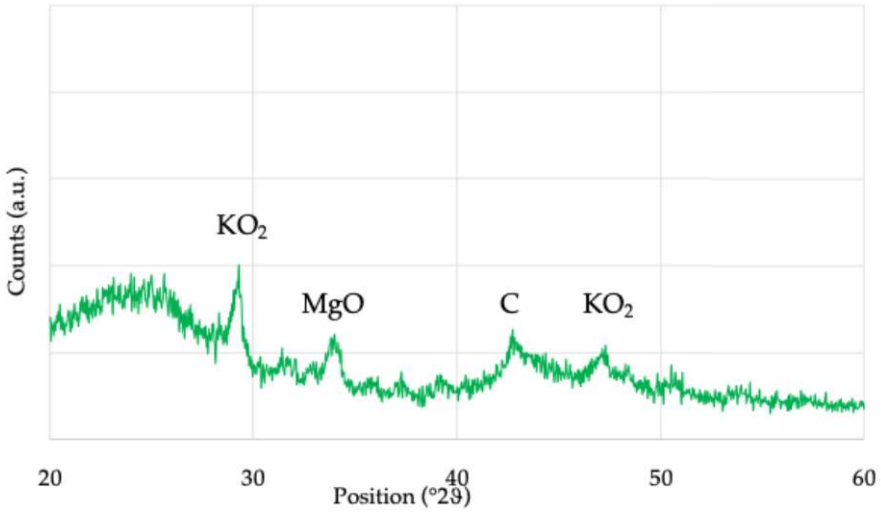

Figure 3.30 – XRD spectrum of RE-CHAR®.

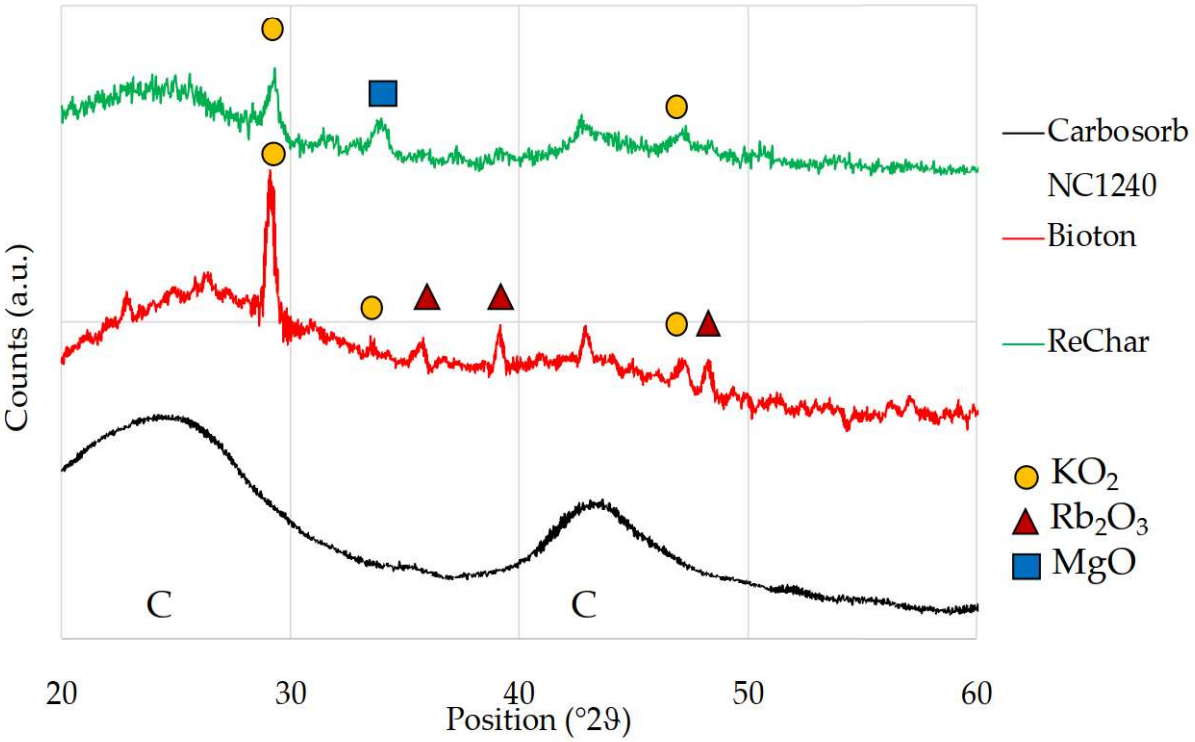

Figure 3.31 – Comparison of XRD spectra of CARBOSORB NC 1240, AMBIOTON® and RE-CHAR®.

The large hump in the area between 20 ° to 30 ° (areas highlighted in purple in the spectrum in Figure 3.31) indicates in both biochar it is due to the index of the crystalline plane C (002). The area between 42 ° and 47 ° of RE-CHAR® is also very similar, which is due to the index of the crystalline plane C (002). For CARBOSORB NC 1240 the wide peak between 40 ° and 50 ° (2ϑ) is due to the axis of the graphite structure [126].

These values are according with the values reported by Huang [772] and Chen [180], which indicates that Sharper peaks indicate a better degree of orientation.

3.1.14 Atomic Force microscopy (AFM)

In AFM the tip (a few μm in size) slides on the surface of a sample that moves along the three axes by means of a movement induced by a piezoelectric mechanism [773]. The forces that typically act between tip and sample vary between 10^{-11} and 10^{-6} N. Considering that between the two atoms joined by covalent bond at a distance of ~ 0.1 nm acts a force of 10^{-9} N approximately, it is understood that the measurements performed using the AFM are not destructive.

The result of the observation consists in the production of a three-dimensional matrix (x, y and z) of the surface being scanned (Figure 3.32 and Figure 3.33). The first two coordinates provide one-dimensional information of the object, the third provides the measurement of the heights (distances between the surface of the sample and the tip).

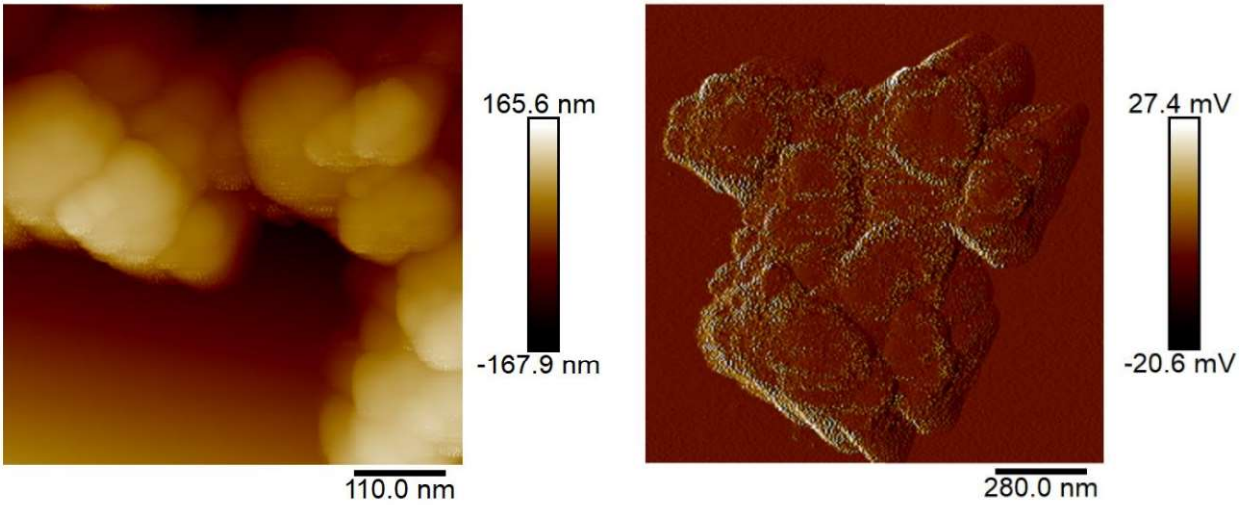

Figure 3.32 – AFM of AMBIOTON® in units of measurement (nm) and electric potential (mV).

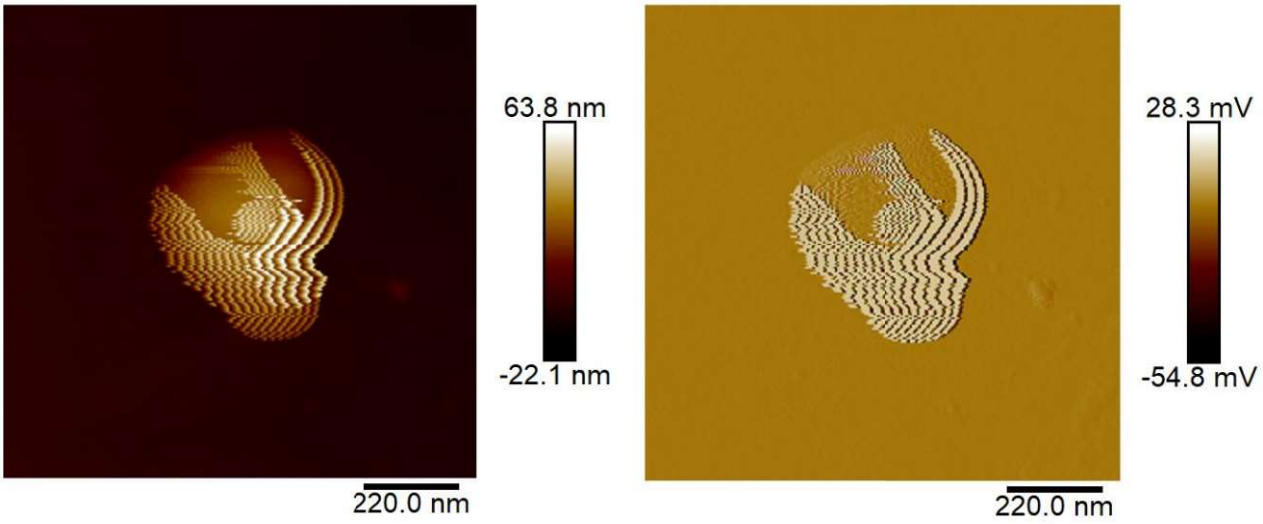

Figure 3.33 – AFM of RE-CHAR® in units of measurement (nm) and electric potential (mV).

Thanks to the AFM it is possible to view the three-dimensional profile of AMBIOTON® and RE-CHAR®. The morphology of the material can be clearly seen. From this qualitative analysis it is possible to show that the depth in AMBIOTON® is more evident than in RE-CHAR®.

It was not possible to carry out the analysis on CARBOSORB NC 1240, due to the size limit that a sample subjected to AFM analysis must have.

3.2 Lead adsorption studies

3.2.1 Influence of contact time

Figure 3.34 shows lead percentage removal versus contact time (h), measured in the batch tests – conducted at initial concentrations of 50 mg L^{-1} and 100 mg L^{-1} Pb – with AMBIOTON® (a) and RE-CHAR® (b). Adsorption temperature, mixing rate and biochar dosage: 20 ± 0.5 °C, 120 rpm, 5 g L^{-1}.

In Figure 3.34 (a) it is shown that, in the case of 50 mg L^{-1}, the slope was still very rapid in the first 30 min, although afterwards it proceeded more slowly reaching R = 100% in about 5 h; in the case of 100 mg L^{-1} the removal rate was very rapid in the first 30 min, and reached almost 100% by the first hour of the test.

In Figure 3.34 (b), it can be observed that removal rate onto RE-CHAR® was initially very fast, reaching values of 70% at 50 mg L^{-1} and 85% at 100 mg L^{-1} after only 30 min. Thereafter, in the case of C_0 = 100 mg L^{-1}, it proceeded at a much lower rate, reaching R% = 100% after 4 h contact time. For C_0 = 50 mg L^{-1}, the removal remained constant at about 70% until the end of the first hour (t = 1 h) and then increased rapidly assuming a profile similar to that observed at C_0 = 100 mg L^{-1}; a complete removal (R% = 100%) was reached at the same time, i.e. t = 4 h. Negligible variations were observed afterwards.

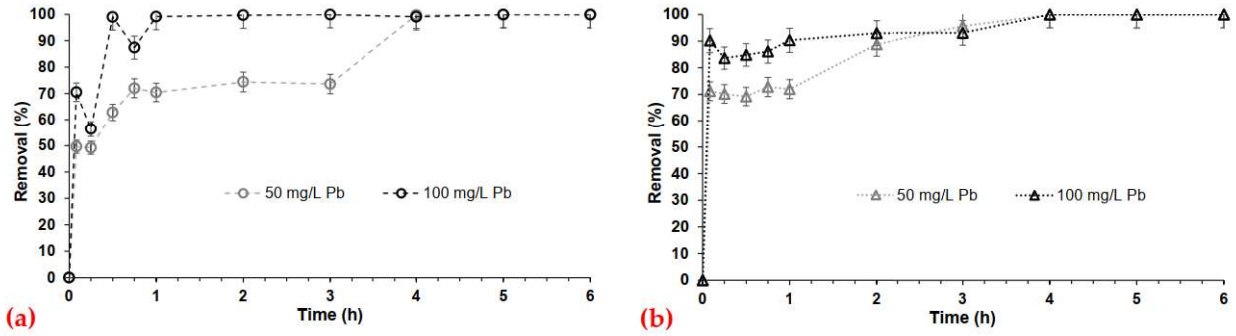

Figure 3.34 – Lead percentage removal (%) onto AMBIOTON® (a) and RE-CHAR® (b) versus contact time (h).

In Figure 3.34, in both biochars, the first removal phase could be attributed to a rapid occupation of the more easily accessible external surface sorption sites, while the slower phase could be related to the formation of inner layer complexes after saturation of outer sorption sites [774].

In addition, unfortunately, the dosage used (5 g L^{-1}) did not allow the optimal description of the kinetics of removal of the contaminant, especially in the first hour.

Compared to the achievement of the equilibrium time, these results are consistent with the scientific literature: for instance, in Kołodyńska et al. [774], a similar time-profile was reported for Pb adsorption at the same initial concentration onto biochar produced from pyrolysis of pig and cow manure at 400 °C and 600 °C, although at a slower rate (equilibria was reached after 5 h contact time). Lead sorption, with initial concentrations ranging from 5 to 200 ppm, onto biochar from pyrolysis of raw sugarcane bagasse also reached equilibrium after about 5 h [775]. Another study indicated equilibrium times after about 2 hour for the adsorption of 50 mg L^{-1} Pb onto a biochar made from a mixture of wood chips, green waste, rice hull, corn cob, nut shells and husks, and cotton gin trash and pomace [776]. In the same paper [776], adsorption on biochar of pinewood and of magnetic switch-grass, at the same Pb concentration, required from 8 to 20 h to reach equilibrium.

Therefore, considering the results obtained in the present study and those reported by the literature, it is evident that feedstock and operating conditions of the production process of AMBIOTON® and RE-CHAR® influence the rate of removal.

The linearized form of the equation of the different kinetic models was used to find out the best fitting of the experimental data, which were analysed using the following models: zero, first, second, saturation, pseudo-first, and pseudo-second order.

The pseudo-second-order (PSO) model provided the best agreement for both Pb concentrations (higher R^2 value), with respect to the other applied models. Figure 3.35 shows the experimental and the modelled data of lead adsorption onto both biochars, respectively, RE-CHAR® (a) and AMBIOTON® (b); in terms of t/q_t versus t. Adsorption temperature, mixing rate and biochar dosage: 20 ± 0.5 °C, 120 rpm, 5 g L^{-1}.

The PSO kinetic equation assumes that the rate of occupation of adsorption sites is proportional to the square of the number of unoccupied activated sites on the surface of the adsorbent [704].

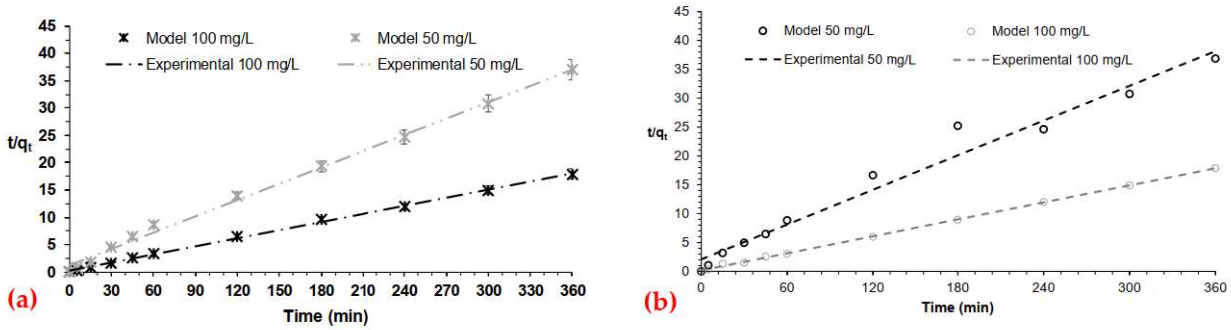

Figure 3.35 – Kinetic experimental data and modelled by the linearized pseudo-second-order equation.

Through the slope and intercept of the regression line, it was possible to determine the values of the pseudo second-order rate parameters, K_{PSO}, and of the amount of Pb adsorbed at equilibrium per unit weight of RE-CHAR® and AMBIOTON®, $q_{e,calc}$, both reported in Table 3.16. The same table also shows $q_{e,exp}$ which represents the value of adsorption capacity experimentally calculated at 300 min, which was assumed to be the equilibrium time based on the batch tests results. It can be noted that experimental and modelled data of the adsorption capacity do not differ appreciably in both cases of 50 mg L^{-1} and 100 mg L^{-1} Pb.

Table 3.16 – PSO kinetic adsorption model parameters onto RE-CHAR® and AMBIOTON®.

C_0 (mg L^{-1})	Biochar	$q_{e,exp}$ (mg g^{-1})	$q_{e,calc}$ (mg g^{-1})	K_{PSO} (g min^{-1})	R^2 -
50.0	AMBIOTON®	9.7340	9.9500	0.0049	0.9730
	RE-CHAR®		9.9957	0.0091	0.9959
100.0	AMBIOTON®	20.0800	20.30	0.0141	0.9993
	RE-CHAR®		20.1462	0.0128	0.9988

Comparing the values obtained for the specific adsorption capacity, it can be noted an almost linear increase of q_e with concentration in both biochars: for instance, rising Pb in solution from 50 mg L^{-1} to 100 mg L^{-1} led to a double q_e value.

Other studies found that the pseudo second order model was that one better representing the biochar adsorption process of lead at the same initial concentration as in the present paper [495,777,778] or at a double concentration [779].

3.2.2 Influence of dosage variation

The ability of AMBIOTON® and RE-CHAR® to remove lead, at 50 mg L^{-1} and 100 mg L^{-1} Pb, as a function of the ratio between adsorbent (mass) and adsorbate (volume) is shown in Figure 3.36, in terms of removal percentage (%) versus adsorbent dosage (g L^{-1}). Adsorption temperature, mixing rate and equilibrium time: 20 ± 0.5 °C, 120 rpm, 5 h.

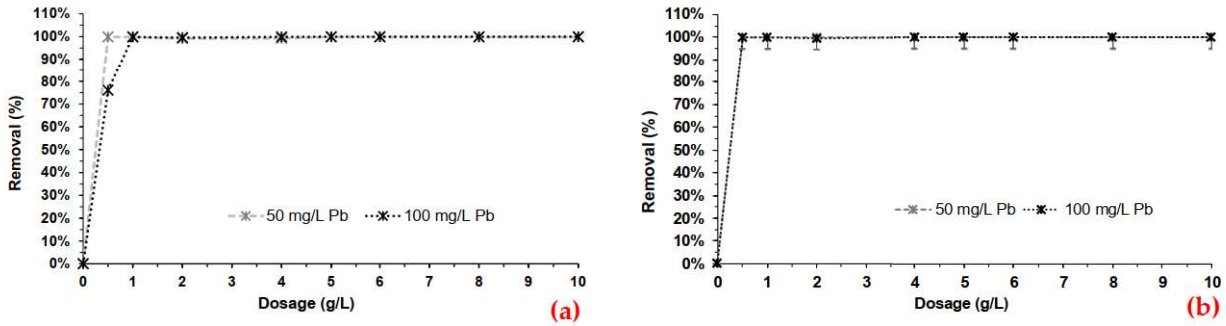

Figure 3.36 – Percentage of lead removal versus different AMBIOTON® (a) and RE-CHAR® dosages (b).

Figure 3.36 (a) shows that the removal percentage increased rapidly by rising the dosage: R% = 100% was reached for 0.5 g L^{-1} and 1 g L^{-1} AMBIOTON®, at 50 and 100 mg L^{-1} Pb concentrations, respectively. Above this dosage, further increases did not determine any appreciable improvement of R%.

In addition, it is highlighted in Figure 3.36 (b) that a dosage of 0.5 g L^{-1} RE-CHAR® was the minimum required to achieve the highest removal percentage, i.e. R% = 100%, at both concentrations of 50 and 100 mg L^{-1} Pb.

From this figure it can be deemed that, for Pb contaminated solutions at 50 mg L^{-1} and 100 mg L^{-1}, using a dosage of 1 g L^{-1} of AMBIOTON® or RE-CHAR® adsorbent makes it possible to comply with the limit set by the Italian legislation for discharge into surface waters and sewage systems (respectively 0.2 mg L^{-1} and 0.3 mg L^{-1}).

Equilibrium data obtained from these tests, for both contaminated solutions at 50 mg L^{-1} and 100 mg L^{-1}, were fitted to Langmuir, Freundlich and BET isotherms. The best fitting model was determined based on the value of R^2.

Figure 3.37 shows the plots of linearized variables for best fitted equilibrium data: Langmuir and BET isotherm model, respectively, onto RE-CHAR® (a) and AMBIOTON® (b), at both Pb aqueous solutions (higher R^2). From the slope and intercept of the regression lines, it was possible to calculate the parameter values of Langmuir and BET adsorption isotherm, which have better fitted the experimental equilibrium data; Table 3.17 shows parameter values.

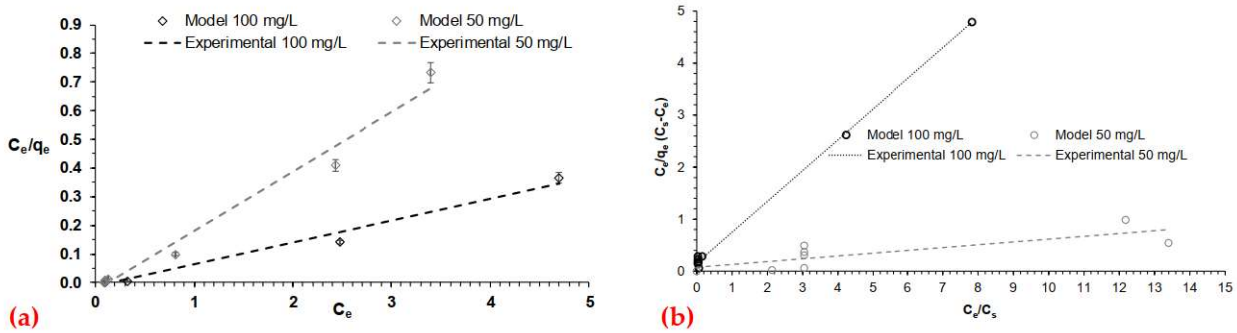

Figure 3.37 – Equilibrium experimental and modelled data by the linearized Langmuir equation onto RE-CHAR® and BET equation onto AMBIOTON®.

Table 3.17 – Parameters of Langmuir (RE-CHAR®) and BET adsorption isotherms (AMBIOTON®).

C_0 (mg L^{-1})	Langmuir isotherm				BET isotherm		
	q_{max} (mg g^{-1})	K_L (L mg^{-1})	R_L -	R^2 -	q_{max} (mg g^{-1})	C_{BET} (L mg^{-1})	R^2 -
50.0	4.6116	11.5804	0.0017	0.9967	22.00	2,530,403.46	0.6952
100.0	9.5895	2.8933	0.0032	0.9863	168.98	373,280.22	0.9981

Specifically, q_{max} represents the maximum adsorption capacity, which is required for the monolayer coverage of the surface (mg g^{-1}); in terms of implementation at full-scale, adsorbents with the highest value of the maximum adsorption capacity are the most desirable.

The values found for both biochars fell within the ranges reported by the literature for different biochars and Pb removal from water [27,30,158,574,775,780–783].

In the case of the contaminated solution at 50 Pb mg L^{-1}: Liu and Zhang (2009), by applying biochar prepared from hydrothermal liquefaction of pinewood (P300), found for the maximum lead sorption capacity a very similar value to that obtained by RE-CHAR® (i.e. 4.25 mg g^{-1} and 4.61 mg g^{-1}, respectively) [574]; Xue et al. (2012), by applying hydrochar produced from peanut hull, found that the value of the maximum lead sorption capacity was very similar to that obtained by AMBIOTON® (i.e., 22.82 mg g^{-1} and 22.00 mg g^{-1}, respectively) [1].

By the contrast, at 100 Pb mg L^{-1}: using biochar produced at 500° C from sugarcane bagasse and Pb concentration of about 80 mg L^{-1}, the adsorption capacity resulted to be. 9.13 mg g^{-1}, which does not differ appreciably from 9.58 mg g^{-1} by RE-CHAR® [784]; Inyang et al. (2011), using biochar derived from anaerobically digested sugarcane bagasse, found a lower value, i.e., 135.48 mg g^{-1}, with respect to 168.98 mg g^{-1} observed by the same biochar [775].

Furthermore, the data equilibrium obtained show a difficulty with respect to the adaptation of isotherm models: after the dosage of 1 g L^{-1} can achieve 100% removal is not a plateau in a manner defined by the non-linear equations.

In fact in the case of 50 mg L^{-1} Pb, onto AMBIOTON®, correlation coefficient was not very high likely due to the fact that the removal process was particularly efficient. Therefore, it was difficult to obtain a good fitting of the data. This suggested the opportunity to use lower dosages at this level of contamination, which would allow saving on adsorbent usage.

3.3 Arsenic adsorption studies

3.3.1 Preliminary tests

Among the two materials investigated as possible adsorbent media, a greater removal efficiency (% R) at natural pH was found in RE-CHAR®. During these tests the dosage was fixed at 2 and 5 g L^{-1}.

To evaluate any variation in the removal rate as a function of pH, preliminary tests were conducted, within which the initial pH (pH_0) of the contaminated solution (5 and 9) was varied.

Although RE-CHAR® still demonstrated a much higher removal efficiency in all tests (75-98%), compared to that found in AMBIOTON® (<1%), the latter showed an encouraging efficiency of removal (> 10%) in the case of the initial pH in acidic conditions, with a dosage equal to 5 g L^{-1}.

This material has not been further investigated although, any further lowering of the pH and the increase in dosage, could be a possible prospect for future research developments, in order to analyse the response of AMBIOTON® in these conditions.

The close relationship between the pH variation and the respective adsorption capacities and removal efficiency was therefore evident. RE-CHAR® showed, in a completely unexpected way, good performances in an alkaline environment (pH: 9-11), reaching excellent removal efficiencies.

From the analysis of literature data, biochar usually obtains acceptable removal efficiencies, only in acidic conditions (pH <5), as also observed in the case of AMBIOTON®.

Therefore, for the moment, AMBIOTON® was excluded from subsequent tests and RE-CHAR® was further characterized.

However, it is suggested that further tests be conducted with both materials, under controlled pH conditions, during each contact time.

In fact, with regard to RE-CHAR®, with contact times greater than 8 hours, by not checking the pH between 10 and 11 – in correspondence with removal efficiency values, close to the unitary value – any desorption emerged by the material, in correspondence with the pH value <9. From the literature data it is assumed that this arsenic in solution is found in the reduced form (III) starting from the oxidized one (V).

Starting from the results obtained, it is assumed that the removal efficiency equilibrium will be achieved, under controlled pH conditions, thus maintaining the residual concentrations in the aqueous phase constant over time.

It is also hypothesized that the decrease in pH, for contact times exceeding 8 hours, may depend on CO_2. It is therefore suggested to conduct further tests in closed batch systems, in order to mitigate any variations in the process parameters, during the entire test.

In the second phase of the preliminary experimental activities for arsenic adsorption, tests were performed in order to determine the optimal dosage for the description of the successive kinetics of removal throughout the entire process, which will be set at 0.5 g L^{-1}.

However, the results obtained showed the difficult experimental correlation of the entire dataset of the values found, starting from the experimental setup used. It is therefore hoped to repeat the tests in a different dosage range (0.5 - 10 g L^{-1}), taking into consideration, for the choice of the experimental setup, the critical issues encountered so far.

3.3.2 Influence of contact time

Figure 3.38 and Figure 3.39 shows the As removal efficiency of the different aqueous solutions, in function of contact time. Adsorption temperature, mixing rate, initial concentration and dosage were maintained at 20 ± 0.5 °C, 120 rpm, 90 μg L^{-1} and 0.5 g L^{-1}, respectively.

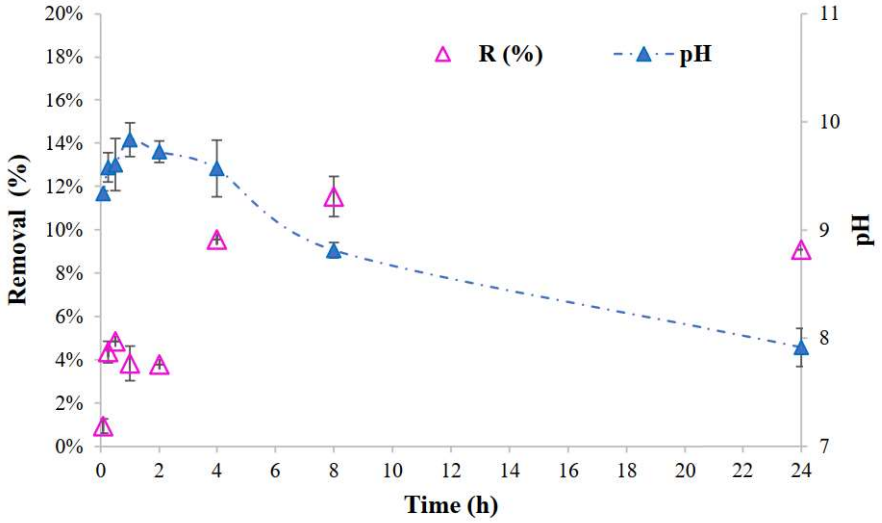

Figure 3.38 – Contact time (h) versus arsenic (As(III)) percentage removal and pH of aqueous solution.

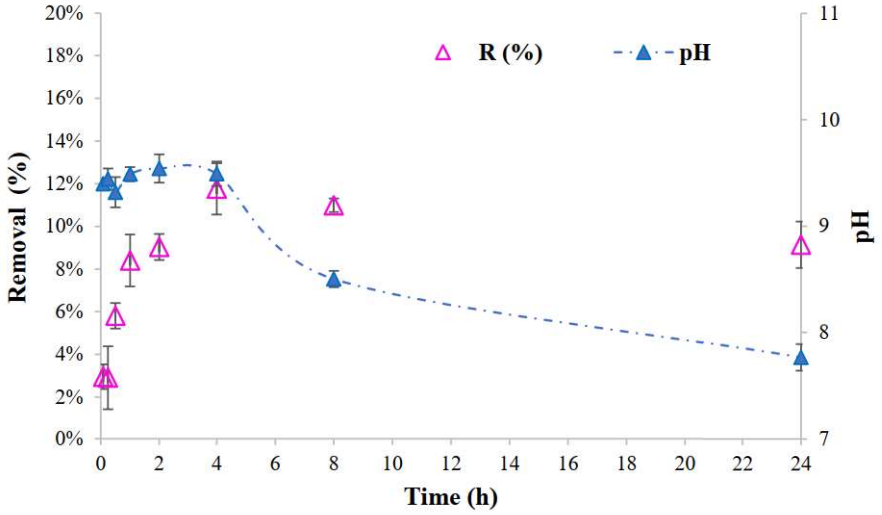

Figure 3.39 – Contact time (h) versus arsenic (As(V)) percentage removal and pH of aqueous solution.

It can be shown that in Figure 3.38 As removal efficiency is slower, as it reaches 10% in 8 hours, while in Figure 3.39 As removal efficiency is more quick, in fact already after 2 hours, 10% is reached. In Figure 3.38, At the equilibrium time (8 hours), there is shown an As removal percentage above 12% at pH about 9, while after 24 hours there is a removal percentage of 10% at pH lower than 8. While in Figure 3.39, at the same equilibrium time (8 hours) there is shown an As removal of 12% at pH about 8.5, while after 24 hours a As removal of 10% at pH lower than 8.

Duan et al. (2017) reported that the equilibrium time was reached at 10 hours, after a contact time between 5 and 7 hours [785]. The removal kinetic start from an initial As(V) concentration of 0.1-5 mg L^{-1} and reaches the maximum adsorption capacity of 1.91 mg g^{-1} at the equilibrium time.

Otherwise, Singh et al. (2020) reported that equilibrium is reached in 12 hours, with a total contact time of 24 hours. The initial As(III) concentration was 0.05 mg L^{-1} and the maximum adsorption capacity (0.096 mg g^{-1}) is reached at the equilibrium time at pH of 7.5 [786].

In the following graphs (Figure 3.40 and Figure 3.41) are shown the trends relating to pH and redox potential (ORP). Adsorption temperature, mixing rate, initial concentration and dosage were maintained at 20 ± 0.5 °C, 120 rpm, 90 µg L^{-1} and 0.5 g L^{-1}, respectively.

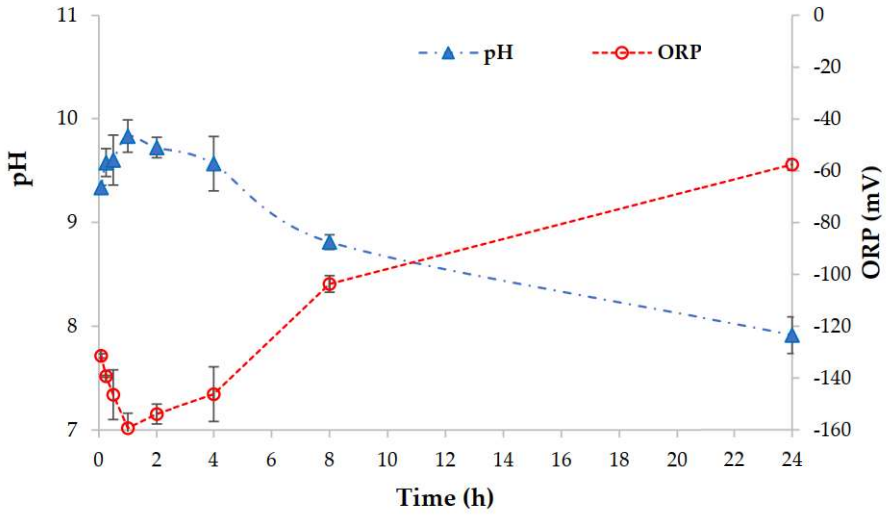

Figure 3.40 – Contact time (h) versus pH and ORP (mV) of aqueous solution (As(III)).

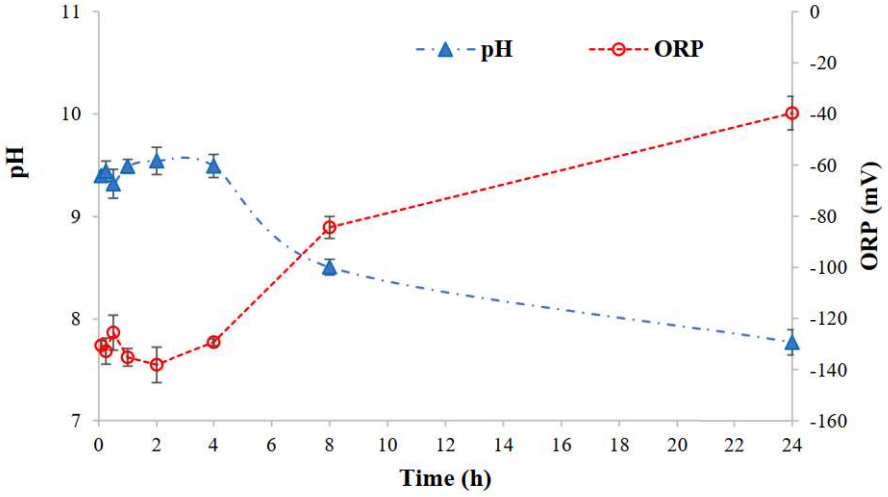

Figure 3.41 – Contact time (h) versus pH and ORP (mV) of aqueous solution (As(V)).

In Figure 3.40 pH increases abruptly in the first two hours and then decreases at 24 h, passing from above 9.75 to 8; at 8 hours pH and OPR were, respectively, 9 and -100 mV. The redox potential instead, up to 2 hours decreases in abruptly and then go up to 24 hours from above -160 to -60 mV.

In Figure 3.41 pH tends to decrease in the first hour and then grows up to 2 hours. Between 2 and 4 hours it appears to be almost constant at 9.5 and then decreases until reaching below 8 after 24 hours; at 8 hours pH and OPR were, respectively, 8.5 and -80 mV The reverse trend is instead done for the redox potential; at 24 h it is reached at -40 mV.

Culler and Reimer (1989) described that the speciation of the predominant arsenic is related to redox potential and pH [87].

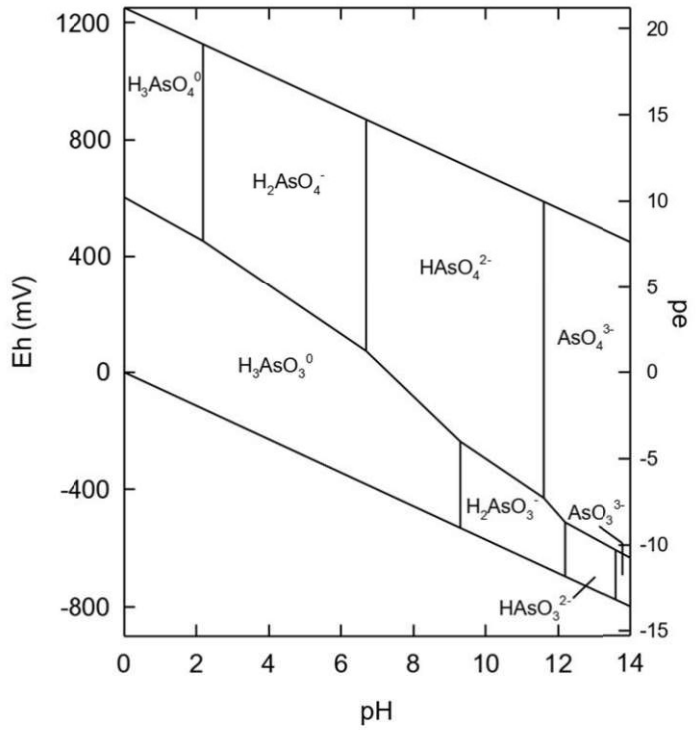

Figure 3.42 – Speciation of arsenic present in aquatic environmental [87].

Furthermore, Horng and Clifford (1997) studied the arsenic speciation fraction (Figure 3.43), present at the different pH of the aqueous solution [787].

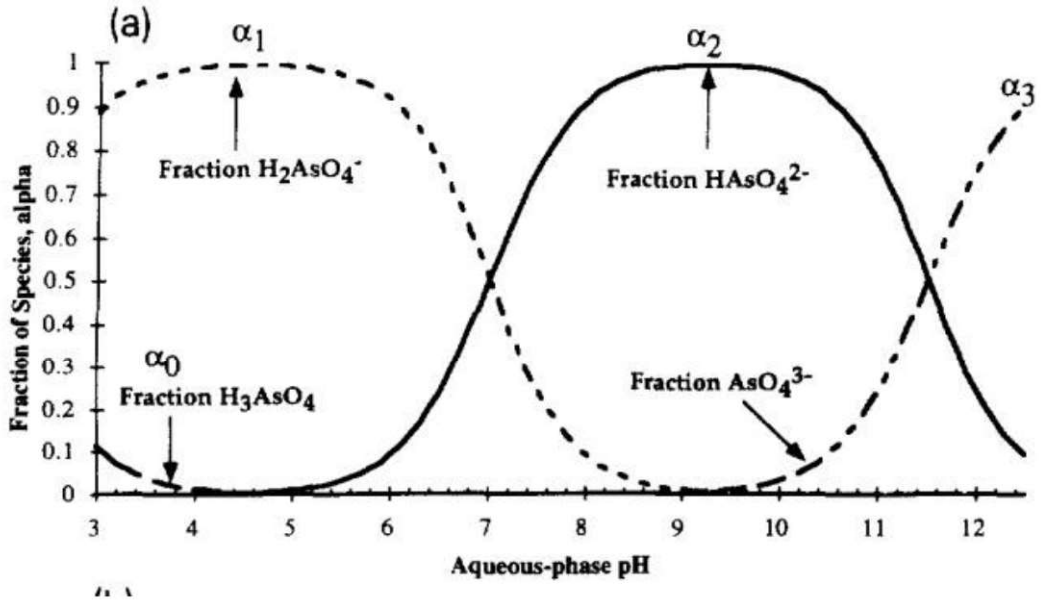

Figure 3.43: Arsenic speciation fraction in function of aqueous-phase pH [788].

At equilibrium time (8 hours): in Figure 3.40, pH and redox potential were, respectively 9 and -100 mV, in Figure 3.41, pH and redox potential were, respectively 8.5 and -80; therefore, in both contaminated solution, the dominant speciation is $HA_sO_4^{2-}$, As(V) [87,788].

Unfortunately, not having the data with respect to speciation, but only on arsenic total, we can assume that it only has only the presence of As (V), having therefore also oxidized to the reduced form.

3.3.3 Influence of dosage variation

Figure 3.44 and Figure 3.45 shows the As removal efficiency of the different aqueous solutions, in function of the variation of dosage (g L^{-1}). Adsorption temperature, mixing rate, initial concentration and equilibrium time were maintained at 20 ± 0.5 °C, 120 rpm , 90 µg L^{-1} and 8 h, respectively.

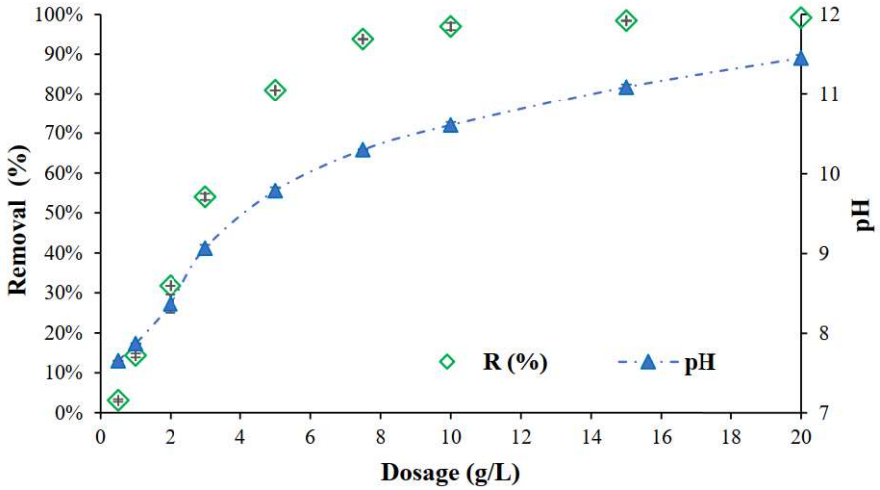

Figure 3.44 – Different RE-CHAR® dosages (g L^{-1}) versus percentage of arsenic removal (As(III)) and pH of aqueous solution.

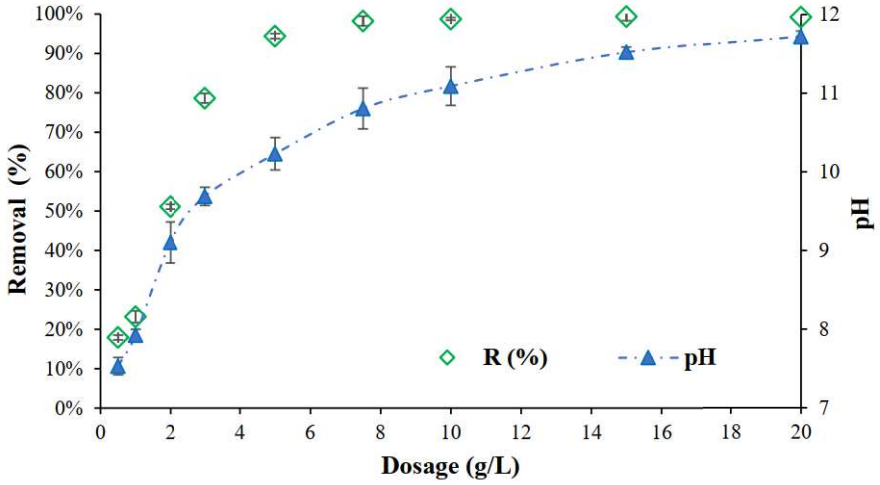

Figure 3.45 – Different RE-CHAR® dosages (g L^{-1}) versus percentage of arsenic removal (As(V)) and pH of aqueous solution.

From the different results obtained from the different aqueous solution, it is evident that the As removal rate over 90% with a dosage greater than 10 and 8 g L^{-1}, respectively, in Figure 3.44 and Figure 3.45. Therefore it is evident the greater aptitude of RE-CHAR® for arsenic removal, dissolved by Na2HAsO4.7H2O.

In the following graphs (Figure 3.46 and Figure 3.47) are shown the trends relating to pH and redox potential (ORP). Adsorption temperature, mixing rate, initial concentration and equilibrium time were maintained at 20 ± 0.5 °C, 120 rpm , 90 µg L^{-1} and 8 h, respectively.

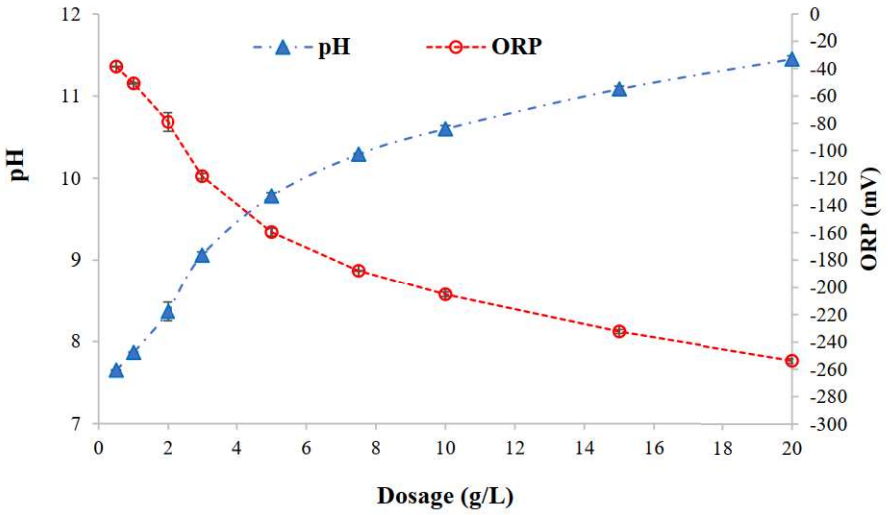

Figure 3.46 – Different RE-CHAR® dosages (g L^{-1}) versus pH and ORP (mV) of aqueous solution (As(III)).

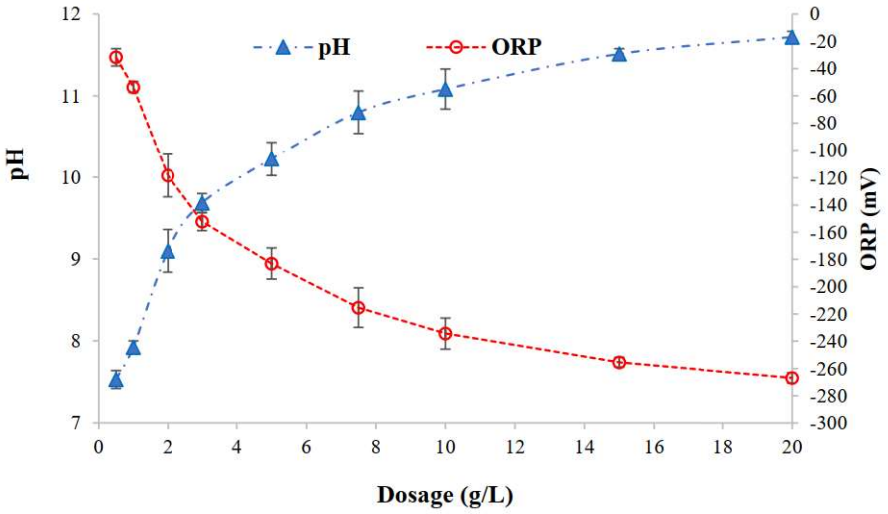

Figure 3.47 – Different RE-CHAR® dosages (g L^{-1}) versus pH and ORP (mV) of aqueous solution (As(V)).

Both Figure 3.46 and Figure 3.47, it shows that until the dosage is increased to 4 g L^{-1}, there is a sharp decrease of the redox potential; subsequently with a dosage of 20 g L^{-1} the rate of change of ORP decreases to stabilize, approximately -250 and -260 mV, respectively, in Figure 3.46 and Figure 3.47.

This is also due to the increase in pH with the dosage variation: the value 8 g L^{-1}, the pH reached 10.5 and 11, respectively, to the solutions of As(III) and As(V). This variation between the two pH is certainly linked to the different redox conditions.

Moreover: in Figure 3.46 (with dosage > 10 g L^{-1}) there is a pH between 10.5 and 11.5 and a ORP of -200 mV, in Figure 3.47 there is a pH between 11 and 12 and a ORP of -220 mV. Comparing with [87] and [88], under reducing conditions, the dominant species is only $HA_sO_4^{2-}$; otherwise in the oxidized form there are two different dominant species ($HA_sO_4^{2-}$, $A_sO_4^{3-}$). In both cases, less than data relating to the concentration of each speciation, the only species remained in solution is to pentavalent arsenic [87,788].

3.3.4 Modelling adsorption Kinetic studies

In this section shows the main results obtained by the arsenic adsorption kinetics onto RE-CHAR®. In fact, the experimental data were used to verify their fit to the most commonly used models including Pseudo-first order (PFO), Pseudo-second order (PSO), Elovich, Weber and Morris (IPD), Avrami and Bangham. Adsorption temperature, mixing rate, initial concentration and dosage were maintained at 20 ± 0.5 °C, 120 rpm, 90 μg L^{-1} and 0.5 g L^{-1}, respectively. Figure 3.48 shows the experimental and the modelled data of Pseudo-first order (PSO) kinetic model for As(III) and As(V) adsorption, respectively, (a) and (b), onto RE-CHAR®.

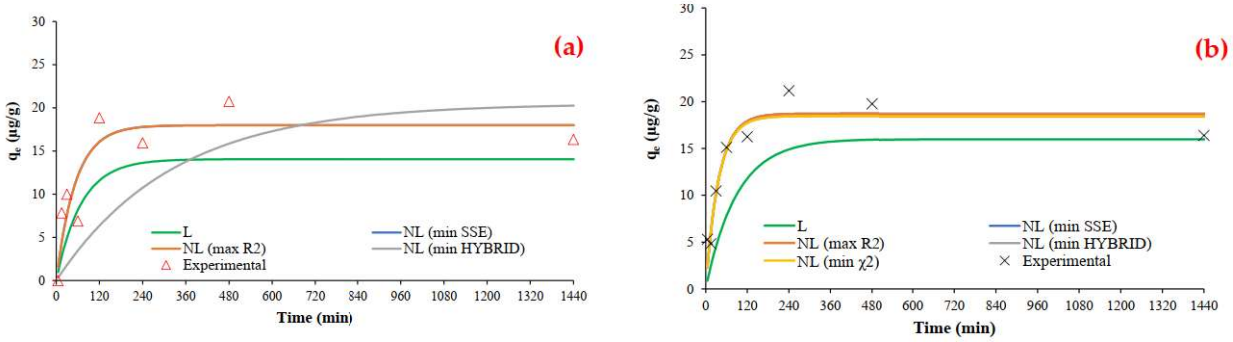

Figure 3.48 – PFO kinetic model for As(III) and As(V) adsorption, respectively, (a) and (b), onto RE-CHAR®.

Through the non-linear and linear regression of the equation, as explained in the previous chapters, it was possible to determine the values of the model parameters and an analysis of the errors was performed; they are therefore reported in Table 3.18.

Table 3.18 – PFO kinetic parameters with error analysis for arsenic adsorption onto RE-CHAR®.

$p = 2$		As(III)		As(V)	
Parameters		**NL regression**	**L regression**	**NL regression**	**L regression**
Symbol	**Unit**				
K_{PFO}	min^{-1}	0.011 ± 2.4E-04	0.014	0.027 ± 3.3E-07	0.011
q_e	μg g^{-1}	19.245 ± 6.3E+00	14.066	18.591 ± 6.5E-02	16.018
Error analysis					
R^2		0.804	0.535	0.902	0.296
R^2_{adj}		0.726	0.349	0.863	0.015
r^2		0.806	0.806	0.912	0.875
SSE		68.464	162.520	26.214	188.925
SAE		21.590	30.996	12.377	35.108
ARE		2001.051	6163.227	16.090	39.658
HYBRID		1258.422	8222.352	48.017	261.179
MSPD		6386.315	20033.805	26.976	53.261
MSE		8.558	20.315	3.277	23.616
RMS		5530.711	17349.784	23.362	46.125
χ^2		75.505	493.341	2.881	15.671
SRE		2134.284	6585.229	16.989	37.770
K_2		0.196	0.465	0.098	99.704
APE		2001.051	6163.227	16.090	39.658
Δq		5912.579	18547.700	24.975	49.310

Figure 3.49 shows the experimental and the modelled data of Pseudo-second order (PSO) kinetic model for As(III) and As(V) adsorption, respe ctively, (a) and (b), onto RE-CHAR®.

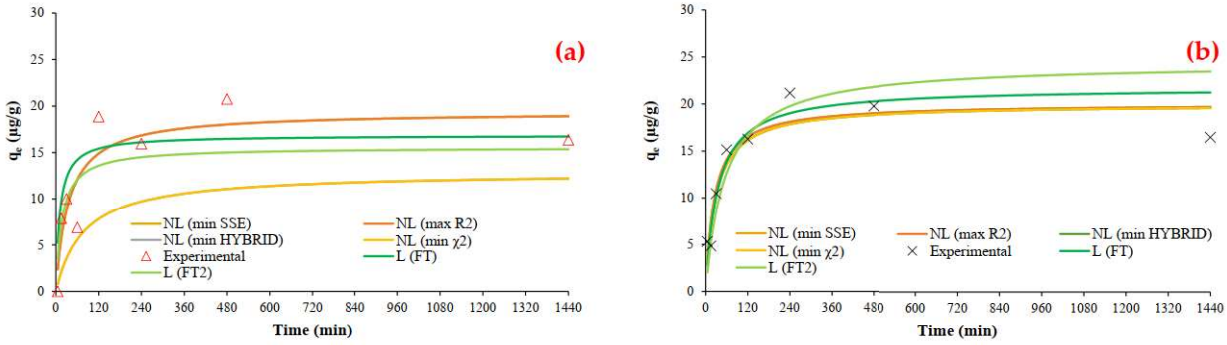

Figure 3.49 – PSO kinetic model for As(III) and As(V) adsorption, respectively, (a) and (b), onto RE-CHAR®.

Through the non-linear and linear regression of the equation, as explained in the previous chapters, it was possible to determine the values of the model parameters and an analysis of the errors was performed; they are therefore reported in Table 3.19.

Table 3.19 – PSO kinetic parameters with error analysis for arsenic adsorption onto RE-CHAR®.

$p = 2$		As(III)		As(V)	
Parameters		**NL regression**	**L regression**	**NL regression**	**L regression**
Symbol	**Unit**				
K_{PSO}	g µg^{-1} min^{-1}	0.001 ± 1.8E-07	0.005	0.002 ± 4.0E-08	0.001
q_e	µg g^{-1}	16.120 ± 4.2E+01	16.854	19.985 ± 3.8E-03	21.718
Error analysis					
R^2		0.802	0.657	0.878	0.852
R^2_{adj}		0.723	0.520	0.829	0.793
r^2		0.804	0.790	0.880	0.877
SSE		69.200	119.837	32.736	39.623
SAE		21.060	24.902	13.406	13.997
ARE		4884.789	32672.088	17.435	17.793
HYBRID		5391.007	227558.057	54.130	60.975
MSPD		15820.509	106627.245	27.451	28.122
MSE		8.650	14.980	4.092	4.953
RMS		13700.963	92341.903	23.774	24.355
χ^2		323.460	13653.483	3.248	3.659
SRE		5216.198	34929.194	18.333	19.368
K_2		0.198	0.343	0.122	0.148
APE		4884.789	32672.088	17.435	17.793
Δq		14646.945	98717.646	25.415	26.036

Figure 3.50 shows the experimental and the modelled data of Elovich kinetic model for As(III) and As(V) adsorption, respectively, (a) and (b), onto RE-CHAR®.

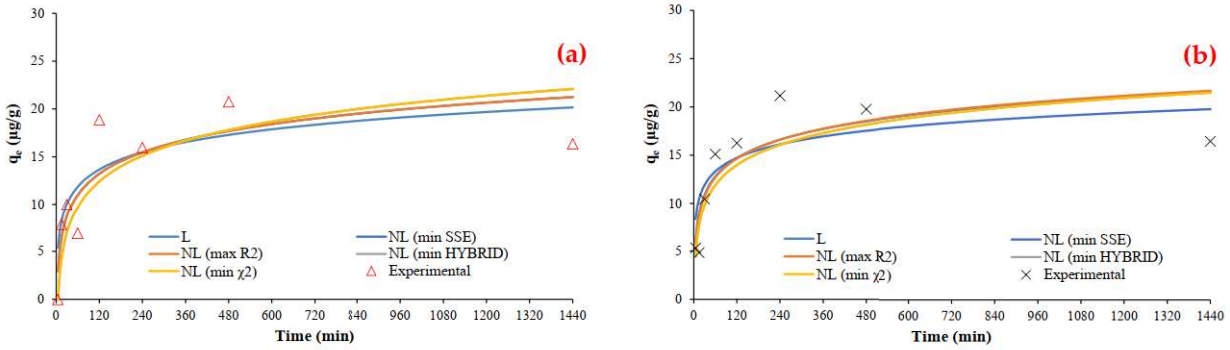

Figure 3.50 – Elovich kinetic model for As(III) and As(V) adsorption, respectively, (a) and (b), onto RE-CHAR®.

Through the non-linear and linear regression of the equation, as explained in the previous chapters, it was possible to determine the values of the model parameters and an analysis of the errors was performed; they are therefore reported in Table 3.20.

Table 3.20 – Elovich kinetic parameters with error analysis for arsenic adsorption onto RE-CHAR®.

$p = 2$		As(III)		As(V)	
Parameters		**NL regression**	**L regression**	**NL regression**	**L regression**
Symbol	**Unit**				
α	µg g^{-1} min^{-1}	1.191 ± 6.7E-01	4.057	8.439 ± 3.4E+02	4.885
β	g µg^{-1}	0.283 ± 2.8E-03	0.383	0.378 ± 1.8E-02	0.365
Error analysis					
R^2		0.731	0.694	0.724	0.723
R^2_{adj}		0.623	0.571	0.614	0.613
r^2		0.731	0.731	0.724	0.724
SSE		94.126	107.111	74.103	74.314
SAE		23.755	23.676	19.675	20.114
ARE		32.387	33480.166	22.173	23.464
HYBRID		139.060	238974.647	97.504	114.707
MSPD		41.181	109285.534	32.095	39.794
MSE		11.766	13.389	9.263	9.289
RMS		35.664	94644.049	27.795	34.462
χ^2		8.344	14338.479	5.850	6.882
SRE		33.733	35792.519	23.709	25.385
K_2		0.269	0.306	0.276	0.277
APE		32.387	33480.166	22.173	23.464
Δq		38.126	101178.744	29.714	36.842

Figure 3.48 shows the experimental and the modelled data of Weber and Morris (IPD) kinetic model for As(III) and As(V) adsorption, respectively, (a) and (b), onto RE-CHAR®.

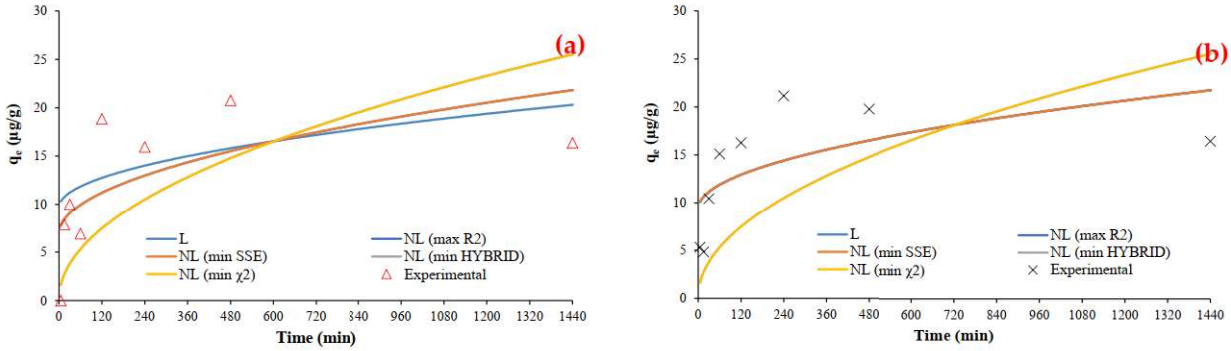

Figure 3.51 – IPD kinetic model for As(III) and As(V) adsorption, respectively, (a) and (b), onto RE-CHAR®.

Through the non-linear and linear regression of the equation, as explained in the previous chapters, it was possible to determine the values of the model parameters and an analysis of the errors was performed; they are therefore reported in Table 3.21.

Table 3.21 – IPD kinetic parameters with error analysis for arsenic adsorption onto RE-CHAR®.

$p = 2$		As(III)		As(V)	
Parameters		**NL regression**	**L regression**	**NL regression**	**L regression**
Symbol	**Unit**				
K_{WM}	µg g^{-1} min$^{-1/2}$	0.531 ± 7.6E-02	0.280	0.375 ± 1.0E-02	0.325
c	µg g^{-1}	3.512 ± 4.6E+01	9.681	7.895 ± 8.8E+00	9.374
Error analysis					
R^2		0.440	0.366	0.393	0.393
R^2_{adj}		0.216	0.112	0.150	0.150
r^2		0.440	0.440	0.393	0.393
SSE		195.757	221.865	163.082	163.082
SAE		33.685	36.327	33.176	33.176
ARE		10193.899	64428.739	35.783	42.469
HYBRID		22375.907	884978.526	218.478	285.646
MSPD		33158.545	210336.198	44.484	65.691
MSE		24.470	27.733	20.385	20.385
RMS		28716.143	182156.491	38.524	56.890
χ^2		1342.554	53098.712	13.109	17.139
SRE		10894.398	68878.596	36.839	45.657
K_2		0.560	0.634	0.607	0.607
APE		10193.899	64428.739	35.783	42.469
Δq		30698.848	194733.480	41.184	60.818

Figure 3.52 shows the experimental and the modelled data of Avrami kinetic model for As(III) and As(V) adsorption, respectively, (a) and (b), onto RE-CHAR®.

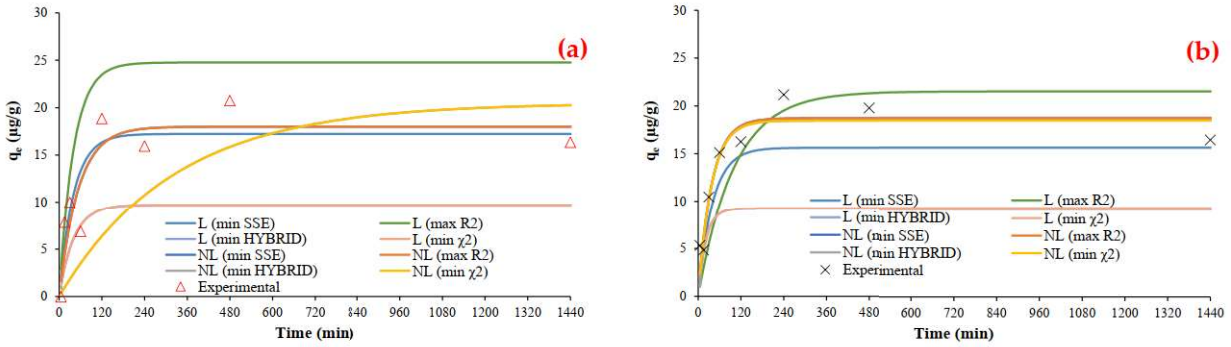

Figure 3.52 – Avrami kinetic model for As(III) and As(V) adsorption, respectively, (a) and (b), onto RE-CHAR®.

Through the non-linear and linear regression of the equation, as explained in the previous chapters, it was possible to determine the values of the model parameters and an analysis of the errors was performed; they are therefore reported in Table 3.22.

Table 3.22 – Avrami kinetic parameters with error analysis for arsenic adsorption onto RE-CHAR®.

p = 3		As(III)		As(V)	
Parameters		**NL regression**	**L regression**	**NL regression**	**L regression**
Symbol	**Unit**				
K_{Av}	µg min^{-1} g^{-1}	0.096 ± 6.5E-03	2.138 ± 0.0	0.163 ± 3.1E-06	2.073 ± 3.2
n_{AV}	-	0.096 ± 6.6E-03	0.012 ± 0.0	0.163 ± 3.1E-06	0.016 ± 2.2E-05
q_e	µg g^{-1}	19.245 ± 6.3	15.346 ± 1.6E+02	18.591 ± 6.5E-02	13.892 ± 1.0E+02
Error analysis					
R^2		0.804	0.790	0.903	0.754
R^2_{adj}		0.657	0.633	0.830	0.570
r^2		0.806	0.792	0.913	0.856
SSE		68.464	73.405	26.098	85.904
SAE		21.590	20.086	12.309	22.139
ARE		2001.051	7040.142	16.065	32.077
HYBRID		1510.107	12982.203	57.493	207.461
MSPD		6995.858	25051.500	29.512	50.219
MSE		8.558	9.176	3.262	10.738
RMS		5530.711	19804.950	23.332	39.702
χ^2		75.505	649.110	2.875	10.373
SRE		2134.284	7520.647	16.949	32.762
K_2		0.196	0.210	0.097	0.246
APE		2001.051	7040.142	16.065	32.077
Δq		5912.579	21172.382	24.943	42.443

Figure 3.53 shows the experimental and the modelled data of Bangham kinetic model for As(III) and As(V) adsorption, respectively, (a) and (b), onto RE-CHAR®.

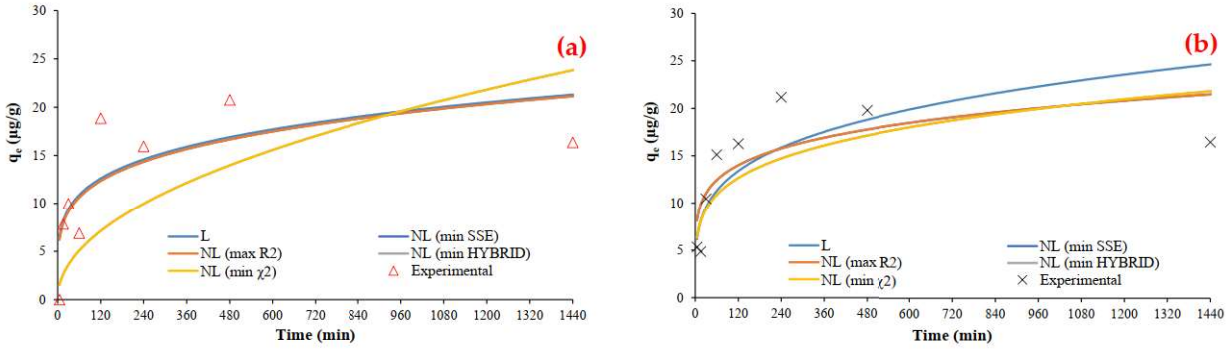

Figure 3.53 – Bangham kinetic model for As(III) and As(V) adsorption, respectively, (a) and (b), onto RE-CHAR®.

Through the non-linear and linear regression of the equation, as explained in the previous chapters, it was possible to determine the values of the model parameters and an analysis of the errors was performed; they are therefore reported in Table 3.23.

Table 3.23 – Bangham kinetic parameters with error analysis for arsenic adsorption onto RE-CHAR®.

$p = 2$		As(III)		As(V)	
Parameters		**NL regression**	**L regression**	**NL regression**	**L regression**
Symbol	**Unit**				
K_B	µg g^{-1}	2.542 ± 1.4E+01	4.596	5.300 ± 3.0	4.147
θ_B	µg min^{-1} g^{-1}	0.351 ± 7.3E-02	0.211	0.195 ± 2.2E-03	0.245
Error analysis					
R^2		0.606	0.605	0.614	0.513
R^2_{adj}		0.448	0.446	0.459	0.318
r^2		0.614	0.617	0.620	0.568
SSE		137.805	138.302	103.747	130.839
SAE		27.824	27.746	25.742	26.138
ARE		9526.479	40340.025	27.848	26.771
HYBRID		19578.254	346933.793	141.700	154.935
MSPD		30976.623	131685.435	37.291	38.479
MSE		17.226	17.288	12.968	16.355
RMS		26826.542	114042.932	32.295	33.323
χ^2		1174.695	20816.028	8.502	9.296
SRE		10180.366	43125.785	28.912	28.727
K_2		0.394	0.395	0.386	0.487
APE		9526.479	40340.025	27.848	26.771
Δq		28678.780	121917.022	34.525	35.624

Compared to the data, in the totality of the investigated kinetic models, both in As(III) and in As(V), the linear regression found an analysis of the errors worse than that of the nonlinear regression.

Between the two aqueous solutions, the study of the As(V) one found some errors, in some cases, excessive; this is probably due to the non-homogeneous dispersion of the data along the curve.

Certainly the analytical limit of speciation determination further increases the non-distribution of data in a representative kinetics.

Values close to the unit of the determination (R^2) and correlation coefficient (r^2) and minimum values of the other errors show an excellent adaptation of the experimental data to the analytical models.

Analysing the errors it emerges that, taking sum square error (SSE) and coefficient of determination (R^2) into consideration, the kinetic that best describes the data, for both aqueous solutions, is the Pseudo-second order (PSO) model, as reported by [789,790].

3.3.5 Modelling adsorption equilibrium studies

This section shows the main results obtained by the arsenic adsorption isotherm onto RE-CHAR®. The experimental data were used to verify their fit to Langmuir, Freundlich, Dubinin-Radushkevich (D–R), Temkin, Redlich-Peterson (R–P) and Koble-Corrigan (K–C) models. Adsorption temperature, mixing rate, initial concentration and equilibrium time were maintained at 20 ± 0.5 °C, 120 rpm , 90 μg L^{-1} and 8 h, respectively. Figure 3.54 shows the experimental and the modelled data of Langmuir isotherm model for As(III) and As(V) adsorption, respectively, (a) and (b), onto RE-CHAR®.

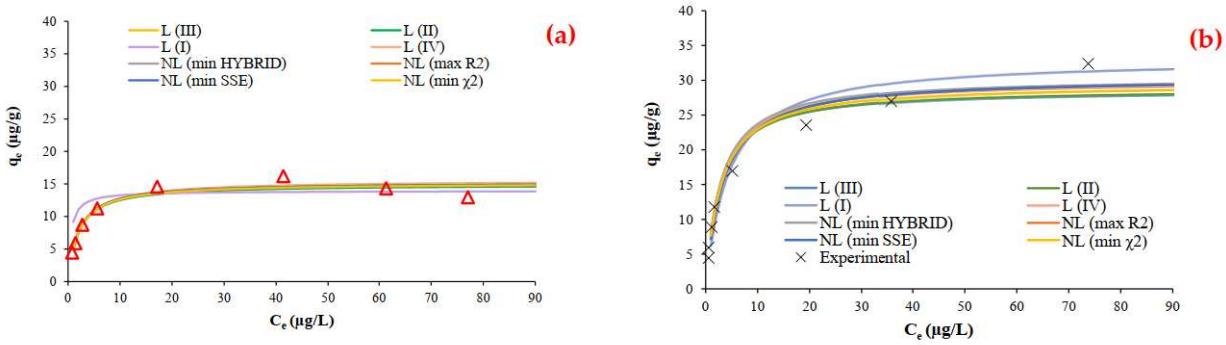

Figure 3.54 – Langmuir isotherm model for As(III) and As(V) adsorption, respectively, (a) and (b), onto RE-CHAR®.

Through the non-linear and linear regression of the equation, as explained in the previous chapters, it was possible to determine the values of the model parameters and an analysis of the errors was performed; they are therefore reported in Table 3.24.

Table 3.24 – Langmuir isotherm parameters with error analysis for arsenic adsorption onto RE-CHAR®.

$p = 2$		As(III)		As(V)	
Parameters		**NL regression**	**L regression**	**NL regression**	**L regression**
Symbol	**Unit**				
K_L	L μg^{-1}	0.503 ± 9.4E-07	0.855 ± 1.6	0.328 ± 1.8E-03	0.337 ± 1.7E-02
q_{max}	$\mu g\ g^{-1}$	15.19 ± 8.2E-03	14.904 ± 1.5	30.269 ± 6.6E-01	30.239 ± 1.3E+01
R_L	-	0.022 ± 1.7E-09	0.015 ± 1.6E-04	0.033 ± 1.7E-05	0.026 ± 1.5E-04
Error analysis					
R^2		0.941	0.940	0.966	0.963
R^2_{adj}		0.917	0.917	0.952	0.949
r^2		0.941	0.941	0.968	0.974
SSE		7.658	7.662	25.593	27.513
SAE		5.628	5.619	11.222	10.832
ARE		5.750	5.682	9.144	8.658
HYBRID		9.245	9.290	20.805	21.566
MSPD		8.410	8.420	11.941	11.912
MSE		0.957	0.958	3.199	3.439
RMS		7.283	7.292	10.342	10.316
χ^2		0.555	0.557	1.248	1.294
SRE		6.162	6.018	9.808	9.265
K_2		0.059	0.060	0.034	0.037
APE		5.750	5.682	9.144	8.658
Δq		7.786	7.795	11.056	11.028

Figure 3.55 shows the experimental and the modelled data of Freundlich isotherm model for As(III) and As(V) adsorption, respectively, (a) and (b), onto RE-CHAR®.

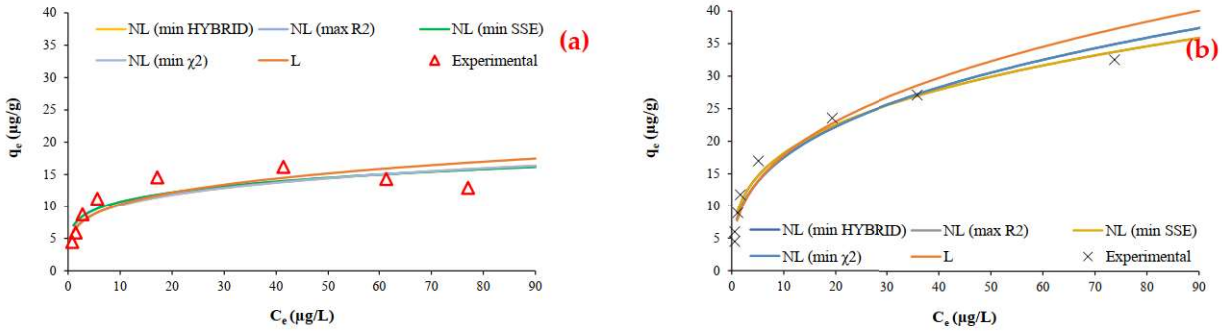

Figure 3.55 – Freundlich isotherm model for As(III) and As(V) adsorption, respectively, (a) and (b), onto RE-CHAR®.

Through the non-linear and linear regression of the equation, as explained in the previous chapters, it was possible to determine the values of the model parameters and an analysis of the errors was performed; they are therefore reported in Table 3.25.

Table 3.25 – Freundlich isotherm parameters with error analysis for arsenic adsorption onto RE-CHAR®.

$p = 2$		As(III)		As(V)	
Parameters		**NL regression**	**L regression**	**NL regression**	**L regression**
Symbol	**Unit**				
K_F	min^{-1}	6.601 ± 5.8E-01	5.952	8.405 ± 9.5E-01	7.652
1/n		0.201 ± 8.0E-04	0.239	0.327 ± 1.2E-03	0.368
q_{max}	µg g^{-1}	16.282 ± 3.6E-02	17.474	36.596 ± 2.3	40.029
Error analysis					
R^2		0.764	0.715	0.971	0.941
R^2_{adj}		0.586	0.601	0.960	0.897
r^2		0.766	0.744	0.972	0.962
SSE		30.428	36.663	21.584	44.533
SAE		14.092	15.153	11.219	15.382
ARE		17.581	17.486	14.253	14.440
HYBRID		47.124	60.672	38.985	44.321
MSPD		22.184	23.901	22.644	21.172
MSE		3.804	4.583	2.698	5.567
RMS		19.212	18.895	19.610	18.336
χ^2		2.827	3.034	2.339	2.659
SRE		18.540	18.738	15.054	15.783
K_2		0.236	0.285	0.029	0.059
APE		17.581	17.486	14.253	14.440
Δq		20.538	20.200	20.964	19.602

Figure 3.56 shows the experimental and the modelled data of Dubinin-Radushkevich (D–R) isotherm model for As(III) and As(V) adsorption, respectively, (a) and (b), onto RE-CHAR®.

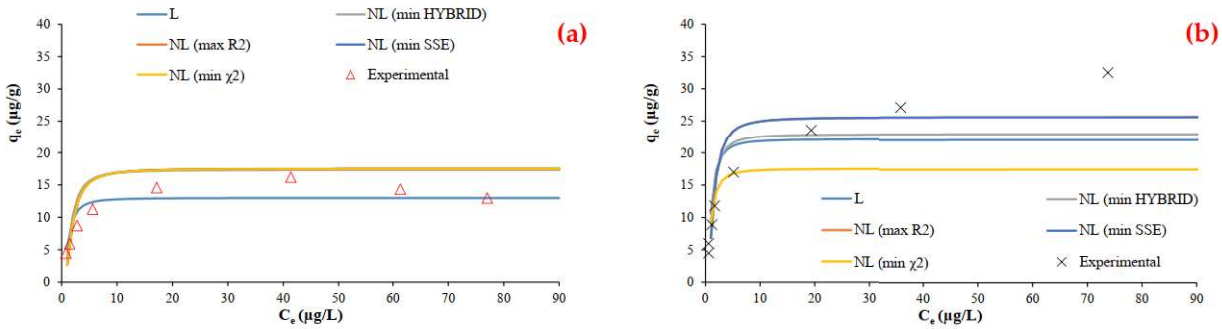

Figure 3.56 – D–R isotherm model for As(III) and As(V) adsorption, respectively, (a) and (b), onto RE-CHAR®.

Through the non-linear and linear regression of the equation, as explained in the previous chapters, it was possible to determine the values of the model parameters and an analysis of the errors was performed; they are therefore reported in Table 3.26.

Table 3.26 – D–R isotherm parameters with error analysis for arsenic adsorption onto RE-CHAR®.

$p = 2$		As(III)		As(V)	
Parameters		**NL regression**	**L regression**	**NL regression**	**L regression**
Symbol	**Unit**				
K_{DR}	$mol^2\ kJ^{-2}$	6.27E-07 ± 1.2E-14	3.06E-07	3.70E-07 ± 4.0E-14	2.57E-07
q_{max}	$\mu g\ g^{-1}$	17.480 ± 1.9E-02	12.989	22.894 ± 4.3E+01	22.143
Error analysis					
R^2		0.368	0.807	0.830	0.760
R^2_{adj}		0.115	0.730	0.762	0.663
r^2		0.896	0.826	0.847	0.790
SSE		81.386	24.836	127.940	181.105
SAE		22.896	12.039	26.289	29.961
ARE		29.516	15.137	20.976	22.614
HYBRID		134.243	38.022	128.355	139.337
MSPD		39.010	20.454	29.567	29.472
MSE		10.173	3.104	15.993	22.638
RMS		33.783	17.714	25.606	25.524
χ^2		8.055	2.281	7.701	8.360
SRE		33.822	16.066	19.318	23.882
K_2		0.632	0.193	0.170	0.240
APE		29.516	15.137	20.976	22.614
Δq		36.116	18.937	27.374	27.286

Figure 3.57 shows the experimental and the modelled data of Temkin isotherm model for As(III) and As(V) adsorption, respectively, (a) and (b), onto RE-CHAR®.

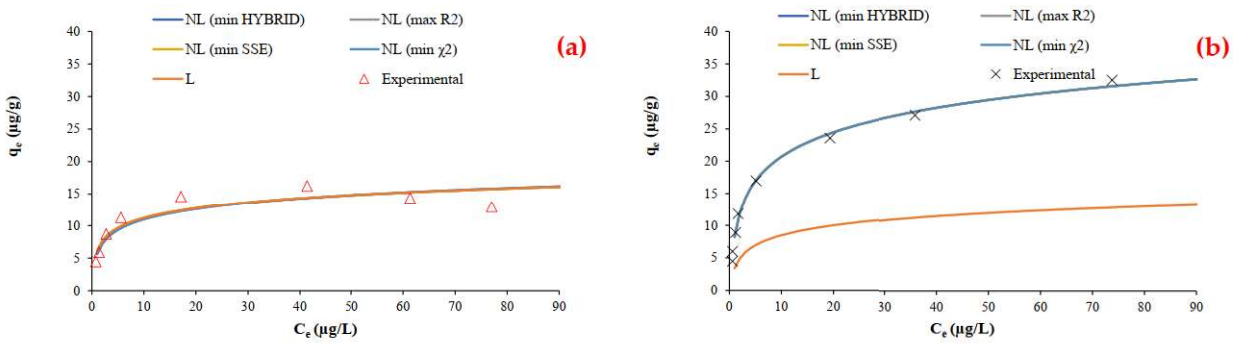

Figure 3.57 – Temkin isotherm model for As(III) and As(V) adsorption, respectively, (a) and (b), onto RE-CHAR®.

Through the non-linear and linear regression of the equation, as explained in the previous chapters, it was possible to determine the values of the model parameters and an analysis of the errors was performed; they are therefore reported in Table 3.27.

Table 3.27 – Temkin isotherm parameters with error analysis for arsenic adsorption onto RE-CHAR®.

$p = 2$		As(III)		As(V)	
Parameters		**NL regression**	**L regression**	**NL regression**	**L regression**
Symbol	**Unit**				
At	L µg^{-1}	13.346 ± 2.3E+01	15.738	4.559 ± 4.5E-03	4.592
bt	J mol^{-1}	2.279 ± 1.6E-02	1099.859	5.421 ± 1.5E-04	449.887
Error analysis					
R^2		0.838	0.838	0.995	0.995
R^2_{adj}		0.774	0.774	0.993	0.993
r^2		0.838	0.838	0.995	0.995
SSE		20.803	20.803	3.540	3.540
SAE		11.407	11.500	4.806	4.884
ARE		12.570	13.957	5.815	5.935
HYBRID		28.015	30.024	5.627	5.670
MSPD		15.462	17.826	9.097	9.266
MSE		2.600	2.600	0.443	0.443
RMS		13.390	15.437	7.878	8.024
χ^2		1.681	1.801	0.338	0.340
SRE		13.327	15.020	6.213	6.384
K_2		0.162	0.162	0.005	0.005
APE		12.570	13.957	5.815	5.935
Δq		14.315	16.503	8.422	8.578

Figure 3.58 shows the experimental and the modelled data of Redlich-Peterson (R–P) isotherm model for As(III) and As(V) adsorption, respectively, (a) and (b), onto RE-CHAR®.

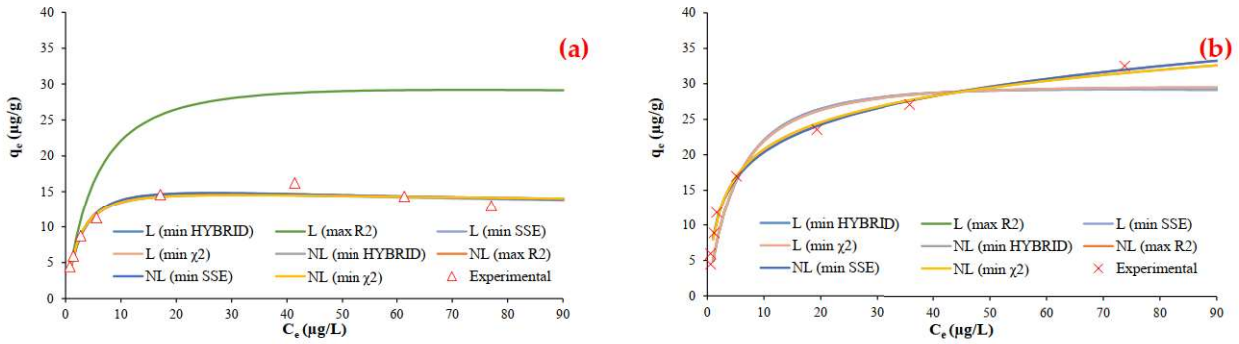

Figure 3.58 – R–P isotherm model for As(III) and As(V) adsorption, respectively, (a) and (b), onto RE-CHAR®.

Through the non-linear and linear regression of the equation, as explained in the previous chapters, it was possible to determine the values of the model parameters and an analysis of the errors was performed; they are therefore reported in Table 3.28.

Table 3.28 – Redlich-Peterson isotherm parameters with error analysis for arsenic adsorption onto RE-CHAR®.

p = 3		As(III)		As(V)	
Parameters		**NL regression**	**L regression**	**NL regression**	**L regression**
Symbol	**Unit**				
K_{RP}	L g^{-1}	5.761 ± 4.4E-01	5.635 ± 5.2E-02	15.987 ± 9.0E	5.635 ± 5.2E-02
b_{RP}	$(L\ \mu g^{-1})^n$	0.257 ± 4.3E-03	0.223 ± 1.4E-02	0.987 ± 9.3E-02	0.133 ± 2.8E-04
n_{RP}	-	1.100 ± 1.0E-03	1.093 ± 6.1E-04	0.839 ± 9.5E-04	1.068 ± 4.4E-04
Error analysis					
R^2		0.962	0.961	0.995	0.927
R^2_{adj}		0.933	0.932	0.991	0.872
r^2		0.964	0.963	0.995	0.966
SSE		4.923	5.005	4.019	55.027
SAE		4.512	4.479	4.505	19.096
ARE		5.656	5.404	6.265	22.375
HYBRID		8.163	8.534	9.463	100.659
MSPD		8.859	9.679	11.909	34.813
MSE		0.615	0.626	0.502	6.878
RMS		7.004	7.652	9.415	27.522
χ^2		0.408	0.427	0.473	5.033
SRE		6.054	5.703	6.782	22.538
K_2		0.038	0.039	0.005	0.073
APE		5.656	5.404	6.265	22.375
Δq		7.487	8.180	10.065	29.422

Figure 3.59 shows the experimental and the modelled data of Koble-Corrigan (K–C) isotherm model for As(III) and As(V) adsorption, respectively, (a) and (b), onto RE-CHAR®.

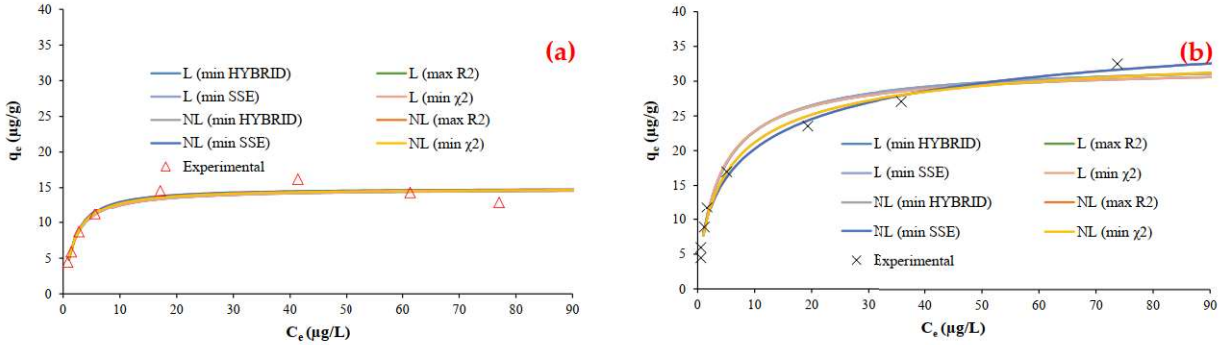

Figure 3.59 – K–C isotherm model for As(III) and As(V) adsorption, respectively, (a) and (b), onto RE-CHAR®.

Through the non-linear and linear regression of the equation, as explained in the previous chapters, it was possible to determine the values of the model parameters and an analysis of the errors was performed; they are therefore reported in Table 3.29.

Table 3.29 – Koble-Corrigan isotherm parameters with error analysis for arsenic adsorption onto RE-CHAR®.

p = 3		As(III)		As(V)	
Parameters		**NL regression**	**L regression**	**NL regression**	**L regression**
Symbol	**Unit**				
A_{KB}	L g^{-1}	7.200 ± 1.4E-01	7.786 ± 1.9E-04	9.999 ± 2.8E-02	10.012 ± 1.7E-02
B_{KB}	L μg^{-1}	0.483 ± 6.4E-04	0.523 ± 5.6E-06	0.259 ± 1.7E-03	0.305 ± 1.3E-04
n_{KB}	-	1.119 ± 5.0E-03	1.006 ± 4.8E-05	0.656 ± 1.9E-02	0.873 ± 4.0E-04
Error analysis					
R^2		0.944	0.938	0.989	0.975
R^2_{adj}		0.902	0.892	0.981	0.956
r^2		0.944	0.941	0.990	0.978
SSE		7.202	7.955	7.963	18.821
SAE		5.648	5.597	6.825	10.814
ARE		6.101	5.683	8.084	9.358
HYBRID		10.761	11.263	15.137	20.168
MSPD		9.344	9.224	13.692	12.766
MSE		0.900	0.994	0.995	2.353
RMS		7.387	7.292	10.824	10.093
χ^2		0.538	0.563	0.757	1.008
SRE		6.531	6.015	8.628	10.372
K_2		0.056	0.062	0.011	0.025
APE		6.101	5.683	8.084	9.358
Δq		7.897	7.795	11.572	10.789

Compared to the data, between the investigated isotherm models, both in As(III) and As(V), the non-linear regression found an analysis of the errors better than that of the linear regression.

Values close to the unit of the determination (R^2) and correlation coefficient (r^2) and minimum values of the other errors show an excellent adaptation of the experimental data to the analytical models.

Analysing the errors it emerges that, taking sum square error (SSE) and coefficient of determination (R^2) into consideration, the isotherm that best describes the data, for both aqueous solutions, is the Redlich-Peterson model, as reported by Yoon et al. [791].

In the following Table 3.30, it is carried out a comparison between the maximum adsorption capacity of arsenic, of some reactive materials (biochar and not), optionally also modified.

Table 3.30 – Values of the maximum adsorption capacity of arsenic.

Reactive material	Co (mg L^{-1})		q_{max} (mg g^{-1})		References
	As(V)	As(V)	As(III)	As(V)	
Biochar impregnated with bismuth	50	n.r.	16.21	n.r.	[792]
Manganese oxid-modified Biochar composite (MBC)	0-50	n.r.	0.80 - 14.36	n.r.	[793]
Magnetic gelatin modified Biochar	n.r.	20	n.r.	45.80	[794]
Iron impregnated Biochar	n.r.	0.1 - 55	n.r.	2.16	[795]
Iron hydro(oxide) onto activated carbon	n.r.	0 - 10	n.r.	4.56	[796]
Fe-impregnated granular activated carbon	n.r.	0.05-5	n.r.	1.95	[797]
Biochar- AlOOH nanocomposite	n.r.	5 - 200	n.r.	15.99	[798]
Fe(II)-loaded activated carbon	n.r.	0.5 - 8.5	n.r.	2.02	[799]
Fe-Mn impregnant BC	50	n.r.	8.25	n.r.	[800]
Biochar / γ-Fe_2O_3 composite	n.r.	50	n.r.	3.147	[529]
Sesbania bispinosa biochar (SBC)	0.1 - 10		7.33		[801]
Sesbania bispinosa biochar with copper oxider (SBC/CuO)			12.47		
Sesbania bispinosa biochar with manganese oxide nanoparticles			7.34		
Raw pine cone Biochar	50 - 200	n.r.	5.7	n.r.	[802]
Zn-loaded Biochar			7.0		
Mesoporous alumina	n.r.	44.70	n.r.	36.60	[803]
Clinoptilolite zeolite	20	n.r.	5-11	n.r.	[706]
Virgin coniferous wood biochar	$90*10^{-3}$	$90*10^{-3}$	$\approx 20*10^{-3}$	$\approx 30*10^{-3}$	This study

Starting from the table, it can be shown that the mentioned aqueous solutions and/or the real waters had an initial arsenic concentration in the order of milligrams per liter. It is therefore complex compare these results with those seen by the experimental activities.

The material probably has not yet exhausted all the sites available for adsorption. It is advisable, therefore, the driving of successive tests stressing the material further.

3.4 Column Test

This paragraph shows the results obtained during the experimental investigation relating to column tests.

3.4.1 Remediation of lead-contaminated water

Figure 3.60 shows the breakthrough curves obtained through the column tests. They were plotted in terms of the percentage of Pb concentration in the eluate with respect to the feeding concentration, C/C0, versus time of operation of the column plant filled with soil only, soil with AMBIOTON® and soil with RE-CHAR® respectively. Adsorption temperature, flow rate and initial concentration were maintained at 20 ± 0.5 °C, 60 mL h^{-1} and 100 mg L^{-1}, respectively. Figure 3.60 shows also two horizontal lines drawn at C/C_0 = 5% and C/C_0 = 95%, assumed to represent breakthrough and the exhaustion conditions, respectively.

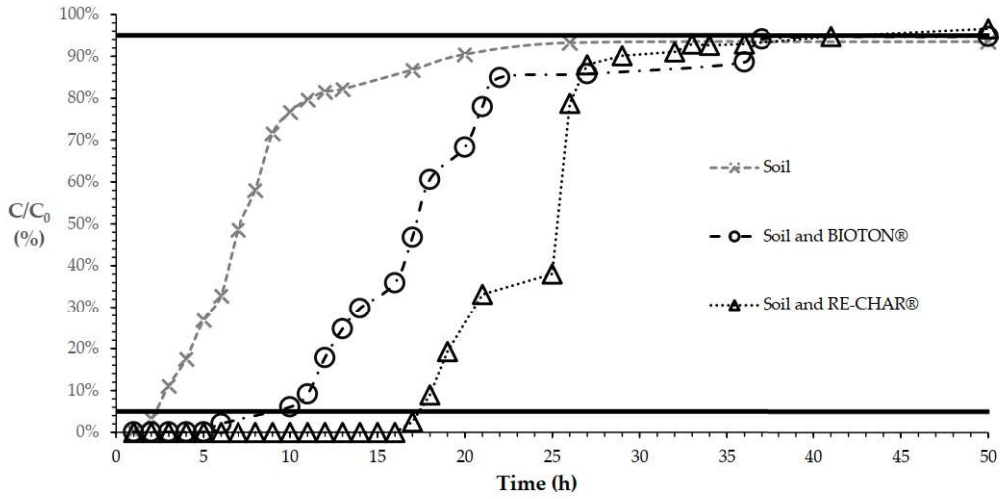

Figure 3.60 –Breakthrough curves for adsorption of Pb onto soil, soil with AMBIOTON® and soil with RE-CHAR®.

The breakthrough curves obtained for soil and soil and biochar columns showed approximately the same shape: a rapid increase of C/C_0 after breakthrough (C/C_0 = 5%), followed by a trend at a much slower rate towards the exhaustion (C/C_0 = 95%).

However, it is worth noting that breakthrough times were reached much faster in the column containing soil only with respect to the column filled with soil (few hours) and the two biochars: i.e. AMBIOTON® and RE-CHAR®, respectively, 5 and 15 h. Similarly, exhaustion times of the columns filled with soil and biochar appeared after about 35 h and 40 h, respectively for AMBIOTON® and RE-CHAR®.

The breakthrough curves of Pb adsorption onto soil, soil and AMBIOTON® and soil and RE-CHAR®, reported in Figure 3.60, highlight that the addition of biochar significantly enhanced the adsorption capacity and the operation time of the column plant with respect to the column containing only soil. This implies a higher amount of metal uptaken by the adsorbent and a less frequency of adsorbent bed replacement/regeneration after exhaustion, which lead to reduced operating costs of the treatment plant.

By integrating the breakthrough curve between t = 0 and t = 50 h (end of the column tests), it was possible to determine the experimental value of the adsorption capacity, which was q_{exp} = 67.07 mg g^{-1} for the column containing soil only, q_{exp} = 177.80 mg g^{-1} for the column filled with soil and AMBIOTON® and q_{exp} = 230.96 mg g^{-1} for the column filled with soil and RE-CHAR®.

This value takes into account the capacity of both biochar, which contributed for 110.73 mg g^{-1} and 163.89 mg g^{-1}, respectively for AMBIOTON® and RE-CHAR®.

Among the three mathematical models applied, the Thomas model provided a better description of the experimental breakthrough curves [715] (R^2 = 0.760 and 0.853, for AMBIOTON® and RE-CHAR®, respectively), when compared to Yoon–Nelson (R^2 = 0.600 and 0.850, for AMBIOTON® and RE-CHAR®, respectively) [714] and Bohart–Adams (R^2 = 0.610 and 0.788, for AMBIOTON® and RE-CHAR®, respectively) [716].

The Thomas rate constant (k_{TH}) and the adsorption capacity (q_0) were obtained from the linearized form of the model equation, by plotting $\ln(C_0 C^{-1})$ versus t (not here shown) and by determining the intercept and the slope of the regression line. The values found were for AMBIOTON® and RE-CHAR®, respectively, k_{TH} = 4.10×10^{-5} mL (min mg)$^{-1}$ and q_0 = 270.57 mg g^{-1}; k_{TH} = 5.28×10^{-5} mL (min mg)$^{-1}$ and q_0 = 334.57 mg g^{-1}.

The value of q_0 predicted by the model was very similar to the data reported in the specialized literature for the lead maximum adsorption capacity by adsorbents other than biochar used in column plants [30,158,574,775,778,780–783],

The adsorption capacity predicted (q_0, mg g^{-1}) by the model of both biochar was higher than that experimentally determined, i.e. q_{exp} = 177.80 mg g^{-1} for RE-CHAR® and q_{exp} = 230.96 mg g^{-1} for AMBIOTON®: the difference indicates that the adsorbent media had not reached complete saturation at the end of the tests, i.e. at t = 50 h and therefore it still possessed adsorption sites which could be potentially occupied by the adsorbate. As expected, the higher driving force of the adsorption process acting in the continuous flow column plant determined a higher uptake capacity than that measured under batch conditions.

Therefore, the findings of the present study can play a key role in view of the implementation of this adsorption process at full-scale which usually applies a column system.

Figure 3.61 – Photographic documentation of the filled columns, connected to the peristaltic pumps.

3.4.2 Adsorption of arsenic from aqueous solutions

Experimental data collected during the two column tests were compared to investigate the suitability of the biochar to remove As(V) from water and to study the influence of the biochar quantity to the removal process [804].

Compared to the column containing only sand, the concentrations of the four ports were compared to the initial concentration to calculate how much arsenic was adsorbed per gram of quartz sand. Based on these tests, the adsorption capacity of sand was determined to be negligible, in the presence of the biochar. Therefore, only influence of the biochar quantity on removal process (Figure 3.62) was considered. As a result, all data subsequently shown and discussed contain corrections made for sand adsorption.

The pH along with the redox potential (ORP) are the most important factors for controlling the speciation of arsenic [88]. In fact, within the samples collected during all the tests, the pH and the ORP were constant, respectively, 7.5 ± 0.2 and 800 ± 100 mV; therefore, it is evident that arsenates ($HAsO_4^{2-}$) remained dominant [87].

Figure 3.62 represents the breakthrough curves obtained by sampling at the four different ports (A, B, C, D), by in two different cases varying the volume ratio (7-3%) of the biochar in the column system. The effect of volume ratio of biochar in the column system on the breakthrough curve shape has been examined with a flow rate (i.e. of 5 mL/min) and initial inlet concentration (i.e. of 1 mg/L).

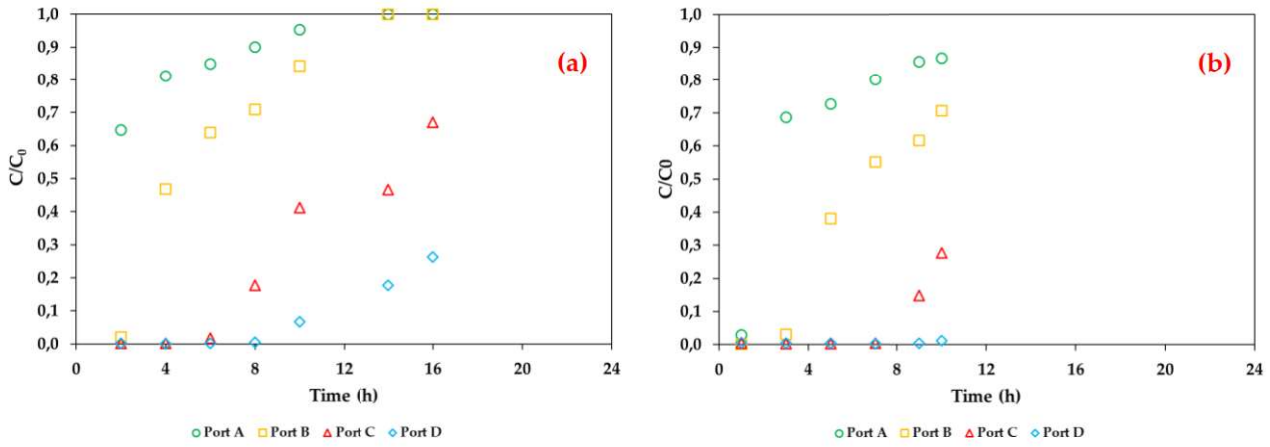

Figure 3.62 – Breakthrough curves for the test 1 (a) and the test 2 (b) with respectively biochar-sand volume ratio of 7:100 and 3:100.

The breakthrough curves of the tests show a higher adsorption of As in the test 1 than in the test 2. This result is related to the biochar physical properties and to its percentage in the two column tests. In the test 1 the quantity of the biochar is higher than in the test 2 and, due to its small grain size, it probably forms zones with low permeability which reduce the contact between the solute and the surface of the biochar.

Figure 3.63 show respectively the mass balances relating to the different column system. The histogram in Figure 3.63 analyzed the amount of accumulated arsenic retained and that entering the column.

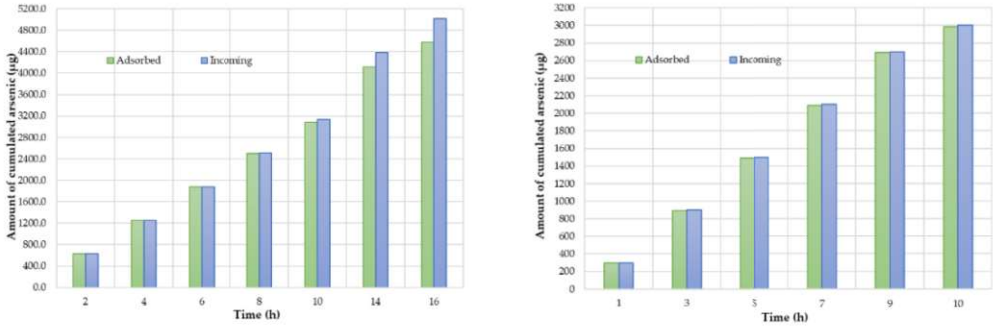

Figure 3.63 – Amount of cumulated arsenic in column test, 7% and 3% by volume, respectively to right and left.

As can be showed from mass balances, both column test show, however, on the whole, a good adsorption capacity.

The numerical model was validated reproducing the laboratory tests and comparing the breakthrough experimental curves with the numerical ones (Figure 3.64, Figure 3.65 and Figure 3.66). Linear, Langmuir and Freundlich isotherms were implemented in the model in order to evaluate the best suitable isotherm to reproduce the experimental data. A preliminary calibration phase was carried out to estimate the values of the hydrodynamic dispersion coefficient, the porosity of the media, the bulk density and the isotherm coefficients by MSE.

Values of the calibrated parameters for the two column tests are reported in Table 3.31. The experimental and simulated data were normalized by the respective highest concentration value for the both columns.

Table 3.31 – Values of the parameters used for the simulation of the two column tests.

Parameter	Unit	Value	
		Test 1	Test 2
p	-	0.25	0.30
D	$m^2\ min^{-1}$	$5*10^{-5}$	$5*10^{-5}$
ρ_b	$g\ cm^{-3}$	1.6	1.6
K_D	$L\ mg^{-1}$	1.6	1.8
q_{max}	$mg\ g^{-1}$	2.6	4.0
K_L	$L\ mg^{-1}$	$9*10^{-1}$	$9*10^{-1}$
n	-	10	10
K_F	$L^{1/n}\ mg\ kg^{-1}\ mg^{-1/n}$	$5*10^{-1}$	$5*10^{-1}$

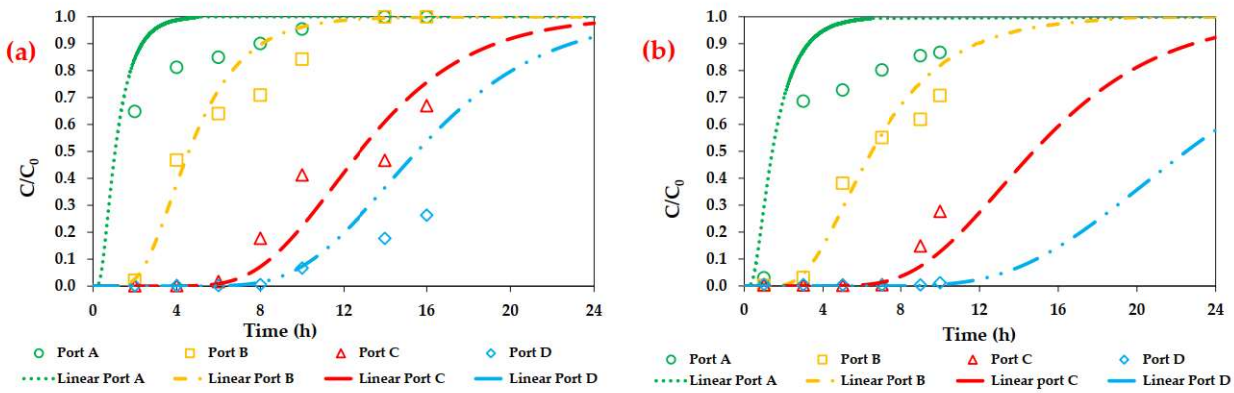

Figure 3.64 – Comparison between the experimental data and the numerical ones obtained using Linear isotherm for test 1 (a) and 2 (b).

(a)

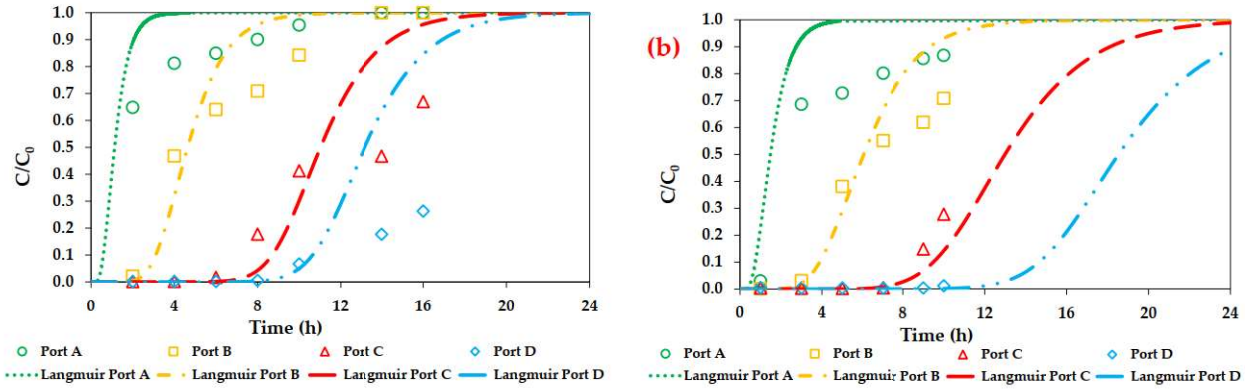

Figure 3.65 – Comparison between the experimental data and the numerical ones obtained using Langmuir isotherm for test 1 (a) and 2 (b).

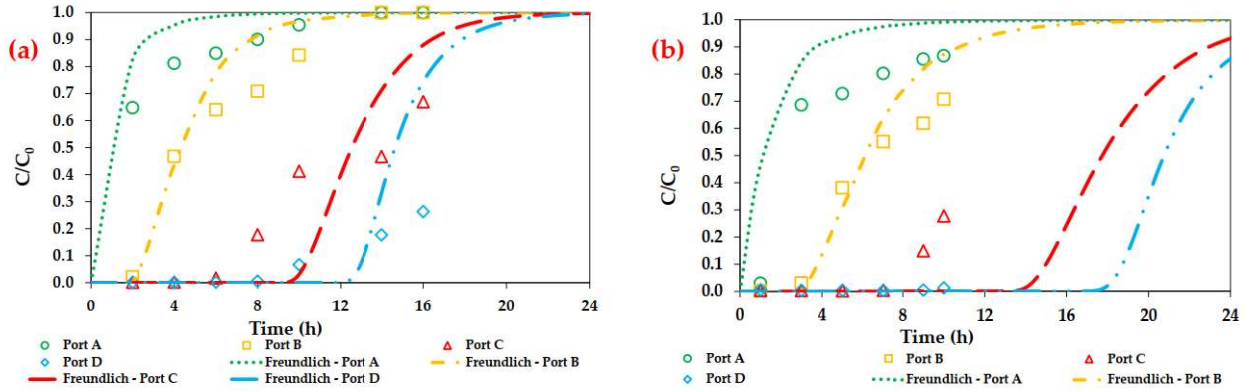

Figure 3.66 – Comparison between the experimental data and the numerical ones obtained using Freundlich isotherm for test 1 (a) and 2 (b).

The comparison between the MSE values calculated for each port of the two tests (Table 3.32) demonstrate the more suitability of the Langmuir isotherm to simulate the experimental data than the Linear and Freundlich isotherm.

Table 3.32 – MSE values between the calculated data and the measured one for each port of the two tests.

Isotherm Model	Test 1				Test 2			
	Sample Port A	*Sample Port B*	*Sample Port C*	*Sample Port D*	*Sample Port A*	*Sample Port B*	*Sample Port C*	*Sample Port D*
Linear	8.83E-01	2.21E-02	2.06E-02	5.23E-01	4.11E-02	6.66E-03	5.49E-03	2.13E-05
Langmuir	3.47E-03	6.43E-03	1.85E-02	1.87E-03	1.90E-02	1.06E-02	1.66E-02	3.51E-05
Freundlich	1.16E-02	1.12E-02	4.02E-02	3.75E-02	5.37E-02	1.35E-02	1.80E-02	4.09E-05

Langmuir isotherm specifically fits with higher accuracy the concentration values of samples collected during the test 1 (Figure 3.65a). The calibrated values of Langmuir isotherm parameters are comparable to the values reported in literature for biochars similar in terms of composition to the investigated biochar (Table 3.33).

Table 3.33 – Values of Langmuir isotherm parameters (q_{max} and K_L) for biochars reported in literature.

Adsorbent media	As concentration (mg L^{-1})	q_{max} (mg g^{-1})	K_L (L mg^{-1})	References
Biochar produced from municipal solid wastes	5.0 - 400	18.06 - 24.49	$7.2*10^{-2}$ - $7.8*10^{-2}$	[805]
Cattle bone char	0.1 – 1.0	0.399	$1.04*10^{-3}$	[806]
Perilla leaf biochar	0.05 – 7.0	3.85 - 7.21	$1.08*10^{-3}$ - $2.14*10^{-3}$	[807]
Peanut shell biochar	5.0	7.94	$2.17*10^{-3}$	[808]
Virgin coniferous wood biochar	1.0	1.80	$9*10^{-2}$	This study

The numerical model implemented with the calibrated parameters of Langmuir isotherm was used to calculate the absorption capacity of the biochar, by the following equations:

$$M_{ads} = V_{cum}\,(T_{max}) \times C_0 - \sum_{t=\Delta t}^{t_{max}} \left[\frac{(C_t + C_{t-\Delta t}) \times \left(V_{cum}(t) - V_{cum}(t-\Delta t)\right)}{2}\right] \quad (74)$$

where M_{ads} is the As mass adsorbed to the biochar (g), C_{Ads} the biochar adsorption capacity (µg L^{-1}), V_{cum} the cumulated volume of injected solution into the column (L), C_0 the As concentration of inflowing solution (µg L^{-1}), t_{max} the duration of the test (h or min) and Δt the numerical time step (h or min).

$$Q_{Ads} = \frac{M_{Ads}}{\rho_b} \quad (75)$$

Values of adsorption capacity (Q_{Ads}) were estimated considering the As concentrations calculated by the model at the outlet of the two columns. The obtained Q_{Ads} values for the two tests are comparable and they are also similar to the adsorption capacity values reported in literature studies (Table 3.34).

Table 3.34 – Values of adsorption capacity of biochars reported in literature.

Adsorbent media	Adsorption capacity (mg g^{-1})	As concentration (mg L^{-1})	References
Biochar produced from Sewage sludge	0.071	1	[809]
Biochar produced from Empty fruit bunch	5.5	3 - 300	[810]
Biochar produced from Rice husk	7.1	3 - 300	
Cattle bone char	0.134	0.1 - 1.0	[806]
Perilla leaf biochar	0.008 - 2.95	0.05 - 7	[807]
Virgin coniferous wood biochar	Test 1: 0.16 Test 2: 0.17	1.0	This study

4 Conclusions and perspective

This Ph.D. thesis in Environmental and Hydraulic Engineering has set itself the goal of studying a possible reactive material for heavy metals removal from contaminated waters.

Biochar, obtained from the controlled thermochemical conversion of products and residues of vegetable origin from agriculture and forestry, could represent a possible environmentally friendly alternative to the adsorbent media, that are currently on the market, since it prefers the valorisation of many wastes, the recovery and reuse of materials with a view to circular economy.

This would also reduce the enormous environmental impact of the industrial production of commercial adsorbents; thus, avoiding the generation of ad hoc production processes.

Compared with the practical use of biochar, the biochar research is really just in its infancy. Even though huge progress has been achieved in biochar research since the beginning of the XXI century, there are still many questions to be answered.

Biochar has been receiving worldwide interest since many years, because of its potential multidisciplinary applications in many fields of environmental engineering, such as bioenergy production via biochar co-products (bio-oil and syngas), global warming mitigation, sustainable agriculture, contaminants removal from environment and other applications.

Biochar can be obtained starting from multiple feedstocks and plant biomasses of all kinds and types. Each Biochar will be so different, just as its properties and potential for application will be different in one field rather than another.

Therefore, it is essential to know the characteristics of biochar which will subsequently be investigated for a specific purpose.

In literature data, the numerous studies relating to the use of different biochars are evident; many of these are produced in laboratory scale and their replicability in terms of production is very complicated.

Therefore, in the choice of biochar to be examined in the experimental activities, the research focused on the production processes already started at the national level. Two different biochars were therefore selected (RE-CHAR® and AMBIOTON®), currently used in agriculture, as their use has been regulated and consolidated in Italy since 2015; both supply chains of these materials are guaranteed, consolidated and certified.

This study provides in the introduction chapter the fundamentals of biochar, such as its concept, feedstock, production technology, uses and benefits and relative environmental impact assessment.

The experimental activities concerned a physico-chemical characterization of these two biochars and a commercial activated carbon, in order to compare their properties; batch and column tests in order to evaluate their performance for heavy metals removal from contaminated water (lead and arsenic were considered as target contaminants).

The concluding remarks of the introductory chapter are highlighted below, as they were necessary for the subsequent evaluations of the experimental results.

Due to the large difference seen in biochar properties, depending on the feedstock and many other factors, predictive knowledge of soil and plant effects is a requirement for development of a market for biochar application to soil. Such understanding would enable the development of a decision-making tool to lead final users in selecting the most suitable biochar for their particular application settings, as well as enabling valid policy guidance.

Biochar production and application to soil is a strategy for carbon (C) sequestration that could contribute to the reduction of emissions, providing simultaneous benefits to soil and opportunities for bioenergy

generation. The thermochemical conversion of biomass into biochar generates a highly stable product with much slower mineralization than the original biomass source; this brings to a long-term C sequestration. Further mitigation can be achieved through reduction in GHG emissions, resulting from reduced fertilizer and irrigation requirements due to improved nutrient and water-use efficiencies and avoidance of conventional disposal routes.

Evidence presented in Greenhouse gases emission paragraph shows that biochar has the potential to mitigate N_2O emissions and CH_4 emissions from soil. However, great uncertainty still exists with respect to biochar use and its GHG reducing effect as associated with different biochars and soil types/conditions. This is due to the lack of understanding of mechanistic biochar effects.

Relating to agriculture, the application of biochar as a soil conditioner can produce abundant benefits, such as the enhancement of the physical, chemical and biological properties of soils.

In particular, in short-term experiments, biochar generally increases plant growth, soil nutrient status and reduce fertilizer and irrigation requirements. However, the mechanisms leading to these benefits are not fully described, and neither the quantitative variability in response nor the duration of the effects are specified. Furthermore, lack of data from long-term studies generates a problem in establishing a distinct link between biochar application and increased crop production.

The production process of both biochars, with its valuable, renewable energy product, seems to be an economically viable conversion technology. Until more certain results are obtained also compared to the benefits of these biochars applied to the soil, it would not be economically convenient to modify the process parameters with the aim of increasing the yield of biochar. However, in order to advance more detailed economic arguments, it would be necessary to carry out an economic analysis of the process, evaluating how revenues would vary, modifying some process parameters.

In Italy, the use of biochar as an agricultural amendment has been legitimized since 2015. Therefore, being biochar a commercial proposition, it will be necessary as soon as possible to establish a reliable predictive knowledge of its impacts in specific soil and agronomic application (as is the case for chemical fertilizers). Moreover, accepting the use of waste as input material for the biochar production, by setting limits on the presence of toxic elements, would allow even greater environmental benefits and would fit perfectly in the context of the circular economy.

All that pointed out the need for a strategic research development that will combine the effects of biochar applied to soil with the details about the characteristics of biochar and soil to be amended, consenting the clarification of differentiated mechanisms for environmental and management factors.

Moreover, Biochar has demonstrated evident potential for the reduction of several organic and inorganic contaminants present in soil and water. The biochar use as an environmental sorbent could have strong consequences: it is not excluded that activated biochar could replace activated carbon, as it could have equivalent or higher adsorption efficiency for various pollutants.

So, first of all, the physicochemical and morphological properties of this carbon-based sorbents, as affected by feedstock sources and pyrolysis temperatures are discussed.

In fact, the various properties depend on two fundamental factors such as: the origin of the raw material and the production conditions. Biochar and active carbon may have very different properties and vary significantly.

The parameters to be investigated have been identified according to the use of these materials as adsorbent media.

The results showed that the various characteristics of the materials analysed are comparable with other biochar or substances used in soil and/or water remediation processes. These characteristics will influence the pollutant removal processes, depending on the matrix where these materials will be applied.

However, the Italian biochar market, like a soil improver, is currently at an early stage. In general, companies have businesses that cater to niche markets and small-scale applications (mainly scientific research).

Producing company, in order to increase the market, could apply for Ecolabel certification to obtain greater visibility even by foreign buyers, where the biochar market is at a more advanced stage.

Also, for this purpose, they may require the product characterization valid for international certification, in addition to the Italian one (i.e. IBI and EBC).

In fact, from a first analysis, the standards required to obtain the EBC certificate would all seem to be respected. This is a good opportunity to give customers a reliable quality basis, end to the company the opportunity of proving that its product meets well-defined quality standards.

In addition, the sustainability assessment of biochar systems would certainly benefit from having a standardized methodological approach. The suggestion is to implement an Environmental Product Declaration (EPD), with guidelines on setting the LCA system boundary, functional unit, impact assessment method and categories.

Considering the possible activation of the biochar, it will be necessary to repeat the characterization of the modified material using the same validated methodology. In addition, in order to perform a bio-activation, it will still be necessary to provide also an estimate of the biological properties of the material as it is, so far not considered.

In batch tests two different studies were conducted related to lead and arsenic removal from contaminated water, using different process parameters, that have been carried out in different timings; so the data collected in the tests are very heterogeneous.

In addition to the analysis of the results of the experimental data on the heavy metals adsorption (Pb and As), the models that more adequately described the kinetics and isotherms of adsorption were investigated.

Among the available models, those that consider the adsorption capacity as a function of time in kinetics (t; $q_t = f(t)$) and concentration (C_e; $q_e = f(C_e)$) in isotherms, respectively, have been selected.

Furthermore, the adsorption isotherms were studied to provide a basis for revealing adsorption behavior, indicating possible adsorption mechanism, and estimating adsorption capacity.

For both contaminants it is essential the role of the characteristic parameters of the adsorption process, such as pH, temperature and redox potential.

As regards the study of lead, both materials (AMBIOTON® and RE-CHAR®) were tested, obtaining different satisfactory results, at high concentrations (50 and 100 mg L^{-1}).

Adsorption kinetic and isotherm models were evaluated using linear regression analysis. Values of coefficient of determination (R^2) showed the isotherms that have higher performance for representing the data.

The data collected are certainly a basis for the execution of further tests: for the equilibrium data, it is possible to carry out tests to modify the concentration instead of the dosage; as regards lead removal kinetics, before proceeding with any modification of the process operating parameters, also for equilibrium tests (i.e. pH, T, rpm, C_0), the dosages (g L^{-1}) must be modified, in order to describe the experimental data in an optimal and systematic way as a function of contact time.

During the experimental activities, specific for As removal, only one of the two materials (RE-CHAR®) was investigated, having completely different performances from the other one.

Moreover, in order to use it for the purification of arsenic contaminated water, it was appropriate to use a particularly high concentration of arsenic; nine times higher than the limits prescribed by law (≈90 μg L^{-1}). This concentration was also chosen for the execution of the preliminary tests, as no data was available regarding the use of this material in the field of arsenic removal.

In order to investigate both arsenic speciation, synthetic solutions were prepared from different arsenic salts: a trivalent (meta-sodium arsenite) and a pentavalent arsenic (disodium hydrogenarsenate heptahydrate).

The models studied, concerning kinetic character and thermodynamic equilibrium, were identified from a major study of literature, in order to best fit the experimental data obtained from laboratory tests and to estimate the errors in a quali-quantitative analysis.

As regards the tests conducted, RE-CHAR® seems to be an effective means for arsenic removal. At equilibrium time (8 hours), RE-CHAR® presented a high percentage of efficiency removal, for both contaminated solutions (dosage ≈ 10 g L^{-1}); residual As concentration were found minor to the detection limit (1 µg L^{-1}).

Furthermore, the removal efficiency is favoured by the alkaline pH of the material (pH_{PZC}); at the end of the tests with the exchange with CO_2 the pH returns to neutrality autonomously.

As regards the analytical methods, it is evident that the determination of arsenic concentrations in its speciations (pentavalent and trivalent), present in the aqueous solution of each sample, would allow a full-range analysis of the fractions of the arsenic species present in contaminated water, in all its forms, concerning both the study of kinetic and thermodynamic character.

At the moment AMBIOTON® has not been characterized as the previous one with respect to As adsorption; it is not excluded that specific studies may be conducted, as for the other one.

Compared to the experimental setup, concentration, rotation speed (0, 60, 120 rpm) and controlled pH tests can be evaluated.

However, with respect to the latter point, to understand the effect of the reduction from one form of Arsenic to another, it would be necessary to carry out batch experiments in order to assume the optimal pH on the material as it is, subsequently it would be possible to investigate the optimal chemical activation, in order to mitigate the conditioning of the water pH and avoid a modification of the chemical characteristics of water. This would not require treatments that would affect a raising/lowering of the pH and subsequent neutral buffer, also because all this would involve an additional cost in the treatment unit of the plant.

Linear regression for the same kinetic and isotherm model resulted in different values. This was due to a linearization method which changes the error distribution. Non-linear regression provided higher correlation with experimental data for both kinetic and isotherm analysis and this is in agreement with the results in literature data.

From the interesting results described above, it is clear that numerous possible variations of the process operating parameters and analytical methods can be taken into consideration during the continuation of the experimental activities.

In order to be used in the treatment of wastewater and/or drinking water, the leaching tests of the material as it is and possibly modified are essential.

In addition, the possibility of activating the biochar both chemically and physically or biologically could be useful for evaluating the possible increase in adsorption capacity and removal rate.

A further deepening of the characteristics of the material could be conducted taking into consideration a contamination of other heavy metals and at the same time from different chemical elements, to test the competitiveness of different contaminants in respect of the adsorption sites of the materials considered.

In column tests, different experimental apparatus, contaminants (As and Pb), operating conditions and subsequent processing of the data obtained were used.

Preliminary laboratory tests showed the suitability of RE-CHAR® and AMBIOTON® to adsorb lead from water solutions.

Based on these first results, it can be assessed that both biochars can be used as effective adsorbents for Pb removal from water even at high metal concentration, considering the order of magnitude of the concentration of real water much lower.

Adsorption of arsenic was investigated onto RE-CHAR® by preliminary laboratory and adaption of experimental data with numerical model.

In particular, two column tests were carried for As removal with a C_0 equal 1 mg/L, by varying the weight and volume ratio of the biochar in the column system.

It is worthwhile to notice that few papers have given values of the possible applicable value of the isotherm parameters indicating at the same time the more suitable isotherm to use in the numerical simulations. It is noticed a considerable difference between the values of isotherm calibrated and the one estimated by batch tests. Specifically, as encountered in other cases, the calibrated values are higher than the values obtained experimentally. This difference is mainly due to the value of initial concentration and the different percentage of biochar used for the two tests. Also, the difference can be due to the smaller contact time between the contaminant and the RE-CHAR® particles during the column test respect to the batch tests.

One of the possible solutions to approach the problem is probably to use non-equilibrium approach, this consideration stems from the fact that the kinetic of the process is largely dependent from the time contact between the water with the dissolved contaminant and the adsorption sites. Batch tests can give a soft idea of the probable value, but maybe they can result, in case of complex processes like those involving a heavy metal, more suitable to identify the right isotherm to use for simulating the process. The estimated values in column simulation are surely much more useful for a real field application where the uncertainties are surely larger than the possible initial or boundary conditions that can be used for a remediation design.

Starting from these preliminary results and the modeling of the breakthrough curves, will be investigated further experimental and optimal conditions (i.e., percentage and grain size of the water flow rate), in order to evaluate the use of biochar in real scale, such as in the water treatment or in remediation site, i.e. as a reactive material of the permeable reactive barrier (PRB), for heavy metals removal from contaminated groundwater.

In view of a possible on-site application in the contest of remediation, with a possible patent for the use of this sustainable material, it should be useful to further investigate the possibility of competitions with other contaminants.

So finally, the possible plant configurations and the methods of applying the remediation technology for contaminated waters by heavy metals will be tested.

In conclusion, considering the encouraging results over the next few experimental activities, some targeted tests, of which this Ph.D. thesis can only be the starting point, should be conducted.

In fact, further experiments are required to better understand the behaviour of both media and to assess their final removal capability.

At the moment, only tests have been carried out in the batch and column systems under neutral conditions of uncontrolled pH, in which the performance capabilities of both materials are limited. Therefore, different controlled pH conditions will have to be taken into consideration, taking into account the appropriate variations in the solid-liquid ratio and contact time, necessarily proportional to the operating conditions of the subsequent application scales (pilot and real).

Within the results of the experimental activities there are also no data relating to the use of activated carbon, mentioned in the material characterization activities (CARBOSORB NC 1240), to be compared with those relating to biochar; this would allow a more complete evaluation of the removal efficiency of the different carbonaceous materials, using the same operating conditions in batch and column tests.

In addition, the study of the appropriate modification/activation of the biochar would allow the optimization of the process operating conditions, in order to also minimize the dosage and the exhaustion time of the carbon-based sorbents.

Starting from the results obtained at the laboratory scale, the activities may eventually be transferred to the pilot scale and to the real scale in order to better test the performance of biochar in the presence of real conditions, i.e., multi-contaminated water (i.e., Cd, Pb, Cu, Hg etc.).

Therefore, potential technologies need to be developed and research gaps still need to be filled in order to optimize the use of biochar as a feasible alternative for treatment of heavy metals contaminated waters.

More research is needed but the results so far obtained by scientific results are so positive that biochar, as soil improver, has been added to the agenda of the upcoming international negotiations on climate change, as the most promising of mitigation strategies.

Although the use of biochar as a substitute for activated carbon is still in an early research phase, with further studies it could become a reality in a short time, finally allowing it to be used as an adsorbent media as well.

The biochar market, as a soil amendment, is however struggling to take off, due to the uncertainty about its benefits, but also to the lower purchasing and applying cost of standard soil improvers and fertilizers, whose effects are well known. Thus, a comprehensive economical study that examines cost and benefit comparison between biochar and standard products over multiple specific time horizons is required. The same argument also applies from an environmental point of view, and LCA should be carried out to evaluate which solution is the least impacting.

For the reasonable and multidisciplinary use of biochar, it would be indispensable a database related to feedstock, production technique parameters, biochar properties, and potential applications of each biochar; through additional experiments and computer simulation.

For a more sustainable society, it is also our responsibility to explore the future of biochar by boosting research and development.

References

1. Xue, Y.; Gao, B.; Yao, Y.; Inyang, M.; Zhang, M.; Zimmerman, A.R.; Ro, K.S. Hydrogen peroxide modification enhances the ability of biochar (hydrochar) produced from hydrothermal carbonization of peanut hull to remove aqueous heavy metals: Batch and column tests. *Chem. Eng. J.* **2012**, *200–202*, 673–680, doi:10.1016/j.cej.2012.06.116.

2. Beiyuan, J.; Tsang, D.C.W.; Yip, A.C.K.; Zhang, W.; Ok, Y.S.; Li, X.-D. Risk mitigation by waste-based permeable reactive barriers for groundwater pollution control at e-waste recycling sites. *Environ. Geochem. Health* **2017**, *39*, 75–88, doi:10.1007/s10653-016-9808-2.

3. Faisal, A.A.H.; Abd Ali, Z.T. Using sewage sludge as a permeable reactive barrier for remediation of groundwater contaminated with lead and phenol. *Sep. Sci. Technol.* **2017**, *52*, 732–742, doi:10.1080/01496395.2016.1251463.

4. Bartoli, M.; Giorcelli, M.; Jagdale, P.; Rovere, M.; Tagliaferro, A. A Review of Non-Soil Biochar Applications. *Materials (Basel).* **2020**, *13*, 261, doi:10.3390/ma13020261.

5. Moreira, M.T.; Noya, I.; Feijoo, G. The prospective use of biochar as adsorption matrix – A review from a lifecycle perspective. *Bioresour. Technol.* **2017**, *246*, 135–141, doi:10.1016/j.biortech.2017.08.041.

6. Ahmed, M.B.; Zhou, J.L.; Ngo, H.H.; Guo, W.; Chen, M. Progress in the preparation and application of modified biochar for improved contaminant removal from water and wastewater. *Bioresour. Technol.* **2016**, *214*, 836–851, doi:10.1016/j.biortech.2016.05.057.

7. Gwenzi, W.; Chaukura, N.; Noubactep, C.; Mukome, F.N.D. Biochar-based water treatment systems as a potential low-cost and sustainable technology for clean water provision. *J. Environ. Manage.* **2017**, *197*, 732–749, doi:10.1016/j.jenvman.2017.03.087.

8. Tan, X. fei; Liu, S. bo heng bo heng bo heng S.; Liu, Y. guo; Gu, Y. ling; Zeng, G. ming; Hu, X. jiang; Wang, X.; Liu, S. bo heng bo heng bo heng S.; Jiang, L. hua Biochar as potential sustainable precursors for activated carbon production: Multiple applications in environmental protection and energy storage. *Bioresour. Technol.* **2017**, *227*, 359–372, doi:10.1016/j.biortech.2016.12.083.

9. Ali, R.M.; Hamad, H.A.; Hussein, M.M.; Malash, G.F. Potential of using green adsorbent of heavy metal removal from aqueous solutions: Adsorption kinetics, isotherm, thermodynamic, mechanism and economic analysis. *Ecol. Eng.* **2016**, *91*, 317–332, doi:10.1016/j.ecoleng.2016.03.015.

10. Enaime, G.; Baçaoui, A.; Yaacoubi, A.; Lübken, M. Biochar for wastewater treatment-conversion technologies and applications. *Appl. Sci.* **2020**, *10*, doi:10.3390/app10103492.

11. Chen, M.; Zhou, S.; Zeng, G.; Zhang, C.; Xu, P. Putting carbon nanomaterials on the carbon cycle map. *Nano Today* **2018**, *20*, 7–9, doi:10.1016/j.nantod.2018.02.001.

12. Wang, H.; Yuan, X.; Wu, Y.; Huang, H.; Peng, X.; Zeng, G.; Zhong, H.; Liang, J.; Ren, M.M. Graphene-based materials: Fabrication, characterization and application for the decontamination of wastewater and wastegas and hydrogen storage/generation. *Adv. Colloid Interface Sci.* **2013**, *195–196*, 19–40, doi:10.1016/j.cis.2013.03.009.

13. Yi, H.; Zeng, G.; Lai, C.; Huang, D.; Tang, L.; Gong, J.; Chen, M.; Xu, P.; Wang, H.; Cheng, M.; Zhang, C.; Xiong, W. Environment-friendly fullerene separation methods. *Chem. Eng. J.* **2017**, *330*, 134–145, doi:10.1016/j.cej.2017.07.143.

14. Xu, P.; Zeng, G.M.; Huang, D.L.; Feng, C.L.; Hu, S.; Zhao, M.H.; Lai, C.; Wei, Z.; Huang, C.; Xie, G.X.; Liu, Z.F. Use of iron oxide nanomaterials in wastewater treatment: A review. *Sci. Total Environ.* **2012**, *424*, 1–10, doi:10.1016/j.scitotenv.2012.02.023.

15. Lee, J.; Kim, K.H.; Kwon, E.E. Biochar as a Catalyst. *Renew. Sustain. Energy Rev.* **2017**, *77*, 70–79,

doi:10.1016/j.rser.2017.04.002.

16. Qambrani, N.A.; Rahman, M.M.; Won, S.; Shim, S.; Ra, C. Biochar properties and eco-friendly applications for climate change mitigation, waste management, and wastewater treatment: A review. *Renew. Sustain. Energy Rev.* **2017**, *79*, 255–273, doi:10.1016/j.rser.2017.05.057.

17. Thengane, S.K.; Kung, K.; York, R.; Sokhansanj, S.; Lim, C.J.; Sanchez, D.L. Technoeconomic and emissions evaluation of mobile in-woods biochar production. *Energy Convers. Manag.* **2020**, *223*, 113305, doi:10.1016/j.enconman.2020.113305.

18. Xu, L.; Fang, H.; Deng, X.; Ying, J.; Lv, W.; Shi, Y.; Zhou, G.; Zhou, Y. Biochar application increased ecosystem carbon sequestration capacity in a Moso bamboo forest. *For. Ecol. Manage.* **2020**, *475*, 118447, doi:10.1016/j.foreco.2020.118447.

19. Criscuoli, I.; Ventura, M.; Sperotto, A.; Panzacchi, P.; Tonon, G. Effect of woodchips biochar on sensitivity to temperature of soil greenhouse gases emissions. *Forests* **2019**, *10*, 1–14, doi:10.3390/f10070594.

20. Ahmad, M.; Rajapaksha, A.U.; Lim, J.E.; Zhang, M.; Bolan, N.; Mohan, D.; Vithanage, M.; Lee, S.S.; Ok, Y.S. Biochar as a sorbent for contaminant management in soil and water: A review. *Chemosphere* **2014**, *99*, 19–23, doi:10.1016/j.chemosphere.2013.10.071.

21. You, S.; Ok, Y.S.; Chen, S.S.; Tsang, D.C.W.; Kwon, E.E.; Lee, J.; Wang, C.H. A critical review on sustainable biochar system through gasification: Energy and environmental applications. *Bioresour. Technol.* **2017**, *246*, 242–253, doi:10.1016/j.biortech.2017.06.177.

22. Keske, C.; Godfrey, T.; Hoag, D.L.K.; Abedin, J. Economic feasibility of biochar and agriculture coproduction from Canadian black spruce forest. *Food Energy Secur.* **2019**, *9*, 1–11, doi:10.1002/fes3.188.

23. Foong, S.Y.; Liew, R.K.; Yang, Y.; Cheng, Y.W.; Yek, P.N.Y.; Wan Mahari, W.A.; Lee, X.Y.; Han, C.S.; Vo, D.V.N.; Van Le, Q.; Aghbashlo, M.; Tabatabaei, M.; Sonne, C.; Peng, W.; Lam, S.S. Valorization of biomass waste to engineered activated biochar by microwave pyrolysis: Progress, challenges, and future directions. *Chem. Eng. J.* **2020**, *389*, 124401, doi:10.1016/j.cej.2020.124401.

24. Buss, W.; Bogush, A.; Ignatyev, K.; Mašek, O. Unlocking the Fertilizer Potential of Waste-Derived Biochar. *ACS Sustain. Chem. Eng.* **2020**, *8*, 12295–12303, doi:10.1021/acssuschemeng.0c04336.

25. Guo, X. xia; Liu, H. tao; Zhang, J. The role of biochar in organic waste composting and soil improvement: A review. *Waste Manag.* 2020, *102*, 884–899.

26. Kaikiti, K.; Stylianou, M.; Agapiou, A. Use of biochar for the sorption of volatile organic compounds (VOCs) emitted from cattle manure. *Environ. Sci. Pollut. Res.* **2020**, 1–9, doi:10.1007/s11356-020-09545-y.

27. Mohan, D.; Sarswat, A.; Ok, Y.S.; Pittman, C.U. Organic and inorganic contaminants removal from water with biochar, a renewable, low cost and sustainable adsorbent - A critical review. *Bioresour. Technol.* **2014**, *160*, 191–202, doi:10.1016/j.biortech.2014.01.120.

28. Tan, X.; Liu, Y.; Zeng, G.; Wang, X.; Hu, X.; Gu, Y.; Yang, Z. Application of biochar for the removal of pollutants from aqueous solutions. *Chemosphere* **2015**, *125*, 70–85, doi:10.1016/j.chemosphere.2014.12.058.

29. De Gisi, S.; Lofrano, G.; Grassi, M.; Notarnicola, M. Characteristics and adsorption capacities of low-cost sorbents for wastewater treatment: A review. *Sustain. Mater. Technol.* **2016**, *9*, 10–40, doi:10.1016/j.susmat.2016.06.002.

30. Inyang, M.I.; Gao, B.; Yao, Y.; Xue, Y.; Zimmerman, A.; Mosa, A.; Pullammanappallil, P.; Ok, Y.S.; Cao, X. A review of biochar as a low-cost adsorbent for aqueous heavy metal removal. *Crit. Rev. Environ. Sci. Technol.* **2016**, *46*, 406–433, doi:10.1080/10643389.2015.1096880.

31. Li, H.; Dong, X.; da Silva, E.B.; de Oliveira, L.M.; Chen, Y.; Ma, L.Q. Mechanisms of metal sorption by

biochars: Biochar characteristics and modifications. *Chemosphere* **2017**, *178*, 466–478, doi:10.1016/j.chemosphere.2017.03.072.

32. Oliveira, F.R.; Patel, A.K.; Jaisi, D.P.; Adhikari, S.; Lu, H.; Khanal, S.K. Environmental application of biochar: Current status and perspectives. *Bioresour. Technol.* **2017**, *246*, 110–122, doi:10.1016/j.biortech.2017.08.122.

33. Zhang, C.; Liu, L.; Zhao, M.; Rong, H.; Xu, Y. The environmental characteristics and applications of biochar. *Environ. Sci. Pollut. Res.* **2018**, 21525–21534, doi:10.1007/s11356-018-2521-1.

34. Lyu, H.; Zhang, Q.; Shen, B. Application of biochar and its composites in catalysis. *Chemosphere* **2020**, *240*, 124842, doi:10.1016/j.chemosphere.2019.124842.

35. Son, E.B.; Poo, K.M.; Chang, J.S.; Chae, K.J. Heavy metal removal from aqueous solutions using engineered magnetic biochars derived from waste marine macro-algal biomass. *Sci. Total Environ.* **2018**, *615*, 161–168, doi:10.1016/j.scitotenv.2017.09.171.

36. Gascó, G.; Álvarez, M.L.; Paz-Ferreiro, J.; Miguel, G.S.; Méndez, A. Valorization of biochars from pinewood gasification and municipal solid waste torrefaction as peat substitutes. *Environ. Sci. Pollut. Res.* **2018**, 1–9, doi:10.1007/s11356-018-2703-x.

37. Dai, Y.; Liang, Y.; Xu, X.; Zhao, L.; Cao, X. An integrated approach for simultaneous immobilization of lead in both contaminated soil and groundwater: Laboratory test and numerical modeling. *J. Hazard. Mater.* **2018**, *342*, 107–113, doi:10.1016/j.jhazmat.2017.08.023.

38. Sanchez-Monedero, M.A.; Cayuela, M.L.; Roig, A.; Jindo, K.; Mondini, C.; Bolan, N. Role of biochar as an additive in organic waste composting. *Bioresour. Technol.* **2018**, *247*, 1155–1164, doi:10.1016/j.biortech.2017.09.193.

39. Weber, K.; Quicker, P. Properties of biochar. *Fuel* **2018**, *217*, 240–261, doi:10.1016/j.fuel.2017.12.054.

40. Sun, X.; Atiyeh, H.K.; Li, M.; Chen, Y. Biochar facilitated bioprocessing and biorefinery for productions of biofuel and chemicals: A review. *Bioresour. Technol.* 2020, *295*, 122252.

41. Schmidt, H.-P. 55 Uses of Biochar. *Ithaka J.* **2012**, *1*, 286–289.

42. Lehmann, J.; Joseph, S. *Biochar for Environmental Management: Science, Technology and Implementation*; Routledge, Ed.; 2nd Editio.; Earthscan Publications Ltd: London, 2015; ISBN 978-0-415-70415-1.

43. Talberg, A.; Abadin, H.; Ashizawa, A.; Stevens, Y.-W.; Llados, F.; Diamond, G.; Sage, G.; Citra, M.; Quinones, A.; Bosch, S.J.; Swarts, S.G. *The basics of biochar*; Australia, 2009; Vol. 10;.

44. Sizmur, T.; Quilliam, R.; Puga, A.P.; Moreno-Jiménez, E.; Beesley, L.; Gomez-Eyles, J.L. Application of Biochar for Soil Remediation. In *Agricultural and Environmental Applications of Biochar: Advances and Barriers. SSSA Special Publication 63.*; Guo, M., He, Z., Uchimiya, S.M., Eds.; Soil Science Society of America: Madison, USA, 2016; pp. 295–324 ISBN 978-0-89118-967-1.

45. Cha, J.S.; Park, S.H.; Jung, S.C.; Ryu, C.; Jeon, J.K.; Shin, M.C.; Park, Y.K. Production and utilization of biochar: A review. *J. Ind. Eng. Chem.* **2016**, *40*, 1–15, doi:10.1016/j.jiec.2016.06.002.

46. Veldkamp, T.I.E.; Wada, Y.; Aerts, J.C.J.H.; Döll, P.; Gosling, S.N.; Liu, J.; Masaki, Y.; Oki, T.; Ostberg, S.; Pokhrel, Y.; Satoh, Y.; Kim, H.; Ward, P.J. Water scarcity hotspots travel downstream due to human interventions in the 20th and 21st century. *Nat. Commun.* **2017**, *8*, 1–12, doi:10.1038/ncomms15697.

47. Ondrasek, G. Water scarcity and water stress in agriculture. In *Physiological Mechanisms and Adaptation Strategies in Plants Under Changing Environment*; Springer New York, 2014; Vol. 1, pp. 75–96 ISBN 9781461485919.

48. Boni, M.R. *Fenomeni di inquinamento degli ambienti naturali: principi e metodi di studio*; Carocci editore, 2007; ISBN 9788843040995.

49. WHO Guidelines for Drinking-water Guidelines for Drinking-water Quality. *Eisei kagaku* **2008**, *1*, 307–312, doi:10.1248/jhs1956.35.307.

50. Zaporozec, A. Ground-Water pollution and its sources. *GeoJournal* **1981**, *5*, 457–471, doi:10.1007/BF02484718.

51. Khatri, N.; Tyagi, S. Influences of natural and anthropogenic factors on surface and groundwater quality in rural and urban areas. *Front. Life Sci.* **2015**, *8*, 23–39, doi:10.1080/21553769.2014.933716.

52. Chen, Y.; Shinogi, Y.; Taira, M. Influence of biochar use on sugarcane growth, soil parameters, and groundwater quality. *Aust. J. Soil Res.* **2010**, *48*, 526–530, doi:10.1071/SR10011.

53. Edokpayi, J.N.; Enitan, A.M.; Mutileni, N.; Odiyo, J.O. Evaluation of water quality and human risk assessment due to heavy metals in groundwater around Muledane area of Vhembe District, Limpopo Province, South Africa. *Chem. Cent. J.* **2018**, *12*, 1–16, doi:10.1186/s13065-017-0369-y.

54. United Nations Educational Scientific and Cultural *Resources of the World and Their Use*; Zektser, I.S., Everett, L.G., Eds.; Paris, 2004; ISBN 9292200070.

55. *Adsorptive Removal of Heavy Metals from Groundwater by Iron Oxide based adsorbents*; ISBN 9781138020641.

56. Hashim, M.A.; Mukhopadhyay, S.; Sahu, J.N.; Sengupta, B. Remediation technologies for heavy metal contaminated groundwater. *J. Environ. Manage.* 2011, *92*, 2355–2388.

57. Paul, D. Research on heavy metal pollution of river Ganga: A review. *Ann. Agrar. Sci.* **2017**, *15*, 278–286, doi:10.1016/j.aasci.2017.04.001.

58. Chowdhury, S.; Mazumder, M.A.J.; Al-Attas, O.; Husain, T. Heavy metals in drinking water: Occurrences, implications, and future needs in developing countries. *Sci. Total Environ.* **2016**, *569–570*, 476–488, doi:10.1016/j.scitotenv.2016.06.166.

59. Oyeku, O.T.; Eludoyin, A.O. Heavy metal contamination of groundwater resources in a Nigerian urban settlement. *African J. Environ. Sci. Technol.* **2010**, *4*, 201–214, doi:10.5897/AJEST09.098.

60. Verma, R.; Dwivedi, P. Heavy metal water pollution- A case study. *Recent Res. Sci. Technol.* **2013**, *5*, 98–99.

61. Egboka, B.C.E.; Nwankwor, G.I.; Orajaka, I.P.; Ejiofor, A.O. Principles and problems of environmental pollution of groundwater resources with case examples from developing countries. *Environ. Health Perspect.* **1989**, *83*, 39–68, doi:10.1289/ehp.898339.

62. Tchounwou, P.B.; Yedjou, C.G.; Patlolla, A.K.; Sutton, D.J. *Molecular, clinical and environmental toxicicology Volume 3: Environmental Toxicology*; 2012; Vol. 101; ISBN 978-3-7643-8339-8.

63. Nagajyoti, P.C.; Lee, K.D.; Sreekanth, T.V.M. Heavy metals, occurrence and toxicity for plants: A review. *Environ. Chem. Lett.* **2010**, *8*, 199–216, doi:10.1007/s10311-010-0297-8.

64. Singh, R.; Gautam, N.; Mishra, A.; Gupta, R. Heavy metals and living systems: An overview. *Indian J. Pharmacol.* **2011**, *43*, 246–253, doi:10.4103/0253-7613.81505.

65. Duffus, J.H. "Heavy metals" a meaningless term? (IUPAC Technical Report). *Pure Appl. Chem.* **2002**, *74*, 793–807, doi:10.1351/pac200274050793.

66. IUPAC International Union of Pure and Applied Chemistry *Compendium of Chemical Terminology Gold Book*; 2.3.3.; 2014; ISBN 9783527320400.

67. Rahman, Z.; Singh, V.P. The relative impact of toxic heavy metals (THMs) (arsenic (As), cadmium (Cd), chromium (Cr)(VI), mercury (Hg), and lead (Pb)) on the total environment: an overview. *Environ. Monit. Assess.* **2019**, *191*, doi:10.1007/s10661-019-7528-7.

68. Roane, T.M.; Pepper, I.L.; Gentry, T.J. Microorganisms and Metal Pollutants. In *Environmental Microbiology: Third Edition*; Elsevier Inc., 2015; pp. 415–439 ISBN 9780123946263.

69. Gadd, G.M. Metals and microorganisms: A problem of definition. *FEMS Microbiol. Lett.* **1992**, *100*, 197–203, doi:10.1016/0378-1097(92)90209-7.

70. Paul, D. Research on heavy metal pollution of river Ganga: A review. *Ann. Agrar. Sci.* **2017**, *15*, 278–286, doi:10.1016/j.aasci.2017.04.001.

71. Azimi, A.; Azari, A.; Rezakazemi, M.; Ansarpour, M. Removal of Heavy Metals from Industrial Wastewaters: A Review. *ChemBioEng Rev.* **2017**, *4*, 37–59, doi:10.1002/cben.201600010.

72. Carolin, C.F.; Kumar, P.S.; Saravanan, A.; Joshiba, G.J.; Naushad, M. Efficient techniques for the removal of toxic heavy metals from aquatic environment: A review. *J. Environ. Chem. Eng.* **2017**, *5*, 2782–2799, doi:10.1016/j.jece.2017.05.029.

73. Isa, N.M.; Aris, A.Z.; Lim, W.Y.; Sulaiman, W.N.A.W.; Praveena, S.M. Evaluation of heavy metal contamination in groundwater samples from Kapas Island, Terengganu, Malaysia. *Arab. J. Geosci.* **2014**, *7*, 1087–1100, doi:10.1007/s12517-012-0818-9.

74. Tiller, K.G. Heavy Metals in Soils and Their Environmental Significance. In *Advances in Soil Science, vol 9*; Stewart, B.A., Ed.; Springer: New York, NY, 1989; pp. 113–142 ISBN 978-1-4612-3532-3.

75. Masindi, V.; Muedi, K.L. Environmental Contamination by Heavy Metals. In *Heavy Metals*; Saleh, H.E.-D.M., Aglan, R.F., Eds.; IntechOpen, 2018; pp. 115–134 ISBN 978-1-78923-361-2.

76. Tchounwou, P.B.; Yedjou, C.G.; Patlolla, A.K.; Sutton, D.J. Heavy Metal Toxicity and the Environment. In *Molecular, Clinical and Environmental Toxicology*; Springer, Basel, 2012; pp. 133–164.

77. Rai, P.K.; Lee, S.S.; Zhang, M.; Tsang, Y.F.; Kim, K.H. Heavy metals in food crops: Health risks, fate, mechanisms, and management. *Environ. Int.* **2019**, *125*, 365–385, doi:10.1016/j.envint.2019.01.067.

78. Zwolak, A.; Sarzyńska, M.; Szpyrka, E.; Stawarczyk, K. Sources of Soil Pollution by Heavy Metals and Their Accumulation in Vegetables: a Review. *Water. Air. Soil Pollut.* **2019**, *230*, doi:10.1007/s11270-019-4221-y.

79. Bretzler, A.; Lalanne, F.; Nikiema, J.; Podgorski, J.; Pfenninger, N.; Berg, M.; Schirmer, M. Corrigendum to "Groundwater arsenic contamination in Burkina Faso, West Africa: Predicting and verifying regions at risk" [Sci. Total Environ. 584–585 (2017) 958–970]. *Sci. Total Environ.* **2017**, *598*, 562, doi:10.1016/j.scitotenv.2017.04.098.

80. Seidl, M.; Balázs, G.; Scheer, M. The Chemistry of Yellow Arsenic. *Chem. Rev.* **2019**, *119*, 8406–8434, doi:10.1021/acs.chemrev.8b00713.

81. Mudhoo, A.; Sharma, S.K.; Garg, V.K.; Tseng, C.H. Arsenic: An overview of applications, health, and environmental concerns and removal processes. *Crit. Rev. Environ. Sci. Technol.* **2011**, *41*, 435–519, doi:10.1080/10643380902945771.

82. Cobbina, J.; Cobbina, S.J.; Nkuah, D.; Tom-Dery, D.; Obiri, S. Non-cancer risk assessment from exposure to mercury (Hg), cadmium (Cd), arsenic (As), copper (Cu) and lead (Pb) in boreholes and surface water in Tinga, in the Bole-Bamboi District, Ghana. *J. Toxicol. Environ. Heal. Sci.* **2013**, *5*, 29–36, doi:10.5897/jtehs12.0253.

83. Nham, N.T.; Tahtamouni, T.M.A.; Nguyen, T.D.; Huong, P.T.; Jitae, K.; Viet, N.M.; Noi, N. Van; Phuong, N.M.; Anh, N.T.H. Synthesis of iron modified rice straw biochar toward arsenic from groundwater. *Mater. Res. Express* **2019**, *6*, doi:10.1088/2053-1591/ab4b98.

84. Zhu, N.; Qiao, J.; Ye, Y.; Yan, T. Synthesis of mesoporous bismuth-impregnated aluminum oxide for arsenic removal: Adsorption mechanism study and application to a lab-scale column. *J. Environ. Manage.* **2018**, *211*, 73–82, doi:10.1016/j.jenvman.2018.01.049.

85. World Health Organization Arsenic in drinking-water. Background document for preparation of WHO Guidelines for drinking-water quality. *World Heal. Organ.* **2011**.

86. Ratnaike, R.N. Acute and chronic arsenic toxicity. *Postgrad. Med. J.* **2003**, *79*, 391–396, doi:10.1136/pmj.79.933.391.

87. Cullen, W.R.; Reimer, K.J. Arsenic speciation in the environment. *Chem. Rev.* **1989**, *89*, 713–764, doi:10.1021/cr00094a002.

88. Bhattacharya, P.; Welch, A.H.; Stollenwerk, K.G.; McLaughlin, M.J.; Bundschuh, J.; Panaullah, G. Arsenic in the environment: Biology and Chemistry. *Sci. Total Environ.* **2007**, *379*, 109–120, doi:10.1016/j.scitotenv.2007.02.037.

89. Ahsan, H. Arsenic in Drinking-water Background document for development of WHO Guidelines for Drinking-water Quality. *Kaohsiung J. Med. Sci.* **2011**, *27*, 358–359, doi:10.1016/j.kjms.2011.05.002.

90. World Health Organization Evaluation of certain contaminants in food. *World Health Organ. Tech. Rep. Ser.* **2011**.

91. Anawar, H.M.; Akai, J.; Mostofa, K.M.G.; Safiullah, S.; Tareq, S.M. Arsenic poisoning in groundwater: Health risk and geochemical sources in Bangladesh. *Environ. Int.* **2002**, *27*, 597–604, doi:10.1016/S0160-4120(01)00116-7.

92. Ćavar, S.; Klapec, T.; Grubešić, R.J.; Valek, M. High exposure to arsenic from drinking water at several localities in eastern Croatia. *Sci. Total Environ.* **2005**, *339*, 277–282, doi:10.1016/j.scitotenv.2004.12.013.

93. Smith, A.H.; Lingas, E.O.; Rahman, M. Contamination of Drinking Water by Arsenic in Bangladesh : A Public Health Emergency . Bulletin of the World Health Organization 78 : Contamination of drinking-water by arsenic in Bangladesh : a public health emergency. *World Heal. Organ. Bull. World Heal. Organ.* **2000**, *78*, 1093, doi:10.1590/S0042-96862000000900005.

94. IARC *Arsenic, metals, fibres, and dusts*; Lyon, 2012; Vol. 100 C;

95. González, M.M.; Gallego, M.; Valcárcel, M. Determination of arsenic in wheat flour by electrothermal atomic absorption spectrometry using a continuous precipitation-dissolution flow system. *Talanta* **2001**, *55*, 135–142, doi:10.1016/S0039-9140(01)00402-7.

96. Košutić, K.; Furač, L.; Sipos, L.; Kunst, B. Removal of arsenic and pesticides from drinking water by nanofiltration membranes. *Sep. Purif. Technol.* **2005**, *42*, 137–144, doi:10.1016/j.seppur.2004.07.003.

97. Ghurye, G.L.; Clifford, D.A.; Tripp, A.R. Combined arsenic and nitrate removal by ion exchange. *J. / Am. Water Work. Assoc.* **1999**, *91*, 85–96, doi:10.1002/j.1551-8833.1999.tb08718.x.

98. Asere, T.G.; Stevens, C. V.; Du Laing, G. Use of (modified) natural adsorbents for arsenic remediation: A review. *Sci. Total Environ.* **2019**, *676*, 706–720, doi:10.1016/j.scitotenv.2019.04.237.

99. Macur, R.E.; Jackson, C.R.; Botero, L.M.; McDermott, T.R.; Inskeep, W.P. Bacterial Populations Associated with the Oxidation and Reduction of Arsenic in an Unsaturated Soil. *Environ. Sci. Technol.* **2004**, *38*, 104–111, doi:10.1021/es034455a.

100. Longhinotti, E.; Pozza, F.; Furlan, L.; Sanchez, M. de N. de M.; Klug, M.; Laranjeira, M.C.M.; Fávere, V.T. Adsorption of Anionic Dyes on the Biopolymer Chitin. *J. Braz. Chem. Soc.* **1998**, *9*, 435–440, doi:10.1590/S0103-50531998000500005.

101. Kuroda, K.; Fukushi, T. Groundwater Contamination in Urban Areas. In *Groundwater Management in Asian Cities: Technology and Policy for Sustainability*; Takizawa, S., Ed.; Springer Japan: tokio, 2009; pp. 125–149.

102. Ok, Y.S.; Usman, A.R.A.; Lee, S.S.; Abd El-Azeem, S.A.M.; Choi, B.; Hashimoto, Y.; Yang, J.E. Effects of rapeseed residue on lead and cadmium availability and uptake by rice plants in heavy metal contaminated paddy soil. *Chemosphere* **2011**, *85*, 677–682, doi:10.1016/j.chemosphere.2011.06.073.

103. Wani, A.L.; Ara, A.; Usmani, J.A. Lead toxicity: a review. *Interdiscip. Toxicol.* **2015**, *8*, 55–64, doi:10.1515/intox-2015-0009.

104. Flora, G.; Gupta, D.; Tiwari, A. Toxicity of lead: A review with recent updates. *Interdiscip. Toxicol.* **2012**, *5*, 47–58, doi:10.2478/v10102-012-0009-2.

105. Abadin, H.; Ashizawa, A.; Stevens, Y.-W.; Llados, F.; Diamond, G.; Sage, G.; Citra, M.; Quinones, A.; Bosch, S.J.; Swarts, S.G. Toxicological Profile for Lead. *U.S Public Heal. Serv. Agency Toxic Subst. Dis. Regist.* **2007**, 582.

106. ATSDR *Toxicological Profile for Lead (Draft for Public Comment)*; Atlanta, Georgia, 2019;

107. Tchounwou, P.B.; Yedjou, C.G.; Patlolla, A.K.; Sutton, D.J. Heavy Metals Toxicity and the Environment. **2012**, *101*, 1–30, doi:10.1007/978-3-7643-8340-4.

108. Goldman, J.G.; Goetz, C.G. *Handbook on the Toxicology of Metals*; Nordberg, G., Fowler, B., Nordberg, M., Eds.; Fourth.; 2012; ISBN 9781439807156.

109. Payne, M. Lead in drinking water. *Can. Med. Assoc. J.* **2008**, *179*, 253–254, doi:10.1503/cmaj.071483.

110. Fu, F.; Wang, Q. Removal of heavy metal ions from wastewaters: A review. *J. Environ. Manage.* **2011**, *92*, 407–418, doi:10.1016/j.jenvman.2010.11.011.

111. Yeh, T.Y.; Chou, C.C.; Pan, C.T. Heavy metal removal within pilot-scale constructed wetlands receiving river water contaminated by confined swine operations. *Desalination* **2009**, *249*, 368–373, doi:10.1016/j.desal.2008.11.025.

112. Tatti, F.; Petrangeli Papini, M.; Torretta, V.; Mancini, G.; Boni, M.R.; Viotti, P. Experimental and numerical evaluation of Groundwater Circulation Wells as a remediation technology for persistent, low permeability contaminant source zones. *J. Contam. Hydrol.* **2019**, *222*, 89–100, doi:10.1016/j.jconhyd.2019.03.001.

113. Tatti, F.; Papini, M.P.; Sappa, G.; Raboni, M.; Arjmand, F.; Viotti, P. Contaminant back-diffusion from low-permeability layers as affected by groundwater velocity: A laboratory investigation by box model and image analysis. *Sci. Total Environ.* **2018**, *622–623*, 164–171, doi:10.1016/j.scitotenv.2017.11.347.

114. Wuana, R.A.; Okieimen, F.E. Heavy Metals in Contaminated Soils: A Review of Sources, Chemistry, Risks and Best Available Strategies for Remediation. *ISRN Ecol.* **2011**, *2011*, 1–20, doi:10.5402/2011/402647.

115. Antonucci, A.; Viotti, P.; Luciano, A.; Mancini, G. A numerical model of the soil flushing remediation in heavy metal contaminated soil. *Chem. Eng. Trans.* **2013**, *32*, 469–474, doi:10.3303/cet1332079.

116. Martorelli, E.; Antonucci, A.; Luciano, A.; Rossi, E.; Raboni, M.; Mancini, G.; Viotti, P. EDTA Chelating Process for Lead Removal: Evaluation of Approaches by Means of a Reactive Transport Model. *Water. Air. Soil Pollut.* **2015**, *226*, doi:10.1007/s11270-015-2377-7.

117. Ali, A.; Sarvajeet, A.; Gill, S.; Gill, R.; Lanza, G.R. *Phytoremediation*; Ansari, A.A., Gill, S.S., Gill, R., Lanza, G., Newman, L., Eds.; 1st ed.; Springer International Publishing, 2016; ISBN 9783319401461.

118. Xu, J.; Liu, C.; Hsu, P.C.; Zhao, J.; Wu, T.; Tang, J.; Liu, K.; Cui, Y. Remediation of heavy metal contaminated soil by asymmetrical alternating current electrochemistry. *Nat. Commun.* **2019**, *10*, 1–8, doi:10.1038/s41467-019-10472-x.

119. Mahar, A.; Wang, P.; Li, R.; Zhang, Z. Immobilization of Lead and Cadmium in Contaminated Soil Using Amendments: A Review. *Pedosphere* **2015**, *25*, 555–568, doi:10.1016/S1002-0160(15)30036-9.

120. Park, J.H.; Lamb, D.; Paneerselvam, P.; Choppala, G.; Bolan, N.; Chung, J.W. Role of organic amendments on enhanced bioremediation of heavy metal(loid) contaminated soils. *J. Hazard. Mater.* **2011**, *185*, 549–574, doi:10.1016/j.jhazmat.2010.09.082.

121. Hua, M.; Zhang, S.; Pan, B.; Zhang, W.; Lv, L.; Zhang, Q. Heavy metal removal from water/wastewater by nanosized metal oxides: A review. *J. Hazard. Mater.* **2012**, *211–212*, 317–331, doi:10.1016/j.jhazmat.2011.10.016.

122. Bokobza, L.; Bruneel, J.-L.; Couzi, M. Raman Spectra of Carbon-Based Materials (from Graphite to Carbon Black) and of Some Silicone Composites. *C* **2015**, *1*, 77–94, doi:10.3390/c1010077.

123. Fedoseeva, Y.V.; Gorodetskiy, D.V.; Baskakova, K.I.; Asanov, I.P.; Bulusheva, L.G.; Makarova, A.A.; Yudin, I.B.; Plotnikov, M.Y.; Emelyanov, A.A.; Rebrov, A.K.; Okotrub, A.V. Structure of Diamond Films Grown Using High-Speed Flow of a Thermally Activated CH4-H2 Gas Mixture. *Materials (Basel).* **2020**, *13*, 219, doi:10.3390/ma13010219.

124. Sweetman, M.; May, S.; Mebberson, N.; Pendleton, P.; Vasilev, K.; Plush, S.; Hayball, J. Activated Carbon, Carbon Nanotubes and Graphene: Materials and Composites for Advanced Water Purification. *C* **2017**, *3*, 18, doi:10.3390/c3020018.

125. Ma, X.; Yang, H.; Yu, L.; Chen, Y.; Li, Y. Preparation, Surface and Pore Structure of High Surface Area Activated Carbon Fibers from Bamboo by Steam Activation. *Materials (Basel).* **2014**, *7*, 4431–4441, doi:10.3390/ma7064431.

126. Liu, X.Y.; Huang, M.; Ma, H.L.; Zhang, Z.Q.; Gao, J.M.; Zhu, Y.L.; Han, X.J.; Guo, X.Y. Preparation of a carbon-based solid acid catalyst by sulfonating activated carbon in a chemical reduction process. *Molecules* **2010**, *15*, 7188–7196, doi:10.3390/molecules15107188.

127. Park, J.; Lee, G.; Hwang, S.; Kim, J.; Hong, B.; Kim, H.; Kim, S. The Effects of Methane Storage Capacity Using Upgraded Activated Carbon by KOH. *Appl. Sci.* **2018**, *8*, 1596, doi:10.3390/app8091596.

128. Chiang, Y.-C.; Yeh, C.-Y.; Weng, C.-H. Carbon Dioxide Adsorption on Porous and Functionalized Activated Carbon Fibers. *Appl. Sci.* **2019**, *9*, 1977, doi:10.3390/app9101977.

129. Liu, Y.; Liu, X.; Zhang, G.; Ma, T.; Du, T.; Yang, Y.; Lu, S.; Wang, W. Adsorptive removal of sulfamethazine and sulfamethoxazole from aqueous solution by hexadecyl trimethyl ammonium bromide modified activated carbon. *Colloids Surfaces A Physicochem. Eng. Asp.* **2019**, *564*, 131–141, doi:10.1016/j.colsurfa.2018.12.041.

130. Gupta, V.K.; Suhas Application of low-cost adsorbents for dye removal - A review. *J. Environ. Manage.* **2009**, *90*, 2313–2342, doi:10.1016/j.jenvman.2008.11.017.

131. Baresel, C.; Harding, M.; Fang, J. Ultrafiltration/granulated active carbon-biofilter: Efficient removal of a broad range of micropollutants. *Appl. Sci.* **2019**, *9*, doi:10.3390/app9040710.

132. Liu, X.; Ao, H.; Xiong, X.; Xiao, J.; Liu, J. Arsenic removal from water by iron-modified bamboo charcoal. *Water. Air. Soil Pollut.* **2012**, *223*, 1033–1044, doi:10.1007/s11270-011-0921-7.

133. Lehmann, J. *Terra Preta Nova – Where to from Here?*; Woods, W.I., Teixeira, W.G., Lehmann, J., Steiner, C., WinklerPrins, A., Rebellato, L., Eds.; Springer Science + Business Media, 2009; ISBN 9781402090301.

134. Lehmann, J.; Joseph, S. Biochar for environmental management: An introduction. In *Biochar for environmental management. Science and technology*; Sterling, VA: London, 2009; Vol. 1, pp. 1–12 ISBN 9781844076581.

135. Glaser, B.; Lehmann, J.; Zech, W. Ameliorating physical and chemical properties of highly weathered soils in the tropics with charcoal - A review. *Biol. Fertil. Soils* **2002**, *35*, 219–230, doi:10.1007/s00374-002-0466-4.

136. *Agricultural and Environmental Applications of Biochar: Advances and Barriers, SSSA Special Publication 63*; Guo, M., He, Z., Uchimiya, S.M., Eds.; 1st ed.; Soil Science Society of America: Madison, USA, 2016; ISBN 978-0-89118-967-1.

137. Chen, W.; Meng, J.; Han, X.; Lan, Y.; Zhang, W. Past, present, and future of biochar. *Biochar* **2019**, *1*, 75–87, doi:10.1007/s42773-019-00008-3.

138. Shackley, S.; Carter, S.; Knowles, T.; Middelink, E.; Haefele, S.; Sohi, S.; Cross, A.; Haszeldine, S. Sustainable gasification-biochar systems? A case-study of rice-husk gasification in Cambodia, Part I:

Context, chemical properties, environmental and health and safety issues. *Energy Policy* **2012**, *42*, 49–58, doi:10.1016/j.enpol.2011.11.026.

139. Verheijen, F.; Jeffery, S.; Bastos, a C.; Van Der Velde, M.; Diafas, I. *Biochar application to soils: a critical review of effects on soil properties, processes and functions*; 2010; ISBN 9789279142932.

140. IBI, I.B.I. Standardized Product Definition and Product Testing Guidelines for Biochar That Is Used in Soil. *Int. Biochar Initiat.* **2015**, 23.

141. Hagemann, N.; Spokas, K.; Schmidt, H.-P.; Kägi, R.; Böhler, M.; Bucheli, T. Activated Carbon, Biochar and Charcoal: Linkages and Synergies across Pyrogenic Carbon's ABCs. *Water* **2018**, *10*, 182, doi:10.3390/w10020182.

142. Agegnehu, G.; Srivastava, A.K.; Bird, M.I. The role of biochar and biochar-compost in improving soil quality and crop performance: A review. *Appl. Soil Ecol.* **2017**, *119*, 156–170, doi:10.1016/j.apsoil.2017.06.008.

143. Jien, S.H.; Chen, W.C.; Ok, Y.S.; Awad, Y.M.; Liao, C. Sen Short-term biochar application induced variations in C and N mineralization in a compost-amended tropical soil. *Environ. Sci. Pollut. Res.* **2017**, 1–11, doi:10.1007/s11356-017-9234-8.

144. Luo, S.; Wang, S.; Tian, L.; Li, S.; Li, X.; Shen, Y.; Tian, C. Long-term biochar application influences soil microbial community and its potential roles in semiarid farmland. *Appl. Soil Ecol.* **2017**, *117–118*, 10–15, doi:10.1016/j.apsoil.2017.04.024.

145. Suliman, W.; Harsh, J.B.; Abu-Lail, N.I.; Fortuna, A.M.; Dallmeyer, I.; Garcia-Pérez, M.; Garcia-Perez, M. The role of biochar porosity and surface functionality in augmenting hydrologic properties of a sandy soil. *Sci. Total Environ.* **2017**, *574*, 139–147, doi:10.1016/j.scitotenv.2016.09.025.

146. Hagemann, N.; Joseph, S.; Schmidt, H.-P.; Kammann, C.I.; Harter, J.; Borch, T.; Young, R.B.; Varga, K.; Taherymoosavi, S.; Elliott, K.W.; McKenna, A.; Albu, M.; Mayrhofer, C.; Obst, M.; Conte, P.; Dieguez-Alonso, A.; Orsetti, S.; Subdiaga, E.; Behrens, S.; Kappler, A. Organic coating on biochar explains its nutrient retention and stimulation of soil fertility. *Nat. Commun.* **2017**, *8*, 1–11, doi:10.1038/s41467-017-01123-0.

147. Burrell, L.D.; Zehetner, F.; Rampazzo, N.; Wimmer, B.; Soja, G. Long-term effects of biochar on soil physical properties. *Geoderma* **2016**, *282*, 96–102, doi:10.1016/j.geoderma.2016.07.019.

148. Blanco-Canqui, H. Biochar and Soil Physical Properties. *Soil Sci. Soc. Am. J.* **2017**, *84*, 687–711, doi:10.2136/sssaj2017.01.0017.

149. Ding, Y.; Liu, Y.; Liu, S.; Li, Z.; Tan, X.; Huang, X.; Zeng, G.; Zhou, L.; Zheng, B. Biochar to improve soil fertility. A review. *Agron. Sustain. Dev.* **2016**, *36*, 1–18, doi:10.1007/s13593-016-0372-z.

150. Ippolito, J.A.; Laird, D.A.; Busscher, W.J. Environmental Benefits of Biochar. *J. Environ. Qual.* **2012**, *41*, 967–972, doi:10.2134/jeq2012.0151.

151. Zong, Y.; Wang, Y.; Sheng, Y.; Wu, C.; Lu, S. Ameliorating soil acidity and physical properties of two contrasting texture Ultisols with wastewater sludge biochar. *Environ. Sci. Pollut. Res.* **2017**, 1–8, doi:10.1007/s11356-017-9509-0.

152. Lomaglio, T.; Hattab-Hambli, N.; Miard, F.; Lebrun, M.; Nandillon, R.; Trupiano, D.; Scippa, G.S.; Gauthier, A.; Motelica-Heino, M.; Bourgerie, S.; Morabito, D. Cd, Pb, and Zn mobility and (bio)availability in contaminated soils from a former smelting site amended with biochar. *Environ. Sci. Pollut. Res.* **2018**, *25*, 25744–25756, doi:10.1007/s11356-017-9521-4.

153. Haider, G.; Steffens, D.; Moser, G.; Müller, C.; Kammann, C.I. Biochar reduced nitrate leaching and improved soil moisture content without yield improvements in a four-year field study. *Agriculture, Ecosyst. Environ.* **2017**, *237*, 80–94, doi:10.1016/j.agee.2016.12.019.

154. Yin, D.; Wang, X.; Chen, C.; Peng, B.; Tan, C.; Li, H. Varying effect of biochar on Cd, Pb and As mobility in a multi-metal contaminated paddy soil. *Chemosphere* **2016**, *152*, 196–206, doi:10.1016/j.chemosphere.2016.01.044.

155. Puga, A.P.; Abreu, C.A.; Melo, L.C.A.; Beesley, L. Biochar application to a contaminated soil reduces the availability and plant uptake of zinc, lead and cadmium. *J. Environ. Manage.* **2015**, *159*, 86–93, doi:10.1016/j.jenvman.2015.05.036.

156. Tang, J.; Zhu, W.; Kookana, R.; Katayama, A. Characteristics of biochar and its application in remediation of contaminated soil. *J. Biosci. Bioeng.* **2013**, *116*, 653–659, doi:10.1016/j.jbiosc.2013.05.035.

157. Rosales, E.; Meijide, J.; Pazos, M.; Sanromán, M.A. Challenges and recent advances in biochar as low-cost biosorbent: From batch assays to continuous-flow systems. *Bioresour. Technol.* **2017**, *246*, 176–192, doi:10.1016/j.biortech.2017.06.084.

158. Uchimiya, M.; Lima, I.M.; Thomas Klasson, K.; Chang, S.; Wartelle, L.H.; Rodgers, J.E. Immobilization of heavy metal ions (CuII, CdII, NiII, and PbII) by broiler litter-derived biochars in water and soil. *J. Agric. Food Chem.* **2010**, *58*, 5538–5544, doi:10.1021/jf9044217.

159. Uchimiya, M.; Klasson, K.T.; Wartelle, L.H.; Lima, I.M. Influence of soil properties on heavy metal sequestration by biochar amendment: 1. Copper sorption isotherms and the release of cations. *Chemosphere* **2011**, *82*, 1431–1437, doi:10.1016/j.chemosphere.2010.11.050.

160. Beesley, L.; Marmiroli, M. The immobilisation and retention of soluble arsenic, cadmium and zinc by biochar. *Environ. Pollut.* **2011**, *159*, 474–480, doi:10.1016/j.envpol.2010.10.016.

161. Beesley, L.; Moreno-Jiménez, E.; Gomez-Eyles, J.L. Effects of biochar and greenwaste compost amendments on mobility, bioavailability and toxicity of inorganic and organic contaminants in a multi-element polluted soil. *Environ. Pollut.* **2010**, *158*, 2282–2287, doi:10.1016/j.envpol.2010.02.003.

162. He, Y.; Zhou, X.; Jiang, L.; Li, M.; Du, Z.; Zhou, G.; Shao, J.; Wang, X.; Xu, Z.; Hosseini Bai, S.; Wallace, H.; Xu, C. Effects of biochar application on soil greenhouse gas fluxes: a meta-analysis. *GCB Bioenergy* **2017**, *9*, 743–755, doi:10.1111/gcbb.12376.

163. Fidel, R.; Laird, D.; Parkin, T. Effect of Biochar on Soil Greenhouse Gas Emissions at the Laboratory and Field Scales. *Soil Syst.* **2019**, *3*, 8, doi:10.3390/soilsystems3010008.

164. Jeffery, S.; Verheijen, F.G.A.; van der Velde, M.; Bastos, A.C. A quantitative review of the effects of biochar application to soils on crop productivity using meta-analysis. *Agriculture, Ecosyst. Environ.* **2011**, *144*, 175–187, doi:10.1016/j.agee.2011.08.015.

165. *Biochar for Environmental Management - Science and Technology*; Lehmann, J., Joseph, S., Eds.; 2009; ISBN 978-1-84407-658-1.

166. Bridgwater, A. V.; Peacocke, G.V.C. Fast pyrolysis processes for biomass. *Renew. Sustain. energy Rev.* **2000**, *4*, 1–73, doi:10.1016/S1364-0321(99)00007-6.

167. Ahmad, M.; Lee, S.S.; Dou, X.; Mohan, D.; Sung, J.-K.K.; Yang, J.E.; Ok, Y.S. Effects of pyrolysis temperature on soybean stover- and peanut shell-derived biochar properties and TCE adsorption in water. *Bioresour. Technol.* **2012**, *118*, 536–544, doi:10.1016/j.biortech.2012.05.042.

168. Suliman, W.; Harsh, J.B.; Abu-Lail, N.I.; Fortuna, A.M.; Dallmeyer, I.; Garcia-Perez, M. Influence of feedstock source and pyrolysis temperature on biochar bulk and surface properties. *Biomass and Bioenergy* **2016**, *84*, 37–48, doi:10.1016/j.biombioe.2015.11.010.

169. Singh, B.; Singh, B.P.; Cowie, A.L. Characterisation and evaluation of biochars for their application as a soil amendment. *Soil Res.* **2010**, *48*, 516, doi:10.1071/SR10058.

170. Sohi, S.; Lopez-capel, E.; Krull, E.; Bol, R. Biochar , climate change and soil : A review to guide future research. *Civ. Eng.* **2009**, *6618*, 64, doi:10.1139/Z03-132.

171. Budai, A.; Wang, L.; Gronli, M.; Strand, L.T.; Antal, M.J.; Abiven, S.; Dieguez-Alonso, A.; Anca-Couce, A.; Rasse, D.P. Surface Properties and Chemical Composition of Corncob and Miscanthus Biochars: Effects of Production Temperature and Method. *J. Agric. Food Chem.* **2014**, *62*, 3791–3799, doi:10.1021/jf501139f.

172. Zhao, B.; O'Connor, D.; Zhang, J.; Peng, T.; Shen, Z.; Tsang, D.C.W.W.; Hou, D.; Connor, D.O.; Zhang, J.; Peng, T.; Shen, Z.; Tsang, D.C.W.W.; Hou, D. Effect of pyrolysis temperature, heating rate, and residence time on rapeseed stem derived biochar. *J. Clean. Prod.* **2018**, *174*, 977–987, doi:10.1016/j.jclepro.2017.11.013.

173. Kong, H.; He, J.; Gao, Y.; Wu, H.; Zhu, X. Cosorption of phenanthrene and mercury(II) from aqueous solution by soybean stalk-based biochar. *J. Agric. Food Chem.* **2011**, *59*, 12116–12123, doi:10.1021/jf202924a.

174. Uchimiya, M.; Ohno, T.; He, Z. Pyrolysis temperature-dependent release of dissolved organic carbon from plant, manure, and biorefinery wastes. *J. Anal. Appl. Pyrolysis* **2013**, *104*, 84–94, doi:10.1016/j.jaap.2013.09.003.

175. Ronsse, F.; van Hecke, S.; Dickinson, D.; Prins, W. Production and characterization of slow pyrolysis biochar: Influence of feedstock type and pyrolysis conditions. *GCB Bioenergy* **2013**, *5*, 104–115, doi:10.1111/gcbb.12018.

176. Enders, A.; Hanley, K.; Whitman, T.; Joseph, S.; Lehmann, J. Characterization of biochars to evaluate recalcitrance and agronomic performance. *Bioresour. Technol.* **2012**, *114*, 644–653, doi:10.1016/j.biortech.2012.03.022.

177. Nanda, S.; Dalai, A.K.; Berruti, F.; Kozinski, J.A. Biochar as an Exceptional Bioresource for Energy, Agronomy, Carbon Sequestration, Activated Carbon and Specialty Materials. *Waste and Biomass Valorization* **2016**, *7*, 201–235, doi:10.1007/s12649-015-9459-z.

178. Brewer, C.E.; Brown, R.C.; Laird, D.A. Biochar characterization and engineering, 2012.

179. Crombie, K.; Mašek, O.; Sohi, S.P.; Brownsort, P.; Cross, A.; Sohi, S.P.; Cross, A.; Crombie, K.; Mašek, O.; Sohi, S.P.; Brownsort, P.; Cross, A. The effect of pyrolysis conditions on biochar stability as determined by three methods. *GCB Bioenergy* **2012**, *5*, 122–131, doi:10.1111/gcbb.12030.

180. Chen, T.; Liu, R.; Scott, N.R. Characterization of energy carriers obtained from the pyrolysis of white ash, switchgrass and corn stover - Biochar, syngas and bio-oil. *Fuel Process. Technol.* **2016**, *142*, 124–134, doi:10.1016/j.fuproc.2015.09.034.

181. Mohamad Aziz, N.S.; Shariff, A.; Abdullah, N.; Mohamed Noor, N. Characteristics of coconut frond as a potential feedstock for biochar via slow pyrolysis. *Malaysian J. Fundam. Appl. Sci.* **2018**, *14*, 408–413, doi:10.11113/mjfas.v14n4.1014.

182. Fryda, L.; Visser, R. Biochar for Soil Improvement: Evaluation of Biochar from Gasification and Slow Pyrolysis. *Agriculture* **2015**, *5*, 1076–1115, doi:10.3390/agriculture5041076.

183. Sun, Y.; Gao, B.; Yao, Y.; Fang, J.; Zhang, M.; Zhou, Y.; Chen, H.; Yang, L. Effects of feedstock type, production method, and pyrolysis temperature on biochar and hydrochar properties. *Chem. Eng. J.* **2014**, *240*, 574–578, doi:10.1016/j.cej.2013.10.081.

184. Windeatt, J.H.; Ross, A.B.; Williams, P.T.; Forster, P.M.; Nahil, M.A.; Singh, S. Characteristics of biochars from crop residues: Potential for carbon sequestration and soil amendment. *J. Environ. Manage.* **2014**, *146*, 189–197, doi:10.1016/j.jenvman.2014.08.003.

185. Gul, S.; Whalen, J.K.; Thomas, B.W.; Sachdeva, V.; Deng, H. Physico-chemical properties and microbial responses in biochar-amended soils: Mechanisms and future directions. *Agriculture, Ecosyst. Environ.* **2015**, *206*, 46–59, doi:10.1016/j.agee.2015.03.015.

186. Vassilev, S. V.; Baxter, D.; Andersen, L.K.; Vassileva, C.G. An overview of the composition and application of biomass ash. Part 1. Phase-mineral and chemical composition and classification. *Fuel* **2013**, *105*, 40–76, doi:10.1016/j.fuel.2012.09.041.

187. Keiluweit, M.; Nico, P.S.; Johnson, M.G.; Kleber, M. Dynamic Molecular Structure of Plant Biomass-Derived Black Carbon (Biochar). *Environ. Sci. Technol.* **2010**, *44*, 1247–1253, doi:10.1021/es9031419.

188. Spokas, K.A. Review of the stability of biochar in soils: Predictability of O:C molar ratios. *Carbon Manag.* **2010**, *1*, 289–303, doi:10.4155/cmt.10.32.

189. Lian, F.; Huang, F.; Chen, W.; Xing, B.; Zhu, L. Sorption of apolar and polar organic contaminants by waste tire rubber and its chars in single- and bi-solute systems. *Environ. Pollut.* **2011**, *159*, 850–857, doi:10.1016/j.envpol.2011.01.002.

190. Xie, T.; Sadasivam, B.Y.; Reddy, K.R.; Wang, C.; Spokas, K. Review of the effects of biochar amendment on soil properties and carbon sequestration. *J. Hazardous, Toxic, Radioact. Waste* **2016**, *20*, doi:10.1061/(ASCE)HZ.2153-5515.0000293.

191. Shinogi, Y.; Kanri, Y. Pyrolysis of plant, animal and human waste: Physical and chemical characterization of the pyrolytic products. *Bioresour. Technol.* **2003**, *90*, 241–247, doi:10.1016/S0960-8524(03)00147-0.

192. Moreno-Castilla, C. Adsorption of organic molecules from aqueous solutions on carbon materials. *Carbon N. Y.* **2004**, *42*, 83–94, doi:10.1016/j.carbon.2003.09.022.

193. Kinney, T.J.; Masiello, C.A.; Dugan, B.; Hockaday, W.C.; Dean, M.R.; Zygourakis, K.; Barnes, R.T. Hydrologic properties of biochars produced at different temperatures. *Biomass and Bioenergy* **2012**, *41*, 34–43, doi:10.1016/j.biombioe.2012.01.033.

194. Basu, P. *Biomass Gasification, Pyrolysis and Torrefaction: Practical Design and Theory*; 2013; ISBN 9780123964885.

195. Antal, M.J.; Allen, S.G.; Dai, X.; Shimizu, B.; Tam, M.S.; Grønli, M. Attainment of the theoretical yield of carbon from biomass. *Ind. Eng. Chem. Res.* **2000**, *39*, 4024–4031, doi:10.1021/ie000511u.

196. Angin, D. Effect of pyrolysis temperature and heating rate on biochar obtained from pyrolysis of safflower seed press cake. *Bioresour. Technol.* **2013**, *128*, 593–597, doi:10.1016/j.biortech.2012.10.150.

197. Lua, A.C.; Guo, J. Preparation and characterization of chars from oil palm waste. *Carbon N. Y.* **1998**, *36*, 1663–1670, doi:10.1016/S0008-6223(98)00161-4.

198. Wang, Y.; Hu, Y.; Zhao, X.; Wang, S.; Xing, G. Comparisons of biochar properties from wood material and crop residues at different temperatures and residence times. *Energy and Fuels* **2013**, *27*, 5890–5899, doi:10.1021/ef400972z.

199. Lawrinenko, M.; Laird, D.A. Anion exchange capacity of biochar. *Green Chem.* **2015**, *17*, 4628–4636, doi:10.1039/c5gc00828j.

200. Cox, J.; Downie, A.; Hickey, M.; Jenkins, A.; Lines-Kelly, R.; McClintock, A.; Van Zwieten, L. *Biochar in horticulture: Prospects for the use of biochar in Australian horticulture*; Cox, J., Ed.; NSW Trade and Investment, 2012; ISBN 978 1 74256 349 7.

201. Lu, K.; Yang, X.; Shen, J.; Robinson, B.; Huang, H.; Liu, D.; Bolan, N.; Pei, J.; Wang, H. Effect of bamboo and rice straw biochars on the bioavailability of Cd, Cu, Pb and Zn to Sedum plumbizincicola. *Agriculture, Ecosyst. Environ.* **2014**, *191*, 124–132, doi:10.1016/j.agee.2014.04.010.

202. Meyer, S.; Glaser, B.; Quicker, P. Technical, economical, and climate-related aspects of biochar production technologies: A literature review. *Environ. Sci. Technol.* **2011**, *45*, 9473–9483, doi:10.1021/es201792c.

203. Zhang, J.; Zhang, J.; Wang, M.; Wu, S.; Wang, H.; Niazi, N.K.; Man, Y.B.; Christie, P.; Shan, S.; Wong,

M.H. Effect of tobacco stem-derived biochar on soil metal immobilization and the cultivation of tobacco plant. *J. Soils Sediments* **2019**, *19*, 2313–2321, doi:10.1007/s11368-018-02226-x.

204. Zhang, Z.; Zhu, Z.; Shen, B.; Liu, L. Insights into biochar and hydrochar production and applications: A review. *Energy* **2019**, *171*, 581–598, doi:10.1016/j.energy.2019.01.035.

205. Xie, T.; Reddy, K.R.; Wang, C.; Yargicoglu, E.; Spokas, K. Characteristics and applications of biochar for environmental remediation: A review. *Crit. Rev. Environ. Sci. Technol.* **2015**, *45*, 939–969, doi:10.1080/10643389.2014.924180.

206. Braghiroli, F.L.; Bouafif, H.; Neculita, C.M.; Koubaa, A. Influence of Pyro-Gasification and Activation Conditions on the Porosity of Activated Biochars: A Literature Review. *Waste and Biomass Valorization* **2019**, doi:10.1007/s12649-019-00797-5.

207. Duku, M.H.; Gu, S.; Hagan, E. Ben Biochar production potential in Ghana - A review. *Renew. Sustain. Energy Rev.* **2011**, *15*, 3539–3551, doi:10.1016/j.rser.2011.05.010.

208. Libra, J.A.; Ro, K.S.; Kammann, C.; Funke, A.; Berge, N.D.; Neubauer, Y.; Titirici, M.M.; Fühner, C.; Bens, O.; Kern, J.; Emmerich, K.H. Hydrothermal carbonization of biomass residuals: A comparative review of the chemistry, processes and applications of wet and dry pyrolysis. *Biofuels* **2011**, *2*, 71–106, doi:10.4155/bfs.10.81.

209. Bridgwater, A. V. Review of fast pyrolysis of biomass and product upgrading. *Biomass and Bioenergy* **2012**, *38*, 68–94, doi:10.1016/j.biombioe.2011.01.048.

210. Funke, A.; Ziegler, F. Hydrothermal carbonization of biomass: A summary and discussion of chemical mechanisms for process engineering. *Biofuels, Bioprod. Biorefining* **2010**, *4*, 160–177, doi:10.1002/bbb.198.

211. Bridgwater, A. V. The production of biofuels and renewable chemicals by fast pyrolysis of biomass. *Int. J. Glob. Energy Issues* **2007**, *27*, 160–203, doi:10.1504/IJGEI.2007.013654.

212. Yan, W.; Acharjee, T.C.; Coronella, C.J.; Vásquez, V.R. Thermal pretreatment of lignocellulosic biomass. *Environ. Prog. Sustain. Energy* **2009**, *28*, 435–440, doi:10.1002/ep.10385.

213. Shankar Tumuluru, J.; Sokhansanj, S.; Hess, J.R.; Wright, C.T.; Boardman, R.D. REVIEW: A review on biomass torrefaction process and product properties for energy applications. *Ind. Biotechnol.* **2011**, *7*, 384–401, doi:10.1089/ind.2011.7.384.

214. Demirbaş, A. Carbonization ranking of selected biomass for charcoal, liquid and gaseous products. *Energy Convers. Manag.* **2001**, *42*, 1229–1238, doi:10.1016/S0196-8904(00)00110-2.

215. Kloss, S.; Zehetner, F.; Dellantonio, A.; Hamid, R.; Ottner, F.; Liedtke, V.; Schwanninger, M.; Gerzabek, M.H.; Soja, G. Characterization of Slow Pyrolysis Biochars: Effects of Feedstocks and Pyrolysis Temperature on Biochar Properties. *J. Environ. Qual.* **2012**, *41*, 990–1000, doi:10.2134/jeq2011.0070.

216. Bridgwater, A.V.; Meier, D.; Radlein, D. An overview of fast pyrolysis of biomass. *Org. Geochem.* **1999**, *30*, 1479–1493, doi:10.1016/S0146-6380(99)00120-5.

217. Shafaghat, H.; Rezaei, P.S.; Daud, W.M.A.W. Catalytic hydrodeoxygenation of simulated phenolic bio-oil to cycloalkanes and aromatic hydrocarbons over bifunctional metal/acid catalysts of Ni/HBeta, Fe/HBeta and NiFe/HBeta. *J. Ind. Eng. Chem.* **2016**, *35*, 268–276, doi:10.1016/j.jiec.2016.01.001.

218. Heidari, A.; Stahl, R.; Younesi, H.; Rashidi, A.; Troeger, N.; Ghoreyshi, A.A. Effect of process conditions on product yield and composition of fast pyrolysis of Eucalyptus grandis in fluidized bed reactor. *J. Ind. Eng. Chem.* **2014**, *20*, 2594–2602, doi:10.1016/j.jiec.2013.10.046.

219. Lee, E.H.; Park, R. su; Kim, H.; Park, S.H.; Jung, S.C.; Jeon, J.K.; Kim, S.C.; Park, Y.K. Hydrodeoxygenation of guaiacol over Pt loaded zeolitic materials. *J. Ind. Eng. Chem.* **2016**, *37*, 18–21, doi:10.1016/j.jiec.2016.03.019.

220. Liu, X.; Li, Z.; Zhang, Y.; Feng, R.; Mahmood, I.B. Characterization of human manure-derived biochar

and energy-balance analysis of slow pyrolysis process. *Waste Manag.* **2014**, *34*, 1619–1626, doi:10.1016/j.wasman.2014.05.027.

221. Gell, K.; van Groenigen, J.W.; Cayuela, M.L. Residues of bioenergy production chains as soil amendments: Immediate and temporal phytotoxicity. *J. Hazard. Mater.* **2011**, *186*, 2017–2025, doi:10.1016/j.jhazmat.2010.12.105.

222. *Biochar for Environmental Management - Science, Technology and Implementation Second Edition*; Lehmann, J., Joseph, S., Eds.; 2015; ISBN 9780415704151.

223. Bridgwater, T. Biomass Pyrolysis. *IEA Bioenergy T34200701* **2007**, 1–20.

224. Shabangu, S.; Woolf, D.; Fisher, E.M.; Angenent, L.T.; Lehmann, J. Techno-economic assessment of biomass slow pyrolysis into different biochar and methanol concepts. *Fuel* **2014**, *117*, 742–748, doi:10.1016/j.fuel.2013.08.053.

225. Mohan, D.; Pittman, C.U.; Steele, P.H. Pyrolysis of Wood/Biomass for Bio-oil: A Critical Review. *Energy & Fuels* **2006**, *20*, 848–889, doi:10.1021/ef0502397.

226. J. W. Gaskin; C. Steiner; K. Harris; K. C. Das; B. Bibens Effect of Low-Temperature Pyrolysis Conditions on Biochar for Agricultural Use. *Trans. ASABE* **2008**, *51*, 2061–2069, doi:10.13031/2013.25409.

227. Bridgwater, A. V. Principles and practice of biomass fast pyrolysis processes for liquids. *J. Anal. Appl. Pyrolysis* **1999**, *51*, 3–22, doi:10.1016/S0165-2370(99)00005-4.

228. Luo, Z.; Wang, S.; Cen, K. A model of wood flash pyrolysis in fluidized bed reactor. *Renew. Energy* **2005**, *30*, 377–392, doi:10.1016/j.renene.2004.03.019.

229. Lima, I.M.; Boateng, A.A.; Klasson, K.T. Physicochemical and adsorptive properties of fast-pyrolysis bio-chars and their steam activated counterparts. *J. Chem. Technol. Biotechnol.* **2010**, *85*, 1515–1521, doi:10.1002/jctb.2461.

230. Russell, S.H.; Turrion-Gomez, J.L.; Meredith, W.; Langston, P.; Snape, C.E. Increased charcoal yield and production of lighter oils from the slow pyrolysis of biomass. *J. Anal. Appl. Pyrolysis* **2017**, *124*, 536–541, doi:10.1016/j.jaap.2017.01.028.

231. Torri, C.; Fabbri, D. Biochar enables anaerobic digestion of aqueous phase from intermediate pyrolysis of biomass. *Bioresour. Technol.* **2014**, *172*, 335–341, doi:10.1016/j.biortech.2014.09.021.

232. Al Arni, S. Comparison of slow and fast pyrolysis for converting biomass into fuel. *Renew. Energy* **2018**, *124*, 197–201, doi:10.1016/j.renene.2017.04.060.

233. Liu, W.J.; Jiang, H.; Yu, H.Q. Development of Biochar-Based Functional Materials: Toward a Sustainable Platform Carbon Material. *Chem. Rev.* **2015**, *115*, 12251–12285, doi:10.1021/acs.chemrev.5b00195.

234. Maschio, G.; Koufopanos, C.; Lucchesi, A. Pyrolysis, a promising route for biomass utilization. *Bioresour. Technol.* **1992**, *42*, 219–231, doi:10.1016/0960-8524(92)90025-S.

235. Demirbas, A. Effects of temperature and particle size on bio-char yield from pyrolysis of agricultural residues. *J. Anal. Appl. Pyrolysis* **2004**, *72*, 243–248, doi:10.1016/j.jaap.2004.07.003.

236. Garcia-Nunez, J.A.; Pelaez-Samaniego, M.R.; Garcia-Perez, M.E.; Fonts, I.; Abrego, J.; Westerhof, R.J.M.; Garcia-Perez, M. *Historical Developments of Pyrolysis Reactors: A Review*; 2017; Vol. 31; ISBN 5093357758.

237. Qian, K.; Kumar, A.; Zhang, H.; Bellmer, D.; Huhnke, R. Recent advances in utilization of biochar. *Renew. Sustain. Energy Rev.* **2015**, *42*, 1055–1064, doi:10.1016/j.rser.2014.10.074.

238. Greenhalf, C.E.; Nowakowski, D.J.; Harms, A.B.; Titiloye, J.O.; Bridgwater, A. V. A comparative study of straw, perennial grasses and hardwoods in terms of fast pyrolysis products. *Fuel* **2013**, *108*, 216–230, doi:10.1016/j.fuel.2013.01.075.

239. Bridgwater, A. V.; Toft, A.J.; Brammer, J.G. *A techno-economic comparison of power production by biomass fast pyrolysis with gasification and combustion*; 2002; Vol. 6; ISBN 4401213593611.

240. Zhang, Q.; Li, Q.; Zhang, L.; Yu, Z.; Jing, X.; Wang, Z.; Fang, Y.; Huang, W. Experimental study on co-pyrolysis and gasification of biomass with deoiled asphalt. *Energy* **2017**, *134*, 301–310, doi:10.1016/j.energy.2017.05.157.

241. Wang, G.; Nie, Z. Synthesis of a novel phosphorus-containing epoxy curing agent and the thermal, mechanical and flame-retardant properties of the cured products. *Polym. Degrad. Stab.* **2016**, *130*, 143–154, doi:10.1016/j.polymdegradstab.2016.06.002.

242. Tremel, A.; Haselsteiner, T.; Nakonz, M.; Spliethoff, H. Coal and char properties in high temperature entrained flow gasification. *Energy* **2012**, *45*, 176–182, doi:10.1016/j.energy.2012.02.028.

243. Wang, B.; Li, X.; Xu, S.; Paterson, N.; Dugwell, D.R.; Kandiyoti, R. Performance of Chinese coals under conditions simulating entrained-flow gasification. *Energy and Fuels* **2005**, *19*, 2006–2013, doi:10.1021/ef050014w.

244. Asthana, S.; Samanta, C.; Voolapalli, R.K.; Saha, B. Direct conversion of syngas to DME: synthesis of new Cu-based hybrid catalysts using Fehling's solution, elimination of the calcination step. *J. Mater. Chem. A* **2017**, *5*, 2649–2663, doi:10.1039/c6ta09038a.

245. Lee, J.; Yang, X.; Cho, S.H.; Kim, J.K.; Lee, S.S.; Tsang, D.C.W.; Ok, Y.S.; Kwon, E.E. Pyrolysis process of agricultural waste using CO2 for waste management, energy recovery, and biochar fabrication. *Appl. Energy* **2017**, *185*, 214–222, doi:10.1016/j.apenergy.2016.10.092.

246. Wang, Z.; Mai, K.; Kumar, N.; Elder, T.; Groom, L.H.; Spivey, J.J. Effect of Steam During Fischer–Tropsch Synthesis Using Biomass-Derived Syngas. *Catal. Letters* **2017**, *147*, 62–70, doi:10.1007/s10562-016-1881-8.

247. Kambo, H.S.; Dutta, A. A comparative review of biochar and hydrochar in terms of production, physico-chemical properties and applications. *Renew. Sustain. Energy Rev.* **2015**, *45*, 359–378, doi:10.1016/j.rser.2015.01.050.

248. Emami Taba, L.; Irfan, M.F.; Wan Daud, W.A.M.; Chakrabarti, M.H. The effect of temperature on various parameters in coal, biomass and CO-gasification: A review. *Renew. Sustain. Energy Rev.* **2012**, *16*, 5584–5596, doi:10.1016/j.rser.2012.06.015.

249. You, S.; Ok, Y.S.; Tsang, D.C.W.; Kwon, E.E.; Wang, C.H. Towards practical application of gasification: a critical review from syngas and biochar perspectives. *Crit. Rev. Environ. Sci. Technol.* **2018**, *48*, 1165–1213, doi:10.1080/10643389.2018.1518860.

250. Hornung, A. *Transformation of Biomass: Theory to Practice*; Wiley, 2014; ISBN 978-1-119-97327-0.

251. Puig-Arnavat, M.; Bruno, J.C.; Coronas, A. Review and analysis of biomass gasification models. *Renew. Sustain. Energy Rev.* **2010**, *14*, 2841–2851, doi:10.1016/j.rser.2010.07.030.

252. Udomsirichakorn, J.; Salam, P.A. Review of hydrogen-enriched gas production from steam gasification of biomass: The prospect of CaO-based chemical looping gasification. *Renew. Sustain. Energy Rev.* **2014**, *30*, 565–579, doi:10.1016/j.rser.2013.10.013.

253. Patra, T.K.; Sheth, P.N. Biomass gasification models for downdraft gasifier: A state-of-the-art review. *Renew. Sustain. Energy Rev.* **2015**, *50*, 583–593, doi:10.1016/j.rser.2015.05.012.

254. Simone, M.; Nicolella, C.; Tognotti, L. Numerical and experimental investigation of downdraft gasification of woody residues. *Bioresour. Technol.* **2013**, *133*, 92–101, doi:10.1016/j.biortech.2013.01.056.

255. Dogru, M.; Howarth, C.R.; Akay, G.; Keskinler, B.; Malik, A.A. Gasification of hazelnut shells in a downdraft gasifier. *Energy* **2002**, *27*, 415–427, doi:10.1016/S0360-5442(01)00094-9.

256. Chaiwat, W.; Hasegawa, I.; Mae, K. Examination of the low-temperature region in a downdraft gasifier

for the pyrolysis product analysis of biomass air gasification. *Ind. Eng. Chem. Res.* **2009**, *48*, 8934–8943, doi:10.1021/ie900264n.

257. De Lasa, H.; Salaices, E.; Mazumder, J.; Lucky, R. Catalytic steam gasification of biomass: Catalysts, thermodynamics and kinetics. *Chem. Rev.* **2011**, *111*, 5404–5433, doi:10.1021/cr200024w.

258. Wilk, M.; Magdziarz, A. Hydrothermal carbonization, torrefaction and slow pyrolysis of Miscanthus giganteus. *Energy* **2017**, *140*, 1292–1304, doi:10.1016/j.energy.2017.03.031.

259. Lee, J.; Lee, K.; Sohn, D.; Kim, Y.M.; Park, K.Y. Hydrothermal carbonization of lipid extracted algae for hydrochar production and feasibility of using hydrochar as a solid fuel. *Energy* **2018**, *153*, 913–920, doi:10.1016/j.energy.2018.04.112.

260. Pala, M.; Kantarli, I.C.; Buyukisik, H.B.; Yanik, J. Hydrothermal carbonization and torrefaction of grape pomace: A comparative evaluation. *Bioresour. Technol.* **2014**, *161*, 255–262, doi:10.1016/j.biortech.2014.03.052.

261. Liu, Z.; Balasubramanian, R. Upgrading of waste biomass by hydrothermal carbonization (HTC) and low temperature pyrolysis (LTP): A comparative evaluation. *Appl. Energy* **2014**, *114*, 857–864, doi:10.1016/j.apenergy.2013.06.027.

262. Yan, W.; Hastings, J.T.; Acharjee, T.C.; Coronella, C.J.; Vásquez, V.R. Mass and energy balances of wet torrefaction of lignocellulosic biomass. *Energy and Fuels* **2010**, *24*, 4738–4742, doi:10.1021/ef901273n.

263. Mašek, O.; Brownsort, P.; Cross, A.; Sohi, S. Influence of production conditions on the yield and environmental stability of biochar. *Fuel* **2013**, *103*, 151–155, doi:10.1016/j.fuel.2011.08.044.

264. Hu, B.; Wang, K.; Wu, L.; Yu, S.-H.; Antonietti, M.; Titirici, M.-M. Engineering Carbon Materials from the Hydrothermal Carbonization Process of Biomass. *Adv. Mater.* **2010**, *22*, 813–828, doi:10.1002/adma.200902812.

265. Kang, C.; Zhu, L.; Wang, Y.; Wang, Y.; Xiao, K.; Tian, T. Adsorption of Basic Dyes Using Walnut Shell-based Biochar Produced by Hydrothermal Carbonization. *Chem. Res. Chinese Univ.* **2018**, *34*, 622–627, doi:10.1007/s40242-018-8018-0.

266. Sevilla, M.; Fuertes, A.B. Sustainable porous carbons with a superior performance for CO2 capture. *Energy Environ. Sci.* **2011**, *4*, 1765–1771, doi:10.1039/c0ee00784f.

267. Krysanova, K.; Krylova, A.; Zaichenko, V. Properties of biochar obtained by hydrothermal carbonization and torrefaction of peat. *Fuel* **2019**, *256*, 115929, doi:10.1016/j.fuel.2019.115929.

268. Liu, Z.; Quek, A.; Kent Hoekman, S.; Balasubramanian, R. Production of solid biochar fuel from waste biomass by hydrothermal carbonization. *Fuel* **2013**, *103*, 943–949, doi:10.1016/j.fuel.2012.07.069.

269. Yu, K.L.; Lau, B.F.; Show, P.L.; Ong, H.C.; Ling, T.C.; Chen, W.H.; Ng, E.P.; Chang, J.S. Recent developments on algal biochar production and characterization. *Bioresour. Technol.* **2017**, *246*, 2–11, doi:10.1016/j.biortech.2017.08.009.

270. Demirbas, A. Biomass Feedstocks. In *Biofuels*; Springer London: London, 2009; pp. 45–85.

271. Demirbas, A. *Biodiesel: A Realistic Fuel Alternative for Diesel Engines*; Springer: London, 2008; ISBN 9781846289941.

272. McKendry, P. Energy production from biomass (part 1): Overview of biomass. *Bioresour. Technol.* **2002**, *83*, 37–46, doi:10.1016/S0960-8524(01)00118-3.

273. Wijitkosum, S.; Jiwnok, P. applied sciences Elemental Composition of Biochar Obtained from Agricultural Waste for Soil Amendment and Carbon Sequestration. **2019**.

274. Abdullah, H.; Wu, H. Biochar as a fuel: 1. Properties and grindability of biochars produced from the pyrolysis of mallee wood under slow-heating conditions. *Energy and Fuels* **2009**, *23*, 4174–4181,

doi:10.1021/ef900494t.

275. Yu, X.Y.; Ying, G.G.; Kookana, R.S. Reduced plant uptake of pesticides with biochar additions to soil. *Chemosphere* **2009**, *76*, 665–671, doi:10.1016/j.chemosphere.2009.04.001.

276. Inyang, M.; Gao, B.; Pullammanappallil, P.; Ding, W.; Zimmerman, A.R. Biochar from anaerobically digested sugarcane bagasse. *Bioresour. Technol.* **2010**, *101*, 8868–8872, doi:10.1016/j.biortech.2010.06.088.

277. Rondon, M.A.; Lehmann, J.; Ramírez, J.; Hurtado, M. Biological nitrogen fixation by common beans (Phaseolus vulgaris L.) increases with bio-char additions. *Biol. Fertil. Soils* **2007**, *43*, 699–708, doi:10.1007/s00374-006-0152-z.

278. Yang, H.; Yan, R.; Chen, H.; Lee, D.H.; Zheng, C. Characteristics of hemicellulose, cellulose and lignin pyrolysis. *Fuel* **2007**, *86*, 1781–1788, doi:10.1016/j.fuel.2006.12.013.

279. Pereira, B.L.C.; Carneiro, A.D.C.O.; Carvalho, A.M.M.L.; Colodette, J.L.; Oliveira, A.C.; Fontes, M.P.F. Influence of Chemical Composition of Eucalyptus Wood on Gravimetric Yield and Charcoal Properties. *BioResources* **2013**, *8*, 4574–4592, doi:10.15376/biores.8.3.4574-4592.

280. Liu, C.; Wang, H.; Karim, A.M.; Sun, J.; Wang, Y. Catalytic fast pyrolysis of lignocellulosic biomass. *Chem. Soc. Rev.* **2014**, *43*, 7594–7623, doi:10.1039/c3cs60414d.

281. Antal, M.J.; Grønli, M. The art, science, and technology of charcoal production. *Ind. Eng. Chem. Res.* **2003**, *42*, 1619–1640, doi:10.1021/ie0207919.

282. Huang, Y.; Wei, Z.; Yin, X.; Wu, C. Pyrolytic characteristics of biomass acid hydrolysis residue rich in lignin. *Bioresour. Technol.* **2012**, *103*, 470–476, doi:10.1016/j.biortech.2011.10.027.

283. Jindo, K.; Mizumoto, H.; Sawada, Y.; Sanchez-Monedero, M.A.; Sonoki, T. Physical and chemical characterization of biochars derived from different agricultural residues. *Biogeosciences* **2014**, *11*, 6613–6621, doi:10.5194/bg-11-6613-2014.

284. Bolognesi, S.; Bernardi, G.; Callegari, A.; Dondi, D.; Capodaglio, A.G. Biochar production from sewage sludge and microalgae mixtures: properties, sustainability and possible role in circular economy. *Biomass Convers. Biorefinery* **2019**, doi:10.1007/s13399-019-00572-5.

285. Tsai, W.T.; Liu, S.C.; Chen, H.R.; Chang, Y.M.; Tsai, Y.L. Textural and chemical properties of swine-manure-derived biochar pertinent to its potential use as a soil amendment. *Chemosphere* **2012**, *89*, 198–203, doi:10.1016/j.chemosphere.2012.05.085.

286. Cantrell, K.B.; Martin, J.H. Stochastic state-space temperature regulation of biochar production. Part II: Application to manure processing via pyrolysis. *J. Sci. Food Agric.* **2012**, *92*, 490–495, doi:10.1002/jsfa.4617.

287. Cao, X.; Harris, W. Properties of dairy-manure-derived biochar pertinent to its potential use in remediation. *Bioresour. Technol.* **2010**, *101*, 5222–5228, doi:10.1016/j.biortech.2010.02.052.

288. Uzoma, K.C.; Inoue, M.; Andry, H.; Fujimaki, H.; Zahoor, A.; Nishihara, E. Effect of cow manure biochar on maize productivity under sandy soil condition. *Soil Use Manag.* **2011**, *27*, 205–212, doi:10.1111/j.1475-2743.2011.00340.x.

289. Dias, B.O.; Silva, C.A.; Higashikawa, F.S.; Roig, A.; Sánchez-Monedero, M.A. Use of biochar as bulking agent for the composting of poultry manure: Effect on organic matter degradation and humification. *Bioresour. Technol.* **2010**, *101*, 1239–1246, doi:10.1016/j.biortech.2009.09.024.

290. Cantrell, K.B.; Hunt, P.G.; Uchimiya, M.; Novak, J.M.; Ro, K.S. Impact of pyrolysis temperature and manure source on physicochemical characteristics of biochar. *Bioresour. Technol.* **2012**, *107*, 419–428, doi:10.1016/j.biortech.2011.11.084.

291. Hossain, M.K.; Strezov Vladimir, V.; Chan, K.Y.; Ziolkowski, A.; Nelson, P.F. Influence of pyrolysis temperature on production and nutrient properties of wastewater sludge biochar. *J. Environ. Manage.*

2011, *92*, 223–228, doi:10.1016/j.jenvman.2010.09.008.

292. Essandoh, M.; Kunwar, B.; Pittman, C.U.; Mohan, D.; Mlsna, T. Sorptive removal of salicylic acid and ibuprofen from aqueous solutions using pine wood fast pyrolysis biochar. *Chem. Eng. J.* **2015**, *265*, 219–227, doi:10.1016/j.cej.2014.12.006.

293. Lucchini, P.; Quilliam, R.S.; DeLuca, T.H.; Vamerali, T.; Jones, D.L. Increased bioavailability of metals in two contrasting agricultural soils treated with waste wood-derived biochar and ash. *Environ. Sci. Pollut. Res.* **2014**, *21*, 3230–3240, doi:10.1007/s11356-013-2272-y.

294. Brown, R.A.; Kercher, A.K.; Nguyen, T.H.; Nagle, D.C.; Ball, W.P. Production and characterization of synthetic wood chars for use as surrogates for natural sorbents. *Org. Geochem.* **2006**, *37*, 321–333, doi:10.1016/j.orggeochem.2005.10.008.

295. He, L.; Liu, Q.; Song, Y.; Deng, Y. Effects of Metal Chlorides on the Solubility of Lignin in the Black Liquor of Prehydrolysis Kraft Pulping. *BioResources* **2014**, *9*, 4636–4642, doi:10.15376/biores.9.3.4636-4642.

296. Feng, Y.; Xu, Y.; Yu, Y.; Xie, Z.; Lin, X. Mechanisms of biochar decreasing methane emission from Chinese paddy soils. *Soil Biol. Biochem.* **2012**, *46*, 80–88, doi:10.1016/j.soilbio.2011.11.016.

297. Lee, J.W.; Kidder, M.; Evans, B.R.; Paik, S.; Buchanan, A.C.; Garten, C.T.; Brown, R.C. Characterization of biochars produced from cornstovers for soil amendment. *Environ. Sci. Technol.* **2010**, *44*, 7970–7974, doi:10.1021/es101337x.

298. Chun, Y.; Sheng, G.; Chiou, G.T.; Xing, B. Compositions and sorptive properties of crop residue-derived chars. *Environ. Sci. Technol.* **2004**, *38*, 4649–4655, doi:10.1021/es035034w.

299. Kizito, S.; Wu, S.; Kipkemoi Kirui, W.; Lei, M.; Lu, Q.; Bah, H.; Dong, R. Evaluation of slow pyrolyzed wood and rice husks biochar for adsorption of ammonium nitrogen from piggery manure anaerobic digestate slurry. *Sci. Total Environ.* **2015**, *505*, 102–112, doi:10.1016/j.scitotenv.2014.09.096.

300. Liu, P.; Liu, W.J.; Jiang, H.; Chen, J.J.; Li, W.W.; Yu, H.Q. Modification of bio-char derived from fast pyrolysis of biomass and its application in removal of tetracycline from aqueous solution. *Bioresour. Technol.* **2012**, *121*, 235–240, doi:10.1016/j.biortech.2012.06.085.

301. Yao, Y.; Gao, B.; Inyang, M.; Zimmerman, A.R.; Cao, X.; Pullammanappallil, P.; Yang, L. Biochar derived from anaerobically digested sugar beet tailings: Characterization and phosphate removal potential. *Bioresour. Technol.* **2011**, *102*, 6273–6278, doi:10.1016/j.biortech.2011.03.006.

302. Wang, Z.; Guo, H.; Shen, F.; Yang, G.; Zhang, Y.; Zeng, Y.; Wang, L.; Xiao, H.; Deng, S. Biochar produced from oak sawdust by Lanthanum (La)-involved pyrolysis for adsorption of ammonium (NH4+), nitrate (NO3-), and phosphate (PO43-). *Chemosphere* 2015, *119*, 646–653.

303. Méndez, A.; Terradillos, M.; Gascó, G. Physicochemical and agronomic properties of biochar from sewage sludge pyrolysed at different temperatures. *J. Anal. Appl. Pyrolysis* **2013**, *102*, 124–130, doi:10.1016/j.jaap.2013.03.006.

304. Song, X.D.; Xue, X.Y.; Chen, D.Z.; He, P.J.; Dai, X.H. Application of biochar from sewage sludge to plant cultivation: Influence of pyrolysis temperature and biochar-to-soil ratio on yield and heavy metal accumulation. *Chemosphere* **2014**, *109*, 213–220, doi:10.1016/j.chemosphere.2014.01.070.

305. Liu, N.; Zhou, J.; Han, L.; Huang, G. Characterization of lignocellulosic compositions' degradation during chicken manure composting with added biochar by phospholipid fatty acid (PLFA) and correlation analysis. *Sci. Total Environ.* **2017**, *586*, 1003–1011, doi:10.1016/j.scitotenv.2017.02.081.

306. Goswami, R.; Shim, J.; Deka, S.; Kumari, D.; Kataki, R.; Kumar, M. Characterization of cadmium removal from aqueous solution by biochar produced from Ipomoea fistulosa at different pyrolytic temperatures. *Ecol. Eng.* **2016**, *97*, 444–451, doi:10.1016/j.ecoleng.2016.10.007.

307. Torri, C.; Samorì, C.; Adamiano, A.; Fabbri, D.; Faraloni, C.; Torzillo, G. Preliminary investigation on the production of fuels and bio-char from Chlamydomonas reinhardtii biomass residue after bio-hydrogen production. *Bioresour. Technol.* **2011**, *102*, 8707–8713, doi:10.1016/j.biortech.2011.01.064.

308. Bird, M.I.; Wurster, C.M.; de Paula Silva, P.H.; Bass, A.M.; de Nys, R. Algal biochar - production and properties. *Bioresour. Technol.* **2011**, *102*, 1886–1891, doi:10.1016/j.biortech.2010.07.106.

309. Srinivasan, P.; Sarmah, A.K.; Smernik, R.; Das, O.; Farid, M.; Gao, W. A feasibility study of agricultural and sewage biomass as biochar, bioenergy and biocomposite feedstock: Production, characterization and potential applications. *Sci. Total Environ.* **2015**, *512–513*, 495–505, doi:10.1016/j.scitotenv.2015.01.068.

310. Wang, Y.; Yin, R.; Liu, R. Characterization of biochar from fast pyrolysis and its effect on chemical properties of the tea garden soil. *J. Anal. Appl. Pyrolysis* **2014**, *110*, 375–381, doi:10.1016/j.jaap.2014.10.006.

311. Touray, N.; Tsai, W.T.; Chen, H.R.; Liu, S.C. Thermochemical and pore properties of goat-manure-derived biochars prepared from different pyrolysis temperatures. *J. Anal. Appl. Pyrolysis* **2014**, *109*, 116–122, doi:10.1016/j.jaap.2014.07.004.

312. Kim, W.-K.K.; Shim, T.; Kim, Y.S.; Hyun, S.; Ryu, C.; Park, Y.K.; Jung, J. Characterization of cadmium removal from aqueous solution by biochar produced from a giant Miscanthus at different pyrolytic temperatures. *Bioresour. Technol.* **2013**, *138*, 266–270, doi:10.1016/j.biortech.2013.03.186.

313. Oh, T.K.; Choi, B.; Shinogi, Y.; Chikushi, J. Effect of pH conditions on actual and apparent fluoride adsorption by biochar in aqueous phase. *Water. Air. Soil Pollut.* **2012**, *223*, 3729–3738, doi:10.1007/s11270-012-1144-2.

314. Chen, B.; Chen, Z. Sorption of naphthalene and 1-naphthol by biochars of orange peels with different pyrolytic temperatures. *Chemosphere* **2009**, *76*, 127–133, doi:10.1016/j.chemosphere.2009.02.004.

315. Ahmad, M.; Lee, S.S.; Rajapaksha, A.U.; Vithanage, M.; Zhang, M.; Cho, J.S.; Lee, S.E.; Ok, Y.S. Trichloroethylene adsorption by pine needle biochars produced at various pyrolysis temperatures. *Bioresour. Technol.* **2013**, *143*, 615–622, doi:10.1016/j.biortech.2013.06.033.

316. Chen, B.; Zhou, D.; Zhu, L. Transitional adsorption and partition of nonpolar and polar aromatic contaminants by biochars of pine needles with different pyrolytic temperatures. *Environ. Sci. Technol.* **2008**, *42*, 5137–5143, doi:10.1021/es8002684.

317. Kim, K.H.; Kim, J.Y.; Cho, T.S.; Choi, J.W. Influence of pyrolysis temperature on physicochemical properties of biochar obtained from the fast pyrolysis of pitch pine (Pinus rigida). *Bioresour. Technol.* **2012**, *118*, 158–162, doi:10.1016/j.biortech.2012.04.094.

318. Chen, Z.; Chen, B.; Chiou, C.T. Fast and slow rates of naphthalene sorption to biochars produced at different temperatures. *Environ. Sci. Technol.* **2012**, *46*, 11104–11111, doi:10.1021/es302345e.

319. Novak, J.M., Lima, I., Xing, B., Gaskin, J.W., Steiner, C., Das, K.C., Ahmedna, M., Rehrah, D., Watts, D.W., Busscher, W.J., Schomberg, H. Characterization of designer biochar produced at different temperatures and their effects on a loamy sand. *Ann. Environ. Sci.* **2009**, *3*, 195–206.

320. Ghani, W.A.W.A.K.; Mohd, A.; da Silva, G.; Bachmann, R.T.; Taufiq-Yap, Y.H.; Rashid, U.; Al-Muhtaseb, A.H. Biochar production from waste rubber-wood-sawdust and its potential use in C sequestration: Chemical and physical characterization. *Ind. Crops Prod.* **2013**, *44*, 18–24, doi:10.1016/j.indcrop.2012.10.017.

321. Dai, Z.; Meng, J.; Muhammad, N.; Liu, X.; Wang, H.; He, Y.; Brookes, P.C.; Xu, J. The potential feasibility for soil improvement, based on the properties of biochars pyrolyzed from different feedstocks. *J. Soils Sediments* **2013**, *13*, 989–1000, doi:10.1007/s11368-013-0698-y.

322. Rajkovich, S.; Enders, A.; Hanley, K.; Hyland, C.; Zimmerman, A.R.; Lehmann, J. Corn growth and nitrogen nutrition after additions of biochars with varying properties to a temperate soil. *Biol. Fertil. Soils* **2012**, *48*, 271–284, doi:10.1007/s00374-011-0624-7.

323. van Zwieten, L.; Kimber, S.; Morris, S.; Chan, K.Y.; Downie, A.; Rust, J.; Joseph, S.; Cowie, A. Effects of biochar from slow pyrolysis of papermill waste on agronomic performance and soil fertility. *Plant Soil* **2010**, *327*, 235–246, doi:10.1007/s11104-009-0050-x.

324. Wang, T.; Camps-Arbestain, M.; Hedley, M.; Bishop, P. Predicting phosphorus bioavailability from high-ash biochars. *Plant Soil* **2012**, *357*, 173–187, doi:10.1007/s11104-012-1131-9.

325. European Biochar Certificate (EBC) European Biochar Certificate - Guidelines for a Sustainable Production of Biochar. *Eur. Biochar Found. Arbaz, Switzerland.* **2012**, *Version 9*.

326. The European Parliament and the Council of the European Union Regulation (EU) 2019/1009 of the European Parliament and of the Council of 5 June 2019 laying down rules on the making available on the market of EU fertilising products and amending Regulation (EC) No 1069/2009 and (EC) No 1107/2009 and repealing Regulat. *Off. J. Eur. Union* **2019**, *2019*, 1–114.

327. MIPAAF Aggiornamento degli allegati 2, 6 e 7 al decreto legislativo n. 75 del 29 aprile 2010. Riordino e revisione della disciplina in materia di fertilizzanti, a norma dell'articolo 13 della legge 7 luglio 2009, n. 88. *Gazz. Uff. della Repubb. Ital.* **2015**.

328. Decreto Legislativo n. 75/2010 e successiva modifica del 10 luglio 2013. Aggiornamento degli allegati del decreto legislativo 29aprile 2010 n. 75, concernente il riordino e la revisione della disciplina in materia di fertilizzanti. *Gazz. Uff. n.121, 26 May 2010, Roma* **2010**.

329. European Parliament and Council Regulation (EC) No 2003/2003 of the European Parliament and of the Council of 13 October 2003 relating to fertilisers. *Off. J. L 304 , 21/11/2003 P. 0001 - 0194* **2003**, 1–194.

330. Sohi, S.P.; Krull, E.; Lopez-Capel, E.; Bol, R. A Review of Biochar and Its Use and Function in Soil. *Adv. Agron.* **2010**, *105*, 47–82, doi:10.1016/S0065-2113(10)05002-9.

331. Manyà, J.J. Pyrolysis for biochar purposes: A review to establish current knowledge gaps and research needs. *Environ. Sci. Technol.* **2012**, *46*, 7939–7954, doi:10.1021/es301029g.

332. Kookana, R.S.; Sarmah, A.K.; Van Zwieten, L.; Krull, E.; Singh, B. *Biochar application to soil. agronomic and environmental benefits and unintended consequences*; 1st ed.; Elsevier Inc., 2011; Vol. 112; ISBN 9780123855381.

333. Glaser, B.; Parr, M.; Braun, C.; Kopolo, G. Biochar is carbon negative. *Nat. Geosci.* **2009**, *2*, 2–2, doi:10.1038/ngeo395.

334. Lehmann, J. A handful of carbon. *Nature* **2007**, *447*, 143–144, doi:10.1038/447143a.

335. Lehmann, J.; Gaunt, J.; Rondon, M. Bio-char Sequestration in Terrestrial Ecosystems – A Review. *Mitig. Adapt. Strateg. Glob. Chang.* **2006**, *11*, 403–427, doi:10.1007/s11027-005-9006-5.

336. Chan, K.Y.; Van Zwieten, L.; Meszaros, I.; Downie, A.; Joseph, S. Agronomic values of greenwaste biochar as a soil amendment. *Aust. J. Soil Res.* **2007**, *45*, 629–634, doi:10.1071/SR07109.

337. Spokas, K.A.; Baker, J.M.; Reicosky, D.C. Ethylene: Potential key for biochar amendment impacts. *Plant Soil* **2010**, *333*, 443–452, doi:10.1007/s11104-010-0359-5.

338. Atkinson, C.J.; Fitzgerald, J.D.; Hipps, N.A. Potential mechanisms for achieving agricultural benefits from biochar application to temperate soils: A review. *Plant Soil* **2010**, *337*, 1–18, doi:10.1007/s11104-010-0464-5.

339. Kimetu, J.M.; Lehmann, J.; Ngoze, S.O.; Mugendi, D.N.; Kinyangi, J.M.; Riha, S.; Verchot, L.; Recha, J.W.; Pell, A.N. Reversibility of soil productivity decline with organic matter of differing quality along a degradation gradient. *Ecosystems* **2008**, *11*, 726–739, doi:10.1007/s10021-008-9154-z.

340. Lehmann, J.; Rillig, M.C.; Thies, J.; Masiello, C.A.; Hockaday, W.C.; Crowley, D. Biochar effects on soil biota - A review. *Soil Biol. Biochem.* **2011**, *43*, 1812–1836, doi:10.1016/j.soilbio.2011.04.022.

341. Ketterings, Q.M.; Bigham, J.M.; Laperche, V. Changes in Soil Mineralogy and Texture Caused by Slash-and-Burn Fires in Sumatra, Indonesia. *Soil Sci. Soc. Am. J.* **2000**, *64*, 1108–1117, doi:10.2136/sssaj2000.6431108x.

342. Riaz, M.; Roohi, M.; Arif, M.S.; Hussain, Q.; Yasmeen, T.; Shahzad, T.; Shahzad, S.M.; Muhammad, H.F.; Arif, M.; Khalid, M. Corncob-derived biochar decelerates mineralization of native and added organic matter (AOM) in organic matter depleted alkaline soil. *Geoderma* **2017**, *294*, 19–28, doi:10.1016/j.geoderma.2017.02.002.

343. Liu, X.; Zhang, A.; Ji, C.; Joseph, S.; Bian, R.; Li, L.; Pan, G.; Paz-Ferreiro, J. Biochar's effect on crop productivity and the dependence on experimental conditions-a meta-analysis of literature data. *Plant Soil* **2013**, *373*, 583–594, doi:10.1007/s11104-013-1806-x.

344. Huang, M.; Yang, L.; Qin, H.; Jiang, L.; Zou, Y. Quantifying the effect of biochar amendment on soil quality and crop productivity in Chinese rice paddies. *F. Crop. Res.* **2013**, *154*, 172–177, doi:10.1016/j.fcr.2013.08.010.

345. Castellini, M.; Giglio, L.; Niedda, M.; Palumbo, A.D.; Ventrella, D. Impact of biochar addition on the physical and hydraulic properties of a clay soil. *Soil Tillage Res.* **2015**, *154*, 1–13, doi:10.1016/j.still.2015.06.016.

346. Ouyang, L.; Wang, F.; Tang, J.; Yu, L.; Zhang, R. Effects of biochar amendment on soil aggregates and hydraulic properties. *J. Soil Sci. Plant Nutr.* **2013**, *13*, 991–1002, doi:10.4067/S0718-95162013005000078.

347. Ramzani, P.M.A.; Shan, L.; Anjum, S.; Khan, W. ud D.; Ronggui, H.; Iqbal, M.; Virk, Z.A.; Kausar, S. Improved quinoa growth, physiological response, and seed nutritional quality in three soils having different stresses by the application of acidified biochar and compost. *Plant Physiol. Biochem.* **2017**, *116*, 127–138, doi:10.1016/j.plaphy.2017.05.003.

348. Ajayi, A.E.; Holthusen, D.; Horn, R. Changes in microstructural behaviour and hydraulic functions of biochar amended soils. *Soil Tillage Res.* **2016**, *155*, 166–175, doi:10.1016/j.still.2015.08.007.

349. Fischer, B.M.C.; Manzoni, S.; Morillas, L.; Garcia, M.; Johnson, M.S.; Lyon, S.W. Improving agricultural water use efficiency with biochar – A synthesis of biochar effects on water storage and fluxes across scales. *Sci. Total Environ.* **2019**, *657*, 853–862, doi:10.1016/j.scitotenv.2018.11.312.

350. Faloye, O.T.; Alatise, M.O.; Ajayi, A.E.; Ewulo, B.S. Effects of biochar and inorganic fertiliser applications on growth, yield and water use efficiency of maize under deficit irrigation. *Agric. Water Manag.* **2019**, *217*, 165–178, doi:10.1016/j.agwat.2019.02.044.

351. Agegnehu, G.; Bass, A.M.; Nelson, P.N.; Bird, M.I. Benefits of biochar, compost and biochar-compost for soil quality, maize yield and greenhouse gas emissions in a tropical agricultural soil. *Sci. Total Environ.* **2016**, *543*, 295–306, doi:10.1016/j.scitotenv.2015.11.054.

352. Batool, A.; Taj, S.; Rashid, A.; Khalid, A.; Qadeer, S.; Saleem, A.R.; Ghufran, M.A. Potential of soil amendments (Biochar and gypsum) in increasing water use efficiency of abelmoschus esculentus L. Moench. *Front. Plant Sci.* **2015**, *6*, 1–13, doi:10.3389/fpls.2015.00733.

353. Yu, O.Y.; Raichle, B.; Sink, S. Impact of biochar on the water holding capacity of loamy sand soil. *Int. J. Energy Environ. Eng.* **2013**, *4*, 1–9, doi:10.1186/2251-6832-4-44.

354. De Melo Carvalho, M.T.; De Holanda Nunes Maia, A.; Madari, B.E.; Bastiaans, L.; Van Oort, P.A.J.; Heinemann, A.B.; Da Silva, M.A.S.; Petter, F.A.; Marimon, B.H.; Meinke, H. Biochar increases plant-available water in a sandy loam soil under an aerobic rice crop system. *Solid Earth* **2014**, *5*, 939–952, doi:10.5194/se-5-939-2014.

355. Kammann, C.I.; Schmidt, H.P.; Messerschmidt, N.; Linsel, S.; Steffens, D.; Müller, C.; Koyro, H.W.; Conte, P.; Stephen, J. Plant growth improvement mediated by nitrate capture in co-composted biochar. *Sci. Rep.* **2015**, *5*, 1–12, doi:10.1038/srep11080.

356. Karhu, K.; Mattila, T.; Bergström, I.; Regina, K. Biochar addition to agricultural soil increased CH4 uptake and water holding capacity - Results from a short-term pilot field study. *Agriculture, Ecosyst. Environ.* **2011**, *140*, 309–313, doi:10.1016/j.agee.2010.12.005.

357. Nelissen, V.; Rütting, T.; Huygens, D.; Staelens, J.; Ruysschaert, G.; Boeckx, P. Maize biochars accelerate short-term soil nitrogen dynamics in a loamy sand soil. *Soil Biol. Biochem.* **2012**, *55*, 20–27, doi:10.1016/j.soilbio.2012.05.019.

358. Yamato, M.; Okimori, Y.; Wibowo, I.F.; Anshori, S.; Ogawa, M. Effects of the application of charred bark of Acacia mangium on the yield of maize, cowpea and peanut, and soil chemical properties in South Sumatra, Indonesia. *Soil Sci. Plant Nutr.* **2006**, *52*, 489–495, doi:10.1111/j.1747-0765.2006.00065.x.

359. Kim, P.; Hensley, D.; Labbé, N. Nutrient release from switchgrass-derived biochar pellets embedded with fertilizers. *Geoderma* **2014**, *232–234*, 341–351, doi:10.1016/j.geoderma.2014.05.017.

360. Liu, Z.; He, T.; Cao, T.; Yang, T.; Meng, J.; Chen, W. Effects of biochar application on nitrogen leaching, ammonia volatilization and nitrogen use efficiency in two distinct soils. *J. Soil Sci. Plant Nutr.* **2017**, *17*, 515–528, doi:10.4067/S0718-95162017005000037.

361. Rovira, P.; Duguy, B.; Vallejo, V.R. Black carbon in wildfire-affected shrubland Mediterranean soils. *J. Plant Nutr. Soil Sci.* **2009**, *172*, 43–52, doi:10.1002/jpln.200700216.

362. Taghizadeh-Toosi, A.; Clough, T.J.; Sherlock, R.R.; Condron, L.M. Biochar adsorbed ammonia is bioavailable. *Plant Soil* **2012**, *350*, 57–69, doi:10.1007/s11104-011-0870-3.

363. Abalos, D.; Sanz-Cobena, A.; Garcia-Torres, L.; van Groenigen, J.W.; Vallejo, A. Role of maize stover incorporation on nitrogen oxide emissions in a non-irrigated Mediterranean barley field. *Plant Soil* **2013**, *364*, 357–371, doi:10.1007/s11104-012-1367-4.

364. Shackley, S. *Biochar in European Soils and Agriculture*; 2016; ISBN 9780415711661.

365. Mukherjee, A.; Zimmerman, A.R.; Harris, W. Surface chemistry variations among a series of laboratory-produced biochars. *Geoderma* **2011**, *163*, 247–255, doi:10.1016/j.geoderma.2011.04.021.

366. Cui, H.J.; Wang, M.K.; Fu, M.L.; Ci, E. Enhancing phosphorus availability in phosphorus-fertilized zones by reducing phosphate adsorbed on ferrihydrite using rice straw-derived biochar. *J. Soils Sediments* **2011**, *11*, 1135–1141, doi:10.1007/s11368-011-0405-9.

367. Galinato, S.P.; Yoder, J.K.; Granatstein, D. The economic value of biochar in crop production and carbon sequestration. *Energy Policy* **2011**, *39*, 6344–6350, doi:10.1016/j.enpol.2011.07.035.

368. Cheng, C.-H.; Lehmann, J.; Thies, J.E.; Burton, S.D. Stability of black carbon in soils across a climatic gradient. *J. Geophys. Res. Biogeosciences* **2008**, *113*, n/a-n/a, doi:10.1029/2007JG000642.

369. Cheng, C.H.; Lehmann, J.; Thies, J.E.; Burton, S.D.; Engelhard, M.H. Oxidation of black carbon by biotic and abiotic processes. *Org. Geochem.* **2006**, *37*, 1477–1488, doi:10.1016/j.orggeochem.2006.06.022.

370. Liang, B.; Lehmann, J.; Solomon, D.; Kinyangi, J.; Grossman, J.; O'Neill, B.; Skjemstad, J.O.; Thies, J.; Luizão, F.J.; Petersen, J.; Neves, E.G. Black Carbon Increases Cation Exchange Capacity in Soils. *Soil Sci. Soc. Am. J.* **2006**, *70*, 1719–1730, doi:10.2136/sssaj2005.0383.

371. Lenton, T.; Vaughan, N. *Geoengineering Responses to Climate Change*; Lenton, T., Vaughan, N., Eds.; Springer New York: New York, NY, 2013; ISBN 978-1-4614-5769-5.

372. Yu, X.Y.; Ying, G.G.; Kookana, R.S. Sorption and desorption behaviors of diuron in soils amended with charcoal. *J. Agric. Food Chem.* **2006**, *54*, 8545–8550, doi:10.1021/jf061354y.

373. Rhodes, A.H.; Carlin, A.; Semple, K.T. Impact of black carbon in the extraction and mineralization of phenanthrene in soil. *Environ. Sci. Technol.* **2008**, *42*, 740–745, doi:10.1021/es071451n.

374. Beck, D.A.; Johnson, G.R.; Spolek, G.A. Amending greenroof soil with biochar to affect runoff water quantity and quality. *Environ. Pollut.* **2011**, *159*, 2111–2118, doi:10.1016/j.envpol.2011.01.022.

375. Slavich, P.G.; Sinclair, K.; Morris, S.G.; Kimber, S.W.L.; Downie, A.; Van Zwieten, L. Contrasting effects of manure and green waste biochars on the properties of an acidic ferralsol and productivity of a subtropical pasture. *Plant Soil* **2013**, *366*, 213–227, doi:10.1007/s11104-012-1412-3.

376. Pietikäinen, J.; Kiikkilä, O.; Fritze, H. Charcoal as a habitat for microbes and its effect on the microbial community of the underlying humus. *Oikos* **2000**, *89*, 231–242, doi:10.1034/j.1600-0706.2000.890203.x.

377. Zackrisson, O.; Nilsson, M.-C.; Wardle, D.A. Key Ecological Function of Charcoal from Wildfire in the Boreal Forest. *Oikos* **1996**, *77*, 10, doi:10.2307/3545580.

378. Smith, J.L.; Collins, H.P.; Bailey, V.L. The effect of young biochar on soil respiration. *Soil Biol. Biochem.* **2010**, *42*, 2345–2347, doi:10.1016/j.soilbio.2010.09.013.

379. Warnock, D.D.; Mummey, D.L.; McBride, B.; Major, J.; Lehmann, J.; Rillig, M.C. Influences of non-herbaceous biochar on arbuscular mycorrhizal fungal abundances in roots and soils: Results from growth-chamber and field experiments. *Appl. Soil Ecol.* **2010**, *46*, 450–456, doi:10.1016/j.apsoil.2010.09.002.

380. Saito, M.; Marumoto, T. Inoculation with arbuscular mycorrhizal fungi: The status quo in Japan and the future prospects. *Plant Soil* **2002**, *244*, 273–279, doi:10.1023/A:1020287900415.

381. Lehmann, J.; Pereira da Silva, J.; Steiner, C.; Nehls, T.; Zech, W.; Glaser, B. Nutrient availability and leaching in an archaeological Anthrosol and a Ferralsol of the Central Amazon basin: fertilizer, manure and charcoal amendments. *Plant Soil* **2003**, *249*, 343–357, doi:https://doi.org/10.1023/A:1022833116184.

382. Spokas, K.A.; Cantrell, K.B.; Novak, J.M.; Archer, D.W.; Ippolito, J.A.; Collins, H.P.; Boateng, A.A.; Lima, I.M.; Lamb, M.C.; McAloon, A.J.; Lentz, R.D.; Nichols, K.A. Biochar: A Synthesis of Its Agronomic Impact beyond Carbon Sequestration. *J. Environ. Qual.* **2012**, *41*, 973–989, doi:10.2134/jeq2011.0069.

383. Laird, D.A.; Brown, R.C.; Amonette, J.E.; Lehmann, J. Review of the pyrolysis platform for coproducing bio-oil and biochar. *Biofuels, Bioprod. Biorefining* **2009**, *3*, 547–562, doi:10.1002/bbb.169.

384. Steiner, C.; Teixeira, W.G.; Lehmann, J.; Nehls, T.; De MacÊdo, J.L.V.; Blum, W.E.H.; Zech, W. Long term effects of manure, charcoal and mineral fertilization on crop production and fertility on a highly weathered Central Amazonian upland soil. *Plant Soil* **2007**, *291*, 275–290, doi:10.1007/s11104-007-9193-9.

385. Vaccari, F.P.; Baronti, S.; Lugato, E.; Genesio, L.; Castaldi, S.; Fornasier, F.; Miglietta, F. Biochar as a strategy to sequester carbon and increase yield in durum wheat. *Eur. J. Agron.* **2011**, *34*, 231–238, doi:10.1016/j.eja.2011.01.006.

386. Gaskin, J.W.; Speir, R.A.; Harris, K.; Das, K.C.; Lee, R.D.; Morris, L.A.; Fisher, D.S. Effect of peanut hull and pine chip biochar on soil nutrients, corn nutrient status, and yield. *Agron. J.* **2010**, *102*, 623–633, doi:10.2134/agronj2009.0083.

387. Van Zwieten, L.; Kimber, S.; Sinclair, K.; Chan, K.Y.; Downie, A. Biochar: Potential for climate change mitigation, improved yield and soil health. *Proc. 23rd Annu. Conf. Grassl. Soc. NSW* **2008**, 30–33.

388. Sinclair, K.; Slavich, P.; Zwieten, L. Van; Downie, A. Productivity and nutrient availability on a Ferrosol : biochar , lime and fertiliser. *Society* **1994**, 119–122.

389. Noguera, D.; Rondón, M.; Laossi, K.R.; Hoyos, V.; Lavelle, P.; Cruz de Carvalho, M.H.; Barot, S. Contrasted effect of biochar and earthworms on rice growth and resource allocation in different soils.

Soil Biol. Biochem. **2010**, *42*, 1017–1027, doi:10.1016/j.soilbio.2010.03.001.

390. Cassman, K.G. Ecological intensification of cereal production systems: Yield potential, soil quality, and precision agriculture. *Proc. Natl. Acad. Sci. U. S. A.* **1999**, *96*, 5952–5959, doi:10.1073/pnas.96.11.5952.

391. Agbna, G.H.D.; Dongli, S.; Zhipeng, L.; Elshaikh, N.A.; Guangcheng, S.; Timm, L.C. Effects of deficit irrigation and biochar addition on the growth, yield, and quality of tomato. *Sci. Hortic. (Amsterdam).* **2017**, *222*, 90–101, doi:10.1016/j.scienta.2017.05.004.

392. El-Naggar, A.; Lee, S.S.; Rinklebe, J.; Farooq, M.; Song, H.; Sarmah, A.K.; Zimmerman, A.R.; Ahmad, M.; Shaheen, S.M.; Ok, Y.S. Biochar application to low fertility soils: A review of current status, and future prospects. *Geoderma* **2019**, *337*, 536–554, doi:10.1016/j.geoderma.2018.09.034.

393. Kim, H.S.; Kim, K.R.; Yang, J.E.; Ok, Y.S.; Owens, G.; Nehls, T.; Wessolek, G.; Kim, K.H. Effect of biochar on reclaimed tidal land soil properties and maize (Zea mays L.) response. *Chemosphere* **2016**, *142*, 153–159, doi:10.1016/j.chemosphere.2015.06.041.

394. Akhtar, S.S.; Andersen, M.N.; Liu, F. Biochar Mitigates Salinity Stress in Potato. *J. Agron. Crop Sci.* **2015**, *201*, 368–378, doi:10.1111/jac.12132.

395. Amer, M. Effect of Biochar, Compost Tea and Magnetic Iron Ore Application on some Soil Properties and Productivity of Some Field Crops under Saline Soils Conditions at North Nile Delta. *Egypt. J. Soil Sci.* **2017**, *0*, 1–17, doi:10.21608/ejss.2017.1097.

396. Akhtar, S.S.; Andersen, M.N.; Liu, F. Residual effects of biochar on improving growth, physiology and yield of wheat under salt stress. *Agric. Water Manag.* **2015**, *158*, 61–68, doi:10.1016/j.agwat.2015.04.010.

397. Mousa, A. Effect of using some soil conditioners on salt affected soil properties and its productivity at El-Tina Plain area - North Sinai - Egypt. *Egypt. J. Soil Sci.* **2017**, *0*, 0–0, doi:10.21608/ejss.2017.1526.

398. Lashari, M.S.; Ye, Y.; Ji, H.; Li, L.; Kibue, G.W.; Lu, H.; Zheng, J.; Pan, G. Biochar-manure compost in conjunction with pyroligneous solution alleviated salt stress and improved leaf bioactivity of maize in a saline soil from central China: A 2-year field experiment. *J. Sci. Food Agric.* **2015**, *95*, 1321–1327, doi:10.1002/jsfa.6825.

399. Zhang, D.; Pan, G.; Wu, G.; Kibue, G.W.; Li, L.; Zhang, X.; Zheng, J.; Zheng, J.; Cheng, K.; Joseph, S.; Liu, X. Biochar helps enhance maize productivity and reduce greenhouse gas emissions under balanced fertilization in a rainfed low fertility inceptisol. *Chemosphere* **2016**, *142*, 106–113, doi:10.1016/j.chemosphere.2015.04.088.

400. Xiao, Q.; Zhu, L.X.; Zhang, H.P.; Li, X.Y.; Shen, Y.F.; Li, S.Q. Soil amendment with biochar increases maize yields in a semi-arid region by improving soil quality and root growth. *Crop Pasture Sci.* **2016**, *67*, 495–507, doi:10.1071/CP15351.

401. Usman, A.R.A.; Al-Wabel, M.I.; Ok, Y.S.; Al-Harbi, A.; Wahb-Allah, M.; El-Naggar, A.H.; Ahmad, M.; Al-Faraj, A.; Al-Omran, A. Conocarpus Biochar Induces Changes in Soil Nutrient Availability and Tomato Growth Under Saline Irrigation. *Pedosphere* **2016**, *26*, 27–38, doi:10.1016/S1002-0160(15)60019-4.

402. Zhang, A.; Cui, L.; Pan, G.; Li, L.; Hussain, Q.; Zhang, X.; Zheng, J.; Crowley, D. Effect of biochar amendment on yield and methane and nitrous oxide emissions from a rice paddy from Tai Lake plain, China. *Agriculture, Ecosyst. Environ.* **2010**, *139*, 469–475, doi:10.1016/j.agee.2010.09.003.

403. Sadaf, J.; Shah, G.A.; Shahzad, K.; Ali, N.; Shahid, M.; Ali, S.; Hussain, R.A.; Ahmed, Z.I.; Traore, B.; Ismail, I.M.I.; Rashid, M.I. Improvements in wheat productivity and soil quality can accomplish by co-application of biochars and chemical fertilizers. *Sci. Total Environ.* **2017**, *607–608*, 715–724, doi:10.1016/j.scitotenv.2017.06.178.

404. Blackwell, P.; Krull, E.; Butler, G.; Herbert, A.; Solaiman, Z. Effect of banded biochar on dryland wheat production and fertiliser use in south-western Australia: an agronomic and economic perspective. *Soil*

Res. **2010**, *48*, 531, doi:10.1071/SR10014.

405. Arif, M.; Ali, K.; Jan, M.T.; Shah, Z.; Jones, D.L.; Quilliam, R.S. Integration of biochar with animal manure and nitrogen for improving maize yields and soil properties in calcareous semi-arid agroecosystems. *F. Crop. Res.* **2016**, *195*, 28–35, doi:10.1016/j.fcr.2016.05.011.

406. Ye, L.; Camps-Arbestain, M.; Shen, Q.; Lehmann, J.; Singh, B.; Sabir, M. Biochar effects on crop yields with and without fertilizer: A meta-analysis of field studies using separate controls. *Soil Use Manag.* **2020**, *36*, 2–18, doi:10.1111/sum.12546.

407. Wang, J.; Zhang, M.; Xiong, Z.; Liu, P.; Pan, G. Effects of biochar addition on N2O and CO2 emissions from two paddy soils. *Biol. Fertil. Soils* **2011**, *47*, 887–896, doi:10.1007/s00374-011-0595-8.

408. Biederman, L.A.; Stanley Harpole, W. Biochar and its effects on plant productivity and nutrient cycling: A meta-analysis. *GCB Bioenergy* **2013**, *5*, 202–214, doi:10.1111/gcbb.12037.

409. Vaccari, F.P.; Maienza, A.; Miglietta, F.; Baronti, S.; Di Lonardo, S.; Giagnoni, L.; Lagomarsino, A.; Pozzi, A.; Pusceddu, E.; Ranieri, R.; Valboa, G.; Genesio, L. Biochar stimulates plant growth but not fruit yield of processing tomato in a fertile soil. *Agriculture, Ecosyst. Environ.* **2015**, *207*, 163–170, doi:10.1016/j.agee.2015.04.015.

410. William, K.; Qureshi, R.A. Evaluation of Biochar as Fertilizer for the Growth of Some Seasonal Vegetables. *J. Bioresour. Manag.* **2015**, *2*, doi:10.35691/jbm.5102.0011.

411. Baronti, S.; Alberti, G.; Vedove, G.D.; di Gennaro, F.; Fellet, G.; Genesio, L.; Miglietta, F.; Peressotti, A.; Vaccari, F.P. The biochar option to improve plant yields: First results from some field and pot experiments in Italy. *Ital. J. Agron.* **2010**, *5*, 3–11, doi:10.4081/ija.2010.3.

412. Rillig, M.C.; Wagner, M.; Salem, M.; Antunes, P.M.; George, C.; Ramke, H.G.; Titirici, M.M.; Antonietti, M. Material derived from hydrothermal carbonization: Effects on plant growth and arbuscular mycorrhiza. *Appl. Soil Ecol.* **2010**, *45*, 238–242, doi:10.1016/j.apsoil.2010.04.011.

413. Genesio, L.; Miglietta, F.; Lugato, E.; Baronti, S.; Pieri, M.; Vaccari, F.P. Surface albedo following biochar application in durum wheat. *Environ. Res. Lett.* **2012**, *7*, doi:10.1088/1748-9326/7/1/014025.

414. IPCC *Climate Change 2007: The Physical Science Basis. Contribution of Working Group I to the Fourth Assessment Report of the Intergovernmental Panel on Climate Change*; Solomon, S., D. Qin, M. Manning, Z. Chen, M. Marquis, K.B. Averyt, M.T. and H.L.M. (eds.)]., Ed.; Cambridge University Press: Cambridge, United Kingdom and New York, NY, USA, 2007; ISBN 978-0-521-88009-1.

415. Oertel, C.; Matschullat, J.; Zurba, K.; Zimmermann, F.; Erasmi, S. Greenhouse gas emissions from soils—A review. *Chemie der Erde* **2016**, *76*, 327–352, doi:10.1016/j.chemer.2016.04.002.

416. Intergovernmental Panel on Climate Change *Climate Change 2014 Mitigation of Climate Change*; Cambridge University Press: Cambridge, 2014; ISBN 9781107415416.

417. Paustian, K.; Lehmann, J.; Ogle, S.; Reay, D.; Robertson, G.P.; Smith, P. Climate-smart soils. *Nature* **2016**, *532*, 49–57, doi:10.1038/nature17174.

418. Lehmann, J.; Kleber, M. The contentious nature of soil organic matter. *Nature* **2015**, *528*, 60–68, doi:10.1038/nature16069.

419. Kwapinski, W.; Byrne, C.M.P.; Kryachko, E.; Wolfram, P.; Adley, C.; Leahy, J.J.; Novotny, E.H.; Hayes, M.H.B. Biochar from biomass and waste. *Waste and Biomass Valorization* **2010**, *1*, 177–189, doi:10.1007/s12649-010-9024-8.

420. Brownsort, P.; Mašek, O. Biomass Pyrolysis Processes: Performance Parameters and their Influence on Biochar System Benefits. *SchoolofGeoSciences* **2009**, *MSc.*, 84.

421. Pratt, K.; Moran, D. Evaluating the cost-effectiveness of global biochar mitigation potential. *Biomass and Bioenergy* **2010**, *34*, 1149–1158, doi:10.1016/j.biombioe.2010.03.004.

422. Lehmann, J.; Rondon, M. Bio-Char Soil Management on Highly Weathered Soils in the Humid Tropics. In *Management*; 2006; pp. 517–529.

423. Baldock, J.A.; Smernik, R.J. Chemical composition and bioavailability of thermally altered Pinus resinosa (Red pine) wood. *Org. Geochem.* **2002**, *33*, 1093–1109, doi:10.1016/S0146-6380(02)00062-1.

424. Hammes, K.; Smernik, R.J.; Skjemstad, J.O.; Herzog, A.; Vogt, U.F.; Schmidt, M.W.I. Synthesis and characterisation of laboratory-charred grass straw (Oryza sativa) and chestnut wood (Castanea sativa) as reference materials for black carbon quantification. *Org. Geochem.* **2006**, *37*, 1629–1633, doi:10.1016/j.orggeochem.2006.07.003.

425. Novak, J.M.; Busscher, W.J.; Laird, D.L.; Ahmedna, M.; Watts, D.W.; Niandou, M.A.S.S. Impact of Biochar Amendment on Fertility of a Southeastern Coastal Plain Soil. *Soil Sci.* **2009**, *174*, 105–112, doi:10.1097/ss.0b013e3181981d9a.

426. Case, S.D.C.; Mcnamara, N.P.; Reay, D.S.; Whitaker, J. Can biochar reduce soil greenhouse gas emissions from a Miscanthus bioenergy crop? *GCB Bioenergy* **2014**, *6*, 76–89, doi:10.1111/gcbb.12052.

427. US EPA *Climate change indicators in the United States 2016 Fourth Edition*; 2016;

428. Lal, R. Sequestration of atmospheric CO2 in global carbon pools. *Energy Environ. Sci.* **2008**, *1*, 86–100, doi:10.1039/b809492f.

429. Karl, T.R.; Trenberth, K.E. Modern Global Climate Change. *Science (80-.).* **2003**, *302*, 1719–1723, doi:10.1126/science.1090228.

430. Korzh, V.; Teh, C.; Kondrychyn, I.; Chudakov, D.M.; Lukyanov, S. Visualizing compound transgenic zebrafish in development: A tale of green fluorescent protein and KillerRed. *Zebrafish* **2011**, *8*, 23–29, doi:10.1089/zeb.2011.0689.

431. IPCC *Global Warming of 1.5°C. An IPCC Special Report on the impacts of global warming of 1.5°C above pre-industrial levels and related global greenhouse gas emission pathways, in the context of strengthening the global response to the threat of cli*; 2018;

432. Conrad, R. Microbial Ecology of Methanogens and Methanotrophs. *Adv. Agron.* **2007**, *96*, 1–63, doi:10.1016/S0065-2113(07)96005-8.

433. Dong, D.; Yang, M.; Wang, C.; Wang, H.; Li, Y.; Luo, J.; Wu, W. Responses of methane emissions and rice yield to applications of biochar and straw in a paddy field. *J. Soils Sediments* **2013**, *13*, 1450–1460, doi:10.1007/s11368-013-0732-0.

434. Reddy, K.R.; Yargicoglu, E.N.; Yue, D.; Yaghoubi, P. Enhanced Microbial Methane Oxidation in Landfill Cover Soil Amended with Biochar. *J. Geotech. Geoenvironmental Eng.* **2014**, *140*, 04014047, doi:10.1061/(asce)gt.1943-5606.0001148.

435. Yaghoubi, P.; Yargicoglu, E.N.; Reddy, K.R. Effects of Biochar-Amendment to Landfill Cover Soil on Microbial Methane Oxidation: Initial Results. **2014**, 1849–1858, doi:10.1061/9780784413272.181.

436. Castro, M.S.; Melillo, J.M.; Steudler, P.A.; Chapman, J.W. Soil moisture as a predictor of methane uptake by temperate forest soils. *Can. J. For. Res.* **1994**, *24*, 1805–1810, doi:10.1139/x94-233.

437. Wang, J.; Pan, X.; Liu, Y.; Zhang, X.; Xiong, Z. Effects of biochar amendment in two soils on greenhouse gas emissions and crop production. *Plant Soil* **2012**, *360*, 287–298, doi:10.1007/s11104-012-1250-3.

438. Kammann, C.; Ratering, S.; Eckhard, C.; Müller, C. Biochar and Hydrochar Effects on Greenhouse Gas (Carbon Dioxide, Nitrous Oxide, and Methane) Fluxes from Soils. *J. Environ. Qual.* **2012**, *41*, 1052–1066, doi:10.2134/jeq2011.0132.

439. Spokas, K.A.; Bogner, J.E. Limits and dynamics of methane oxidation in landfill cover soils. *Waste Manag.* **2011**, *31*, 823–832, doi:10.1016/j.wasman.2009.12.018.

440. Pandey, A.; Mai, V.T.; Vu, D.Q.; Bui, T.P.L.; Mai, T.L.A.; Jensen, L.S.; de Neergaard, A. Organic matter and water management strategies to reduce methane and nitrous oxide emissions from rice paddies in Vietnam. *Agriculture, Ecosyst. Environ.* **2014**, *196*, 137–146, doi:10.1016/j.agee.2014.06.010.

441. Singla, A.; Inubushi, K. Effect of biochar on CH4 and N2O emission from soils vegetated with paddy. *Paddy Water Environ.* **2014**, *12*, 239–243, doi:10.1007/s10333-013-0357-3.

442. Zhang, A.; Bian, R.; Hussain, Q.; Li, L.; Pan, G.; Zheng, J.; Zhang, X.; Zheng, J. Change in net global warming potential of a rice-wheat cropping system with biochar soil amendment in a rice paddy from China. *Agriculture, Ecosyst. Environ.* **2013**, *173*, 37–45, doi:10.1016/j.agee.2013.04.001.

443. Spokas, K.A.; Reicosky, D.C. Impacts of sixteen different biochars on soil greenhouse gas production. *Ann. Environ. Sci.* **2009**, *3*, 179–193.

444. Wang, C.; Liu, J.; Shen, J.; Chen, D.; Li, Y.; Jiang, B.; Wu, J. Effects of biochar amendment on net greenhouse gas emissions and soil fertility in a double rice cropping system: A 4-year field experiment. *Agriculture, Ecosyst. Environ.* **2018**, *262*, 83–96, doi:10.1016/j.agee.2018.04.017.

445. Ly, P.; Duong Vu, Q.; Jensen, L.S.; Pandey, A.; de Neergaard, A. Effects of rice straw, biochar and mineral fertiliser on methane (CH4) and nitrous oxide (N2O) emissions from rice (Oryza sativa L.) grown in a rain-fed lowland rice soil of Cambodia: a pot experiment. *Paddy Water Environ.* **2015**, *13*, 465–475, doi:10.1007/s10333-014-0464-9.

446. Chen, D.; Wang, C.; Shen, J.; Li, Y.; Wu, J. Response of CH4 emissions to straw and biochar applications in double-rice cropping systems: Insights from observations and modeling. *Environ. Pollut.* **2018**, *235*, 95–103, doi:10.1016/j.envpol.2017.12.041.

447. Khan, S.; Chao, C.; Waqas, M.; Arp, H.P.H.; Zhu, Y.G. Sewage sludge biochar influence upon rice (Oryza sativa L) yield, metal bioaccumulation and greenhouse gas emissions from acidic paddy soil. *Environ. Sci. Technol.* **2013**, *47*, 8624–8632, doi:10.1021/es400554x.

448. Ravishankara, A.R.; Daniel, J.S.; Portmann, R.W. Nitrous oxide (N2O): The dominant ozone-depleting substance emitted in the 21st century. *Science (80-.).* **2009**, *326*, 123–125, doi:10.1126/science.1176985.

449. Ussiri, D.; Lal, R. *Soil emission of nitrous oxide and its mitigation*; 2012; ISBN 9789400753648.

450. Cayuela, M.L.; van Zwieten, L.; Singh, B.P.; Jeffery, S.; Roig, A.; Sánchez-Monedero, M.A. Biochar's role in mitigating soil nitrous oxide emissions: A review and meta-analysis. *Agriculture, Ecosyst. Environ.* **2014**, *191*, 5–16, doi:10.1016/j.agee.2013.10.009.

451. Rubasinghege, G.; Spak, S.N.; Stanier, C.O.; Carmichael, G.R.; Grassian, V.H. Abiotic mechanism for the formation of atmospheric nitrous oxide from ammonium nitrate. *Environ. Sci. Technol.* **2011**, *45*, 2691–2697, doi:10.1021/es103295v.

452. Butterbach-Bahl, K.; BagDannenmann; R., K.; S., Z.-B. Nitrous oxide emissions from soils: How well do we understand the processes and their controls? Philosophical Transactions of the Royal Society,. *Philos. Trans. R. Soc.* **2013**, *368*, 1–13.

453. Jia, J.; Li, B.; Chen, Z.; Xie, Z.; Xiong, Z. Effects of biochar application on vegetable production and emissions of n2o and ch4. *Soil Sci. Plant Nutr.* **2012**, *58*, 503–509, doi:10.1080/00380768.2012.686436.

454. RENNER, R. Rethinking biochar. *Environ. Sci. Technol.* **2007**, *41*, 5932–5933, doi:10.1021/es0726097.

455. Van Zwieten, L.; Kimber, S.; Morris, S.; Downie, A.; Berger, E.; Rust, J.; Scheer, C. Influence of biochars on flux of N2O and CO2 from Ferrosol. *Aust. J. Soil Res.* **2010**, *48*, 555–568, doi:10.1071/SR10004.

456. Troy, S.M.; Lawlor, P.G.; O' Flynn, C.J.; Healy, M.G. Impact of biochar addition to soil on greenhouse gas emissions following pig manure application. *Soil Biol. Biochem.* **2013**, *60*, 173–181, doi:10.1016/j.soilbio.2013.01.019.

457. Bruun, E.W.; Müller-Stöver, D.; Ambus, P.; Hauggaard-Nielsen, H. Application of biochar to soil and

N2O emissions: Potential effects of blending fast-pyrolysis biochar with anaerobically digested slurry. *Eur. J. Soil Sci.* **2011**, *62*, 581–589, doi:10.1111/j.1365-2389.2011.01377.x.

458. Kettunen, R.; Saarnio, S. Biochar can restrict N2O emissions and the risk of nitrogen leaching from an agricultural soil during the freeze-thaw period. *Agric. Food Sci.* **2013**, *22*, 373–379, doi:10.23986/afsci.7887.

459. Case, S.D.C.; McNamara, N.P.; Reay, D.S.; Whitaker, J. The effect of biochar addition on N2O and CO2 emissions from a sandy loam soil - The role of soil aeration. *Soil Biol. Biochem.* **2012**, *51*, 125–134, doi:10.1016/j.soilbio.2012.03.017.

460. Augustenborg, C.A.; Hepp, S.; Kammann, C.; Hagan, D.; Schmidt, O.; Müller, C. Biochar and Earthworm Effects on Soil Nitrous Oxide and Carbon Dioxide Emissions. *J. Environ. Qual.* **2012**, *41*, 1203, doi:10.2134/jeq2011.0119.

461. Rogovska, N.; Laird, D.; Cruse, R.; Fleming, P.; Parkin, T.; Meek, D. Impact of Biochar on Manure Carbon Stabilization and Greenhouse Gas Emissions. *Soil Sci. Soc. Am. J.* **2011**, *75*, 871–879, doi:10.2136/sssaj2010.0270.

462. Wang, Z.; Zheng, H.; Luo, Y.; Deng, X.; Herbert, S.; Xing, B. Characterization and influence of biochars on nitrous oxide emission from agricultural soil. *Environ. Pollut.* **2013**, *174*, 289–296, doi:10.1016/j.envpol.2012.12.003.

463. Hale, S.E.; Lehmann, J.; Rutherford, D.; Zimmerman, A.R.; Bachmann, R.T.; Shitumbanuma, V.; O'Toole, A.; Sundqvist, K.L.; Arp, H.P.H.; Cornelissen, G. Quantifying the total and bioavailable polycyclic aromatic hydrocarbons and dioxins in biochars. *Environ. Sci. Technol.* **2012**, *46*, 2830–2838, doi:10.1021/es203984k.

464. Quin, P.R.; Cowie, A.L.; Flavel, R.J.; Keen, B.P.; Macdonald, L.M.; Morris, S.G.; Singh, B.P.; Young, I.M.; Van Zwieten, L. Oil mallee biochar improves soil structural properties-A study with x-ray micro-CT. *Agriculture, Ecosyst. Environ.* **2014**, *191*, 142–149, doi:10.1016/j.agee.2014.03.022.

465. Rondon, M.A.; Ramirez, J.A.; Lehmann, J. *Greenhouse Gas Emissions Decrease with Charcoal Additions to Tropical Soils*; Baltimore, MD. 21–24 Mar, University of Delaware, USA, pp. 208, 2005;

466. Yanai, Y.; Toyota, K.; Okazaki, M. Effects of charcoal addition on N2O emissions from soil resulting from rewetting air-dried soil in short-term laboratory experiments: Original article. *Soil Sci. Plant Nutr.* **2007**, *53*, 181–188, doi:10.1111/j.1747-0765.2007.00123.x.

467. Borchard, N.; Schirrmann, M.; Cayuela, M.L.; Kammann, C.; Wrage-Mönnig, N.; Estavillo, J.M.; Fuertes-Mendizábal, T.; Sigua, G.; Spokas, K.; Ippolito, J.A.; Novak, J. Biochar, soil and land-use interactions that reduce nitrate leaching and N2O emissions: A meta-analysis. *Sci. Total Environ.* **2019**, *651*, 2354–2364, doi:10.1016/j.scitotenv.2018.10.060.

468. Cayuela, M.L.; Sánchez-Monedero, M.A.; Roig, A.; Hanley, K.; Enders, A.; Lehmann, J. Biochar and denitrification in soils: When, how much and why does biochar reduce N2O emissions? *Sci. Rep.* **2013**, *3*, 1–7, doi:10.1038/srep01732.

469. Ameloot, N.; Maenhout, P.; De Neve, S.; Sleutel, S. Biochar-induced N2O emission reductions after field incorporation in a loam soil. *Geoderma* **2016**, *267*, 10–16, doi:10.1016/j.geoderma.2015.12.016.

470. Liu, Y.; Yang, M.; Wu, Y.; Wang, H.; Chen, Y.; Wu, W. Reducing CH4 and CO2 emissions from waterlogged paddy soil with biochar. *J. Soils Sediments* **2011**, *11*, 930–939, doi:10.1007/s11368-011-0376-x.

471. Spokas, K.A.; Koskinen, W.C.; Baker, J.M.; Reicosky, D.C. Impacts of woodchip biochar additions on greenhouse gas production and sorption/degradation of two herbicides in a Minnesota soil. *Chemosphere* **2009**, *77*, 574–581, doi:10.1016/j.chemosphere.2009.06.053.

472. Clough, T.J.; Bertram, J.E.; Ray, J.L.; Condron, L.M.; O'Callaghan, M.; Sherlock, R.R.; Wells, N.S. Unweathered Wood Biochar Impact on Nitrous Oxide Emissions from a Bovine-Urine-Amended Pasture Soil. *Soil Sci. Soc. Am. J.* **2010**, *74*, 852–860, doi:10.2136/sssaj2009.0185.

473. Taghizadeh-Toosi, A.; Clough, T.J.; Condron, L.M.; Sherlock, R.R.; Anderson, C.R.; Craigie, R.A. Biochar Incorporation into Pasture Soil Suppresses in situ Nitrous Oxide Emissions from Ruminant Urine Patches. *J. Environ. Qual.* **2011**, *40*, 468–476, doi:10.2134/jeq2010.0419.

474. Singh, B.P.; Hatton, B.J.; Singh, B.; Cowie, A.L.; Kathuria, A. Influence of Biochars on Nitrous Oxide Emission and Nitrogen Leaching from Two Contrasting Soils. *J. Environ. Qual.* **2010**, *39*, 1224–1235, doi:10.2134/jeq2009.0138.

475. Castaldi, S.; Riondino, M.; Baronti, S.; Esposito, F.R.; Marzaioli, R.; Rutigliano, F.A.; Vaccari, F.P.; Miglietta, F. Impact of biochar application to a Mediterranean wheat crop on soil microbial activity and greenhouse gas fluxes. *Chemosphere* **2011**, *85*, 1464–1471, doi:10.1016/j.chemosphere.2011.08.031.

476. Shaheen, S.M.; Niazi, N.K.; Hassan, N.E.E.; Bibi, I.; Wang, H.; Tsang, D.C.W.; Ok, Y.S.; Bolan, N.; Rinklebe, J. Wood-based biochar for the removal of potentially toxic elements in water and wastewater: a critical review. *Int. Mater. Rev.* **2019**, *64*, 216–247, doi:10.1080/09506608.2018.1473096.

477. Zhang, K.; Cheng, X.; Dang, H.; Ye, C.; Zhang, Y.; Zhang, Q. Linking litter production, quality and decomposition to vegetation succession following agricultural abandonment. *Soil Biol. Biochem.* **2013**, *57*, 803–813, doi:10.1016/j.soilbio.2012.08.005.

478. Zhang, C.; Zeng, G.; Huang, D.; Lai, C.; Chen, M.; Cheng, M.; Tang, W.; Tang, L.; Dong, H.; Huang, B.; Tan, X.; Wang, R. Biochar for environmental management: Mitigating greenhouse gas emissions, contaminant treatment, and potential negative impacts. *Chem. Eng. J.* **2019**, *373*, 902–922, doi:10.1016/j.cej.2019.05.139.

479. Karami, N.; Clemente, R.; Moreno-Jiménez, E.; Lepp, N.W.; Beesley, L. Efficiency of green waste compost and biochar soil amendments for reducing lead and copper mobility and uptake to ryegrass. *J. Hazard. Mater.* **2011**, *191*, 41–48, doi:10.1016/j.jhazmat.2011.04.025.

480. Méndez, A.; Gómez, A.; Paz-Ferreiro, J.; Gascó, G. Effects of sewage sludge biochar on plant metal availability after application to a Mediterranean soil. *Chemosphere* **2012**, *89*, 1354–1359, doi:10.1016/j.chemosphere.2012.05.092.

481. Yao, Y.; Gao, B.; Chen, H.; Jiang, L.; Inyang, M.; Zimmerman, A.R.; Cao, X.; Yang, L.; Xue, Y.; Li, H. Adsorption of sulfamethoxazole on biochar and its impact on reclaimed water irrigation. *J. Hazard. Mater.* **2012**, *209–210*, 408–413, doi:10.1016/j.jhazmat.2012.01.046.

482. Teixidó, M.; Hurtado, C.; Pignatello, J.J.; Beltrán, J.L.; Granados, M.; Peccia, J. Predicting contaminant adsorption in black carbon (Biochar)-amended soil for the veterinary antimicrobial sulfamethazine. *Environ. Sci. Technol.* **2013**, *47*, 6197–6205, doi:10.1021/es400911c.

483. Hale, S.E.; Hanley, K.; Lehmann, J.; Zimmerman, A.R.; Cornelissen, G. Effects of Chemical, Biological, and Physical Aging As Well As Soil Addition on the Sorption of Pyrene to Activated Carbon and Biochar. *Environ. Sci. Technol.* **2012**, *46*, 2479–2480, doi:10.1021/es3001097.

484. Inyang, M.; Dickenson, E. The potential role of biochar in the removal of organic and microbial contaminants from potable and reuse water: A review. *Chemosphere* **2015**, *134*, 232–240, doi:10.1016/j.chemosphere.2015.03.072.

485. Jung, C.; Oh, J.; Yoon, Y. Removal of acetaminophen and naproxen by combined coagulation and adsorption using biochar: influence of combined sewer overflow components. *Environ. Sci. Pollut. Res.* **2015**, *22*, 10058–10069, doi:10.1007/s11356-015-4191-6.

486. Xu, R. kou; Xiao, S. cheng; Yuan, J. hua; Zhao, A. zhen Adsorption of methyl violet from aqueous solutions by the biochars derived from crop residues. *Bioresour. Technol.* **2011**, *102*, 10293–10298,

doi:10.1016/j.biortech.2011.08.089.

487. Mondal, S.; Bobde, K.; Aikat, K.; Halder, G. Biosorptive uptake of ibuprofen by steam activated biochar derived from mung bean husk: Equilibrium, kinetics, thermodynamics, modeling and eco-toxicological studies. *J. Environ. Manage.* **2016**, *182*, 581–594, doi:10.1016/j.jenvman.2016.08.018.

488. Cao, X.; Ma, L.; Liang, Y.; Gao, B.; Harris, W. Simultaneous immobilization of lead and atrazine in contaminated soils using dairy-manure biochar. *Environ. Sci. Technol.* **2011**, *45*, 4884–4889, doi:10.1021/es103752u.

489. Lyu, H.; Gong, Y.; Gurav, R.; Tang, J. Potential Application of Biochar for Bioremediation of Contaminated Systems. In *Biochar Application: Essential Soil Microbial Ecology*; Elsevier Inc., 2016; pp. 221–246 ISBN 9780128034361.

490. Anawar, H.M.; Akter, F.; Solaiman, Z.M.; Strezov, V. Biochar: An Emerging Panacea for Remediation of Soil Contaminants from Mining, Industry and Sewage Wastes. *Pedosphere* **2015**, *25*, 654–665, doi:10.1016/S1002-0160(15)30046-1.

491. Qin, G.; Gong, D.; Fan, M.Y. Bioremediation of petroleum-contaminated soil by biostimulation amended with biochar. *Int. Biodeterior. Biodegrad.* **2013**, *85*, 150–155, doi:10.1016/j.ibiod.2013.07.004.

492. Brown, D.M.; Okoro, S.; van Gils, J.; van Spanning, R.; Bonte, M.; Hutchings, T.; Linden, O.; Egbuche, U.; Bruun, K.B.; Smith, J.W.N. Comparison of landfarming amendments to improve bioremediation of petroleum hydrocarbons in Niger Delta soils. *Sci. Total Environ.* **2017**, *596–597*, 284–292, doi:10.1016/j.scitotenv.2017.04.072.

493. Hu, B.; Song, Y.; Wu, S.; Zhu, Y.; Sheng, G. Slow released nutrient-immobilized biochar: A novel permeable reactive barrier filler for Cr(VI)removal. *J. Mol. Liq.* **2019**, *286*, doi:10.1016/j.molliq.2019.04.153.

494. Dong, X.; Ma, L.Q.; Li, Y. Characteristics and mechanisms of hexavalent chromium removal by biochar from sugar beet tailing. *J. Hazard. Mater.* **2011**, *190*, 909–915, doi:10.1016/j.jhazmat.2011.04.008.

495. Lu, H.; Zhang, W.; Yang, Y.; Huang, X.; Wang, S.; Qiu, R. Relative distribution of Pb2+ sorption mechanisms by sludge-derived biochar. *Water Res.* **2012**, *46*, 854–862, doi:10.1016/j.watres.2011.11.058.

496. Jiang, T.Y.; Jiang, J.; Xu, R.K.; Li, Z. Adsorption of Pb(II) on variable charge soils amended with rice-straw derived biochar. *Chemosphere* **2012**, *89*, 249–256, doi:10.1016/j.chemosphere.2012.04.028.

497. Peng, X.; Ye, L.L.; Wang, C.H.; Zhou, H.; Sun, B. Temperature- and duration-dependent rice straw-derived biochar: Characteristics and its effects on soil properties of an Ultisol in southern China. *Soil Tillage Res.* **2011**, *112*, 159–166, doi:10.1016/j.still.2011.01.002.

498. Kwon, S.; Pignatello, J.J. Effect of natural organic substances on the surface and adsorptive properties of environmental black carbon (char): Pseudo pore blockage by model lipid components and its implications for N2-probed surface properties of natural sorbents. *Environ. Sci. Technol.* **2005**, *39*, 7932–7939, doi:10.1021/es050976h.

499. Lu-Lu Kong , Wei-Tao Liu, and Q.-X.Z. Biochar: An Effective Amendment for Remediating Contaminated Soil. *Rev. Environ. Contam. Toxicol.* **2014**, *228*, 83–99.

500. Dai, Y.; Zhang, N.; Xing, C.; Cui, Q.; Sun, Q. The adsorption, regeneration and engineering applications of biochar for removal organic pollutants: A review. *Chemosphere* 2019, *223*, 12–27.

501. Alloway, B.J. *Heavy Metals in Soils*; Alloway, B.J., Ed.; Environmental Pollution; Third Edit.; Springer Netherlands: Dordrecht, 2013; Vol. 22; ISBN 978-94-007-4469-1.

502. Ross, S.M. *Toxic Metals in Soil-Plant Systems*; Ross, S.M., Ed.; John Wiley & Sons: Chichester, 1994;

503. Komárek, M.; Vaněk, A.; Ettler, V. Chemical stabilization of metals and arsenic in contaminated soils using oxides - A review. *Environ. Pollut.* **2013**, *172*, 9–22, doi:10.1016/j.envpol.2012.07.045.

504. Kumpiene, J. Trace Element Immobilization in Soil Using Amendments. *Trace Elem. Soils* **2010**, 353–379, doi:10.1002/9781444319477.ch15.

505. Uchimiya, M.; Chang, S.C.; Klasson, K.T. Screening biochars for heavy metal retention in soil: Role of oxygen functional groups. *J. Hazard. Mater.* **2011**, *190*, 432–441, doi:10.1016/j.jhazmat.2011.03.063.

506. Beesley, L.; Marmiroli, M.; Pagano, L.; Pigoni, V.; Fellet, G.; Fresno, T.; Vamerali, T.; Bandiera, M.; Marmiroli, N. Biochar addition to an arsenic contaminated soil increases arsenic concentrations in the pore water but reduces uptake to tomato plants (Solanum lycopersicum L.). *Sci. Total Environ.* **2013**, *454–455*, 598–603, doi:10.1016/j.scitotenv.2013.02.047.

507. Jiang, J.; Xu, R. kou; Jiang, T. yu; Li, Z. Immobilization of Cu(II), Pb(II) and Cd(II) by the addition of rice straw derived biochar to a simulated polluted Ultisol. *J. Hazard. Mater.* **2012**, *229–230*, 145–150, doi:10.1016/j.jhazmat.2012.05.086.

508. Kumar, S.; Loganathan, V.A.; Gupta, R.B.; Barnett, M.O. An Assessment of U(VI) removal from groundwater using biochar produced from hydrothermal carbonization. *J. Environ. Manage.* **2011**, *92*, 2504–2512, doi:10.1016/j.jenvman.2011.05.013.

509. Yang, X.; Wan, Y.; Zheng, Y.; He, F.; Yu, Z.; Huang, J.; Wang, H.; Ok, Y.S.; Jiang, Y.; Gao, B. Surface functional groups of carbon-based adsorbents and their roles in the removal of heavy metals from aqueous solutions: A critical review. *Chem. Eng. J.* 2019, *366*, 608–621.

510. Zhang, X.; Wang, H.; He, L.; Lu, K.; Sarmah, A.; Li, J.; Bolan, N.S.; Pei, J.; Huang, H. Using biochar for remediation of soils contaminated with heavy metals and organic pollutants. *Environ. Sci. Pollut. Res.* **2013**, *20*, 8472–8483, doi:10.1007/s11356-013-1659-0.

511. Inyang, M.; Gao, B.; Yao, Y.; Xue, Y.; Zimmerman, A.R.; Pullammanappallil, P.; Cao, X. Removal of heavy metals from aqueous solution by biochars derived from anaerobically digested biomass. *Bioresour. Technol.* **2012**, *110*, 50–56, doi:10.1016/j.biortech.2012.01.072.

512. Yang, Y.; Sheng, G. Pesticide adsorptivity of aged particulate matter arising from crop residue burns. *J. Agric. Food Chem.* **2003**, *51*, 5047–5051, doi:10.1021/jf0345301.

513. Gomez-Eyles, J.L.; Ghosh, U. Enhanced biochars can match activated carbon performance in sediments with high native bioavailability and low final porewater PCB concentrations. *Chemosphere* **2018**, *203*, 179–187, doi:10.1016/j.chemosphere.2018.03.132.

514. Huang, P.; Ge, C.; Feng, D.; Yu, H.; Luo, J.; Li, J.; Strong, P.J.; Sarmah, A.K.; Bolan, N.S.; Wang, H. Effects of metal ions and pH on ofloxacin sorption to cassava residue-derived biochar. *Sci. Total Environ.* **2018**, *616–617*, 1384–1391, doi:10.1016/j.scitotenv.2017.10.177.

515. Huang, S.; Bao, J.; Shan, M.; Qin, H.; Wang, H.; Yu, X.; Chen, J.; Xu, Q. Dynamic changes of polychlorinated biphenyls (PCBs) degradation and adsorption to biochar as affected by soil organic carbon content. *Chemosphere* **2018**, *211*, 120–127, doi:10.1016/j.chemosphere.2018.07.133.

516. Bogusz, A.; Nowak, K.; Stefaniuk, M.; Dobrowolski, R.; Oleszczuk, P. Synthesis of biochar from residues after biogas production with respect to cadmium and nickel removal from wastewater. *J. Environ. Manage.* **2017**, *201*, 268–276, doi:10.1016/j.jenvman.2017.06.019.

517. Fabietti, G.; Biasioli, M.; Barberis, R.; Ajmone-Marsan, F. Soil contamination by organic and inorganic pollutants at the regional scale: The case of piedmont, Italy. *J. Soils Sediments* **2010**, *10*, 290–300, doi:10.1007/s11368-009-0114-9.

518. Sarmah, A.K.; Srinivasan, P.; Smernik, R.J.; Manley-Harris, M.; Antal, M.J.; Downie, A.; Van Zwieten, L. Retention capacity of biochar-amended New Zealand dairy farm soil for an estrogenic steroid hormone and its primary metabolite. *Aust. J. Soil Res.* **2010**, *48*, 648–658, doi:10.1071/SR10013.

519. He, L.; Fan, S.; Müller, K.; Wang, H.; Che, L.; Xu, S.; Song, Z.; Yuan, G.; Rinklebe, J.; Tsang, D.C.W.; Ok,

Y.S.; Bolan, N.S. Comparative analysis biochar and compost-induced degradation of di-(2-ethylhexyl) phthalate in soils. *Sci. Total Environ.* **2018**, *625*, 987–993, doi:10.1016/j.scitotenv.2018.01.002.

520. Chen, Y.; Jiang, Z.; Wu, D.; Wang, H.; Li, J.; Bi, M.; Zhang, Y. Development of a novel bio-organic fertilizer for the removal of atrazine in soil. *J. Environ. Manage.* **2019**, *233*, 553–560, doi:10.1016/j.jenvman.2018.12.086.

521. Teixidó, M.; Pignatello, J.J.; Beltrán, J.L.; Granados, M.; Peccia, J. Speciation of the ionizable antibiotic sulfamethazine on black carbon (Biochar). *Environ. Sci. Technol.* **2011**, *45*, 10020–10027, doi:10.1021/es202487h.

522. Xu, X.; Cao, X.; Zhao, L. Comparison of rice husk- and dairy manure-derived biochars for simultaneously removing heavy metals from aqueous solutions: Role of mineral components in biochars. *Chemosphere* **2013**, *92*, 955–961, doi:10.1016/j.chemosphere.2013.03.009.

523. Larsbo, M.; Löfstrand, E.; De Veer, D.V.A.; Ulén, B. Pesticide leaching from two Swedish topsoils of contrasting texture amended with biochar. *J. Contam. Hydrol.* **2013**, *147*, 73–81, doi:10.1016/j.jconhyd.2013.01.003.

524. Sopeña, F.; Semple, K.; Sohi, S.; Bending, G. Assessing the chemical and biological accessibility of the herbicide isoproturon in soil amended with biochar. *Chemosphere* **2012**, *88*, 77–83, doi:10.1016/j.chemosphere.2012.02.066.

525. Zhang, P.; Sheng, G.; Feng, Y.; Miller, D.M. Predominance of char sorption over substrate concentration and soil pH in influencing biodegradation of benzonitrile. *Biodegradation* **2006**, *17*, 1–8, doi:10.1007/s10532-005-1919-x.

526. Martin, S.M.; Kookana, R.S.; Van Zwieten, L.; Krull, E. Marked changes in herbicide sorption-desorption upon ageing of biochars in soil. *J. Hazard. Mater.* **2012**, *231–232*, 70–78, doi:10.1016/j.jhazmat.2012.06.040.

527. Zheng, W.; Guo, M.; Chow, T.; Bennett, D.N.; Rajagopalan, N. Sorption properties of greenwaste biochar for two triazine pesticides. *J. Hazard. Mater.* **2010**, *181*, 121–126, doi:10.1016/j.jhazmat.2010.04.103.

528. Ghosh, U.; Gomez-Eyles, J.; Yupanqui, C.; Xia, H.; Beckingham, B. *Activated Biochars with Iron for In-Situ Sequestration of Organics, Metals and Carbon*; 2012;

529. Zhang, M.; Gao, B.; Varnoosfaderani, S.; Hebard, A.; Yao, Y.; Inyang, M. Preparation and characterization of a novel magnetic biochar for arsenic removal. *Bioresour. Technol.* **2013**, *130*, 457–462, doi:10.1016/j.biortech.2012.11.132.

530. Chiou, C.T.; Cheng, J.; Hung, W.N.; Chen, B.; Lin, T.F. Resolution of Adsorption and Partition Components of Organic Compounds on Black Carbons. *Environ. Sci. Technol.* **2015**, *49*, 9116–9123, doi:10.1021/acs.est.5b01292.

531. Gao, J.; Liu, Q.; Song, L.; Shi, B. Risk assessment of heavy metals in pipe scales and loose deposits formed in drinking water distribution systems. *Sci. Total Environ.* **2019**, *652*, 1387–1395, doi:10.1016/j.scitotenv.2018.10.347.

532. Soto, D.X.; Koehler, G.; Wassenaar, L.I.; Hobson, K.A. Spatio-temporal variation of nitrate sources to Lake Winnipeg using N and O isotope (δ15N, δ18O) analyses. *Sci. Total Environ.* **2019**, *647*, 486–493, doi:10.1016/j.scitotenv.2018.07.346.

533. Chen, H.; Xie, A.; You, S. A Review: Advances on Absorption of Heavy Metals in the Waste Water by Biochar. *IOP Conf. Ser. Mater. Sci. Eng.* **2018**, *301*, doi:10.1088/1757-899X/301/1/012160.

534. Palansooriya, K.N.; Yang, Y.; Tsang, Y.F.; Sarkar, B.; Hou, D.; Cao, X.; Meers, E.; Rinklebe, J.; Kim, K.H.; Ok, Y.S. Occurrence of contaminants in drinking water sources and the potential of biochar for water

quality improvement: A review. *Crit. Rev. Environ. Sci. Technol.* **2020**, *50*, 549–611, doi:10.1080/10643389.2019.1629803.

535. Yao, Y.; Gao, B.; Zhang, M.; Inyang, M.; Zimmerman, A.R. Effect of biochar amendment on sorption and leaching of nitrate, ammonium, and phosphate in a sandy soil. *Chemosphere* **2012**, *89*, 1467–1471, doi:10.1016/j.chemosphere.2012.06.002.

536. Mayakaduwa, S.S.; Kumarathilaka, P.; Herath, I.; Ahmad, M.; Al-Wabel, M.; Ok, Y.S.; Usman, A.; Abduljabbar, A.; Vithanage, M. Equilibrium and kinetic mechanisms of woody biochar on aqueous glyphosate removal. *Chemosphere* **2016**, *144*, 2516–2521, doi:10.1016/j.chemosphere.2015.07.080.

537. He, J.; Song, Y.; Chen, J.P. Development of a novel biochar/PSF mixed matrix membrane and study of key parameters in treatment of copper and lead contaminated water. *Chemosphere* **2017**, *186*, 1033–1045, doi:10.1016/j.chemosphere.2017.07.028.

538. Peng, B.; Chen, L.; Que, C.; Yang, K.; Deng, F.; Deng, X.; Shi, G.; Xu, G.; Wu, M. Adsorption of Antibiotics on Graphene and Biochar in Aqueous Solutions Induced by π-π Interactions. *Sci. Rep.* **2016**, *6*, 1–10, doi:10.1038/srep31920.

539. Naeem, A.; Westerhoff, P.; Mustafa, S. Vanadium removal by metal (hydr)oxide adsorbents. *Water Res.* **2007**, *41*, 1596–1602, doi:10.1016/j.watres.2007.01.002.

540. Li, Y.; Wang, Z.; Xie, X.; Zhu, J.; Li, R.; Qin, T. Removal of Norfloxacin from aqueous solution by clay-biochar composite prepared from potato stem and natural attapulgite. *Colloids Surfaces A Physicochem. Eng. Asp.* **2017**, *514*, 126–136, doi:10.1016/j.colsurfa.2016.11.064.

541. Li, X.; Zhao, C.; Zhang, M. *Biochar for Anionic Contaminants Removal From Water*; Elsevier Inc., 2019; ISBN 9780128117293.

542. Karunanayake, A.G.; Todd, O.A.; Crowley, M.; Ricchetti, L.; Pittman, C.U.; Anderson, R.; Mohan, D.; Mlsna, T. *Lead and cadmium remediation using magnetized and nonmagnetized biochar from Douglas fir*; 2018; Vol. 331; ISBN 6623251618.

543. Boni, M.R.; Chiavola, A.; Marzeddu, S. Remediation of Lead-Contaminated Water by Virgin Coniferous Wood Biochar Adsorbent: Batch and Column Application. *Water, Air, Soil Pollut.* **2020**, *231*, 171, doi:10.1007/s11270-020-04496-z.

544. Mohan, D.; Rajput, S.; Singh, V.K.; Steele, P.H.; Pittman, C.U. Modeling and evaluation of chromium remediation from water using low cost bio-char, a green adsorbent. *J. Hazard. Mater.* **2011**, *188*, 319–333, doi:10.1016/j.jhazmat.2011.01.127.

545. Hsu, N.H.; Wang, S.L.; Liao, Y.H.; Huang, S.T.; Tzou, Y.M.; Huang, Y.M. Removal of hexavalent chromium from acidic aqueous solutions using rice straw-derived carbon. *J. Hazard. Mater.* **2009**, *171*, 1066–1070, doi:10.1016/j.jhazmat.2009.06.112.

546. Hsu, N.H.; Wang, S.L.; Lin, Y.C.; Sheng, G.D.; Lee, J.F. Reduction of Cr(VI) by crop-residue-derived black carbon. *Environ. Sci. Technol.* **2009**, *43*, 8801–8806, doi:10.1021/es901872x.

547. Lou, L.; Wu, B.; Wang, L.; Luo, L.; Xu, X.; Hou, J.; Xun, B.; Hu, B.; Chen, Y. Sorption and ecotoxicity of pentachlorophenol polluted sediment amended with rice-straw derived biochar. *Bioresour. Technol.* **2011**, *102*, 4036–4041, doi:10.1016/j.biortech.2010.12.010.

548. Wu, S.C.; Lin, F.; Yang, J.Y. Modular biochar torrefaction system for rural Taiwan. *Int. Conf. Manag. Serv. Sci. MASS 2011* **2011**, 0–3, doi:10.1109/ICMSS.2011.5998655.

549. Uchimiya, M.; Wartelle, L.H.; Lima, I.M.; Klasson, K.T. Sorption of deisopropylatrazine on broiler litter biochars. *J. Agric. Food Chem.* **2010**, *58*, 12350–12356, doi:10.1021/jf102152q.

550. Jang, H.M.; Kan, E. Engineered biochar from agricultural waste for removal of tetracycline in water. *Bioresour. Technol.* **2019**, *284*, 437–447, doi:10.1016/j.biortech.2019.03.131.

551. Regkouzas, P.; Diamadopoulos, E. Adsorption of selected organic micro-pollutants on sewage sludge biochar. *Chemosphere* **2019**, *224*, 840–851, doi:10.1016/j.chemosphere.2019.02.165.

552. Qiu, Y.; Zheng, Z.; Zhou, Z.; Sheng, G.D. Effectiveness and mechanisms of dye adsorption on a straw-based biochar. *Bioresour. Technol.* **2009**, *100*, 5348–5351, doi:10.1016/j.biortech.2009.05.054.

553. Inyang, M.; Gao, B.; Zimmerman, A.; Zhou, Y.; Cao, X. Sorption and cosorption of lead and sulfapyridine on carbon nanotube-modified biochars. *Environ. Sci. Pollut. Res.* **2015**, *22*, 1868–1876, doi:10.1007/s11356-014-2740-z.

554. Tang, J.; Lv, H.; Gong, Y.; Huang, Y. Preparation and characterization of a novel graphene/biochar composite for aqueous phenanthrene and mercury removal. *Bioresour. Technol.* **2015**, *196*, 355–363, doi:10.1016/j.biortech.2015.07.047.

555. Chu, K.H.; Shankar, V.; Park, C.M.; Sohn, J.; Jang, A.; Yoon, Y. Evaluation of fouling mechanisms for humic acid molecules in an activated biochar-ultrafiltration hybrid system. *Chem. Eng. J.* **2017**, *326*, 240–248, doi:10.1016/j.cej.2017.05.161.

556. Jin, J.; Sun, K.; Wang, Z.; Han, L.; Du, P.; Wang, X.; Xing, B. Effects of chemical oxidation on phenanthrene sorption by grass- and manure-derived biochars. *Sci. Total Environ.* **2017**, *598*, 789–796, doi:10.1016/j.scitotenv.2017.04.160.

557. Shankar, V.; Heo, J.; Al-Hamadani, Y.A.J.; Park, C.M.; Chu, K.H.; Yoon, Y. Evaluation of biochar-ultrafiltration membrane processes for humic acid removal under various hydrodynamic, pH, ionic strength, and pressure conditions. *J. Environ. Manage.* **2017**, *197*, 610–618, doi:10.1016/j.jenvman.2017.04.040.

558. Liu, W.; Zhang, J.; Zhang, C.; Ren, L. Sorption of norfloxacin by lotus stalk-based activated carbon and iron-doped activated alumina: Mechanisms, isotherms and kinetics. *Chem. Eng. J.* **2011**, *171*, 431–438, doi:10.1016/j.cej.2011.03.099.

559. Li, L.; Zou, D.; Xiao, Z.; Zeng, X.; Zhang, L.; Jiang, L.; Wang, A.; Ge, D.; Zhang, G.; Liu, F. Biochar as a sorbent for emerging contaminants enables improvements in waste management and sustainable resource use. *J. Clean. Prod.* **2019**, *210*, 1324–1342, doi:10.1016/j.jclepro.2018.11.087.

560. Essandoh, M.; Wolgemuth, D.; Pittman, C.U.; Mohan, D.; Mlsna, T. *Phenoxy herbicide removal from aqueous solutions using fast pyrolysis switchgrass biochar*; Elsevier Ltd, 2017; Vol. 174; ISBN 6623251618.

561. Essandoh, M.; Wolgemuth, D.; Pittman, C.U.; Mohan, D.; Mlsna, T. Adsorption of metribuzin from aqueous solution using magnetic and nonmagnetic sustainable low-cost biochar adsorbents. *Environ. Sci. Pollut. Res.* **2017**, *24*, 4577–4590, doi:10.1007/s11356-016-8188-6.

562. Li, Y.; Shao, J.; Wang, X.; Deng, Y.; Yang, H.; Chen, H. Characterization of modified biochars derived from bamboo pyrolysis and their utilization for target component (furfural) adsorption. *Energy and Fuels* **2014**, *28*, 5119–5127, doi:10.1021/ef500725c.

563. Mayakaduwa, S.S.; Herath, I.; Ok, Y.S.; Mohan, D.; Vithanage, M. Insights into aqueous carbofuran removal by modified and non-modified rice husk biochars. *Environ. Sci. Pollut. Res.* **2017**, *24*, 22755–22763, doi:10.1007/s11356-016-7430-6.

564. Chen, B.; Chen, Z.; Lv, S. A novel magnetic biochar efficiently sorbs organic pollutants and phosphate. *Bioresour. Technol.* **2011**, *102*, 716–723, doi:10.1016/j.biortech.2010.08.067.

565. Nabiul Afrooz, A.R.M.; Boehm, A.B. Effects of submerged zone, media aging, and antecedent dry period on the performance of biochar-amended biofilters in removing fecal indicators and nutrients from natural stormwater. *Ecol. Eng.* **2017**, *102*, 320–330, doi:10.1016/j.ecoleng.2017.02.053.

566. Lau, A.Y.T.; Tsang, D.C.W.; Graham, N.J.D.; Ok, Y.S.; Yang, X.; Li, X. dong Surface-modified biochar in a bioretention system for Escherichia coli removal from stormwater. *Chemosphere* **2017**, *169*, 89–98,

doi:10.1016/j.chemosphere.2016.11.048.

567. Dowhan, W.; Bogdanov, M.; Mileykovskaya, E.; Vitrac, H. Biogenesis of Fatty Acids, Lipids and Membranes. *Biog. Fat. Acids, Lipids Membr.* **2017**, doi:10.1007/978-3-319-43676-0.

568. Wu, E.L.; Fleming, P.J.; Yeom, M.S.; Widmalm, G.; Klauda, J.B.; Fleming, K.G.; Im, W. E. coli outer membrane and interactions with OmpLA. *Biophys. J.* **2014**, *106*, 2493–2502, doi:10.1016/j.bpj.2014.04.024.

569. Lima, I.M.; Boateng, A.A.; Klasson, K.T. Pyrolysis of broiler manure: Char and product gas characterization. *Ind. Eng. Chem. Res.* **2009**, *48*, 1292–1297, doi:10.1021/ie800989s.

570. Tong, X.J.; Li, J.Y.; Yuan, J.H.; Xu, R.K. Adsorption of Cu(II) by biochars generated from three crop straws. *Chem. Eng. J.* **2011**, *172*, 828–834, doi:10.1016/j.cej.2011.06.069.

571. Qian, L.; Chen, B. Dual role of biochars as adsorbents for aluminum: The effects of oxygen-containing organic components and the scattering of silicate particles. *Environ. Sci. Technol.* **2013**, *47*, 8759–8768, doi:10.1021/es401756h.

572. Chen, X.; Chen, G.; Chen, L.; Chen, Y.; Lehmann, J.; McBride, M.B.; Hay, A.G. Adsorption of copper and zinc by biochars produced from pyrolysis of hardwood and corn straw in aqueous solution. *Bioresour. Technol.* **2011**, *102*, 8877–8884, doi:10.1016/j.biortech.2011.06.078.

573. Zhang, Z. Bin; Cao, X.H.; Liang, P.; Liu, Y.H. Adsorption of uranium from aqueous solution using biochar produced by hydrothermal carbonization. *J. Radioanal. Nucl. Chem.* **2013**, *295*, 1201–1208, doi:10.1007/s10967-012-2017-2.

574. Liu, Z.; Zhang, F.S. Removal of lead from water using biochars prepared from hydrothermal liquefaction of biomass. *J. Hazard. Mater.* **2009**, *167*, 933–939, doi:10.1016/j.jhazmat.2009.01.085.

575. Zhang, W.; Mao, S.; Chen, H.; Huang, L.; Qiu, R. Pb(II) and Cr(VI) sorption by biochars pyrolyzed from the municipal wastewater sludge under different heating conditions. *Bioresour. Technol.* **2013**, *147*, 545–552, doi:10.1016/j.biortech.2013.08.082.

576. Li, M.; Liu, Q.; Guo, L.; Zhang, Y.; Lou, Z.; Wang, Y.; Qian, G. Cu(II) removal from aqueous solution by Spartina alterniflora derived biochar. *Bioresour. Technol.* **2013**, *141*, 83–88, doi:10.1016/j.biortech.2012.12.096.

577. Sun, L.; Wan, S.; Luo, W. Biochars prepared from anaerobic digestion residue, palm bark, and eucalyptus for adsorption of cationic methylene blue dye: Characterization, equilibrium, and kinetic studies. *Bioresour. Technol.* **2013**, *140*, 406–413, doi:10.1016/j.biortech.2013.04.116.

578. Jia, M.; Wang, F.; Bian, Y.; Jin, X.; Song, Y.; Kengara, F.O.; Xu, R.; Jiang, X. Effects of pH and metal ions on oxytetracycline sorption to maize-straw-derived biochar. *Bioresour. Technol.* **2013**, *136*, 87–93, doi:10.1016/j.biortech.2013.02.098.

579. Tsai, W.T.; Chen, H.R. Adsorption kinetics of herbicide paraquat in aqueous solution onto a low-cost adsorbent, swine-manure-derived biochar. *Int. J. Environ. Sci. Technol.* **2013**, *10*, 1349–1356, doi:10.1007/s13762-012-0174-z.

580. Yao, H.; Lu, J.; Wu, J.; Lu, Z.; Wilson, P.C.; Shen, Y. Adsorption of fluoroquinolone antibiotics by wastewater sludge biochar: Role of the sludge source. *Water. Air. Soil Pollut.* **2013**, *224*, doi:10.1007/s11270-012-1370-7.

581. Nacu, G.; Bulgariu, D.; Cristina Popescu, M.; Harja, M.; Toader Juravle, D.; Bulgariu, L. Removal of Zn(II) ions from aqueous media on thermal activated sawdust. *Desalin. Water Treat.* **2016**, *57*, 21904–21915, doi:10.1080/19443994.2015.1128366.

582. Fagbohungbe, M.O.; Herbert, B.M.J.; Hurst, L.; Ibeto, C.N.; Li, H.; Usmani, S.Q.; Semple, K.T. The challenges of anaerobic digestion and the role of biochar in optimizing anaerobic digestion. *Waste Manag.* **2017**, *61*, 236–249, doi:10.1016/j.wasman.2016.11.028.

583. Mumme, J.; Srocke, F.; Heeg, K.; Werner, M. Use of biochars in anaerobic digestion. *Bioresour. Technol.* **2014**, *164*, 189–197, doi:10.1016/j.biortech.2014.05.008.

584. Shen, Y.; Linville, J.L.; Ignacio-de Leon, P.A.A.; Schoene, R.P.; Urgun-Demirtas, M. Towards a sustainable paradigm of waste-to-energy process: Enhanced anaerobic digestion of sludge with woody biochar. *J. Clean. Prod.* **2016**, *135*, 1054–1064, doi:10.1016/j.jclepro.2016.06.144.

585. Schmidt, H.P.; Hagemann, N.; Draper, K.; Kammann, C. The use of biochar in animal feeding. *PeerJ* **2019**, *2019*, 1–54, doi:10.7717/peerj.7373.

586. Joseph, S.; Pow, D.; Dawson, K.; Mitchell, D.R.G.; Rawal, A.; Hook, J.; Taherymoosavi, S.; Van Zwieten, L.; Rust, J.; Donne, S.; Munroe, P.; Pace, B.; Graber, E.; Thomas, T.; Nielsen, S.; Ye, J.; Lin, Y.; Pan, G.; Li, L.; Solaiman, Z.M. Feeding Biochar to Cows: An Innovative Solution for Improving Soil Fertility and Farm Productivity. *Pedosphere* **2015**, *25*, 666–679, doi:10.1016/S1002-0160(15)30047-3.

587. Leng, R.A.; Inthapanya, S.; Preston, T.R. Biochar lowers net methane production from rumen fluid in vitro. *Livest. Res. Rural Dev.* **2012**, *24*, 1–8.

588. KAMMANN, C.; IPPOLITO, J.; HAGEMANN, N.; BORCHARD, N.; CAYUELA, M.L.; ESTAVILLO, J.M.; FUERTES-MENDIZABAL, T.; JEFFERY, S.; KERN, J.; NOVAK, J.; RASSE, D.; SAARNIO, S.; SCHMIDT, H.-P.; SPOKAS, K.; WRAGE-MÖNNIG, N. BIOCHAR AS A TOOL TO REDUCE THE AGRICULTURAL GREENHOUSE-GAS BURDEN – KNOWNS, UNKNOWNS AND FUTURE RESEARCH NEEDS. *J. Environ. Eng. Landsc. Manag.* **2017**, *25*, 114–139, doi:10.3846/16486897.2017.1319375.

589. Mekbungwan, A.; Yamauchi, K.; Sakaida, T. Intestinal Villus Histological Alterations in Piglets fed Dietary Charcoal Powder Including Wood Vinegar Compound Liquid. *J. Vet. Med. Ser. C Anat. Histol. Embryol.* **2004**, *33*, 11–16, doi:10.1111/j.1439-0264.2004.00501.x.

590. Olson, K.R. Activated Charcoal for Acute Poisoning: One Toxicologist's Journey. *J. Med. Toxicol.* **2010**, *6*, 190–198, doi:10.1007/s13181-010-0046-1.

591. Chyka, P.A. *Activated Charcoal in Medical Applications*; 1995; Vol. 29; ISBN 9781482206883.

592. Minocha, A.; Herold, D.A.; Barth, J.T.; Gideon, D.A.; Spyker, D.A. Activated Charcoal in Oral Ethanol Absorption: Lack of Effect in Humans. *J. Toxicol. Clin. Toxicol.* **1986**, *24*, 225–234, doi:10.3109/15563658608990460.

593. Jürgens, G.; Groth Hoegberg, L.; Graudal, N. The Effect of Activated Charcoal on Drug Exposure in Healthy Volunteers: A Meta-Analysis. *Clin. Pharmacol. Ther.* **2009**, *85*, 501–505, doi:10.1038/clpt.2008.278.

594. Jiang, J.; Zhang, L.; Wang, X.; Holm, N.; Rajagopalan, K.; Chen, F.; Ma, S. Highly ordered macroporous woody biochar with ultra-high carbon content as supercapacitor electrodes. *Electrochim. Acta* **2013**, *113*, 481–489, doi:10.1016/j.electacta.2013.09.121.

595. Liu, M.; Kong, L.; Zhang, P.; Luo, Y.; Kang, L. Porous wood carbon monolith for high-performance supercapacitors. *Electrochim. Acta* **2012**, *60*, 443–448, doi:10.1016/j.electacta.2011.11.100.

596. Wan, C.; Jiao, Y.; Li, J. Core-shell composite of wood-derived biochar supported MnO2 nanosheets for supercapacitor applications. *RSC Adv.* **2016**, *6*, 64811–64817, doi:10.1039/c6ra12043a.

597. Li, Z.; Huang, Y.; Yuan, L.; Hao, Z.; Huang, Y. Status and prospects in sulfur-carbon composites as cathode materials for rechargeable lithium-sulfur batteries. *Carbon N. Y.* **2015**, *92*, 41–63, doi:10.1016/j.carbon.2015.03.008.

598. Elleuch, A.; Boussetta, A.; Yu, J.; Halouani, K.; Li, Y. Experimental investigation of direct carbon fuel cell fueled by almond shell biochar: Part I. Physico-chemical characterization of the biochar fuel and cell performance examination. *Int. J. Hydrogen Energy* **2013**, *38*, 16590–16604,

doi:10.1016/j.ijhydene.2013.08.090.

599. Yu, J.; Zhao, Y.; Li, Y. Utilization of corn cob biochar in a direct carbon fuel cell. *J. Power Sources* **2014**, *270*, 312–317, doi:10.1016/j.jpowsour.2014.07.125.

600. Myers, P. *Handbook of porous solids volume 4*; 2003; Vol. 57; ISBN 3527303391.

601. Sircar, S.; Golden, T.C.; Rao, M.B. Activated carbon for gas separation and storage. *Carbon N. Y.* **1996**, *34*, 1–12, doi:10.1016/0008-6223(95)00128-X.

602. Yates, M.; Blanco, J.; Avila, P.; Martin, M.P. Honeycomb monoliths of activated carbons for effluent gas purification. *Microporous Mesoporous Mater.* **2000**, *37*, 201–208, doi:10.1016/S1387-1811(99)00266-8.

603. Shen, Y.; Fu, Y. Advances in: In situ and ex situ tar reforming with biochar catalysts for clean energy production. *Sustain. Energy Fuels* **2018**, *2*, 326–344, doi:10.1039/c7se00553a.

604. Bhandari, P.N.; Kumar, A.; Huhnke, R.L. Simultaneous Removal of Toluene (Model Tar), NH 3 , and H 2 S, from Biomass-Generated Producer Gas Using Biochar-Based and Mixed-Metal Oxide Catalysts. *Energy & Fuels* **2014**, *28*, 1918–1925, doi:10.1021/ef4016872.

605. Ren, S.; Lei, H.; Wang, L.; Bu, Q.; Chen, S.; Wu, J. Hydrocarbon and hydrogen-rich syngas production by biomass catalytic pyrolysis and bio-oil upgrading over biochar catalysts. *RSC Adv.* **2014**, *4*, 10731–10737, doi:10.1039/C4RA00122B.

606. Liu, W.-J.; Ling, L.; Wang, Y.-Y.; He, H.; He, Y.-R.; Yu, H.-Q.; Jiang, H. One-pot high yield synthesis of Ag nanoparticle-embedded biochar hybrid materials from waste biomass for catalytic Cr(vi) reduction. *Environ. Sci. Nano* **2016**, *3*, 745–753, doi:10.1039/C6EN00109B.

607. Ahmetli, G.; Kocaman, S.; Ozaytekin, I.; Bozkurt, P. Epoxy composites based on inexpensive char filler obtained from plastic waste and natural resources. *Polym. Compos.* **2013**, *34*, 500–509, doi:10.1002/pc.22452.

608. Zhao, M.Y.; Enders, A.; Lehmann, J. Short- and long-term flammability of biochars. *Biomass and Bioenergy* **2014**, *69*, 183–191, doi:10.1016/j.biombioe.2014.07.017.

609. Wang, P.; Wang, G.; Zhang, J.; Lee, J.Y.; Li, Y.; Wang, C. Co-combustion characteristics and kinetic study of anthracite coal and palm kernel shell char. *Appl. Therm. Eng.* **2018**, *143*, 736–745, doi:10.1016/j.applthermaleng.2018.08.009.

610. Wang, B.; Gao, B.; Fang, J. Recent advances in engineered biochar productions and applications. *Crit. Rev. Environ. Sci. Technol.* **2017**, *47*, 2158–2207, doi:10.1080/10643389.2017.1418580.

611. Premarathna, K.S.D.; Rajapaksha, A.U.; Sarkar, B.; Kwon, E.E.; Bhatnagar, A.; Ok, Y.S.; Vithanage, M. Biochar-based engineered composites for sorptive decontamination of water: A review. *Chem. Eng. J.* **2019**, *372*, 536–550, doi:10.1016/j.cej.2019.04.097.

612. Rajapaksha, A.U.; Chen, S.S.; Tsang, D.C.W.; Zhang, M.; Vithanage, M.; Mandal, S.; Gao, B.; Bolan, N.S.; Ok, Y.S. Engineered/designer biochar for contaminant removal/immobilization from soil and water: Potential and implication of biochar modification. *Chemosphere* **2016**, *148*, 276–291, doi:10.1016/j.chemosphere.2016.01.043.

613. Ho, S.H.; Chen, Y. di; Yang, Z. kai; Nagarajan, D.; Chang, J.S.; Ren, N. qi High-efficiency removal of lead from wastewater by biochar derived from anaerobic digestion sludge. *Bioresour. Technol.* **2017**, *246*, 142–149, doi:10.1016/j.biortech.2017.08.025.

614. Safaei Khorram, M.; Zhang, Q.; Lin, D.; Zheng, Y.; Fang, H.; Yu, Y. Biochar: A review of its impact on pesticide behavior in soil environments and its potential applications. *J. Environ. Sci. (China)* **2016**, *44*, 269–279, doi:10.1016/j.jes.2015.12.027.

615. Tripathi, M.; Sahu, J.N.; Ganesan, P. Effect of process parameters on production of biochar from biomass waste through pyrolysis: A review. *Renew. Sustain. Energy Rev.* **2016**, *55*, 467–481,

doi:10.1016/j.rser.2015.10.122.

616. Hassan, M.; Liu, Y.; Naidu, R.; Parikh, S.J.; Du, J.; Qi, F.; Willett, I.R. Influences of feedstock sources and pyrolysis temperature on the properties of biochar and functionality as adsorbents: A meta-analysis. *Sci. Total Environ.* 2020, *744*, 140714.

617. Rollinson, A.N. Gasification reactor engineering approach to understanding the formation of biochar properties. *Proc. R. Soc. A Math. Phys. Eng. Sci.* **2016**, *472*, doi:10.1098/rspa.2015.0841.

618. Akhil, D.; Lakshmi, D.; Kartik, A.; Vo, D.V.N.; Arun, J.; Gopinath, K.P. Production, characterization, activation and environmental applications of engineered biochar: a review. *Environ. Chem. Lett.* 2021, *1*, 3.

619. Kazemi Shariat Panahi, H.; Dehhaghi, M.; Ok, Y.S.; Nizami, A.S.; Khoshnevisan, B.; Mussatto, S.I.; Aghbashlo, M.; Tabatabaei, M.; Lam, S.S. A comprehensive review of engineered biochar: Production, characteristics, and environmental applications. *J. Clean. Prod.* **2020**, *270*, 122462, doi:10.1016/j.jclepro.2020.122462.

620. Kuang, Y.; Zhang, X.; Zhou, S. Adsorption of methylene blue in water onto activated carbon by surfactant modification. *Water (Switzerland)* **2020**, *12*, 1–19, doi:10.3390/w12020587.

621. Rajapaksha, A.U.; Vithanage, M.; Ahmad, M.; Seo, D.C.; Cho, J.S.; Lee, S.E.S.S.S.E.; Lee, S.E.S.S.S.E.; Ok, Y.S. Enhanced sulfamethazine removal by steam-activated invasive plant-derived biochar. *J. Hazard. Mater.* **2015**, *290*, 43–50, doi:10.1016/j.jhazmat.2015.02.046.

622. Li, F.; Cao, X.; Zhao, L.; Wang, J.; Ding, Z. Effects of Mineral Additives on Biochar Formation: Carbon Retention, Stability, and Properties. *Environ. Sci. & Technol.* **2014**, *48*, 11211–11217, doi:10.1021/es501885n.

623. Yan, L.; Kong, L.; Qu, Z.; Li, L.; Shen, G. Magnetic Biochar Decorated with ZnS Nanocrytals for Pb (II) Removal. *ACS Sustain. Chem. & Eng.* **2014**, *3*, 125–132, doi:10.1021/sc500619r.

624. Wang, L.; Wang, Y.; Ma, F.; Tankpa, V.; Bai, S.; Guo, X.; Wang, X. Mechanisms and reutilization of modified biochar used for removal of heavy metals from wastewater: A review. *Sci. Total Environ.* **2019**, *668*, 1298–1309, doi:10.1016/j.scitotenv.2019.03.011.

625. Sun, Y.; Zhang, B.; Zheng, T.; Wang, P. Regeneration of activated carbon saturated with chloramphenicol by microwave and ultraviolet irradiation. *Chem. Eng. J.* **2017**, *320*, 264–270, doi:10.1016/j.cej.2017.03.007.

626. Guo, D.; Shi, Q.; He, B.; Yuan, X. Different solvents for the regeneration of the exhausted activated carbon used in the treatment of coking wastewater. *J. Hazard. Mater.* **2011**, *186*, 1788–1793, doi:10.1016/j.jhazmat.2010.12.068.

627. Lu, P.J.; Lin, H.C.; Yu, W. Te; Chern, J.M. Chemical regeneration of activated carbon used for dye adsorption. *J. Taiwan Inst. Chem. Eng.* **2011**, *42*, 305–311, doi:10.1016/j.jtice.2010.06.001.

628. Li, C.; Zhang, L.; Xia, H.; Peng, J.; Cheng, S.; Shu, J.; Zhang, Q.; Jiang, X. Analysis of devitalization mechanism and chemical constituents for fast and efficient regeneration of spent carbon by means of ultrasound and microwaves. *J. Anal. Appl. Pyrolysis* **2017**, *124*, 42–50, doi:10.1016/j.jaap.2017.02.025.

629. Xin-hui, D.; Srinivasakannan, C.; Jin-sheng, L. Process optimization of thermal regeneration of spent coal based activated carbon using steam and application to methylene blue dye adsorption. *J. Taiwan Inst. Chem. Eng.* **2014**, *45*, 1618–1627, doi:10.1016/j.jtice.2013.10.019.

630. Salvador, F.; Martin-Sanchez, N.; Sanchez-Hernandez, R.; Sanchez-Montero, M.J.; Izquierdo, C. Regeneration of carbonaceous adsorbents. Part II: Chemical, Microbiological and Vacuum Regeneration. *Microporous Mesoporous Mater.* **2015**, *202*, 277–296, doi:10.1016/j.micromeso.2014.08.019.

631. Preston, F. A Global Redesign? Shaping the Circular Economy. *Energy, Environ. Resour. Gov.* **2012**, 1–

20.

632. Rizos, V.; Tuokko, K.; Behrens, A. *The Circular Economy: A review of definitions, processes and impacts*; 2017;

633. Marshall, A.J. (Sandy) *Commercial Application of Pyrolysis Technology in Agriculture*; 2013;

634. Bhange, V.P.; William, S.P.M.P.; Vaidya, A.N. Evaluation of treatment options for garden biomass with specific reference to reduction in greenhouse gases. *Int. J. Multidiscip. Res. Dev.* **2015**, *2*, 320–324.

635. CEC Burning Agricultural Waste: A Source of Dioxins. *Montr. Canada Comm. Environ. Coop.* **2014**, 6.

636. Ahmed, M.B.; Zhou, J.L.; Ngo, H.H.; Guo, W. Insight into biochar properties and its cost analysis. *Biomass and Bioenergy* **2016**, *84*, 76–86, doi:10.1016/j.biombioe.2015.11.002.

637. Chiavola, A.; Tchieda, V.K.; D'Amato, E.; Chianese, A.; Kanaev, A. Synthesis and characterization of nanometric titania coated on granular alumina for arsenic removal. *Chem. Eng. Trans.* **2016**, *47*, 331–336, doi:10.3303/CET1647056.

638. Chiavola, A.; D'Amato, E.; Boni, M.R. Comparison of different iron oxide adsorbents for combined arsenic, vanadium and fluoride removal from drinking water. *Int. J. Environ. Sci. Technol.* **2019**, *16*, 6053–6064, doi:10.1007/s13762-019-02316-4.

639. Deka, K.; Medhi, B.K.; Kandali, G.G.; Pathak, K.; Das, R.; Nath, D.C.; Hazarika, P.P. Physicochemical Characteristics of Activated Biochar Derived from Different Sources. *Int. J. Biochem. Res. Rev.* **2018**, *22*, 1–9, doi:10.9734/IJBCRR/2018/42571.

640. Vilardi, G.; Verdone, N.; Bubbico, R. Combined production of metallic-iron nanoparticles: exergy and energy analysis of two alternative processes using Hydrazine and NaBH4 as reducing agents. *J. Taiwan Inst. Chem. Eng.* **2020**, doi:10.1016/j.jtice.2020.11.020.

641. Azari, A.; Nabizadeh, R.; Nasseri, S.; Mahvi, A.H.; Mesdaghinia, A.R. Comprehensive systematic review and meta-analysis of dyes adsorption by carbon-based adsorbent materials: Classification and analysis of last decade studies. *Chemosphere* 2020, *250*, 126238.

642. Viglašová, E.; Galamboš, M.; Danková, Z.; Krivosudský, L.; Lengauer, C.L.; Hood-Nowotny, R.; Soja, G.; Rompel, A.; Matík, M.; Briančin, J. Production, characterization and adsorption studies of bamboo-based biochar/montmorillonite composite for nitrate removal. *Waste Manag.* **2018**, *79*, 385–394, doi:10.1016/j.wasman.2018.08.005.

643. Yefremova, S.; Terlikbayeva, A.; Zharmenov, A.; Kablanbekov, A.; Bunchuk, L.; Kushakova, L.; Shumskiy, V.; Sukharnikov, Y.; Yermishin, S. Coke-Based Carbon Sorbent: Results of Gold Extraction in Laboratory and Pilot Tests. *Minerals* **2020**, *10*, 508, doi:10.3390/min10060508.

644. Ying, A.; Evans, S.F.; Tsouris, C.; Parans Paranthaman, M. Magnetic sorbent for the removal of selenium(IV) from simulated industrial wastewaters: Determination of column kinetic parameters. *Water (Switzerland)* **2020**, *12*, 1234, doi:10.3390/W12051234.

645. Galeotti, F.; Maccari, F.; Fachini, A.; Volpi, N. Chemical Composition and Antioxidant Activity of Propolis Prepared in Different Forms and in Different Solvents Useful for Finished Products. *Foods* **2018**, *7*, 41, doi:10.3390/foods7030041.

646. Chiavola, A.; Stoller, M.; Di Palma, L.; Boni, M.R. Magnetic core nanoparticles coated by titania and alumina for water and wastewater remediation from metal contaminants. *Chem. Eng. Trans.* **2017**, *60*, 205–210, doi:10.3303/CET1760035.

647. Boni, M.R.; Sbaffoni, S. Chemical Oxidation by Sodium Persulphate for the Treatment of Contaminated Groundwater. Laboratory Tests. *Chem. Eng. Trans.* **2012**, *28*, 157–162, doi:10.3303/CET1228027.

648. Hájková, P. Kaolinite Claystone-Based Geopolymer Materials: Effect of Chemical Composition and Curing Conditions. *Minerals* **2018**, *8*, 444, doi:10.3390/min8100444.

649. Alkurdi, S.S.A.; Herath, I.; Bundschuh, J.; Al-Juboori, R.A.; Vithanage, M.; Mohan, D. Biochar versus bone char for a sustainable inorganic arsenic mitigation in water: What needs to be done in future research? *Environ. Int.* **2019**, *127*, 52–69, doi:10.1016/j.envint.2019.03.012.

650. Pituello, C.; Francioso, O.; Simonetti, G.; Pisi, A.; Torreggiani, A.; Berti, A.; Morari, F. Characterization of chemical–physical, structural and morphological properties of biochars from biowastes produced at different temperatures. *J. Soils Sediments* **2015**, *15*, 792–804, doi:10.1007/s11368-014-0964-7.

651. CEFIC *Test Methods for activated carbon*; 1986;

652. Bansode, R.R.; Losso, J.N.; Marshall, W.E.; Rao, R.M.; Portier, R.J. Adsorption of volatile organic compounds by pecan shell- and almond shell-based granular activated carbons. *Bioresour. Technol.* **2003**, *90*, 175–184, doi:10.1016/S0960-8524(03)00117-2.

653. Noh, J.S.; Schwarz, J.A. Effect of HNO3 treatment on the surface acidity of activated carbons. *Carbon N. Y.* **1990**, *28*, 675–682, doi:10.1016/0008-6223(90)90069-B.

654. Boehm, H.P. Surface oxides on carbon and their analysis: A critical assessment. *Carbon N. Y.* **2002**, *40*, 145–149, doi:10.1016/S0008-6223(01)00165-8.

655. Moreno-Castilla, C.; Rivera-Utrilla, J. Carbon materials as adsorbents for the removal of pollutants from the aqueous phase. *MRS Bull.* **2001**, *26*, 890–894, doi:10.1557/mrs2001.230.

656. Aranda, P.R.; Colombo, L.; Perino, E.; De Vito, I.E.; Raba, J. Solid-phase preconcentration and determination of mercury(II) using activated carbon in drinking water by X-ray fluorescence spectrometry. *X-Ray Spectrom.* **2013**, *42*, 100–104, doi:10.1002/xrs.2440.

657. Leyva, D.; Estévez, J.; Montero, A.; Pupo, I. Sub-ppm determination of Hg and Cr in water: Cr speciation. *X-Ray Spectrom.* **2007**, *36*, 27–34, doi:10.1002/xrs.

658. Kim, Y.S.; Yang, S.J.; Lim, H.J.; Kim, T.; Lee, K.; Park, C.R. Effects of carbon dioxide and acidic carbon compounds on the analysis of Boehm titration curves. *Carbon N. Y.* **2012**, *50*, 1510–1516, doi:10.1016/j.carbon.2011.11.021.

659. Funk, J.E.; Dinger, D.R. Methylene Blue Index. In *Predictive Process Control of Crowded Particulate Suspensions*; Springer, Boston, MA, 1994; pp. 669–689 ISBN 978-1-4615-3118-0.

660. Wu, R.; Beutler, J.; Price, C.; Baxter, L.L. Biomass char particle surface area and porosity dynamics during gasification. *Fuel* **2020**, *264*, 116833, doi:10.1016/j.fuel.2019.116833.

661. Di Natale, M.; Musmarra, D.; Capasso, S.; Lama, A. Tecniche di capping per il trattamento dei sedimenti marini contaminati nelle aree costiere.

662. Matshitse, R. *Brunauer-Emmett-Teller (BET) surface area analysis*; 2010;

663. BEL JAPAN, I. *Belsorp High Precision Gas/vapor adsorpion apparatus*; ISBN 0717-6163.

664. Barrett, E.P.; Joyner, L.G.; Halenda, P.P. The Determination of Pore Volume and Area Distributions in Porous Substances. I. Computations from Nitrogen Isotherms. *J. Am. Chem. Soc.* **1951**, *73*, 373–380, doi:10.1021/ja01145a126.

665. Dutta, S.; Sharma, R.K. Sustainable Magnetically Retrievable Nanoadsorbents for Selective Removal of Heavy Metal Ions From Different Charged Wastewaters. In *Separation Science and Technology (New York)*; Elsevier Inc., 2019; Vol. 11, pp. 371–416.

666. *Standard Methods for the Examination of Water and Wastewater*; Clesceri, L.S., Greenberg, A.E., Eaton, A.D., Eds.; 20th ed.; American Public Health Association (APHA): Washington, DC, USA, 1998; ISBN 978-0875532356.

667. Kołodyńska, D.; Krukowska, J.; Thomas, P. Comparison of sorption and desorption studies of heavy metal ions from biochar and commercial active carbon. *Chem. Eng. J.* **2017**, *307*, 353–363,

doi:10.1016/j.cej.2016.08.088.

668. Kumar, K.V.; Porkodi, K.; Rocha, F. Isotherms and thermodynamics by linear and non-linear regression analysis for the sorption of methylene blue onto activated carbon: Comparison of various error functions. *J. Hazard. Mater.* **2008**, *151*, 794–804, doi:10.1016/j.jhazmat.2007.06.056.

669. Batool, F.; Akbar, J.; Iqbal, S.; Noreen, S.; Bukhari, S.N.A. Study of Isothermal, Kinetic, and Thermodynamic Parameters for Adsorption of Cadmium: An Overview of Linear and Nonlinear Approach and Error Analysis. *Bioinorg. Chem. Appl.* **2018**, *2018*, doi:10.1155/2018/3463724.

670. Salarirad, M.M.; Behnamfard, A. Modeling of equilibrium data for free cyanide adsorption onto activated carbon by linear and non-linear regression methods. In *2011 International Conference on Environment and Industrial Innovation IPCBEE*; IACSIT Press: Singapore, 2011; Vol. 12, pp. 79–84.

671. Langmuir, I. The adsorption of gases on plane surfaces of glass, mica and platinum. *J. Am. Chem. Soc.* **1918**, *40*, 1361–1403, doi:10.1021/ja02242a004.

672. Al-Ghouti, M.A.; Da'ana, D.A. Guidelines for the use and interpretation of adsorption isotherm models: A review. *J. Hazard. Mater.* **2020**, *393*, 122383, doi:10.1016/j.jhazmat.2020.122383.

673. Ayawei, N.; Ebelegi, A.N.; Wankasi, D. Modelling and Interpretation of Adsorption Isotherms. *J. Chem.* **2017**, *2017*, 11, doi:10.1155/2017/3039817.

674. Kinniburgh, D.G. General purpose adsorption isotherms. *Environ. Sci. Technol.* **1986**, *20*, 895–904, doi:10.1021/es00151a008.

675. Lineweaver, H.; Burk, D. The Determination of Enzyme Dissociation Constants. *J. Am. Chem. Soc.* **1934**, *56*, 658–666, doi:10.1021/ja01318a036.

676. Eadie, G.S. The inhibition of cholinesterase by physostigmine and prostigmine. *J. Biol. Chem.* **1942**, *146*, 85–93.

677. Hofstee, B.H.J. Non-inverted versus inverted plots in enzyme kinetics. *Nature* **1959**, *184*, 1296–1298, doi:10.1038/1841296b0.

678. Scatchard, G. The Attraction of Proteins for Small Molecules and Ions. *Ann. N. Y. Acad. Sci.* **1949**, *51*, 660–672, doi:10.1111/j.1749-6632.1949.tb27297.x.

679. Yakout, S.M.; Elsherif, E. Batch kinetics, isotherm and thermodynamic studies of adsorption of strontium from aqueous solutions onto low cost rice-straw based carbons. *Carbon - Sci. Technol.* **2010**, *3*, 144–153.

680. Weber, T.W.; Chakravorti, R.K. Pore and solid diffusion models for fixed-bed adsorbers. *AIChE J.* **1974**, *20*, 228–238, doi:10.1002/aic.690200204.

681. Hall, K.R.; Eagleton; Acrivos, A.; Vermeulen, T.; Eagleton, L.C.; Acrivos, A.; Vermeulen, T. Pore- and solid-diffusion kinetics in fixed-bed adsorption under constant-pattern conditions. *Ind. Eng. Chem. Fundam.* **1966**, *5*, 212–223, doi:10.1021/i160018a011.

682. Freundlich, H.M.F. Über die Adsorption in Lösungen. *Zeitschrift für Phys. Chemie* **1907**, *57*, 385–470, doi:10.1515/zpch-1907-5723.

683. Ho, Y.S.; Porter, J.F.; McKay, G. Equilibrium isotherm studies for the sorption of divalent metal ions onto peat: Copper, nickel and lead single component systems. *Water. Air. Soil Pollut.* **2002**, *141*, 1–33, doi:10.1023/A:1021304828010.

684. Ringot, D.; Lerzy, B.; Chaplain, K.; Bonhoure, J.P.; Auclair, E.; Larondelle, Y. In vitro biosorption of ochratoxin A on the yeast industry by-products: Comparison of isotherm models. *Bioresour. Technol.* **2007**, *98*, 1812–1821, doi:10.1016/j.biortech.2006.06.015.

685. Halsey, G.D. The role of surface heterogeneity. *Adv. Synth. Catal.* **1952**, *4*, 259–269.

686. Dubinin, M.M.; Radushkevich, L.V. The equation of the characteristic curve of activated charcoal. In *Proceedings of the Academy of Sciences, Physical Chemistry Section*; 1947; Vol. 55, pp. 331–337.

687. Ayoob, S.; Gupta, A.K. Insights into isotherm making in the sorptive removal of fluoride from drinking water. *J. Hazard. Mater.* **2008**, *152*, 976–985, doi:10.1016/j.jhazmat.2007.07.072.

688. Sumanjit; Rani, S.; Mahajan, R.K. Equilibrium, kinetics and thermodynamic parameters for adsorptive removal of dye Basic Blue 9 by ground nut shells and Eichhornia. *Arab. J. Chem.* **2016**, *9*, S1464–S1477, doi:10.1016/j.arabjc.2012.03.013.

689. Inyinbor, A.A.; Adekola, F.A.; Olatunji, G.A. Kinetics, isotherms and thermodynamic modeling of liquid phase adsorption of Rhodamine B dye onto Raphia hookerie fruit epicarp. *Water Resour. Ind.* **2016**, *15*, 14–27, doi:10.1016/j.wri.2016.06.001.

690. Hamdaoui, O.; Naffrechoux, E. Modeling of adsorption isotherms of phenol and chlorophenols onto granular activated carbon. Part I. Two-parameter models and equations allowing determination of thermodynamic parameters. *J. Hazard. Mater.* **2007**, *147*, 381–394, doi:10.1016/j.jhazmat.2007.01.021.

691. Largitte, L.; Pasquier, R. A review of the kinetics adsorption models and their application to the adsorption of lead by an activated carbon. *Chem. Eng. Res. Des.* **2016**, *109*, 495–504, doi:10.1016/j.cherd.2016.02.006.

692. Redlich, O.; Peterson, D.L. A useful adsorption isotherm. *J. Physic Chem.* **1959**, *63*, 1024, doi:10.1021/j150576a611.

693. Wu, F.C.; Liu, B.L.; Wu, K.T.; Tseng, R.L. A new linear form analysis of Redlich-Peterson isotherm equation for the adsorptions of dyes. *Chem. Eng. J.* **2010**, *162*, 21–27, doi:10.1016/j.cej.2010.03.006.

694. Rojas, J.; Suarez, D.; Moreno, A.; Silva-Agredo, J.; Torres-Palma, R.A. Kinetics, isotherms and thermodynamic modeling of liquid phase adsorption of crystal violet dye onto shrimp-waste in its raw, pyrolyzed material and activated charcoals. *Appl. Sci.* **2019**, *9*, doi:10.3390/app9245337.

695. Kumara, N.T.R.N.; Hamdan, N.; Petra, M.I.; Tennakoon, K.U.; Ekanayake, P. Equilibrium Isotherm Studies of Adsorption of Pigments Extracted from Kuduk-kuduk (Melastoma malabathricum L.) Pulp onto TiO 2 Nanoparticles. *J. Chem.* **2014**, *2014*, 1–6, doi:10.1155/2014/468975.

696. Ngakou, C.S.; Anagho, G.S.; Ngomo, H.M. Non-linear Regression Analysis for the Adsorption Kinetics and Equilibrium Isotherm of Phenacetin onto Activated Carbons. *Curr. J. Appl. Sci. Technol.* **2019**, *36*, 1–18, doi:10.9734/cjast/2019/v36i430246.

697. Nemr, A. El; El-Sikaily, A.; Khaled, A. Modeling of adsorption isotherms of Methylene Blue onto rice husk activated carbon. *Egypt. J. Aquat. Res.* **2010**, *36*, 403–425.

698. Shahbeig, H.; Bagheri, N.; Ghorbanian, S.A.; Hallajisani, A.; Poorkarimi, S. A new adsorption isotherm model of aqueous solutions on granular activated carbon. *World J. Model. Simul.* **2013**, *9*, 243–254.

699. Farouq, R.; Yousef, N.S. Equilibrium and Kinetics Studies of adsorption of Copper (II) Ions on Natural Biosorbent. *Int. J. Chem. Eng. Appl.* **2015**, *6*, 319–324, doi:10.7763/ijcea.2015.v6.503.

700. Lagergren, S.Y. Zur theorie der sogenannten adsorption geloster stoffe, Kungliga Svenska Vetenskapsakademiens. *Handlingar* **1898**, *24*, 1–39.

701. Antuña-Nieto, C.; Rodríguez, E.; López-Antón, M.A.; García, R.; Martínez-Tarazona, M.R. Mercury adsorption in the gas phase by regenerable Au-loaded activated carbon foams: A kinetic and reaction mechanism study. *New J. Chem.* **2020**, *44*, 12009–12018, doi:10.1039/d0nj00898b.

702. Febrianto, J.; Kosasih, A.N.; Sunarso, J.; Ju, Y.H.; Indraswati, N.; Ismadji, S. Equilibrium and kinetic studies in adsorption of heavy metals using biosorbent: A summary of recent studies. *J. Hazard. Mater.* **2009**, *162*, 616–645, doi:10.1016/j.jhazmat.2008.06.042.

703. Tan, K.L.; Hameed, B.H. Insight into the adsorption kinetics models for the removal of contaminants

from aqueous solutions. *J. Taiwan Inst. Chem. Eng.* **2017**, *74*, 25–48, doi:10.1016/j.jtice.2017.01.024.

704. Ho, Y.S.; McKay, G. Pseudo-second order model for sorption processes. *Process Biochem.* **1999**, *34*, 451–465, doi:10.1016/S0032-9592(98)00112-5.

705. Simonin, J.P. On the comparison of pseudo-first order and pseudo-second order rate laws in the modeling of adsorption kinetics. *Chem. Eng. J.* **2016**, *300*, 254–263, doi:10.1016/j.cej.2016.04.079.

706. Karadag, D.; Koc, Y.; Turan, M.; Ozturk, M. A comparative study of linear and non-linear regression analysis for ammonium exchange by clinoptilolite zeolite. *J. Hazard. Mater.* **2007**, *144*, 432–437, doi:10.1016/j.jhazmat.2006.10.055.

707. Liu, Q.; Shi, J.; Zheng, S.; Tao, M.; He, Y.; Shi, Y. Kinetics studies of CO2 adsorption/desorption on amine-functionalized multiwalled carbon nanotubes. *Ind. Eng. Chem. Res.* **2014**, *53*, 11677–11683, doi:10.1021/ie502009n.

708. Andrade, C.A.; Zambrano-Intriago, L.A.; Oliveira, N.S.; Vieira, J.S.; Quiroz-Fernández, L.S.; Rodríguez-Díaz, J.M. Adsorption Behavior and Mechanism of Oxytetracycline on Rice Husk Ash: Kinetics, Equilibrium, and Thermodynamics of the Process. *Water. Air. Soil Pollut.* **2020**, *231*, doi:10.1007/s11270-020-04473-6.

709. Boni, M.R.; Chiavola, A.; Antonucci, A.; Di Mattia, E.; Marzeddu, S. A novel treatment for Cd-contaminated solution through adsorption on beech charcoal: the effect of bioactivation. *Desalin. Water Treat.* **2018**, *127*, 104–110, doi:10.5004/dwt.2018.22664.

710. Chiavola, A.; Marzeddu, S.; Boni, M.R. Remediation of Water Contaminated by Pb(II) Using Virgin Coniferous Wood Biochar as Adsorbent. In *Frontiers in Water-Energy-Nexus—Nature-Based Solutions, Advanced Technologies and Best Practices for Environmental Sustainability. Advances in Science, Technology & Innovation (IEREK Interdisciplinary Series for Sustainable Development)*; Naddeo, V., Balakrishnan, M., Choo, K.-H., Eds.; Springer, Cham: Salerno, Italy, 2020; pp. 363–366 ISBN 978-3-030-13067-1.

711. Perry, R.H.; Green, D.W. *Perry's chemical engineers' handbook*; 8°th Ed.; McGraw-Hill: New York, Chicago, San Francisco, Lisbon, London, Madrid, Mexico City, Milan, New Delhi, San Juan, Seoul, Singapore, Sydney, Toronto, 2008; ISBN 9780071422949.

712. Hai, F.I.; Yamamoto, K.; Jegatheesan, J.V. *Wastewater Treatment and Reuse Technologies*; Hai, F.I., Yamamoto, K., Jegatheesan, J.V., Eds.; 1st ed.; MDPI, 2018; ISBN 9783038971016.

713. Chern, J.M.; Chien, Y.W. Adsorption of nitrophenol onto activated carbon: Isotherms and breakthrough curves. *Water Res.* **2002**, *36*, 647–655, doi:10.1016/S0043-1354(01)00258-5.

714. Yoon, Y.H.; Nelson, J.H. Application of Gas Adsorption Kinetics I. A Theoretical Model for Respirator Cartridge Service Life. *Am. Ind. Hyg. Assoc. J.* **1984**, *45*, 509–516, doi:10.1080/15298668491400197.

715. Thomas, H.C. Heterogeneous Ion Exchange in a Flowing System. *J. Am. Chem. Soc.* **1944**, *66*, 1664–1666, doi:10.1021/ja01238a017.

716. Bohart, G.S.; Adams, E.Q. Some aspects of the behavior of charcoal with respect to chlorine. *J. Am. Chem. Soc.* **1920**, *42*, 523–544, doi:10.1021/ja01448a018.

717. Boni, M.R.; Chiavola, A.; Sbaffoni, S. Pretreated waste landfilling: Relation between leachate characteristics and mechanical behaviour. *Waste Manag.* **2006**, *26*, 1156–1165, doi:10.1016/j.wasman.2006.01.001.

718. Boni, M.R.; Leoni, S.; Sbaffoni, S. Co-landfilling of pretreated waste: Disposal and management strategies at lab-scale. *J. Hazard. Mater.* **2007**, *147*, 37–47, doi:10.1016/j.jhazmat.2006.12.049.

719. Rose, P.; Hager, S.; Glas, K.; Rehmann, D.; Hofmann, T. Coating techniques for glass beads as filter media for removal of manganese from water. *Water Sci. Technol. Water Supply* **2017**, *17*, 95–106, doi:10.2166/ws.2016.116.

720. Perry, R.H.; Green, D.W.; Maloney, J.O. *Perry's chemical engineer's handbook*; McGraw-Hill, Ed.; 7th ed.; McGraw-Hill: New York, USA, 1997; Vol. 27; ISBN 0070498415.

721. Luciano, A.; Viotti, P.; Torretta, V.; Mancini, G. Numerical approach to modelling pulse-mode soil flushing on a Pb-contaminated soil. *J. Soils Sediments* **2013**, *13*, 43–55, doi:10.1007/s11368-012-0567-0.

722. Vilardi, G.; Mpouras, T.; Dermatas, D.; Verdone, N.; Polydera, A.; Di Palma, L. Nanomaterials application for heavy metals recovery from polluted water: The combination of nano zero-valent iron and carbon nanotubes. Competitive adsorption non-linear modeling. *Chemosphere* **2018**, *201*, 716–729, doi:10.1016/j.chemosphere.2018.03.032.

723. Karahan, H. Unconditional stable explicit finite difference technique for the advection-diffusion equation using spreadsheets. *Adv. Eng. Softw.* **2007**, *38*, 80–86, doi:10.1016/j.advengsoft.2006.08.001.

724. Saul'yev, V.K. *Integration of Equations of Parabolic Type by the Method of Nets*; Pergamon Press Ltd, 1964; ISBN 978-0-08-010195-8.

725. Kumar, K.V.; Sivanesan, S. Pseudo second order kinetics and pseudo isotherms for malachite green onto activated carbon: Comparison of linear and non-linear regression methods. *J. Hazard. Mater.* **2006**, *136*, 721–726, doi:10.1016/j.jhazmat.2006.01.003.

726. Ng, J.C.Y.; Cheung, W.H.; McKay, G. Equilibrium studies for the sorption of lead from effluents using chitosan. *Chemosphere* **2003**, *52*, 1021–1030, doi:10.1016/S0045-6535(03)00223-6.

727. Ng, J.C.Y.; Cheung, W.H.; McKay, G. Equilibrium studies of the sorption of Cu(II) ions onto chitosan. *J. Colloid Interface Sci.* **2002**, *255*, 64–74, doi:10.1006/jcis.2002.8664.

728. Sarici-Özdemir, Ç.; Önal, Y. Error anlaysis studies of dye adsorption onto activated carbon from aqueous solutions. *Part. Sci. Technol.* **2014**, *32*, 20–27, doi:10.1080/02726351.2013.791360.

729. Kundu, S.; Gupta, A.K. Arsenic adsorption onto iron oxide-coated cement (IOCC): Regression analysis of equilibrium data with several isotherm models and their optimization. *Chem. Eng. J.* **2006**, *122*, 93–106, doi:10.1016/j.cej.2006.06.002.

730. Hekmatzadeh, A.A.; Karimi-Jashni, A.; Talebbeydokhti, N.; Kløve, B. Adsorption kinetics of nitrate ions on ion exchange resin. *Desalination* **2013**, *326*, 125–134, doi:10.1016/j.desal.2013.07.017.

731. Ahmadvand, M.; Soltani, J.; Hashemi Garmdareh, S.E.; Varavipour, M. The relationship between the characteristics of Biochar produced at different temperatures and its impact on the uptake of NO 3- -N. *Environ. Heal. Eng. Manag. J.* **2018**, *5*, 67–75, doi:10.15171/EHEM.2018.10.

732. Hekmatzadeh, A.A.; Karimi-Jashani, A.; Talebbeydokhti, N.; Kløve, B. Modeling of nitrate removal for ion exchange resin in batch and fixed bed experiments. *Desalination* **2012**, *284*, 22–31, doi:10.1016/j.desal.2011.08.033.

733. Klasson, K.T. Biochar characterization and a method for estimating biochar quality from proximate analysis results. *Biomass and Bioenergy* **2017**, *96*, 50–58, doi:10.1016/j.biombioe.2016.10.011.

734. William Kajjumba, G.; Emik, S.; Öngen, A.; Kurtulus Özcan, H.; Aydın, S. Modelling of Adsorption Kinetic Processes—Errors, Theory and Application. In *Advanced Sorption Process Applications*; Edebali, S., Ed.; IntechOpen, 2019; pp. 1–19 ISBN 978-1-83962-029-4.

735. Allen, S.J.; Mckay, G.; Porter, J.F. Adsorption isotherm models for basic dye adsorption by peat in single and binary component systems. *J. Colloid Interface Sci.* **2004**, *280*, 322–333, doi:10.1016/j.jcis.2004.08.078.

736. Tosun, İ. Ammonium Removal from Aqueous Solutions by Clinoptilolite: Determination of Isotherm and Thermodynamic Parameters and Comparison of Kinetics by the Double Exponential Model and Conventional Kinetic Models. *Int. J. Environ. Res. Public Health* **2012**, *9*, 970–984, doi:10.3390/ijerph9030970.

737. Foo, K.Y.; Hameed, B.H. Insights into the modeling of adsorption isotherm systems. *Chem. Eng. J.* **2010**,

156, 2–10, doi:10.1016/j.cej.2009.09.013.

738. Marquardt, D.W. An Algorithm for Least-Squares Estimation of Nonlinear Parameters. *J. Soc. Ind. Appl. Math.* **1963**, *11*, 431–441, doi:10.1137/0111030.

739. Tran, H.N.; You, S.J.; Chao, H.P. Effect of pyrolysis temperatures and times on the adsorption of cadmium onto orange peel derived biochar. *Waste Manag. Res.* **2016**, *34*, 129–138, doi:10.1177/0734242X15615698.

740. Pillai, R.S.N.; Bagavathi, V. *Statistics. Theory and Practice*; 8th ed.; S. Chand Publishing, 2016; ISBN 9781461378365.

741. Boulinguiez, B.; Le Cloirec, P.; Wolbert, D. Revisiting the determination of langmuir parameters-application to tetrahydrothiophene adsorption onto activated carbon. *Langmuir* **2008**, *24*, 6420–6424, doi:10.1021/la800725s.

742. Agarwal, A.K.; Kadu, M.S.; Pandhurnekar, C.P.; Muthreja, I.L. Langmuir , Freundlich and BET Adsorption Isotherm Studies for Zinc ions onto coal fly ash. *Int. J. Appl. or Innov. Eng. Manag.* **2014**, *3*, 64–71.

743. Major, J.; Steiner, C.; Downie, A.; Lehmann, J. Biochar Effects on Nutrient Leaching. In; Routledge, 2012; pp. 303–320.

744. Singh, A.; Singh, A.P.; Purakayastha, T.J. Characterization of biochar and their influence on microbial activities and potassium availability in an acid soil. *Arch. Agron. Soil Sci.* **2019**, *65*, 1302–1315, doi:10.1080/03650340.2018.1563291.

745. McLauglin, H. Characterizing biochars: attributes, indicators, and at-home tests. In *The Biochar Revolution: Transforming Agriculture & Environment*; Taylor, P., Ed.; NuLife Publishing, 2010; pp. 89–111 ISBN 9781921630415.

746. Yargicoglu, E.N.; Yamini, B.; Reddy, K.R.; Spokas, K.; Sadasivam, B.Y.; Reddy, K.R.; Spokas, K. Physical and chemical characterization of waste wood derived biochars. *Waste Manag.* **2015**, *36*, 256–268, doi:10.1016/j.wasman.2014.10.029.

747. Leeq, J.W.; Kidder, M.; Evans, B.R.; Paik, S.; Buchanan, A.C.; Garten, C.T.; Brown, R.C. Characterization of biochars produced from cornstovers for soil amendment. *Environ. Sci. Technol.* **2010**, *44*, 7970–7974, doi:10.1021/es101337x.

748. Brewer, C.E.; Schmidt-Rohr, K.; Satrio, J.A.; Browna, R.C. Characterization of Biochar from Fast Pyrolysis and Gasification Systems. *Environ. Prog. Sustain. Energy* **2009**, 11, doi:10.1002/ep.10378.

749. Federico, E. Adsorbimento composti organici volatili (VOCs) in soluzione acquosa su materiali sorbenti granulari, Università degli studi di Napoli Federico II.

750. Smider, B.; Singh, B. Agronomic performance of a high ash biochar in two contrasting soils. *Agriculture, Ecosyst. Environ.* **2014**, *191*, 99–107, doi:10.1016/j.agee.2014.01.024.

751. Lawrinenko, M.; Laird, D.A. Anion Exchange Capacity of Biochar Cite. *Green Chem.* **2012**, doi:10.1039/x0xx00000x.

752. Yuan, J.H.; Xu, R.K.; Zhang, H. The forms of alkalis in the biochar produced from crop residues at different temperatures. *Bioresour. Technol.* **2011**, *102*, 3488–3497, doi:10.1016/j.biortech.2010.11.018.

753. Basu, P. *Biomass Gasification and Pyrolysis: Pratical Design and Theory*; Elsevier, Ed.; 2010; ISBN 978-0-12-374988-8.

754. Tsechansky, L.; Graber, E.R. Methodological limitations to determining acidic groups at biochar surfaces via the Boehm titration. *Carbon N. Y.* **2014**, *66*, 730–733, doi:10.1016/j.carbon.2013.09.044.

755. Dehouli, H.; Chedeville, O.; Cagnon, B.; Caqueret, V.; Porte, C. Influences of pH, temperature and

activated carbon properties on the interaction ozone/activated carbon for a wastewater treatment process. *Desalination* **2010**, *254*, 12–16, doi:10.1016/j.desal.2009.12.021.

756. Allwar, A. Characteristics of Pore Structures and Surface Chemistry of Activated Carbons by Physisorption, Ftir And Boehm Methods. *IOSR J. Appl. Chem.* **2012**, *2*, 09–15, doi:10.9790/5736-0210915.

757. Saka, C. BET, TG-DTG, FT-IR, SEM, iodine number analysis and preparation of activated carbon from acorn shell by chemical activation with ZnCl2. *J. Anal. Appl. Pyrolysis* **2012**, *95*, 21–24, doi:10.1016/j.jaap.2011.12.020.

758. Zhang, P.; O'Connor, D.; Wang, Y.; Jiang, L.; Xia, T.; Wang, L.; Tsang, D.C.W.; Ok, Y.S.; Hou, D. A green biochar/iron oxide composite for methylene blue removal. *J. Hazard. Mater.* **2020**, *384*, 121286, doi:10.1016/j.jhazmat.2019.121286.

759. Luperto, A.A. Il carbone attivo, Università degli studi di Lecce- Facoltà di Ingegneria, 2002.

760. Nimmo, J.R. Porosity and Pore-Size Distribution. *Encycl. Soils Environ.* **2004**, *4*, 295–303, doi:10.1016/B0-12-348530-4/00404-5.

761. Alsabry, A.; Backiel-Brzozowska, B.; Nikitsin, V.I. Dependencies for Determining the Thermal Conductivity of Moist Capillary-Porous Materials. *Energies* **2020**, *13*, 3211, doi:10.3390/en13123211.

762. Sampath, U.; Ching, Y.; Chuah, C.; Sabariah, J.; Lin, P.-C. Fabrication of Porous Materials from Natural/Synthetic Biopolymers and Their Composites. *Materials (Basel).* **2016**, *9*, 991, doi:10.3390/ma9120991.

763. Yang, Z.; Chen, J. Preparation, characterization and adsorption performance of reed biochar. *Chem. Eng. Trans.* **2017**, *62*, 1243–1248, doi:10.3303/CET1762208.

764. Rahman; Muttakin; Pal; Shafiullah; Saha A Statistical Approach to Determine Optimal Models for IUPAC-Classified Adsorption Isotherms. *Energies* **2019**, *12*, 4565, doi:10.3390/en12234565.

765. Inyang, M.I.; Gao, B.; Yao, Y.; Xue, Y.; Zimmerman, A.; Mosa, A.; Pullammanappallil, P.; Ok, Y.S.; Cao, X. A review of biochar as a low-cost adsorbent for aqueous heavy metal removal. *Crit. Rev. Environ. Sci. Technol.* **2016**, *46*, 406–433, doi:10.1080/10643389.2015.1096880.

766. Qiu, Y.; Xu, X.; Xu, Z.; Liang, J.; Yu, Y.; Cao, X. Contribution of different iron species in the iron-biochar composites to sorption and degradation of two dyes with varying properties. *Chem. Eng. J.* **2020**, *389*, 124471, doi:10.1016/j.cej.2020.124471.

767. Wan, Z.; Sun, Y.; Tsang, D.C.W.; Xu, Z.; Khan, E.; Liu, S.H.; Cao, X. Sustainable impact of tartaric acid as electron shuttle on hierarchical iron-incorporated biochar. *Chem. Eng. J.* **2020**, *395*, 125138, doi:10.1016/j.cej.2020.125138.

768. Wang, Y.; Xiao, X.; Xu, Y.; Chen, B. Environmental Effects of Silicon within Biochar (Sichar) and Carbon-Silicon Coupling Mechanisms: A Critical Review. *Environ. Sci. Technol.* **2019**, *53*, 13570–13582, doi:10.1021/acs.est.9b03607.

769. Joseph, S.; Kammann, C.I.; Shepherd, J.G.; Conte, P.; Schmidt, H.-P.; Hagemann, N.; Rich, A.M.; Marjo, C.E.; Allen, J.; Munroe, P.; Mitchell, D.R.G.; Donne, S.; Spokas, K.; Graber, E.R. Microstructural and associated chemical changes during the composting of a high temperature biochar: Mechanisms for nitrate, phosphate and other nutrient retention and release. *Sci. Total Environ.* **2018**, *618*, 1210–1223, doi:10.1016/j.scitotenv.2017.09.200.

770. Mazzei, L. *Lab Manual: Raman Spectroscopy*; 2014;

771. Miraglia, L. Caratteristiche del sistema analitico SEM-EDS valutazione dell'accuratezza e della precisione delle analisi eseguite su standard internazionali di minerali e vetri. *Rapp. Tec. INGV* **2012**, *ISSN 2039-*, 7–9.

772. Huang, Y.; Yin, X.; Wu, C.; Wang, C.; Xie, J.; Zhou, Z.; Ma, L.; Li, H. Effects of metal catalysts on CO2

gasification reactivity of biomass char. *Biotechnol. Adv.* **2009**, *27*, 568–572, doi:10.1016/j.biotechadv.2009.04.013.

773. Colombo, C.M.; Fontana, F.; Barron, V. Microscopia di forza atomica. *Metod. di Anal. Mineral. del suolo* 1–25.

774. Kołodyńska, D.; Wnetrzak, R.; Leahy, J.J.; Hayes, M.H.B.; Kwapiński, W.; Hubicki, Z. Kinetic and adsorptive characterization of biochar in metal ions removal. *Chem. Eng. J.* **2012**, *197*, 295–305, doi:10.1016/j.cej.2012.05.025.

775. Inyang, M.; Gao, B.; Ding, W.; Pullammanappallil, P.; Zimmerman, A.R.; Cao, X. Enhanced lead sorption by biochar derived from anaerobically digested sugarcane bagasse. *Sep. Sci. Technol.* **2011**, *46*, 1950–1956, doi:10.1080/01496395.2011.584604.

776. Karunanayake, A.G.; Todd, O.A.; Crowley, M.; Ricchetti, L.; Pittman, C.U.; Anderson, R.; Mohan, D.; Mlsna, T. Lead and cadmium remediation using magnetized and non magnetized biochar from Douglas fir. *Chem. Eng. J.* **2018**, *331*, 480–491, doi:10.1016/j.cej.2017.08.124.

777. Deng, J.; Liu, Y.; Liu, S.; Zeng, G.; Tan, X.; Huang, B.; Tang, X.; Wang, S.; Hua, Q.; Yan, Z. Competitive adsorption of Pb(II), Cd(II) and Cu(II) onto chitosan-pyromellitic dianhydride modified biochar. *J. Colloid Interface Sci.* **2017**, *506*, 355–364, doi:10.1016/j.jcis.2017.07.069.

778. Boni, M.R.; Chiavola, A.; Marzeddu, S. Application of Biochar to the Remediation of Pb-Contaminated Solutions. *Sustainability* **2018**, *10*, 4440, doi:10.3390/su10124440.

779. Ifthikar, J.; Wang, T.; Khan, A.; Jawad, A.; Sun, T.; Jiao, X.; Chen, Z.; Wang, J.; Wang, Q.; Wang, H.; Jawad, A. Highly Efficient Lead Distribution by Magnetic Sewage Sludge Biochar: Sorption Mechanisms and Bench Applications. *Bioresour. Technol.* **2017**, *238*, 399–406, doi:10.1016/j.biortech.2017.03.133.

780. Mohan, D.; Pittman, C.U.; Bricka, M.; Smith, F.; Yancey, B.; Mohammad, J.; Steele, P.H.; Alexandre-Franco, M.F.; Gómez-Serrano, V.; Gong, H. Sorption of arsenic, cadmium, and lead by chars produced from fast pyrolysis of wood and bark during bio-oil production. *J. Colloid Interface Sci.* **2007**, *310*, 57–73, doi:10.1016/j.jcis.2007.01.020.

781. Harris, W. Dairy-Manure Derived Biochar Effectively Sorbs Lead and Atrazine. *Environ. Sci. Technol.* **2009**, *1*, 3285–3291, doi:Doi 10.1021/Es803092k.

782. Li, Y.-H.; Ding, J.; Luan, Z.; Di, Z.; Zhu, Y.; Xu, C.; Wu, D.; Wei, B. Competitive adsorption of Pb2+, Cu2+ and Cd2+ ions from aqueous solutions by multiwalled carbon nanotubes. *Carbon N. Y.* **2003**, *41*, 2787–2792, doi:10.1016/S0008-6223(03)00392-0.

783. Mahdi, Z.; Yu, Q.J.; El Hanandeh, A. Removal of lead(II) from aqueous solution using date seed-derived biochar: batch and column studies. *Appl. Water Sci.* **2018**, *8*, 181, doi:10.1007/s13201-018-0829-0.

784. Ding, W.; Dong, X.; Ime, I.M.; Gao, B.; Ma, L.Q. Pyrolytic temperatures impact lead sorption mechanisms by bagasse biochars. *Chemosphere* **2014**, *105*, 68–74, doi:10.1016/j.chemosphere.2013.12.042.

785. Duan, X.; Zhang, C.; Srinivasakannan, C.; Wang, X. Waste walnut shell valorization to iron loaded biochar and its application to arsenic removal. *Resour. Technol.* **2017**, *3*, 29–36, doi:10.1016/j.reffit.2017.01.001.

786. Singh, P.; Sarswat, A.; Pittman, C.U.; Mlsna, T.; Mohan, D. Sustainable Low-Concentration Arsenite [As(III)] Removal in Single and Multicomponent Systems Using Hybrid Iron Oxide–Biochar Nanocomposite Adsorbents—A Mechanistic Study. *ACS Omega* **2020**, *5*, 2575–2593, doi:10.1021/acsomega.9b02842.

787. Horng, L.-L.; Clifford, D. The behavior of polyprotic anions in ion-exchange resins. *React. Funct. Polym.*

1997, *35*, 41–54, doi:10.1016/S1381-5148(97)00048-5.

788. Horng, L.-L.; Clifford, D. The behavior of polyprotic anions in ion-exchange resins. *React. Funct. Polym.* **1997**, *35*, 41–54, doi:10.1016/S1381-5148(97)00048-5.

789. Nguyen, T.H.; Pham, T.H.; Nguyen Thi, H.T.; Nguyen, T.N.; Nguyen, M.V.; Tran Dinh, T.; Nguyen, M.P.; Do, T.Q.; Phuong, T.; Hoang, T.T.; Mai Hung, T.T.; Thi, V.H.T. Synthesis of Iron-Modified Biochar Derived from Rice Straw and Its Application to Arsenic Removal. *J. Chem.* **2019**, *2019*, doi:10.1155/2019/5295610.

790. Liang, T.; Li, L.; Zhu, C.; Liu, X.; Li, H.; Su, Q.; Ye, J.; Geng, B.; Tian, Y.; Sardar, M.F.; Huang, X.; Li, F. Adsorption of As(V) by the Novel and Efficient Adsorbent Cerium-Manganese Modified Biochar. *Water* **2020**, *12*, 2720, doi:10.3390/w12102720.

791. Yoon, K.; Cho, D.W.; Tsang, D.C.W.W.; Bolan, N.; Rinklebe, J.; Song, H. Fabrication of engineered biochar from paper mill sludge and its application into removal of arsenic and cadmium in acidic water. *Bioresour. Technol.* **2017**, *246*, 69–75, doi:10.1016/j.biortech.2017.07.020.

792. Zhu, N.; Yan, T.; Qiao, J.; Cao, H. Adsorption of arsenic, phosphorus and chromium by bismuth impregnated biochar: Adsorption mechanism and depleted adsorbent utilization. *Chemosphere* **2016**, *164*, 32–40, doi:10.1016/j.chemosphere.2016.08.036.

793. Yu, Z.; Zhou, L.; Huang, Y.; Song, Z.; Qiu, W. Effects of a manganese oxide-modified biochar composite on adsorption of arsenic in red soil. *J. Environ. Manage.* **2015**, *163*, 155–162, doi:10.1016/j.jenvman.2015.08.020.

794. Zhou, Z.; Liu, Y. guo; Liu, S. bo; Liu, H. yu; Zeng, G. ming; Tan, X. fei; Yang, C. ping; Ding, Y.; Yan, Z. li; Cai, X. xi Sorption performance and mechanisms of arsenic(V) removal by magnetic gelatin-modified biochar. *Chem. Eng. J.* **2017**, *314*, 223–231, doi:10.1016/j.cej.2016.12.113.

795. Hu, X.; Ding, Z.; Zimmerman, A.R.; Wang, S.; Gao, B. Batch and column sorption of arsenic onto iron-impregnated biochar synthesized through hydrolysis. *Water Res.* **2015**, *68*, 206–216, doi:10.1016/j.watres.2014.10.009.

796. Nieto-Delgado, C.; Rangel-Mendez, J.R. Anchorage of iron hydro(oxide) nanoparticles onto activated carbon to remove As(V) from water. *Water Res.* **2012**, *46*, 2973–2982, doi:10.1016/j.watres.2012.03.026.

797. Chang, Q.; Lin, W.; Ying, W. chi Preparation of iron-impregnated granular activated carbon for arsenic removal from drinking water. *J. Hazard. Mater.* **2010**, *184*, 515–522, doi:10.1016/j.jhazmat.2010.08.066.

798. Zhang, M.; Gao, B. Removal of arsenic, methylene blue, and phosphate by biochar/AlOOH nanocomposite. *Chem. Eng. J.* **2013**, *226*, 286–292, doi:10.1016/j.cej.2013.04.077.

799. Tuna, A.Ö.A.; özdemir, E.; şimşek, E.B.; Beker, U. Removal of As(V) from aqueous solution by activated carbon-based hybrid adsorbents: Impact of experimental conditions. *Chem. Eng. J.* **2013**, *223*, 116–128, doi:10.1016/j.cej.2013.02.096.

800. Lin, L.; Qiu, W.; Wang, D.; Huang, Q.; Song, Z.; Chau, H.W. Arsenic removal in aqueous solution by a novel Fe-Mn modified biochar composite: Characterization and mechanism. *Ecotoxicol. Environ. Saf.* **2017**, *144*, 514–521, doi:10.1016/j.ecoenv.2017.06.063.

801. Imran, M.; Iqbal, M.M.; Iqbal, J.; Shah, N.S.; Khan, Z.U.H.; Murtaza, B.; Amjad, M.; Ali, S.; Rizwan, M. Synthesis, characterization and application of novel MnO and CuO impregnated biochar composites to sequester arsenic (As) from water: Modeling, thermodynamics and reusability. *J. Hazard. Mater.* **2021**, *401*, 123338, doi:10.1016/j.jhazmat.2020.123338.

802. Baker, D.E.; Chesnin, L. Chemical monitoring of soils for environmental quality and animal and human health. *Adv. Agron.* **1975**, *27*, 305–374, doi:10.1016/S0065-2113(08)70013-0.

803. Han, C.; Li, H.; Pu, H.; Yu, H.; Deng, L.; Huang, S.; Luo, Y. Synthesis and characterization of

mesoporous alumina and their performances for removing arsenic(V). *Chem. Eng. J.* **2013**, *217*, 1–9, doi:10.1016/j.cej.2012.11.087.

804. Boni, M.R.; Marzeddu, S.; Tatti, F.; Raboni, M.; Mancini, G.; Luciano, A.; Viotti, P. Experimental and Numerical Study of Biochar Fixed Bed Column for the Adsorption of Arsenic from Aqueous Solutions. *Water (Switzerland)* **2021**, *13*, 915, doi:10.3390/w13070915.

805. Jin, H.; Capareda, S.; Chang, Z.; Gao, J.; Xu, Y.; Zhang, J. Biochar pyrolytically produced from municipal solid wastes for aqueous As(V) removal: Adsorption property and its improvement with KOH activation. *Bioresour. Technol.* **2014**, *169*, 622–629, doi:10.1016/j.biortech.2014.06.103.

806. Begum, S.A.; Golam Hyder, A.H.M.; Vahdat, N. Adsorption isotherm and kinetic studies of As(V) removal from aqueous solution using cattle bone char. *J. Water Supply Res. Technol. - AQUA* **2016**, *65*, 244–252, doi:10.2166/aqua.2016.089.

807. Niazi, N.K.; Bibi, I.; Shahid, M.; Ok, Y.S.; Burton, E.D.; Wang, H.; Shaheen, S.M.; Rinklebe, J.; Lüttge, A. Arsenic removal by perilla leaf biochar in aqueous solutions and groundwater: An integrated spectroscopic and microscopic examination. *Environ. Pollut.* **2018**, *232*, 31–41, doi:10.1016/j.envpol.2017.09.051.

808. Sattar, M.S.; Shakoor, M.B.; Ali, S.; Rizwan, M.; Niazi, N.K.; Jilani, A. Comparative efficiency of peanut shell and peanut shell biochar for removal of arsenic from water. *Environ. Sci. Pollut. Res.* **2019**, *26*, 18624–18635, doi:10.1007/s11356-019-05185-z.

809. Tavares, D.S.; Lopes, C.B.; Coelho, J.P.; Sánchez, M.E.; Garcia, A.I.; Duarte, A.C.; Otero, M.; Pereira, E. Removal of arsenic from aqueous solutions by sorption onto sewage sludge-based sorbent. *Water. Air. Soil Pollut.* **2012**, *223*, 2311–2321, doi:10.1007/s11270-011-1025-0.

810. Samsuri, A.W.; Sadegh-Zadeh, F.; Seh-Bardan, B.J. Adsorption of As(III) and As(V) by Fe coated biochars and biochars produced from empty fruit bunch and rice husk. *J. Environ. Chem. Eng.* **2013**, *1*, 981–988, doi:10.1016/j.jece.2013.08.009.